BRUNEL UNIVERSITY LONDON

Time-Frequency Analysis based on Split Spectrum Applied to Audio and Ultrasonic Signals

by:

Seyed Kamran Pedram Rad

A thesis submitted in partial fulfilment for the

degree of Doctor of Philosophy

in the

Centre for Electronic Systems Research (CESR)

College of Engineering, Design and Physical Sciences

April 2017

BRUNEL UNIVERSITY LONDON

Abstract

College of Engineering, Design and Physical Sciences

Doctorate of Philosophy

By Seyed Kamran Pedram Rad

Signal processing is a large subject with applications integral to a number of technological fields such as communication, audio, Voice over IP (VoIP), pattern recognition, sonar, radar, ultrasound and medical imaging. Techniques exist for the analysis, modelling, extraction, recognition and synthesis of signals of interest.

The focus of this thesis is signal processing for acoustics (both sonic and ultrasonic). In the applications examined, signals of interest are usually incomplete, distorted and/or noisy. Therefore, reconstructing the signal, noise reduction and removal of any distortion/interference are the main goals of the signal processing techniques presented. The primary aim is to study and develop an advanced time-frequency signal processing technique for acoustic applications to enhance the quality of the signals.

In the first part of the thesis, a technique is presented that models and maintains the correlation between temporal and spectral parameters of audio signals. A novel Packet Loss Concealment (PLC) method is developed with applications to VoIP, audio broadcasting, and streaming. The problem of modelling the time-varying frequency spectrum in the context of PLC is addressed, and a novel solution is proposed for tracking and using the temporal motion of spectral flow to reconstruct the signal. The proposed method utilises a Time-Frequency Motion (TFM) matrix representation of the audio signal, where each frequency is tagged with a motion vector estimate that is assessed by cross-correlation of the movement of spectral energy within sub-bands across time frames. The missing packets are estimated using extrapolation or interpolation algorithms using a TFM matrix and then inverse transformed to the time-domain for reconstruction of the signal. The proposed method is compared with conventional approaches using objective Performance Evaluation of Speech Quality (PESQ), and subjective Mean Opinion Scores (MOS) in a range of packet loss from 5% to 20%. The evaluation results demonstrate that the proposed algorithm substantially improves performance by an average of 2.85% and 5.9% in terms of PESQ and MOS respectively.

In the second part of the thesis, the proposed method is extended and modified to address challenges of excessive coherent noise arising from ultrasonic signals gathered during Guided Wave Testing (GWT). It is an advanced Non-destructive testing technique which is used over several branches of industry to inspect large structures for defects where the structural integrity is of concern. In such systems, signal interpretation can often be challenging due to the multi-modal and dispersive propagation of Ultrasonic Guided Waves (UGWs). The multi-modal and dispersive nature of the received signals hampers the ability to detect defects in a given structure. The Split-Spectrum Processing (SSP) method with application for such signal has been studied and reviewed quantitatively to measure the enhancement in terms of Signal-to-Noise Ratio (SNR) and spatial resolution. In this thesis, the influence of SSP filter bank parameters on these signals is studied and optimised to improve SNR and spatial resolution considerably. The proposed method is compared analytically and experimentally with conventional approaches. The proposed SSP algorithm substantially improves SNR by an average of 30dB. The conclusions reached in this thesis will contribute to the progression of the GWT technique through considerable improvement in defect detection capability.

Acknowledgement

I would like to take this opportunity to thank my project supervisors Dr. Lu Gan and Prof. Wamadeva Balachandran for the continuous support of my PhD study and related research, for their patience, motivation, and immense knowledge. I would like to express my sincere gratitude to my industrial supervisors Dr. Peter Mudge and Dr. Keith Thornicroft for their insightful comments and encouragement. Particular thanks goes out to Dr. Alex Haig and Dr. Sina Fateri for their advice and direction on programming, signal processing and surviving my PhD.

I would like to thank all of my colleagues within Plant Integrity Ltd., with particular thanks to Dr. Paul Jackson for providing me with the equipment, support and guidance in carrying out the empirical work.

I would like to thank Prof. Saeed Vaseghi for his support and guidance.

I would like to thank my fellow research colleagues within Plant Integrity Ltd., TWI and Brunel University London for their feedback, cooperation and of course friendship.

For the project funding, thanks and recognition must also be apportioned to the Centre for Electronic Systems Research (CESR) of Brunel University London, The National Structural Integrity Research Centre (NSIRC) and TWI Ltd., without whom the research would not have been possible.

And last but not least I would like to thank my family for supporting me spiritually throughout writing this thesis and my life.

Declaration

The work described in this thesis has not been previously submitted for a degree in this or any other university, and unless otherwise referenced it is the author’s own work.

Table of contents

Abstract ii

Acknowledgement iii

Declaration iv

Table of contents v

List of Figures x

List of Tables xv

List of Abbreviations xvi

List of Symbols xviii

Chapter 1 1

1 Introduction 1

1.1 Chapter overview 1

1.2 Motivation for Research 1

1.2.1 Motivation for Audio Signal Processing 2

1.2.2 Motivation for Ultrasound Signal Processing 2

1.3 Acoustic Signal Processing 4

1.3.1 Audio Signal Processing 5

1.3.2 Signal Processing for Ultrasonics 6

1.4 Aim and Objectives 7

1.5 Research Methods 7

1.6 Thesis Outline 11

1.7 Contributions to Knowledge 12

1.8 List of Publications arising from this research 14

Chapter 2 16

2 Fundamental knowledge and background review 16

2.1 Chapter overview 16

2.2 Principle of Acoustics 16

2.3 Signal Processing Techniques 17

2.3.1 Fourier Transform 17

2.3.1.1 Discrete Fourier Transform (DFT) 18

2.3.1.2 Short-Time Fourier Transform (STFT) 19

2.3.2 Windowing 20

2.3.3 Cross-correlation 22

2.3.4 Sampling Rate 22
2.3.5 Zero-Padding 23
2.3.6 Split-Spectrum Processing (SSP) 24
2.3.7 SSP Recombination Algorithms 25
2.3.7.1 Polarity Thresholding (PT) 25
2.3.7.2 PT with Minimisation (PTM) 26
2.3.7.3 Mean 26
2.3.7.4 Minimisation 27
2.3.7.5 Frequency Multiplication (FM) 27
2.4 Sonic Applications 28
2.4.1 Bandwidths of Voice and Music 28
2.4.2 Streaming Media 29
2.4.3 Streaming Protocol 29
2.4.4 Packet Loss Concealment Domains 30
2.4.5 Review of Audio Flow 33
2.4.6 Kalman Filter 35
2.5 Ultrasonic Applications 35
2.5.1 Propagation of Elastic Waves 36
2.5.2 Longitudinal Waves 37
2.5.3 Shear Waves 37
2.5.4 Surface Waves 38
2.6 Guided Waves 38
2.6.1 Lamb waves 39
2.6.2 Guided Wave in Hollow Cylinders 39
2.6.3 Propagation of UGW 40
2.6.4 Commercial Applications of UGW 42
2.6.5 Phase and Group Velocity 43
2.6.6 Dispersion Curve 45
2.6.7 Mode Conversion of UGWs 49
2.6.8 Coherent Noise 50
2.6.9 Guided Wave Inspection Methods 50
2.7 Summary 51
Chapter 3 52
3 Literature Review 52

3.1 Sonic Applications 52
3.1.1 Packet Loss Recovery Techniques 52
3.1.2 Receiver-Based Techniques 53
3.2 Ultrasonics Guided Wave 58
3.2.1 Literature review of SSP 59
Chapter 4 71
4 Time-Varying Signal Models Using Spectral Motion Detection 71
4.1 Chapter overview 71
4.2 Introduction 72
4.3 Reconstruction of Lost Audio Samples 73
4.3.1 Extrapolation/Interpolation Techniques 74
4.3.2 Bandwidth Extension 76
4.3.3 Phase Prediction 76
4.4 Spectral Flow and Motion in Time-Frequency Domain 77
4.4.1 Fourier Transform and Spectrogram 78
4.5 Time-Varying Spectral Motion Vector (SMV) Model 81
4.5.1 Spectral Motion Vector Estimation 81
4.6 Reconstruction in TFM Matrix 83
4.6.1 Extrapolation in TFM Matrix 84
4.6.2 Interpolation in TFM Matrix 84
4.7 Performance Evaluation 85
4.7.1 Packet Loss Model 85
4.7.2 Experiment Setup 86
4.7.3 Experiments on Synthesised Time-Varying Signals 87
4.7.4 Experiments on Audio/Speech signals 89
4.7.5 Objective Evaluation 89
4.7.6 Subjective Listening Test 91
4.8 Conclusions 93
Chapter 5 94
5 Optimisation of SSP input parameters for Synthesised UGW Signals 94
5.1 Chapter overview 94
5.2 Split-Spectrum Processing (SSP) 95
5.3 Implementation of SSP 96
5.3.1 Filter Bank Parameters 96

5.3.1.1 Total Bandwidth for Processing 97
5.3.1.2 Sub-band Filter Bandwidth 98
5.3.1.3 Filter Separation 99
5.3.2 Implementation of the Filter Bank 100
5.3.3 Selection of SSP Filter Bank Parameters for UGW testing 101
5.4 Signal Synthesis 102
5.4.1 Synthesised UGW Data 102
5.4.2 Implementation of Synthesised UGW Signals 105
5.5 SSP of Synthesised UGW Signal 107
5.5.1 First Synthesised Signal Analysis 107
5.5.2 Second Synthesised Signal Analysis 110
5.6 Discussion of Initial SSP Studies 114
5.7 Conclusions 115
Chapter 6 116
6 Application of SSP to experimental GWT data and field trials for validation 116
6.1 Chapter overview 116
6.2 Application of SSP to experimental signal 116
6.2.1 Experiment #1: using Pitch-Catch Technique 117
6.2.2 Experiment #2: using Pulse-Echo Technique 122
6.2.3 SNR Calculations 131
6.3 Experiment with Two Saw Cut Defects 135
6.3.1 Objectives 135
6.3.2 Overview 135
6.3.3 Experiment Setup Up 135
6.3.4 Implementation of SSP 136
6.4 Application of SSP to field data 137
6.4.1 Objectives 138
6.4.2 Field data collection 138
6.4.3 Pre-Processing 139
6.4.4 Data Analysis and Results 139
6.5 Discussion 148
6.5.1 Experiment #1: Pitch-catch using Teletest Focus+ and 3D-LDV scan (no defect) 148

6.5.2 Experiment #2: Pulse-echo using Teletest Focus+ system (single saw cut defect) 149

6.5.3 Experiment #3: Pulse-echo using Teletest Focus+ system, (two saw cut defects) 149

6.5.4 Field data analysis using SSP 150

6.6 Conclusions 151

Chapter 7 153

7 Conclusions and Recommendations for Future Work 153

7.1 Main Finding of this Thesis 153

7.1.1 Signal processing technique applied to Audio Signal 153

7.1.2 Signal processing method applied to Ultrasonic Guided Wave Signal 154

7.2 Recommendation for Future Works 157

7.2.1 Time-Frequency Motion Matrix using Modified Discrete Cosine Transform or Wavelet Transform 157

7.2.2 Automation of SSP Algorithm 158

7.2.3 Application of the SSP Method on Flexural Wave Modes 158

7.2.4 Apply the SSP Method on Hybrid Active Focusing Technique 158

References 160

List of Figures

Figure 1-1a) Trans-Alaskan pipeline, USA [2], b) Clean-up efforts after failure [3], ...3

Figure 2-1: a) Time domain Hann window, sine wave and windowed, b) Frequency spectrum of the sine wave and its windowed form. 22

Figure 2-2: Block diagram of SSP 25

Figure 2-3: Distribution of displacements for the vertical shear wave (left) and the horizontal shear wave (right) [78].....38

Figure 2-4: Distribution of displacements pattern of a) Symmetric (S0) or b) Anti-symmetric (A0) Lamb waves [81] 39

Figure 2-5: A Finite Element Analysis (FEA) representation of the T(0,1), L(0,2), and F(3,2) wave modes. 42

Figure 2-6: Illustration of commercial UGW pipe inspection equipment, Teletest®Focus+ system including the transducer array, the ultrasonic pulser/receiver, and an operator with a laptop [14], [16]. 44

Figure 2-7: Wave propagations including phase velocity where the phase is changing but the wave propagate with zero group velocity (green dots), and group velocity where the pulse envelope propagates but the phase is not changing (red dots). 45

Figure 2-8 : Dispersion curves diagram for a six-inch steel pipe with 168.3mm outer diameter and 7.11mm wall thickness. a) phase velocity and b) group velocity for different axisymmetric modes and their family of flexural modes are illustrated in this figure. 48

Figure 2-9: Frequency spectrum of a 50kHz, 10-cycles Hann windowed pulse overlaid with the phase velocity dispersion curve of the F(4,2) mode for a six-inch steel pipe schedule 40. The main and first side lobes are illustrated to present that the pulse has a frequency bandwidth from 35kHz to 65kHz. 49

Figure 4-1: Time-frequency motion algorithms of audio signal 80

Figure 4-2: Transformation of a time-domain signal with gaps into TFMs with spectral motion vectors for each sub-bands appended. 80

Figure 4-3: Illustration of spectral time-frequency matrix of a signal with a missing gap. 83

Figure 4-4: Illustration of a speech segment where the spectral power is moving across the frequency over the time frames.....84

Figure 4-5: Gilbert-Elliott 2-state HMM model for packet loss. 85

Figure 4-6: Spectrogram of synthesised signal, from top: original signal, DFT-TFM, DFT, and signal with 20% Bernoulli frame loss 88

Figure 4-7: Spectrogram of the synthesised time-varying signal, from top: original signal, lossy signal, DFT- Extrapolation, DFTI- Interpolation and DFT-TFM signal. 88

Figure 4-8: Spectrogram of the Civil Rights speech from the - United States, from top: original signal, lossy signal, DFT-without motion and DFT-TFM signal. 90

Figure 4-9: Time-domain signal of Civil Rights speech, from top: original signal, lossy signal, DFT-without motion and DFT-TFM (with motion) signal 90

Figure 5-1: SSP filter bank parameters 97

Figure 5-2: A Gaussian filter function 101

Figure 5-3: Phase velocity dispersion curves for a six-inch pipe overlaid with the frequency spectrum of a 50kHz 10-cycle Hann windowed pulse. The main and first side lobes are displayed to clarify that the pulse will have a frequency bandwidth corresponding to a phase velocity bandwidth of each wave modes. 104

Figure 5-4: Synthesised dispersive propagation of, F(5,2) wave mode. Frequency = 50kHz 105

Figure 5-5: Synthesised UGW signals: Torsional T(0,1) and its family of flexural wave modes: F(1,2), F(2,2), F(3,2), F(4,2), F(5,2) ,F(6,2).....106

Figure 5-6: Synthesised UGW signal: a) ideal reflection signal T(0,1), b) spectrum of ideal reflection signal c) received signal including T(0,1) and its family of flexural wave modes: F(1,2),…, F(2,6), and d) spectrum of received signal.....106

Figure 5-7: Received synthesised UGW signal: a) Time domain, b) frequency domain with Gaussian band-pass filters.....108

Figure 5-8: Results of synthesised UGW signal before and after applying SSP: a) Unprocessed input signal, b) Mean, c) Minimisation, d) Frequency Multiplication, e) Polarity Thresholding, f) Polarity Thresholding with Minimisation 110

Figure 5-9: Synthesised setup for eight-inch pipe with WT =8.179 mm and OD=219.08 mm. 111

Figure 5-10: Results for synthesised UGW signal before and after applying SSP (PT & PTM algorithms). The defect and the pipe end are located at X=3 m and X=4.5 m from the excitation signal. The defect sizes are a)10% CSA, b)8% CSA, c)6% CSA, d)4% CSA, e)2% CSA and f)1% CSA 112

Figure 5-11: Results for synthesised UGW signal before and after applying SSP (PT & PTM). The defect location (X=3.5m) is moved towards the pipe end (X=4.5 m) with steps of 0.1m. 113

Figure 6-1: Illustration of 3D-LDVexperimental set-up 118

Figure 6-2: Excitation Time-domain signal 118

Figure 6-3: Experimental signal using 3D-LDV: a) sum of 118 points b) one point scan 119

Figure 6-4: Results from applying various SSP techniques: a) unprocessed signal, b) result of mean, c) result of minimisation, d) result of frequency multiplication, e) result of polarity thresholding f) result of polarity thresholding with minimisation 121

Figure 6-5: Re-scaled results from applying various SSP techniques: a) unprocessed signal, b) result of mean, c) result of minimisation, d) result of FM, e) result of PT f) result of PTM 121

Figure 6-6: Experimental setup up for eight-inch steel pipe with a wall thickness of 8.179 mm and OD of 219.08 m 123

Figure 6-7: Result of unprocessed signal vs. SSP- 3% CSA defect - 44kHz: a) result b) zoom-in 125

Figure 6-8: Result of unprocessed signal vs. SSP- 2% CSA defect- 44kHz: a) result b) zoom-in 127

Figure 6-9: Illustrates the zoom-in result of experimental data for the defect's reflection from baseline up to 8% CSA, obtained by a) Teletest unit and b) the proposed SSP technique using PT algorithms. 129

Figure 6-10: Zoom in around defect area from 0.5% CSA up to 8% CSA 130

Figure 6-11: Result with 8% CSA; Unprocessed Signal (blue) and SSP Signal (red) ... 130

Figure 6-12: Regions to calculate SNR 131

Figure 6-13: SNR calculation - peak amplitude of the defect (S) to the RMS value of the noise region (N) for 28 kHz, 36 kHz, 44 kHz, 64 kHz and 72 kHz. 132

Figure 6-14: Result of SNR for original respond and SSP respond for different frequencies 133

Figure 6-15: Result of SNR calculation a) peak of pipe end to RMS of noise region, b) peak of pipe end to peak of defect 134

Figure 6-16: Experimental setup for the same eight-inch pipe with two saw cut defects. 136

Figure 6-17: Zoom in result with two defects a) Unprocessed Signal b) SSP -PT 137

Figure 6-18: Comparison between unprocessed signal and proposed SSP with PT and PTM algorithms. Test ID: TK104, 8-inch pipe with OD: 8.625 and WT: 8.18mm at 36 kHz. 139

Figure 6-19: Comparison between unprocessed signal and proposed SSP with PT and PTM algorithms. Test ID: Tank 13, 16-inch pipe with at 36kHz, forward direction. 141

Figure 6-20: Comparison between unprocessed signal and proposed SSP with PT and PTM algorithms. Test ID: Tank 13, 16-inch pipe with at 36 kHz, backward direction. 142

Figure 6-21: Comparison between unprocessed signal and proposed SSP with PT and PTM algorithms. Test ID: C9 Sewage, 12-inch pipe with OD: 12.75 and WT: 19.05mm at 44kHz, forward direction. 143

Figure 6-22: Comparison between unprocessed signal and proposed SSP with PT and PTM algorithms. Test ID: C9 Sewage, 12-inch pipe with OD: 12.75 and WT: 19.05mm at 44kHz, backward direction. 144

Figure 6-23: Comparison between unprocessed signal and proposed SSP with PT and PTM algorithms. Test ID: GW SES, 12-inch pipe with OD: 12.75 and WT: 5.16mm at 64kHz, forward direction.....145

Figure 6-24: Comparison between unprocessed signal and proposed SSP with PT and PTM algorithms. Test ID: 153, 14-inch pipe with OD: 14 and WT: 7.92mm at 36kHz, forward direction. 146

Figure 6-25: Comparison between unprocessed signal and proposed SSP with PT and PTM algorithms. Test ID: 516, 12-inch pipe with OD: 12.75 and WT: 10.31mm at 54kHz, forward direction.....147

Figure 7-1: Focusing technique a) HTRF set up b) HTRF signal c) result of SSP-PT ..159

List of Tables

Table 2-1: Summary of commercial UGW systems 44

Table 4-1. Performance of different algorithms for restoration of Bernoulli generated gaps (PESQ Result).....92

Table 4-2. Audio, speech and music samples 92

Table 4-3. Comparative subjective results of proposed methods with a loss rate of 20% against LP-HNM and G.711 92

Table 5-1: The recommended values for SSP parameters 98

Table 5-2: SNR enhancement of synthesised UGW signal.....110

Table 6-1: SNR and DCR enhancement of experimental UGW signal 122

Table 6-2: Flaw size plan for eight-inch steel pipe 124

Table 6-3: SNR enhancement of experimental UGW signal with 3% CSA 126

Table 6-4: Peak to peak measurement of pipe-end to defect with 3% CSA 127

Table 6-5: SNR enhancement of experimental UGW signal with 2% CSA 129

Table 6-6: SNR enhancement of experimental UGW signal with two defects.....137

Table 6-7: Schedule of field tests.....138

Table 6-8: SNR of all test files.....140

List of Abbreviations

BS	**B**ritish **S**tandard
CC	**C**ross-**C**orrelation
CSA	**C**ross-**S**ectional **A**rea
DAC	**D**istance **A**mplitude **C**orrection
DCR	**D**efect to **C**oherent Noise **R**atio
DCT	**D**iscrete **C**osine **T**ransform
DFT	**D**iscrete **F**ourier **T**ransform
DST	**D**iscrete **S**ine **T**ransform
DSTFT	**D**iscrete **S**hort-**T**ime **F**ourier **T**ransform
DWM	**D**ispersive **W**ave **M**odes
EMAT	**E**lectromagnetic **A**coustic **T**ransducer
FEA	**F**inite **E**lement **A**nalysis
FFT	**F**ast **F**ourier **T**ransform
FIR	**F**inite **I**mpulse **R**esponse
FM	**F**requency **M**ultiplication
GWT	**G**uided **W**ave **T**esting
ID	**I**dentification
IID	**I**ndependent **I**dentically **D**istributed
ITU	**I**nternational **T**elecommunication **U**nion
LP	**L**inear **P**rediction
LRUT	**L**ong-**R**ange **U**ltrasonic **T**esting
MDCT	**M**odified **D**iscrete **C**osine **T**ransform
MMSE	**M**inimum **M**ean **S**quare **E**rror
MOS	**M**ean **O**pinion **S**core
NDE	**N**on-Destructive **E**valuation
NDT	**N**on-**D**estructive **T**esting
OD	**O**utside **D**iameter
PESQ	**P**erformance **E**valuation of **S**peech **Q**uality
PLC	**P**acket **L**oss **C**oncealment
PT	**P**olarity **T**hresholding
PTM	**P**olarity **T**hresholding with **M**inimisation

RMS	**R**oot **M**ean **S**quare
RTP	**R**eal-Time **T**ransport **P**rotocol
Rx	**R**eception
SH	**S**hear **H**orizontal
SHM	**S**tructural **H**ealth **M**onitoring
SNR	**S**ignal to **N**oise **R**atio
SSP	**S**plit-Spectrum **P**rocessing
ST-DFT	**S**hort-**T**ime **D**iscrete **F**ourier **T**ransform
STFT	**S**hort-**T**ime **F**ourier **T**ransform
STSA	**S**hort-**T**ime **S**pectral **A**mplitude
3D-LDV	**3D** - **L**aser **D**oppler **V**ibrometry
TCP	**T**ransmission **C**ontrols **P**rotocol
TFM	**T**ime-**F**requency **M**otion
TFR	**T**ime-**F**requency **R**epresentation
TWI	**T**he **W**elding **I**nstitute
Tx	**T**ransmission
UDP	**U**ser **D**atagram **P**rotocol
UGW	**U**ltrasonic **G**uided **W**aves
UT	**U**ltrasonic **T**esting
VOIP	**V**oice **O**ver **IP**
WT	**W**all **T**hickness

List of Symbols

A_l……..state transition matrix coefficient

B……..Total bandwidth for processing, Hz

B_{filt}……SSP filter bandwidth, Hz

c_j……..coefficients of an extrapolation polynomial

d……..Wave propagation distance, Metre

f_0……..Start frequency, Hz

f_1……..Final frequency, Hz

f……centre frequency , Hz

f_l……..lower cut-off frequency for SSP filter, Hz

f_h……higher cut-off frequency for SSP filter, Hz

f_{min}……lower cut off frequency for each sub-band, Hz

f_k……..frequency bandwidth of side lobe k, Hz

F……..SSP filter separation, Hz

F_s……..Sampling frequency, Sample/Second

$F(n,m)$……..Flexural wave mode

G…….. Gaussian function

G_c……Centre of Gaussian function

i……..Imaginary number

j……..Iterator

k……..*Wavenumber or spatial frequency*

k……*discrete-frequency index*

$\hat{k}_{SB}$……*frequency bandwidth for each sub-bands*

$\ddot{k}$……*lag position for audio*

L……*Window Length*

l……*Length of propagation, Metre*

$L(0,m)$……*Longituidinal wave mode*

m……*Discrete time index*

$\mathcal{M}$……*spectral motion vector*

M_{filt}…… *Number of samples in 3 dB bandwidth*

n……*Number of cycles*

N…… *number of SSP filters*

n_{sample}…… *Sampling index*

R……*Cross-correlation*

$s(t)$……*audio input stream*

SB……*number of sub-bands*

t……*Time, Second*

t_{ToA}……*Time of Arrival, Second*

T……*Sampling time, Second*

$\tilde{T}$……*Period of the signal, Second*

$T(0,m)$……..*Torsional wave mode*

T_s……..*Input sampling interval, Second*

T'_s……..*Output sampling interval, Second*

u……*Sample Signal*

u_t……..*vector containing any control inputs*

v_l…… *random driving variable*

v_{gr}……..*Group velocity, Metre/Second*

v_{ph}……..*Phase velocity, Metre/Second*

ω……..*Angular Velocity/Frequency, Radians/Second*

w……..*Window function*

w_t……..*vector containing noise*

W_s……..*Windowed sine wave*

w_n……..*Weighting factor*

x……..*Distance, Metre*

$x_i[m]$……..*sub-band signals*

X……..*Spectral vector across time and frequency*

X_{SB}……*Spectral motion-compensated extrapolation –interpolation*

y_{FM}…… ……*FM output signal*

y_{mean}…… *Mean output signal*

y_{min}……*Minimisation output signal*

y_{PT}……..*PT output signal*

y_{PTM}……..*PTM output signal*

τ……..*Rate converted time, Second*

$\tilde{\tau}$……..*STFT time, Second*

p_{δ}……..*new crossover point*

Δf……..*frequency resolution*

α_L……..*average gap length*

β_L……..*2-state model*

δ……..*filter crossover point*

γ……..*segment overlap*

λ……..*Wavelength, Metre*

Chapter 1

1 Introduction

1.1 Chapter overview

This introductory chapter provides a background to the content of the thesis. This includes the motivation for this research, the fundamentals of acoustic signal processing and some current applications. The general approach applied throughout this research is described here, followed by the contributions to knowledge alongside a list of submitted publications arising from this thesis. The structure of the thesis is also provided in order to help guide the reader through the document.

1.2 Motivation for Research

The field of signal processing has grown over recent decades with a large proportion of research dedicated to enhancing the quality of digital signals. The removal of noise and the estimation of lost segments within digital signals are two specific areas that are dedicated to improving signal quality. However, the implementation of each method is slightly different. Most methods are only capable of enhancing the signal in particular situations but do not perform well in other scenarios, and in some cases, failing to offer any improvement at all. Thus, more advanced signal processing techniques are required to enhance the quality of signals.

Numerous methods, employing hardware and/or specialist software designs, have been studied to enhance the quality of signals with the aim of understanding the behaviour of signals and to find a solution that helps improve signal quality in terms of noise, dropouts, lost packets, etc. Hardware designs are typically not cost-effective, whereas specialist software is usually more affordable, especially in commercial examples where conventional devices are already designed such as pipeline inspection tools. This work focuses on denoising techniques for acoustic applications and is described in the following subsections.

1.2.1 Motivation for Audio Signal Processing

Use of the Internet for the transmission and reception of music, wideband speech, broadcast audio, and podcasts is pervasive. Audio streaming facilities are increasingly accessible over the Internet. This involves coding short segments of a digital audio signal, packing them into small data packets, transmitting, and then decompressing into waveforms at the destination. Data packets can be lost, discarded or delayed during transmission for many reasons such as router congestion, the fading of signals, etc.

There are many approaches to mitigating the degradation in quality due to audio packet loss, which have been fully covered in the literature in Chapter 3. However, most of these methods do not specifically address the important issue of time-variation of the audio spectral parameters. A number of methods that may lend themselves to adaptation for time-varying of signals have not been fully investigated in terms of their capacity to provide an improvement in the reconstruction of a lost packet. Due to the challenges mentioned above, these methods are not suitable for wideband audio signals that contain a combination of inputs from several instruments with several fundamental frequencies and spectral envelopes. Hence, the aim of the audio part of the research is to develop an algorithm to reconstruct the packet loss in audio streaming to address these challenges.

1.2.2 Motivation for Ultrasound Signal Processing

A slightly different signal processing technique has been extended and applied to address another challenging problem in the Guided Wave Testing (GWT) industry, where shortcomings in inspections could result in:

i) Public health and safety issues arising from the catastrophic failure of plant

ii) Adversely affecting the surrounding environment

iii) Enormous financial costs for associated repairs

iv) Loss of production revenue

It is essential to find a robust inspection method for pipelines but in an economically viable way. GWT offers an efficient method of inspecting for corrosion and losses of pipe wall section, but the confidence in defect detectability needs to improve.

There are millions of miles of pipeline all around the world, carrying fluids such as oil, gas, water, etc. These structures are vulnerable to attack by internal and external damage

mechanisms such as corrosion or erosion. Leaks in pipelines carrying dangerous fluids such as petroleum pose health and safety risks to the public and if the leak or rupture is severe enough an environmental catastrophe could result, such as the Trans-Alaskan pipeline spill in the USA. Figure 1-1.a) illustrates the Trans-Alaskan pipeline itself, and Figure 1-1.b) shows the failure [1], which poses a huge risk to the environment[1].

In order to monitor the integrity of these structures periodic inspection and in some cases, where the damage mechanism is shown to be aggressive, real-time Structural Health Monitoring (SHM) can be employed. An inspection methodology such as this reduces the likelihood of failure by identifying damage or flaws before they reach a critical state.

a)

b)

Figure 1-1a) Trans-Alaskan pipeline, USA [2], b) Clean-up efforts after failure [3],

[1] Leakage of over 200,000 gallons of crude oil into clean water due to severe internal corrosion that made British Petroleum (BP) pay $12 million fine [1].

There are many techniques used for pipeline inspection including visual inspection, Phased Array Ultrasonic Testing [4], Radiographic Testing [5], etc. GWT using Ultrasonic Guided Waves (UGW) [6] is a relatively recent Non-Destructive Testing (NDT) technique that can cover up to 100m from a single test location. GWT applications and the limitations of this technique are discussed in Chapter 2.

Signal interpretation for GWT can be challenging due to the potential presence of multiple so-called wave modes and their dispersive effects. The wave mode purity of excitation and response of the structure directly affects the Signal-to-Noise Ratio (SNR) and spatial resolution (the ability to distinguish echoes from closely spaced reflectors). Hence, an advanced signal processing technique is required to improve the quality of the received GWT signal. The consequence of applying the proposed and optimised technique to GWT is an improved defect detection capability and therefore increased industrial confidence in the technology.

1.3 Acoustic Signal Processing

Signal processing appears in a wide range of digital and analogue systems, its main purpose is to identify the nature of signals; employing patterns, modelling, and structures to convert and improve the signal. Signals are usually incomplete, distorted and noisy. Therefore, reconstructing the signal of interest or reducing noise and removing distortion/interference in the signal are the main aims of signal processing.

In general, signal processing techniques can be employed for pre-processing and/or the post-processing of signals to facilitate interpretation over different domains such as time and/or frequency domains. Hence *time-frequency analysis*, which studies a signal in both time and frequency domains simultaneously, has become subject to increased attention.

The main purpose of time-frequency analysis is that phase and magnitude are represented on orthogonal planes when Fourier methods are applied (using complex representation) and that there is no feel for time-related information in the frequency domain, only phase and magnitude. A stationary signal does not have a frequency dependent parameter within it whereas a *non-stationary* signal has a variable contained within the function that varies with frequency. In practice, many signals are non-stationary, which means their frequency domain representation changes substantially over time. Therefore, the fundamental

aspects of signal processing, as well as time-frequency analysis, are briefly discussed in Chapter 3.

1.3.1 Audio Signal Processing

One of the main challenges regarding a reduction in the quality of audio signals in telecommunication systems is the presence of random frame losses. Packet loss in VoIP systems is a well-known scenario of this problem, where the signals suffer from effects of signal dropouts, background noise, and corruption during transference, etc. In order to play the audio signal continuously without any disruption at the receiver side, a technique is required to deal with the packet loss problem so that the end user remains unaware of the loss.

Many studies have been conducted to develop and enhance the quality of audio signals; these studies are covered in the literature review of thesis research, along with a discussion of the shortcomings of different packet loss recovery technique. In the first technical chapter, (Chapter 4) a novel solution is proposed to address this issue. The technique has been developed to enhance the quality of the audio signal where there are packet losses in a received signal. The aim of the solution described is to model and synthesise the signal and then to reconstruct the lost packet by employing a *time-frequency signal processing technique* for reconstruction of the missing part of the signal throughout the gap.

Therefore, a Packet Loss Concealment (PLC) method is developed with applications to VoIP. A novel contribution of this research is the introduction of the *Time-Frequency Motion (TFM) matrix* and its application to motion-compensated extrapolation and/or interpolation for audio signals. The proposed PLC algorithm utilises the TFM matrix representation of the audio signal where each frequency is tagged with a motion vector estimate. These investigations are described in Chapter 4, where the PLC model is developed, evaluated and discussed for reconstructing the audio signals.

The proposed algorithm is applied to synthesised and real audio signals that contain random frame loss or gaps, in order to reconstruct/estimate the missing frames and enhance the quality of audio signals that have been degraded by packet loss. Evaluation of the results demonstrates that the proposed algorithm substantially improves performance in comparison to alternative approaches. In addition, the results presented here are also published in two conference proceedings and one journal paper [7], [8].

Furthermore, while the proposed technique is developed to address the problem of packet loss in audio signals, attempts have been made to expand the proposed algorithm to be applicable to other signals, such as UGWs. References, therefore, have been given to the appropriate application, wherever necessary, and the results are applicable to any signal. Therefore, the application of the proposed algorithms developed throughout the first technical chapter is extended and modified to address another problem in a seemingly unrelated industry that suffers from a similar issue; corrosion detection using UGWs. A failure to identify problems during these types of inspection increases the risk of catastrophic failure of the asset under examination and could result in harm to the environment and to nearby residents.

1.3.2 Signal Processing for Ultrasonics

As mentioned in Section 1.2.2, a failure in a pipeline inspection could result in catastrophe. It is, therefore, crucial to implement a robust inspection method for pipelines that assesses the integrity of their structure and can provide a forewarning of failure. In this section, the focus is on a signal processing technique that could be utilised as the *post-processing technique* for a UGW response and improve the confidence in the pipeline inspection technique. This has been achieved by employing the modified version of time-frequency algorithms that were proposed and developed for audio signals in Section 1.3.

Pipelines in the petrochemical, oil and gas sectors are subject to damage mechanisms such as corrosion and cracking during their operational lifetime. These damage mechanisms are triggered by factors associated with the environments they operate within and the products they contain. In-service flaws that result from these damage mechanisms are the main cause of pipeline failure [1][9-10]. Therefore a reliable technique is required that can use to perform periodic, automated and rapid inspection for the analysis of the structural integrity of these structures to identify flaws before they become a problem.

As mentioned previously, one of the aims of ultrasonic part of this research is to develop a technique to enhance the capabilities and sensitivity of UGW inspection by the suppression of unwanted signals that form the coherent noise. A time-frequency signal processing technique called *Split Spectrum Processing (SSP)* is therefore proposed, examined and developed to enhance the SNR and spatial resolution of UGW responses. This is achieved by reducing the effect of dispersive wave modes (DWM), which is one of the main sources of the coherent noise, by utilising optimised SSP filter bank

parameters. The use of SSP is relatively new in the field of UGW testing; therefore, the main object of investigating SSP is to understand the factors that contribute to the sensitivity of filter bank parameters when applying the algorithm to UGW signals. The proposed method is compared synthetically and experimentally with conventional UGW inspection data; the results of this comparison show that the proposed method substantially improves the reliability and sensitivity of UGW testing. Furthermore, the results presented here are also published in two conference proceedings and two journal papers [11], [12].

1.4 Aim and Objectives

The overall aim of this research is to study and develop an advanced signal processing technique based on time-frequency analysis for acoustic applications. The main goal is therefore to enhance the quality of signals of interest by recovering and reconstructing missing frames or minimising unwanted segments of signals in a system response. The specific objectives of this research are listed as follow:

- To review the current state-of-the-art in signal processing for acoustic applications (audio and ultrasound).
- To develop a time-frequency signal processing technique to enhance the quality of signals (audio and UGW).
- To develop spectral motion models for audio spectral flow and apply this model to reconstruct the lost packets.
- To obtain transparent quality for low and medium packet loss for 5% to 20% in terms of Mean Opinion Score (MOS) and objective Performance Evaluation of Speech Quality (PESQ) at the receiver side.
- To develop a novel method that reduces the presence of dispersive wave modes in multimodal UGW signals.
- To propose pre-defined parameters for post-processing algorithms to maximise the efficiency of the UGW testing by increasing the sensitivity and inspection range.

1.5 Research Methods

Time-frequency signal processing algorithms are widely employed in many industrial fields such as sonic and ultrasonic applications for the analysis of a signal to facilitate

better signal interpretation. In most scenarios, signal interpretation is one of the most challenging parts of such analysis. Therefore, a signal processing technique based on time-frequency analysis is studied, and a model developed to reconstruct gaps created by lost packets, with applications to VoIP, audio broadcast, and streaming. The problem of modelling the *time-varying frequency spectrum* in the context of PLC is addressed, and a novel solution is proposed for tracking and using the temporal motion of spectral flow. The proposed PLC utilises a *TFM matrix* representation of the audio signal, where each frequency is tagged with a motion vector estimate. The spectral motion vectors are estimated by cross-correlating the movement of spectral energy within sub-bands across time frames. The missing packets are estimated in the TFM domain and inverse transformed to the time-domain to improve performance.

Of particular note is that the proposed technique operates on Short-Time discrete Fourier transform (ST-DFT) of audio signal utilising the TFM matrix. The performance of the TFM matrix for PLC is evaluated employing subjective and objective measurement, and their outcomes are discussed. To design such algorithms, numerous parameters are considered, including the statistical distribution assumptions of audio signals (e.g. music, speech, and noise). However, most of such algorithms are based on Independent identically distributed (IID) assumptions on successive frames of the signal. According to a statistical model of the signal, it is assumed that DFT values are independent of each other across both time and frequency. Furthermore, a statistical interpolator based on time-frequency interpolation is developed for this application.

In addition, a signal processing technique is developed based on time-frequency analysis for UGW. UGW testing is widely utilised for pipeline inspection to find defects/damages in the structure. However, the presence of coherent noise in the received signals is a significant challenge for pipeline inspection, which may limit the inspection range, as well as the sensitivity of inspection. This challenge is mainly due to the multi-modal, dispersive propagation nature of UGW, and mode conversions that contribute to the coherent noise. This results in degradation of the signals regarding SNR and spatial resolution. Therefore, a technique is required to reduce the level of coherent noise and enhance the quality of received signal. Hence, a technique is proposed for post-processing of the received UGW signal known as "*split-spectrum processing*" (SSP) for pipeline inspection.

This algorithm is similar to the one developed in the first technical chapter. It should be mentioned that the SSP technique has already been developed for conventional UT for

SNR enhancement; however, the use of SSP and its optimum parameters have not yet been applied in UGW testing. The extant literature identifies that the performance of SSP is highly sensitive to the selection of filter bank parameters. To the best of the author's knowledge, other than Mallet [13], no one else has investigated the use of SSP in UGW testing. However, Mallet's result indicates that he was not able to find the optimum parameter values of SSP for UGW testing, and his proposed parameters created some erroneous features for both synthesised and field data. Mallet stated regarding his work, the SSP with the parameters that he employed was not suitable to use in industry and future work was necessary to address the limitation of his approach. Therefore, an investigation is provided to clarify the sensitivity of SSP performance to the filter bank parameter values for UGWs such as processing bandwidth, filter bandwidth, filter separation, etc. to find the optimum values to enhance the SNR and spatial resolution of such signal.

In order to apply the proposed technique, information such as the centre frequency of the test, the number of cycles, and the group velocity of a wave mode of interest are required to be known. These data ease the detection process of features of the structure under investigation. The excitation signal employs multiple cycle Hann windowed sinusoidal pulse at a particular frequency range to excite a pure axisymmetric signal. However, some other wave modes are usually excited during excitation, which is dispersive and spread out in time and space that converts to coherent noise[2].

It is found that the proposed algorithms reduce the effect of DWM; thus, reducing the coherent noise in the received UGWs. It is also indicated that this algorithm is best suited for one-dimensional structures such as pipes, bars, rods, etc. The proposed method is synthetically and experimentally tested using a brute force search algorithm to evaluate the effectiveness of the proposed technique. The synthesised UGWs involve the modelling of an axisymmetric with its flexural wave modes' family to generate the UGWs. The results show that the proposed method significantly improves the SNR of received UGWs.

Moreover, two laboratory experiments are carried out in this research using two pipes in the laboratory with some defects. In the first experiment, the Teletest Focus+ system [14] is employed to transmit a signal (Tx), and a Polytec 3D Laser Doppler Vibrometer (3D-

[2] The problem of coherent noise in the UGWs testing is discussed in Chapter 2 and a novel solution developed for reduction of coherent noise is outlined in Chapter 5.

LDV) [15] scan is utilised to receive the signal (Rx) on a six-inch diameter pipe. The pipe included an axisymmetric defect of a 12.5% depth, which represented a loss in cross-section area (CSA) of 13.5%. The results show that the proposed technique substantially enhances the SNR and spatial resolution of the received UGWs. In the second experiment, the Teletest system [14] [16] is utilised for both transmitting and receiving the signal on an eight-inch diameter pipe. The experiment introduces a saw-cut, of increasing size between repeated tests, from 0.5% to 8% CSA.

It is shown that *SSP* in both cases has the potential to reduce the presence of coherent noise significantly and is able to identify the smaller size of defect down to 3% CSA where it is hidden below noise level for the unprocessed signals. Furthermore, the proposed algorithm is applied to a set of field data from pipelines in Alaska. These pipelines contain a number of known features that were used to assess our method. The SNR, as well as the spatial resolution of these data, is greatly improved. These signals are far more complex than the lab's data and as a result, contain a number of unidentified peaks in the processed signals. Some of these may correspond to unidentified peaks in the unprocessed signals, and some may be erroneous features introduced by the technique and requiring further investigation.

However, this research identifies that *SSP* has some limitations especially when two features are very close to each other, as shown in the synthesised signals where two features merge in the output of processed signal and present as a single feature. This leads to a loss of resolution. The limitations are identified, some of which are addressed in Chapter 6. Overall, the proposed technique shows promise regarding the use for UGW inspection and has great potential to enhance the SNR, sensitivity, and spatial resolution of UGW response. Hence, these enhancements can lead to the detection of smaller defects and an increase in inspection range. However, further development is required to address the current limitations of this algorithm, which is recognised by this work.

Moreover, the outcome of the research conducted in this thesis paves the way to enhance the quality of the audio signal by reconstructing the lost packets in audio applications and enhance the reliability and sensitivity of UGW inspections by removing the coherent noise and thus increasing the SNR and spatial resolution of the UGW response.

1.6 Thesis Outline

The organisation of the rest of this document is set out as follows:

Chapter 2 presents an overview of the background review of the acoustic application and the fundamental knowledge of signal processing techniques and related concepts, e.g. Fourier transforms, windowing, SSP, etc. followed by introducing the important theory of streaming audio signal to reconstruct audio packet loss. Then provides some of the main points of UGW theory includes the fundamental knowledge of ultrasonic applications, particularly the development of GWT for pipe inspection to help the reader to understand the concept of UGW testing as it is repeatedly referred throughout the thesis.

Chapter 3 covers the literature review of acoustic application for both sonic and ultrasonic guided wave signal includes the history of packet loss recovery techniques in particular receiver-based techniques followed by the literature review of SSP method that is introduced and developed for the use in NDT techniques to enhance SNR.

Chapter 4 provides the development of the time-frequency signal processing application in audio signals that are degraded by audio packet loss and discusses the different reconstruction methods includes the extrapolation and the interpolation techniques that utilised for estimating the missing frames.

Chapter 5 suggests a signal processing technique called split-spectrum processing (SSP) that is developed for UGW testing for reduction of the effect of dispersive wave modes in multimodal UGW signals. The optimisation of SSP parameters for some synthesised signals is investigated within this chapter.

An empirical investigation of the SSP technique followed by reusability study for the optimum filter bank parameters and validation with a defect detection trial in a real structure is studied in Chapter 6. The application of SSP to experimental data is discussed, evaluated and implemented in this chapter followed by field data analysis in order to validate the effectiveness of the proposed technique.

The conclusion of the research is discussed in Chapter 7, where the contributions to the knowledge are thoroughly reviewed in the wider context of the published literature before recommendations for future research work are presented.

1.7 Contributions to Knowledge

In addressing the objectives of this research, by employing a combination of signal synthesis, laboratory experiments, and field data to evaluate the proposed techniques, and to study the characteristics of the signals, signal processing methods based on time-frequency analysis are suggested and implemented, leading to two distinct contributions to knowledge. The detailed descriptions of the contributions are listed below.

Demonstration of a signal processing technique based on time-frequency analysis for enhancement of the quality of audio signals that are degraded by audio packet loss

The problem of the restoration of gaps in an audio signal is addressed, and a novel solution of packet loss concealment is presented for audio signals based on *Time-Frequency Motion (TFM) matrix* using a discrete Fourier transform (DFT) or discrete cosine transform (DCT) method. The novel aspect of this methodology is the introduction of TFM and its application to motion-compensated extrapolation/interpolation for audio. The spectral motion vectors are estimated by dividing the signal bandwidth into several sub-bands. The cross-correlation of the frequency bands across time frames are used for motion estimation. The objective and subjective evaluation experiment reveal that the proposed method compares well with the conventional methods, resulting in superior output quality in terms of PESQ and MOS scores.

Demonstration of a signal processing technique called SSP for UGWs in pipelines via experimentation

I. An advanced signal processing technique called *SSP* is investigated for the reduction of coherent noise in UGW testing due to the presence of unwanted, dispersive wave modes. The research into this application of *SSP* demonstrates that the performance of the technique is sensitive to the parameter values employed in its implementation. This research therefore investigates a parametric study of the filter bank parameter values to determine their influence on *SSP* performance for pipe inspection using UGWs. Parameters such as processing bandwidth, filter bandwidth, and filter separation with resultant estimated optimum values were investigated for pipeline

inspection. The results show that SSP with optimal filter bank parameters applied has the capability to significantly enhance the SNR and spatial resolution of an UGW response. To the best of the author's knowledge, these optimum parameters have not previously been recognised or identified in the field of UGW testing.

II. A range of SSP recombination algorithms are studied in this research, before being selected for synthesised and experimental data. *Polarity Thresholding (PT)* and *PT with Minimisation (PTM)* algorithms were found to be the best SSP method for recombining the signal. An SNR improvement of up to 38dB of received UGWs was observed. In addition, the SSP technique shows promise in improving the SNR and spatial resolution of focused UGWs up to 6dB when applying a Hybrid Active Focusing technique.

III. The limitations of each of the SSP algorithms are investigated in this research. The research identifies that if the distance of two features (e.g. defect and weld) is less than 0.4cm, the SSP algorithm combines the reflection of two features as a single feature and presents a single peak. The amplitude of this single peak is the value of the larger of the two original peaks this effect reduces the temporal resolution. A minimum distance of 0.5cm is found to be effective with the proposed technique. It should be mentioned that, this examination utilises an excitation frequency of 44kHz with 10-cycles. However, this result may vary slightly for different excitation frequencies and pulse widths. Therefore, the frequency optimisation study indicates that the distance limitation can be reduced up to 0.35cm by increasing the excitation frequency up to 70kHz.

IV. The defect sensitivity of the SSP algorithm is examined in this study. The results reveal that the SSP algorithm has the potential to identify defects down to 2% Cross-Sectional Area (CSA). In addition, SSP shows good potential to increase the inspection range from a single test location as it significantly reduces the level of coherent noise, enhancing the SNR, and improves the spatial resolution of UGW response.

1.8 List of Publications arising from this research

1. S. K. Pedram, L. Gan, W. Balachandran, " Spectral Extrapolation for Audio Packet Loss Concealment using Motion Compensation," Accepted on Speech Communication Journal Paper, March 2017.
2. S. K. Pedram, S. Fateri, L. Gan, A. Haig, and K. Thornicroft, "Split-Spectrum Processing Technique for SNR Enhancement of Ultrasonic Guided Wave," In Press, Corrected Proof on Special Issue of Ultrasonics on ‘‘Ultrasonic advances applied to materials science”, Feb 2017.
3. S. K. Pedram, “Split-Spectrum Processing Technique for High-Resolution Ultrasonic Guided Wave Response,” in 2nd National Structural Integrity Research Centre (NSIRC) Annual Conference, TWI Cambridge, United Kingdom, 27–28 June 2016.
4. S. K. Pedram, A. Haig, P. S. Lowe, K. Thornicroft, L. Gan, and P. Mudge, "Split-Spectrum Signal Processing for Reduction of the Effects of Dispersive Wave Modes in Long-Range Ultrasonic Testing," Physics Procedia, 70:388-392, 2015.
5. S. K. Pedram, “Reduction of Dispersive Wave Modes in Guided Wave Testing using Split-Spectrum Processing,” in 3rd Iranian International NDT (IRNDT) Conference, Olympic Hotel, Tehran, Iran, 21–22 February 2016.
6. S. K. Pedram, “Split-Spectrum Signal Processing for the Reduction of Dispersive Wave Modes in Guided Waves,” in 1st National Structural Integrity Research Centre (NSIRC) Annual Conference, TWI Cambridge, United Kingdom, 23 June 2015.
7. P. S. Lowe, R. Sanderson, S. K. Pedram, N. V. Boulgouris and P. Mudge, "Inspection of Pipelines using the First Longitudinal Guided Wave Mode," in *International Congress of Ultrasonic*, Metz, France, 2015.
8. S. K. Pedram, S. Vaseghi, B, Langari, "Audio Packet Loss Concealment using Spectral Motion," *Acoustics, Speech, and Signal Processing (ICASSP), 2014 IEEE International Conference on*, vol., no., pp. 6707,6710, 4–9 May 2014.

9. S. K. Pedram, “Audio Packet Loss Concealment using Spectral Motion,” in 7th Annual Student Research Conference, Brunel University London, United Kingdom, 23–26 June 2014.

10. S. K. Pedram, S. Vaseghi, B Langari, "Audio Packet Loss Concealment using Motion-compensated Spectral Extrapolation," *Signal Processing and Information Technology(ISSPIT), 2013 IEEE International Symposium on*, vol., no., pp. 434, 439, 12–15 December 2013.

11. B. Langari, S. Vaseghi, S. K. Pedram, "Multi-resolution Edge-guided Image Gap Restoration," *Signal Processing and Information Technology (ISSPIT), 2013 IEEE International Symposium on*, vol., no., pp. 374, 379, 12–15 December 2013.

Chapter 2

2 Fundamental Knowledge and Background Review

2.1 Chapter overview

This chapter introduces the theoretical background of acoustic applications includes the principles of acoustics, a fundamental knowledge of signal processing techniques such as Fourier transform, split spectrum processing (SSP) technique with its various recombination algorithms which is necessary for Chapters 5 and 6 are explored in this chapter. In addition, the fundamental knowledge of sound, streaming media/protocol, Kalman filter, etc. are discussed within this chapter to equip the reader with an understanding of the concept of time-frequency analysis for sonic signals that are employed in Chapter 4.

Furthermore the theoretical background of ultrasonic guided waves (UGWs), in particular, the development of GWT that has been achieved in recent years is explored, to help the reader to understand the concept of UGW testing. The explanation of different wave modes and the relationship between concepts such as phase and group velocities, dispersion curve and relevant concepts, an understanding of which is required in Chapters 5 and 6, is also covered in this chapter.

2.2 Principle of Acoustics

Acoustics is the interdisciplinary science of sound that deals with the study of mechanical waves, including sound wave production, transmission, detection and its effects. The scope of acoustics is not limited to those phenomena that can be heard by the normal human ear, but also contains all phenomena that are governed by the same physical principles. Hence, disturbances with low frequencies (infrasound) or high frequencies (ultrasound), which cannot be heard by the normal human ear, can also be considered within the sound wave category. In general, the sound is a periodic vibration that travels through any medium.

Many researches and studies in acoustic applications show that the transmission of sound is affected by, and consequently gives information concerning, the medium through which it passes. Isaac Newton's (1642–1727) [17] investigation of the mathematical theory of sound propagation included a mechanical interpretation of sound as being "pressure" pulses transmitted through neighbouring fluid particles. The mathematical analysis was limited to waves of constant frequency and was universally difficult to decipher. Newton theoretically calculated the speed of sound; however, he miscalculated by about 16% (lower than the accepted value today) because he assumed an isothermal (constant temperature) instead of an adiabatic (no heat exchange) process. Numerous researches have been done in the field of acoustic applications for sonic and ultrasonic sound propagations [17][18]. The fundamental knowledge regarding sonic and ultrasonic applications is discussed in greater detail in this chapter.

2.3 Signal Processing Techniques

Various signal processing techniques have been studied, and are employed in this thesis to facilitate the analysis and interpretation of signals. In this regard, the fundamentals of signal processing techniques as well as the time-frequency analysis employed throughout this thesis are explored below, which provides further details in respect of signal processing techniques that are required in the following chapters.

2.3.1 Fourier Transform

The Fourier transform, named after Joseph Fourier, is a mathematical transformation utilised to transform signals between time and frequency domains regarding the way in which signals can be viewed, analysed, and processed. In signal processing applications, frequency spectrum and bandwidth are the fundamental concepts that result from the Fourier representation of signals, which are widely applied for signal analysis. The Fourier transform is employed to analyse the spectral content (frequency components) of a signal by breaking the signal down into sine waves of different amplitudes and frequencies.

The Fourier transform, and its discrete implementations, such as the discrete Fourier transform (DFT), as well as Fourier-related transforms, such as discrete sine transform (DST), discrete cosine transform (DCT), and modified DCT (MDCT), employ a set of time-invariant fixed sinusoidal basis functions. For a segment of N samples, the DFT basis function is $\left[1, e^{-j\frac{2\pi k}{N}}, e^{-j\frac{4\pi k}{N}}, \cdots, e^{-j\frac{2\pi(N-1)k}{N}}\right]$ with a fixed complex sinusoidal kernel

of $e^{-j\frac{2\pi}{N}}$, a frequency resolution of $\Delta f = \frac{F_S}{N}$ and a time resolution of $\Delta T = NT_s$ where $F_s = \frac{1}{T_s}$ is the sampling frequency.

The main shortcoming of the Fourier transform is that its basis functions are time-invariant and consequently it is assumed that the input signal is non-stationary. While the short-time Fourier transform (i.e. essentially the DFT of a window of N samples of a signal) mitigates the problem, the DFT does not provide any explicit functional information on time-variations of the frequencies of the input signal.

There are a variety of time-varying transforms for non-stationary signals, such as the Gabor transform [19], the Wigner distribution function [20], and complex wavelets [21]. These transforms, in combination, provide a set of parameter differences: frequencies, window lengths (scales), window shape, and in the case of two-dimensional transforms, window orientations. However, while these transforms provide a set of time-frequency resolutions, they do not provide a systematic functional relationship on how the time-varying frequencies evolve over time.

Due to its relative simplicity and efficiency, the Fourier transform remains the most powerful spectral analysis technique widely used in consumer applications, such as for coding of audio, filtering, image and video signals, radar, spectral analysis, ultrasound, and in scientific research. Hence, augmenting the DFT and its variants with additional tags that will explicitly indicate the direction and magnitude of the movement of spectral energy across time frames will be of practical and theoretical interest. Fourier transform has been employed throughout this thesis as it facilitates the manipulation and interpretation of a signal and leads to the perception of frequency analysis and synthesis. The discrete implementation of the Fourier transform method is discussed in greater detail in the following section.

2.3.1.1 Discrete Fourier Transform (DFT)

DFT is a discrete implementation of the Fourier transform of a signal, which is obtained by sampling the discrete-time Fourier transform (DTFT) at N discrete frequencies by sample times T. The DTFT can be derived by numerical integration of the Fourier transform as shown in (2-1):

$$X(j\omega) = \sum_{-\infty}^{+\infty} \left(x(nT_s)e^{-j\omega nT_s}\right) \times T_s \tag{2-1}$$

When $x[n] = x(nT_s)$ and $\omega = 2\pi F_s/N$. Then, using the normalised frequency $\hat{\omega} = 2\pi F/F_s$, we have:

$$X(e^{j\,\hat{\omega}}) = \sum_{-\infty}^{+\infty} x[n]e^{-j\,\hat{\omega}n} \tag{2-2}$$

where the value of T_s has been neglected. The DFT is obtained from (2-1) and (2-2) as:

$$X(k) = \sum_{n=0}^{N-1} x[n]e^{-j\frac{2\pi}{N}kn} \tag{2-3}$$

This equation gives a complex number that describes the magnitude and phase of $x[n]$ at that frequency. Thus, the DFT generates the frequency domain components in discrete values or bins. Furthermore, the fast Fourier transform (FFT), which is presented by Cooley and Tukey [22] is an optimised implementation of DFT that takes less computation to perform. The FFT runs in $O(NlogN)$ whereas DFT runs in $O(N^2)$. Overall, the frequency domain representation of a signal may be of more help to understand and troubleshoot signals compared to the time domain signal. FFT by itself performs well and provides great insight of the signal; however, to improve the signal quality, a windowing function is also required in the processing procedure.

2.3.1.2 Short-Time Fourier Transform (STFT)

The spectral content of signals in the acoustic application is not stationary and changes over time, therefore applying DFT over a long window does not reveal transitions in spectral content. Hence, to solve this issue, the DFT is applied over a short period in such a way that the signal can be considered stationary.

Therefore, Short-Time Fourier Transform (STFT) [23] is developed, which is a Fourier-related transform that is employed to determine the sinusoidal phase and frequency element of sections of a signal that is not stationary. This is achieved by splitting a longer time signal into shorter segments of equal length and then computing the Fourier transform for each shorter segment individually. However, the drawback of STFT is that once the

size of the time window is selected, it must be the same for all frequencies, while sometimes it is required to have a more flexible approach.

The Fourier transform of the windowed signal waveform can be calculated as;

$$X(n,\omega) = \sum_{m=-\infty}^{+\infty} x[m]w[n-m]e^{-j\,\omega n} \tag{2-4}$$

where w is a window function and the sequence $x[m]w[n-m]$ is a short-time section of the signal $x[m]$ at time n. Hence, the discrete STFT is defined as:

$$X(n,k) = X(n,\omega)|_{\omega=\frac{2\pi}{N}k} \tag{2-5}$$

In addition, the spectrogram, which is a graphical display of the magnitude of the discrete STFT, is calculated as:

$$S(n,k) = \log|X(n,k)|^2 \tag{2-6}$$

This is a 2D plot of the relative energy content in frequency at different time locations. According to Cohen [23], there is a time-frequency trade-off that limits the resolution of time and frequency to the uncertain principle. Many researchers have performed investigations with the intention of balancing the uncertainty in Time-Frequency Representation (TFR) [such as [23][24]]. In UGW applications, this has been achieved by comparing TFR signals with the theoretical dispersion curves, which is fully covered in the literature.

2.3.2 Windowing

Windowing functions are usually utilised in signal processing applications to enhance the quality of signal from spectral leakage in the frequency domain that is caused by discontinuities in the signal. This is achieved by reducing the amplitude of the discontinuities at the boundaries of each finite sequence acquired by the digitizer. This involves multiplying the time record by a finite-length window with an amplitude that varies smoothly and gradually toward zero at the edges to meet the requirement of the endpoints of the waveform. Thus, it creates a continuous waveform without sharp transitions. In order to localise any signals in time, a windowing function $w\,[n,\tau\,]$ is defined, which tapers the signal at its ends to avoid unnatural discontinuities in the segment. Several different window types exist that could affect the spectral leakage of the

signal, which are usually selected as a trade-off between the width of its main lobe and attenuation of its side lobe. The main lobe is centred at each frequency element of the time-domain signal and the side lobes approach to zero.

The height of the side lobes shows the effect of windowing on frequencies around main lobes. The side lobe response of a strong sinusoidal signal may suppress the response of the main lobe of a nearby weak sinusoidal signal. Lower side lobes reduce leakage in the measured FFT but increase the bandwidth of the major lobe. The side lobe roll-off rate is the asymptotic decay rate of the side lobe peaks. Thus, the spectral leakage will be reduced by increasing the side lobe roll-off rate.

The Hann, Hamming, and Gaussian windows are among the most common windows widely employed in signal processing applications. These window functions provide a wide peak with low side lobes. The Hann window drops to zero at both ends. Therefore it eliminates discontinuity, whereas the Hamming window does not reach zero; thus, the signal after windowing contains some discontinuity at the edges, so it is good for cancelling the nearest side lobe but gives a poorer result for cancelling the others.

In addition, the Gaussian function extends to infinity. Thus it is required to be either truncated at the ends of the window or to be windowed itself with another zero-ended window. Therefore, these window functions are more suitable for noise measurement and enhanced frequency resolution compared to the other window functions.

Nuttal [25] described and compared the different window functions. The Hann window, developed by Cawley and Alleyne [26], and the Gaussian window function are utilised throughout this thesis in order to implement the research methodology for both sonic and ultrasonic applications. The Hann window function is a discrete window function, named after the Austrian meteorologist Julius Von Hann, which can be defined as:

$$\omega(t) = 0.5\ (\ 1 - \cos\left(\frac{2\pi t}{\acute{L} - 1}\right)),\qquad 0 \le t \le \acute{L} - 1 \tag{2-7}$$

Where t is time, $\acute{L}$ is the window length. The Hann windowed sine wave can be defined as follows:

$$W_s(t) = \sin(\omega t)(\ 0.5\ (\ 1 - \cos\left(\frac{2\pi t}{\acute{L} - 1}\right)),\qquad 0 \le t \le \acute{L} - 1 \tag{2-8}$$

Figure 2-1 illustrated a 50kHz continuous sine wave modulated by a 10-cycles sinusoidal tone burst and its windowed form (Hann window) in a) time and b) frequency domains. As shown in Figure 2-1 b) the window function helps to reduce the effect of spectral leakage created in the frequency spectrum due to the cut-off between the last sample and the repeated first sample which creates artefacts. Therefore, the window function could smooth out these discontinuities by reducing artefacts in the spectrum.

2.3.3 Cross-correlation

Cross-correlation (CC) is a signal processing technique that measures the similarity of two signals as a function of the lag position of one relative to the other. CC has the capability to compare the values of samples at one time to the value of the samples at another time [27]. The CC function of the sampled signal, $R(m)$ can be defined as:

$$R(m) = \sum_{n=0}^{N-1} x[n]y[n+m] \tag{2-9}$$

where $x[n]$ and $y[n]$ is a function of time, m is the lag position that could be negative, zero or positive and R is the cross correlation.

2.3.4 Sampling Rate

In general, continuous signals require to be sampled for transmission, processing, etc. to obtain a discrete signal such as conversion of a sound wave to a sequence of samples.

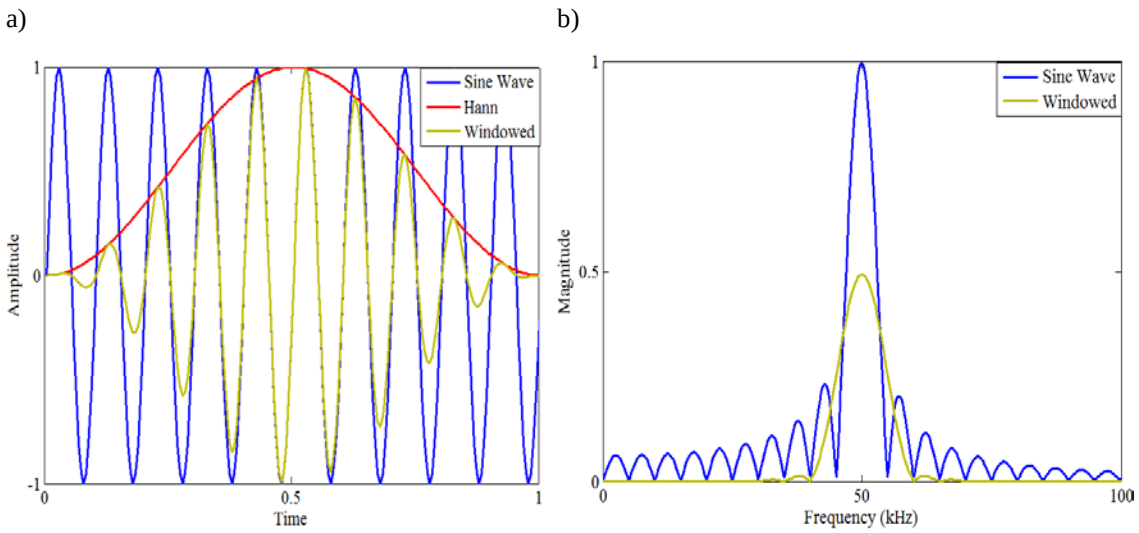

Figure 2-1: a) Time domain Hann window, sine wave and windowed, b) Frequency spectrum of the sine wave and its windowed form.

These samples present the values at a point in time/space. The sampling frequency (sampling rate), F_s is the average number of samples achieved in one second that could be calculated as follow:

$$F_s = 1/T_s \tag{2-10}$$

where T_s is the sampling period. In some cases, the sampled signal requires conversion to a new sampled signal at a different sampling period, $\hat{T}_s$ in order that the resulting signal corresponds to the same analog function. Therefore, the new sampling frequency $\hat{F}_s$ will be obtained as:

$$\hat{F}_s = 1/\hat{T}_s \tag{2-11}$$

The process of changing the sampling frequency, F_s of a discrete signal to obtain a new sampling frequency, $\hat{F}_s$ of a discrete signal from the same continuous signal is called sample rate conversion (SRC) [28], which is widely employed in different areas such as audio/visual systems, communication systems and radar systems [29]. The process of SRC is a linear time-varying system that is usually compulsory in audio/speech signal when converting a signal from one sampling rate (such as studio quality $192kHz$) to another sampling rate (such as CD quality $44.1kHz$).

2.3.5 Zero-Padding

Zero padding is widely utilised in signal processing applications and adds zeros to the end of a time-domain signal to increase its length. This allows longer FFT, which results in more frequency bins that are more closely spaced in frequency, making the spectrum look smoother when plotted without interpolation. In general, zero padding is utilised before a DFT/FFT as it is a computationally efficient method of interpolating many points.

The number of samples that structure each filter function depends on the DFT of a signal, which contains the same number of samples as the input signal. Thus, zero padding is usually added to the input signal to increase the resolution and improve the resolution of the filters (e.g. Gaussian). In GWT the number of samples (M_{filt}) within the 3dB bandwidth (B_{filt}) of a Gaussian filter could be obtained as:

$$M_{filt} = M\frac{B_{filt}}{F_s} \tag{2-12}$$

where F_s is the sampling frequency and M is the total number of samples of the original signal. Hence, to achieve a desired number of samples, $\widehat{M}_{filt}$, in the 3dB bandwidth of the Gaussian filter, it is required to zero pad the original signal to make sure that the input length is at least $\widehat{M}$ samples long. Hence, $\widehat{M}$ is calculated as follows:

$$\widehat{M} = \frac{\widehat{M}_{filt} f_s}{B_{filt} f_s} \tag{2-13}$$

However, if the input length by itself is sufficient $\left(M > \widehat{M}\right)$, then zero padding is not required. Zero padding is utilised in both sonic and ultrasonic applications, as proposed in Chapters 4 and 5.

2.3.6 Split-Spectrum Processing (SSP)

SSP is an advanced signal processing technique that was initially developed from the frequency agility techniques used in radar. This method was then considered for SNR enhancement in NDT application such as conventional UT to reduce grain scatter in the received signal. A significant amount of research has been undertaken over the last few decades in this area with respect to the reduction of non-random noise (coherent signals) in NDT applications due to ultrasonic scattering. These developments are fully described in the literature review of SSP in Chapter 3. The application of SSP in UGW testing is relatively new and, to the best of the author's knowledge, this technique has not been previously utilised in the field of UGW testing [except for Mallet thesis[3] [13]].

SSP application divides the spectrum of a received UGW signal in a frequency domain using a bank of bandpass filters in order to generate a set of sub-band signals at incremental centre frequencies. These sub-band signals are normalised and then subjected to a number of possible non-linear processing algorithms in the time domain to generate an output signal. The block diagram shown in Figure 2-2 describes the steps to implement the SSP application where the input time domain signal $x(t)$, is transformed into the frequency domain using the FFT and is then filtered by a bank of band-pass filters. Subsequently, the outputs from the filter banks , $X_k(f)$ $(k = 1,2, \dots, n)$, are converted back into the time domain using the inverse FFT (IFFT) and normalised by a weighting

[3] The review of Mallet thesis [13] is fully covered in the literature review of SSP in Chapter 3.

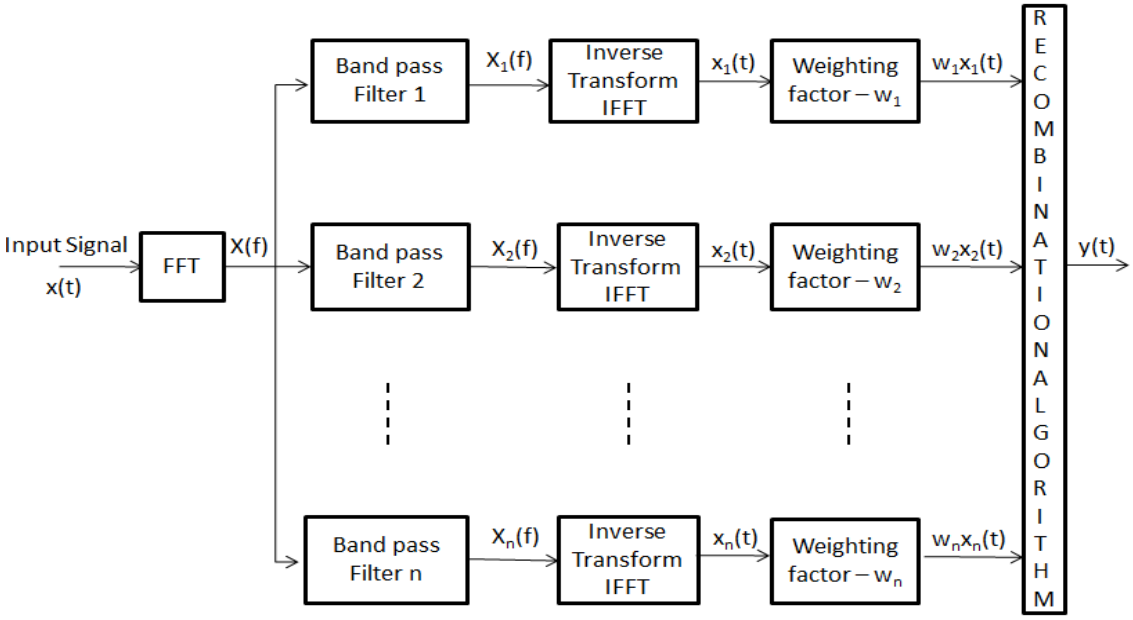

Figure 2-2: Block diagram of SSP

factor, w_k. These non-linear signals are combined using one of the SSP recombination algorithms, which are described in the following section, to generate the output signal, $y(t)$.

In general, SSP application shows potential to reduce those signal components that vary across a frequency range, and to suppress the regions of the signal of interest that are constant in that frequency range.

2.3.7 SSP Recombination Algorithms

Several SSP recombination algorithms exist that could be utilised for the reduction of coherent noise in NDT applications [30]. The five most common algorithms, which have been employed in this work for UGW testing, are described here in detail:

2.3.7.1 Polarity Thresholding (PT)

The PT algorithm is defined as;

$$\begin{aligned} y_{PT}[m] &= x[m] && \text{if all } x_i[m] > 0, && i = 1, \dots, n \\ y_{PT}[m] &= x[m] && \text{if all } x_i[m] < 0, && i = 1, \dots, n \\ y_{PT}[m] &= 0 && \text{Otherwise} \end{aligned} \tag{2-14}$$

where y_{PT} is the output result obtained after processing of the signal at m, $x[m]$ is the unprocessed (input) signal, n is the number of filter band signals and $x_i[m]$ are the sub-

band signals. This algorithm is somewhat similar in operation to the "sign detector" utilised in the past to detect signals. Hence, it looks at the signal sub-bands at each sample time, and if the samples are all positive or all negative then the signal is unchanged. Otherwise, the output is zero. This has the effect of only passing time samples where polarity is not affected by frequency. Therefore, those parts of the signal that are highly frequency-dependent should be removed. The amplitude of the signal of interest must be greater than the amplitude of the noise, as if the noise has larger amplitude it will be change the signal's sign.

2.3.7.2 PT with Minimisation (PTM)

This technique is the combination of the PT algorithm with minimisation (PTM) and the output of this algorithm, y_{PTM}, is the minimum amplitude of PT when there is no change in polarity, which is defined in (2-15);

$$\begin{aligned} y_{PTM}[m] &= min(xi[m]) && \text{if all } x_i[m] > 0, \quad i = 1, \dots, n \\ y_{PTM}[m] &= min(xi[m]) && \text{if all } x_i[m] < 0, \quad i = 1, \dots, n \\ y_{PTM}[m] &= 0 && \text{Otherwise} \end{aligned} \tag{2-15}$$

The aim of this method is to suppress noise further than is achieved by the PT algorithm, by taking the minimum points that PT has passed. Since the variance of the points containing noise is usually greater than those are containing the signal of interest, the use of minimisation reduces those that are the result of noise. However, this technique becomes less effective when the noise level is greater than the actual signal's amplitude, so reducing the noise level will significantly reduce the signal amplitude in certain sub-bands and gives minimum values for the PTM's output in that region.

2.3.7.3 Mean

The output of mean algorithm, y_{mean} is the summation of the mean of each sub-band sample at that sample time, as given in (2-16);

$$y_{mean}[m] = \frac{1}{N}\sum_{i=1}^{N} x_i[m] \tag{2-16}$$

where N is the number of sub-bands signals and x_i are the sub-band signals. Using the mean of sub-band samples as the output could reduce the noise as the value of noise

fluctuates between negative and positive values at each sub-band, as they are frequency-dependent. On the other hand, the value of the signal of interest should have a constant value across the sub-bands and remain unchanged for all sub-bands. As the noises are not constant, the amplitude of the signal across the sub-bands varies. This is the result of combination between signal and noise. However, this recombination algorithm is more suitable for signals with low noise level, and as the output is the mean of sub-band, thus the amplitude will decrease when the noise level is high. Thus, this method is not suitable for a noisy signal.

2.3.7.4 Minimisation

The output of each sample for this algorithm is simply the minimum magnitude of amplitude of each sub-band sample as given in (2-17);

$$y_{min}[m] = min(|x_1[m]|, \dots, |x_n[m]|) \tag{2-17}$$

This algorithm, similar to the mean algorithm, will reduce noise as the noise level varies across each sub-band. It is expected that the variation of the noise will be greater than the signal variance so that it will reduce the noise. This method will be effective only in cases where the level of noise is considerably lower than the signal. Therefore, it is only useful when the amplitude of the signals of interest is significantly higher than the noise level.

2.3.7.5 Frequency Multiplication (FM)

The outputs of each sub-band signal are multiplied by each other in this algorithm to generate the FM output signal, $y_{FM}[m]$, as given in (2-18);

$$y_{FM}[m] = x_1[m] \times x_2[m] \times \dots \times x_n[m] \tag{2-18}$$

This algorithm is relatively similar to the algorithms called Geometric Mean algorithm without applying the square root operation to the sub-bands' outputs. Therefore, the output of this algorithm compared to the square root of the product is capable of enhancing the amplitudes of larger signals but has a greater distortion level. It is less complex and uses fewer bands. However, this algorithm is not suitable for highly dispersive materials and only works for low dispersive material.

2.4 Sonic Applications

Most of our daily experience with acoustics applications is related to sonic signals for communication or pleasure, such as audio, speech, music, etc. In this work, the aim is to develop a technique to enhance the quality of modern telecommunication systems where such signals suffer from the effects of signal dropouts, background noise, and corruption during transference, etc.

One of the main challenges in telecommunication systems that result in a reduction of the quality of signals is the presence of random frame losses in the received signal. Packet-switching techniques are widely employed to deliver the audio signal in VoIP networks to maximise the network efficiency. This means that the audio signals are divided into small data packets, each of which is then sent independently over the network. Hence, the packets can travel by different routes to reach a destination and may suffer differing amounts of delay to arrive. Some packets may never reach their endpoint because of reasons such as congestion at the routers, overloaded server's buffer, and link failure. It is clear that a late arriving packet is as good as one that has never arrived, as the audio signal needs to be played continuously at the receiver side. Therefore, a technique is required to deal with the packet loss problem such that the end-user does not perceive the loss.

2.4.1 Bandwidths of Voice and Music

Normal hearing is usually in the range from 10Hz to 20kHz, although some individuals may have an ability to hear a wider range of frequencies. In general, sounds below 10Hz and above 20kHz are called infrasound and ultrasound respectively. The sound information of speech is mostly in the traditional telephony bandwidth of 300Hz to 3.5kHz. Sound energy with a frequency beyond 3.5kHz is mainly utilised for high-quality applications such as music. A singing voice requires a wider bandwidth than speech as it has a wider dynamic range, and usually contains energy in the frequencies well above that of ordinary speech. The bandwidth range for music is between 10Hz and 20kHz. A regular CD is sampled at 44.1kHz or 48kHz and is quantised with the equivalent of 16bits to 24bits of uniform quantisation, which gives a SNR of about 100dB at which point the quantisation noise is inaudible and the signal is transparent [31]. A sound wave's wavelength λ depends on its propagation speed c and the frequency of vibration f and can be calculated as below:

$$\lambda = \frac{c}{f} \tag{2-19}$$

2.4.2 Streaming Media

Streaming media is a term used to describe multimedia (audio, video, text, and data) that is delivered, or streamed, constantly by a provider to an end-user client to provide the opportunity to play the data in real-time without the need to download or transmit the entire file. Audio streaming is one of the fast-growing technologies and is increasingly accessible all around the world via the Internet, which has become the global broadcasting and distribution standard. The technical simplicity of using one global technology to communicate, along with its convenience, worldwide access, and especially its low cost, makes web broadcasting irresistible to media distributors and consumers. This involves coding short segments of a digital audio signal, packing them into small data packets, transmitting, and then decompressing into waveforms at the destination [32].

Hence, as the data arrives, it is buffered for a few seconds at the destination before the audio starts to play; meanwhile, more data is constantly streaming (arriving), which allows the user to hear constant audio. Thus, the data should always be available in the buffer to achieve constant audio; however, due to congestion on the Internet, the buffer may sometimes be empty, which causes a delay in receiving data.

2.4.3 Streaming Protocol

Real-Time Transport Protocol (RTP) and Real-Time Streaming Protocol (RTSP) are widely employed for delivering streamed media over IP networks by using either User Datagram Protocol (UDP), Transmission Controls Protocol (TCP), or IP multicast transmission channels. However, most applications are developed to use UDP as it supports the timely delivery of information, which is highly important for real-time delivery, whereas TCP favours reliability over timeliness [33].

UDP compresses audio files into extremely small data packets for transmitting data over the Internet and is a connectionless transport layer protocol that does not require any previous setup to communicate between the hosts. Hence, data packets can choose different directions to transfer; this simplicity provides an unreliable message delivery and, unlike TCP, adds no flow control, reliability, or error-recovery functions to IP. In addition, UDP streams continuously, which means if a packet is delayed or lost during transmission, the server preserves the sending data and only a small gap occurs rather than

a huge gap of silence, whereas in TCP transmission, the server tries to resend the lost packet before delivering the next packet, that makes for greater delays with larger gaps.

To summarise, UDP does not guarantee a reliable data stream service or retransmission service. Therefore, data packets can be lost, discarded or delayed for the following reasons: (a) router congestion; (b) excessive delays that may be caused due to routeing and congestion at a number of nodes; (c) network outages; or (d) fading of radio signals [32]. The audio packets usually correspond to 20-30msec of audio, hence a gap that is created by just a single frame loss is relatively wide (around 882-1,323 samples at 44.1kHz sampling rate), hence restoring gaps is usually difficult, especially if there is no access to the sender side and the only solution is to estimate the missing frames [32]. Each lost packet creates a gap in the streamed audio and must be concealed and replaced somehow to prevent an annoying disturbance to the end-user. Reconstructing the gap to approximate the original waveform is the common methods used to replace the missing packet.

Bolot et al. [34] investigated some fundamental characteristics of audio streaming over the Internet by measuring the audio loss process for each connection utilising UDP. They found that when the network load is low/moderate then the number of consecutively lost audio packets and the length of the gaps, are small. Bolot [35] studied the loss rates in such cases as a function of the network load (δ), where δ indicates the constant interval between the sending times of two successive UDP packets. The results indicate that the packet losses are accidental, especially when the traffic employs less than 10% of the available capacity of the connection to send the packets. However, losses become more correlated at higher rates; also, the buffer will experience overflows and lead to dropping more packets. Bolot showed that packet loss occurred in most scenarios. However, when the network load is low, the loss rate is low (typically less than 10%); conversely, when the network load is high, the gaps are wider and more frequent, which leads to connection drop-out with poor quality service. Therefore, it is clear that the majority of users are confronted with some packet losses when using media streaming. Thus, finding a solution to replace lost packets is essential.

2.4.4 Packet Loss Concealment Domains

Many domains could be utilised for packet loss concealment (PLC) such as time-domain, frequency-domain, compressed domain, spectral domain, linear prediction coding (LPC) methods, and etc., which are utilised for audio coding to reconstruct waveform samples.

Traditionally, LPC was employed for time-domain speech coder, but it has more recently been applied to the frequency-domain coders and achieved promising results in terms of audio and speech coding standards such as that used in audio coding and MPEG-D unified speech to enhance voice services and coding efficiency [36].

As an example, the audio signal in MPEG-audio coders such as MP3 is compressed in the MDCT domain. An advantage of this is a single packet loss in the MDCT domain is translated to a gap of only two coefficients per frequency bin. Hence, it is easier to interpolate the missing packets in this domain compared to the time domain [37], which suggests reconstructing the missing MDCT coefficients separately for each frequency bin based on the available coefficients from neighbouring packets at the same frequency.

One of the main issues of working in the MDCT domain rather than the time domain is the window type employed in the MPEG-audio coders during transforming in the MDCT domain. Window type is directly related to the packets, which means that if a packet is lost, its window type and the information about it is lost too. Also, choosing the wrong window type reduces the quality of construction as it will not eliminate the aliasing. However, there is a possibility to recover and estimate the window types of the lost packets by checking the window types of the packets that surrounded the missing segment.

The second issue that can occur in the MDCT domain is the use of different window types with different frequency resolutions: the MDCT coefficients sometimes represent different resolutions at a certain frequency bin even for two consecutive segments. Therefore, it is not an accurate estimation to reconstruct the coefficient of a missing segment from another coefficient that represented a different resolution of the frequency band. To solve this problem, the MDCT coefficient should be converted back to the time domain, and then the same window length applied for all segments to convert them once more to the frequency domain. Another limitation of the MDCT domain that makes it difficult to use is the rapid sign changes of MDCT coefficients from frame to frame, at each frequency bin, which reflect phase changes in the complex spectral domain [38]. Therefore, in order to reduce the fluctuating representation of the audio signal, it is necessary to employ another domain that could cover these limitations and provide better results. An alternative domain that could function as the concealment domain to overcome those limitations is the DSTFT domain.

In the last few decades, a variety of approaches has been developed to enhance audio signals; these approaches are mainly based on the restoration of the short-time spectral amplitude (STSA) of the audio signal. In most cases, a short-time phase distortion is assumed that has negligible effects on the perceptual quality of audio signals [39][40]. There are many researches [41]-[43] that estimate the STSA of speech by utilising a spectral subtraction algorithm that estimates the average noise spectrum by subtracting it from the noisy signal. The spectral subtraction's disadvantage is the 'musical noise' artefact that is like an annoying narrowband with short-life bursts of noise in the restored signal [44][45].

In order to solve the problem of STSA estimation, a method based on Bayesian interference algorithms is investigated that employ a priori probability knowledge of distributions for a short time discrete Fourier transform (ST-DFT) of the signal [45]. Estimation of the ST-DFT parts of the signal is another way of enhancing the audio signal. Although the first approach is more suitable in general, estimating the ST-DFT has the potential to be used for more statistical models. Martin [46][47] utilised Laplacian and Gamma distributions to develop the ST-DFT approach of the speech signal. He derived the corresponding closed form of estimators for modelling the imaginary and real part of the ST-DFT of the signal, whereas Chen and Loizou [48][49] proposed a numerical integration and discovered that a closed form solution obtained with Laplacian prediction was impractical for an STSA estimator. They suggested a numerical integration algorithm instead, which was not suitable for many real-time applications, as it requires a high power computational device with a lot of memory, which in many cases is not affordable.

The Wiener filter method [46] is one of the optimum solutions for finding ST-DFT components utilising Gaussian priors. Ephraim and Malah [50] proposed technique, utilising a derived minimum mean square error (MMSE) STSA estimator based on the assumption of Gaussian distribution for the imaginary and real part of the ST-DFT of speech. They assume that ST-DFT components are statistically independent and, based on this assumption, they demonstrate that the amplitude of the DFT has a Rayleigh distribution and its phase is uniformly distributed. Hence, they state that the amplitude and the phase of the signal cannot be optimally predicted simultaneously. On the other hand, there are some methods that were introduced for tracking the temporal variation of SNR and observe that STSA typically follows successive speech frames [43][45][51][52].

It is notable that the successive short-time frames of the audio/speech spectrum in signal processing approach are usually assumed to be independent and identically distributed (IID) across both frequency and time. However, according to Cohen [51], there is an apparent contradiction about this idea. These techniques use the IID assumption as well as the assumption of the dependency of successive frames for the estimation and smoothing of the main audio/speech parameters, such as a priori SNR spectrum[46], [47], [50], [53]. Cohen [54] has obtained more robust speech enhancement by utilising the correlation between successive samples of the short-time speech spectrum. Therefore, the main challenge of audio enhancement to improve the performance of signals could be overcome by utilising a realistic model of the temporal trajectory of the audio spectrum.
In general, audio signals have a slow varying nature; therefore, it could be argued from a signal processing point of view that the overlap between successive frames of such signals, which is usually considered in the short-time frequency analysis, is another way to achieve correlation between successive frames. Essi [55], [56] proposed an autoregressive (AR) technique to model the temporal correlation of the ST-DFT components of speech utilising the framework of Kalman filters for optimal prediction of speech in the presence of noise. He assumed that both speech and noise ST-DFT components had Gaussian distributions; he then extended the algorithm to incorporate the AR techniques of the ST-DFT trajectories of noise signal in the Kalman filter framework and obtained a good result.

2.4.5 Review of Audio Flow

A major obstacle in audio processing applications is the requirement for an appropriate algorithm that smoothly reconstructs the gap between two sounds. For example, the spectral mismatch at concatenation join points must be reduced for speech synthesis, reconstruction between two decoded spectra is required in speech compression, and interpolation between different people's phonemes for adaptation purposes is required for speech recognition [57].

Measuring the motion of two smoothed envelopes in audio flow is inspired by the idea of optical flow from computer vision applications, as proposed by Horn and Schunck [58], which measures the motion of objects between two images. The easiest way to interpolate two envelopes is to linearly cross-fade between them [59], or to linearly cross-fade alternative representations of the envelopes such as line spectral frequencies [60]. However, neither method is acceptable for shifting between two sounds [61], [62]. A

nearest neighbour correspondence estimation technique is employed in sinusoidal methods that track partials across a spectrogram [63]. However, it is difficult to track partials due to their noisy nature, plus partial movement is affected by pitch/formant changes. Goncharoff and Kaine-Krolak [64] proposed the pole-shifting method, which attempts to establish a correspondence between poles in the linear predictive coding (LPC) representation of the envelopes. The relationship between formants and poles was not one-to-one; therefore, pole matching was difficult to achieve. Pfitzinger [62] proposed a dynamic frequency warping (DFW) method where a morphing algorithm is employed to generate the intermediate envelopes as well as using DFW to establish correspondence non-parametrically between two LPC envelopes. However, the DFW method was direct with no access to any data, which is not acceptable for long losses.

Ezzat [57] proposed several techniques whereby each one improves further the computation of the audio flow[4]. He employed *Audio flow* technique to estimate the correspondence between envelopes to ensure that the warping process preserves the desired alignment between the geometric attributes of the objects during the morphing. Ezzat focused on interpolating smoothed spectral magnitude envelopes and defined how spectral energy at each frequency bin moved between two envelopes [65]. He then proposed a morphing algorithm that morphs smoothly between any two spectral magnitude envelopes of speech. This technique captures the formant resonances of the vocal tract and interpolates formant shapes, locations and amplitudes between the two envelopes. In addition, an inverse audio flow between envelopes is calculated by utilising cross-dissolving or blending the warped intermediates. This method performs better than the DFW method [62] as it is data-driven, and can extract natural flow estimation in most cases. However, the formant trajectories follow the linear paths (even for bandwidths). Hence, it is not suitable and accurate enough for a nonlinear trajectory, as the change of bandwidths during the sound transition is nonlinear. In addition, in terms of algorithm performance, the audio flow is only tested for a 20-second corpus of audio. If the corpus' size is smaller than this value, there will not be enough data to generate smooth paths through the graph, and even for a 20-second corpus, which is sufficiently large, this technique sometimes produces incorrect results.

[4] Audio flow defines the movement of spectral energy at each frequency bin between two envelopes to check the formant shifting that occurs from one sound to another [57].

2.4.6 Kalman Filter

Rudolf Kalman developed the Kalman filter, which is an efficient recursive filter that predicts the state of a dynamic system from a series of incomplete, noisy signals [66], [67]. It can produce an estimation of unknown variables more precisely compared to other methods that are based on a single measurement, such as Bayesian inference. Therefore, it has been widely utilised during the last few decades in different technology fields, such as tracking algorithms (e.g. visual tracking [68]), speech enhancement (e.g. noisy signal [69], [70]) and noise reduction applications (e.g. white Gaussian noise [71]).

The main advantage of the Kalman filter compared to other filters such as the Wiener filter is the dependencies of successive predictions, which are explicitly modelled in the Kalman filter. In addition, the Kalman filter employs the former values of the received signal for estimation of the signal. The Kalman filter application is widely utilised for speech enhancement and focuses on the time-domain processing of the speech signal. Hence, it gains was calculated and applied to reconstruct the speech signal or remove the effect of any unwanted signal (e.g., noise) to improve the signal's quality. The basic Kalman filter can be calculated as follows:

$$x_t = F_t x_{t-1} + B_t u_t + w_t \tag{2-20}$$

where x_t is the state vector containing the terms of interest for the system at time t, F_t is the state transition model that is applied to the previous state x_{t-1}, u_t is the vector containing any control inputs, B_t is the control-input model that is applied to the control vector u_t and finally w_t is the vector containing the process noise terms for each parameter in the state vector. Yan and Zavarehei [56], investigated the use of the Kalman filter for inter-frame correlations of the speech spectrum based on the DFT trajectories of noisy speech. They also considered the Kalman filter's application in the frequency domain, which has a very different implication to that of time domain. The Kalman filter algorithm is utilised in the proposed method, developed in Chapter 4.

2.5 Ultrasonic Applications

As mentioned in Section 2.4.1, frequencies above 20kHz that are beyond the limit of hearing are called ultrasonic waves. The main features of ultrasonic waves are: i) they are highly energetic; ii) the speed of propagation depends upon their frequencies; iii) they can

be transmitted over a long distance without any appreciable loss of energy. Ultrasonic waves are widely utilised in many applications, such as: ultrasonic flaw detection, ultrasonic guided wave, applications in medicine, welding, cutting and matching of hard materials, communication, etc.

A wave mode is a way in which sound energy propagates through the structure, which can be defined by its displacement characteristics (shape of the mode) at a particular frequency. Since the geometries and materials can vary, different wave modes can be generated at different frequencies. Wave modes can be plastic, anisotropic, etc.; however only elastic wave modes are considered in this work.

2.5.1 Propagation of Elastic Waves

The fundamental theory of wave propagation within an elastic solid is discussed in many papers, such as [125]-[127]. In this work, a brief explanation of elastic waves propagating in an elastic medium is given. The characteristics of wave propagation depend on the boundary conditions of an elastic medium such as its density and geometry. A differential equation of motion is defined by Navier, which can be applied for these propagation conditions for an isotropic elastic unbounded media, as given in (2-21):

$$(\lambda + \mu)\nabla\nabla.u + \mu\nabla^2 u = \rho\left(\frac{\partial^2 u}{\partial t^2}\right) \tag{2-21}$$

where u is a three dimentional vector, μ and λ are two constant materials (Lam*é*), ρ is the material density and ∇ is a three dimentional differential operator. The full details of this can be found in [75], [76]. Equation (2-21) is capable of calculating the motion of elastic wave propagation within the material. This is a linear equation; it is not able to integrate without using the Helmholt decomposition as follows:

$$u = \nabla\emptyset + \nabla \times \Phi \tag{2-22}$$

where $\emptyset$ is a summed scalar potential, (compressional), Φ is the vector filed and $\nabla . \Phi = 0$. By combining equations (2-21) and (2-22), the two unknown parameters can be calculated using two separate equations that govern longitudinal and shear waves respectively, as given in equations (2-23) and (2-24):

$$\left(\frac{\partial^2 \emptyset}{\partial t^2}\right) = c_l^2 \nabla^2 \emptyset \tag{2-23}$$

$$\left(\frac{\partial^2 \Phi}{\partial t^2}\right) = c_s^2 \nabla^2 \Phi \tag{2-24}$$

where c_l and c_s are the longitudinal and shear wave velocities in the infinite isotropic medium, which are given as follows:

$$c_l = \sqrt{\frac{\lambda + 2\mu}{\rho}} \tag{2-25}$$

$$c_s = \sqrt{\frac{\mu}{\rho}} \tag{2-26}$$

These are the only waves that can propagate in an unbounded isotropic medium, which is independent of each other. Wave propagation can vary in character depending on the restrictions imposed by an elastic medium. A guided wave is only applicable when there is a physical boundary within the medium, similar to the bulk waves (longitudinal waves and shear waves) when applied to wave propagation in an infinite media. Surface waves can propagate in a three-dimensional medium along a bounding surface of a medium, such as Rayleigh waves and Love waves.

The propagation of bulk waves and surface waves is used to describe the seismic wave phenomena that travel through the Earth's surface layer. Lamb waves are generated by the interaction of longitudinal and shear waves in a bounded elastic medium where there are two equidistant surfaces. Some of these wave modes are briefly described here.

2.5.2 Longitudinal Waves

Longitudinal waves are also known as compression or pressure waves. These waves are characterised by alternating particle motion (i.e. stretching and compression). The vibration displacements of longitudinal waves are exclusively oriented in the same direction as the direction of travel of the wave mode, and the velocity of compression waves, c_l, is given in equation (2-25).

2.5.3 Shear Waves

Shear waves are also referred as transverse waves as their vibration displacements are aligned perpendicularly to the direction of propagation. This means that it is shearing the

material transversely. This vibration displacement can occur vertically (shear vertical wave, SV) or horizontally (shear horizontal wave, SH), as displayed in Figure 2-3.

The velocity of these waves, c_s, is given in equation (2-26). It is notable that shear stress does not work for materials with fluids inside them, thus shear waves do not propagate through them.

2.5.4 Surface Waves

Surface waves (e.g. Rayleigh and Love waves) are another type of wave modes that propagate in a three-dimensional medium along a bounding surface of a medium, such as earthquakes [77]. These waves are widely studied in many fields, i.e. NDT, electronics and geophysics, which are characterised by vibration displacement of an elliptical manner. Rayleigh waves are usually utilised in NDT to inspect surface flaws and can be produced by employing electro-magnetic acoustic transducers (EMATs) or wedge probes. The amplitude of these waves decays exponentially with depth, starting from the wave crest.

2.6 Guided Waves

The term ‘guided waves’ is utilised when there is a free boundary restricting an elastic body that guides and drives waves, which means two boundaries are present in the structures, unlike surface waves, which exist when there is only one boundary between two mediums. Since the particle oscillations are guided during displacement, these waves can be said to form a ‘wave guide’. UGWs have been broadly employed in several NDT applications over recent decades, in applications where structural integrity is of concern. Longitudinal and transverse wave modes are the only wave modes that occur in an infinite medium. However, many other type of ‘guided waves’ exists for a medium with multiple boundaries. In addition, there will be an infinite number of wave modes depending on the geometry of a specimen that could be propagated with a much more complex velocity,

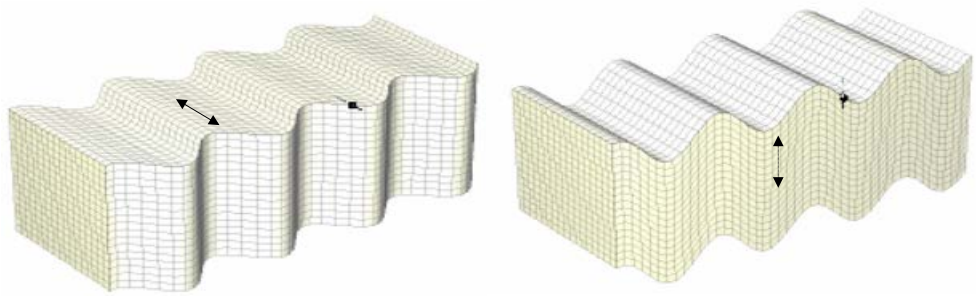

Figure 2-3: Distribution of displacements for the vertical shear wave (left) and the horizontal shear wave (right) [78].

where velocity is a function of material properties as well as the geometry itself. Therefore, the shape of the wave modes can be changed according to geometry structure and wavelength. This means that some wave modes are *frequency dependent*, where the same wave mode at a different frequency/different wavelength is capable of propagating with a different velocity and different mode shape. The frequency dependent behaviour of wave modes, which is known as "*dispersion"*, will be explained in more detail in Section 2.6.6.

2.6.1 Lamb waves

Horace Lamb developed the theory of the propagation of Lamb waves in 1917 [79], but he was not able to generate the waves that he discovered. These waves were physically generated by Worlton [80], who also discovered the potential use of Lamb waves for damage detection.

Lamb discovered that there are an infinite number of modes of propagation in an infinite media that are bounded by two surfaces such as plates. These waves arise because of the superposition of multiple reactions of shear and longitudinal waves from the bounding surfaces, which are often complex in terms of particle motions in the structure. The displacement form of Lamb waves can be classified according to the distribution of the displacements in the structure; as shown in

Figure 2-4, Lamb waves can be classified as 'Symmetric' ($S0$) and 'Anti-symmetric' ($A0$) in a plate structure[5].

2.6.2 Guided Wave in Hollow Cylinders

A cylindrical specimen such as pipe, rod, etc. can be considered as a plate where it has been shaped into a cylinder by joining along an axial part. The axial cross-section of the specimen wall will support Lamb waves that propagate along the length of the specimen, and since there are circumferences that lead to an additional boundary condition, other

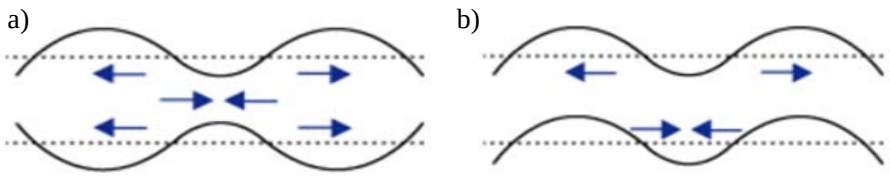

Figure 2-4: Distribution of displacements pattern of a) Symmetric (S0) or b) Anti-symmetric (A0) Lamb waves [81]

[5] The nomenclature of symmetric and anti-symmetric waves will be increased by n for higher order mode, so for the symmetric modes is $S0, S1, \dots, Sn$ and for the anti-symmetric modes is $A0, A1, \dots, An$.

wave modes can be generated. The UGW propagation in cylinders is investigated, analysed and explained in detail in many works [82]-[85]. In general, cylindrical wave modes can be categorised into three main families, based upon their particle movement:

- Torsional wave modes that are similar to the Shear horizontal (SH) plate modes where T(0,1) is the fundamental member of this family. Note that except T(0,1), all the other waves modes in this family are dispersive.
- Longitudinal wave modes that have the similar particle movement to the Lamb waves in plates where the L(0,1) and L(0,2) wave modes are equivalent to A0 and S0 respectively. These wave modes in the frequency that is utilised in GWT are dispersive.
- Flexural wave modes are attributed to those presenting a particle movement pattern around the circumference that incorporates a harmonic oscillation that is distributed. These wave modes can be categorised into two groups, which are attached to either the torsional or the longitudinal family, where F(1,1) and F(1,2), and F(2,1) are the fundamental flexural waves in these types of structures.

It should be mentioned that the relationship between the thickness of the specimen and the wavelength of a guided wave mode is considered in terms of wave propagation through the specimen. This is usually expressed as a function of the product of the frequency and thickness, $f.d$ in $H_z.m$. In addition, the fundamental wave modes are the modes that exist from $f.d = 0\ H_z.m$ upward. Other wave modes, referred to as higher order wave modes, require a minimum $f.d$ to exist. Thus, a cut-off frequency has been introduced to present the frequencies where each wave mode comes into existence. This means that below that frequency, the specimen will not support the particular wave mode with that particular thickness. Therefore, additional modes will come into existence by increasing the frequency. These higher-order modes contain a more complex displacement pattern compared to the fundamental wave modes. As a result, in order to reduce the level of coherent noise that is mainly produced by the higher- order modes, it is beneficial to work towards fewer wave modes, to receive the test data with higher quality.

2.6.3 Propagation of UGW

The nature of sound has been explored over recent decades by many researches, including those by Helmholtz [86], Rayleigh [87], and Lamb [88], whereas the UGW technique is a

relatively new method. The potential of using Lamb waves for the use of NDT, particularly in plates applications, is recognised by Worlton [80]. Viktorov [89] investigated the use of Lamb and Rayleigh wave modes for flaw detection in plates, tubes, and thin-walled structures of a complex shape. Meitzler [84], in 1961, considered the propagation of elastic waves in wires and proposed particular notations for the different propagation wave modes in UGW testing, widely utilised by researchers. He introduced the naming scheme of the wave mode family for hollow cylinders in terms of their particle displacement patterns around the circumference. The wave modes are defined in the form of *X(m,n)* where X will be replaced by either T, L or F for torsional, longitudinal or flexural modes respectively; *m* is the integer number of harmonic variation in particle displacement around the circumference; n is a counter variable of modes with order m of family X referring to the cut-off frequency. Since the displacement patterns for torsional and longitudinal modes do not vary around the circumference, the value of *m* is always zero for them, and they are referred to as axisymmetric modes. Flexural wave modes on the other hand, show a non-axisymmetric variation whose displacements vary around the circumference during propagation, and the value of m will present its order. Figure 2-5 illustrates a finite element analysis of fundamental axisymmetric modes, T(0,1), L(0,2), and a random flexural, F(3,2) mode.

Silk & Bainton [90] empirically investigated the generation of UGWs by referring to Meitzler's work in thin-walled metal tubing, employing a piezoelectric probe. They studied the interaction of UGWs with artefact defects in pipes using longitudinal wave modes (i.e. L(0,1) and L(0,2)), and stated that the propagation of the L(0,1) wave mode, when compared to the L(0,2) wave mode, is more efficient. Böttger *et al.* [91] employed the UGW inspection method to propose a prototype system of ferritic tubes with the aid of electro-magnetic acoustic transducers (EMATs). They claimed that there is a linear relationship between the amplitude of the T(0,1) mode and the reflection of the defect's cross section area.

In the early 1990s, researchers such as Mudge et al. [92], and Cawley and Alleyne [26], investigated the use of UGWs into NDT applications for different types of structures (e.g. plates, pipes, bars, rods) [147-150]. It was suggested by Cawley and Alleyne to use an appropriate frequency region in which the Lamb mode(s) are non-dispersive. They also considered the frequency thickness of the specimens. They utilised the L(0,2) wave mode for their inspections on 3-inch diameter pipes in the region where it was non-dispersive.

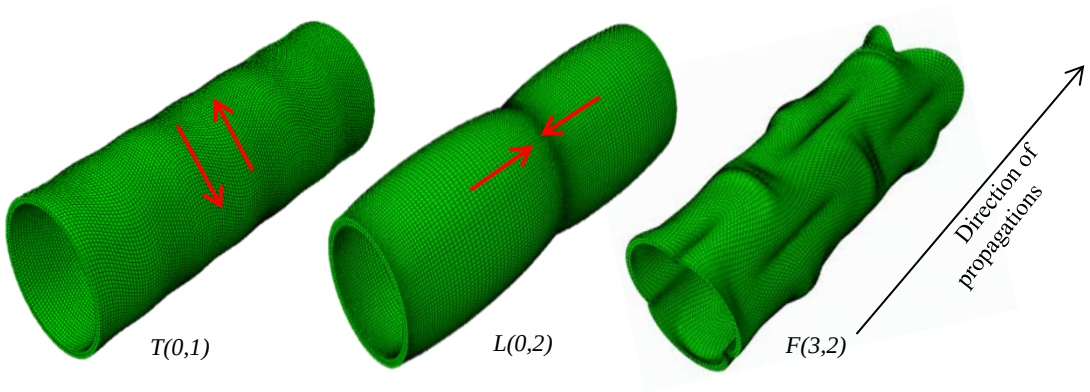

Figure 2-5: A Finite Element Analysis (FEA) representation of the T(0,1), L(0,2), and F(3,2) wave modes.

They employed a ring of shear mode piezoelectric transducers coupled around the circumference with axial alignment to generate the L(0,2) wave mode [95]. In order to suppress the generation of the L(0,1) wave mode, two rings of transducers were employed along the surface of the waveguide, where the transducers were separated by the wavelength of L(0,1) exciting with reverse polarities. Furthermore, in order to amplify the L(0,2) wave mode, another ring was added to create constructive interference of the desired mode. Since it is desirable to propagate in one direction/forward only, the signal is transmitted by the first two rings, with a phase delayed from the third ring's signal, by the ratio of their separation and phase velocity of L(0,2) [95]. Alleyne and Lowe [96], a few years later, investigated the use of T(0,1) wave mode instead of L(0,2) wave mode, as it was non-dispersive across the frequency range of interest. However, the velocity of T(0,1) is much less than that of L(0,2) which means that the test range as well as the resolution of inspection can be reduced due to the shorter wavelengths.

2.6.4 Commercial Applications of UGW

The majority of commercial applications of UGW testing comprise the in situ inspection of industrial pipelines [97]. Conventional units usually include three main parts: the transducer array, the ultrasonic pulser/receiver device, and an operator that uses this equipment to collect data using a laptop/PC. As shown in Figure 2-6 an array of shear mode transducers is located around the circumference of a pipe [16] and is pneumatically forced against the surface, which is excited with a windowed (e.g. Hann, Hamming) tone burst signal of between 10-100kHz. This generates a signal in the pipe metal, which UGW propagates along its length. The wave is sensitive to changes in the CSA of the pipe, such as defects, welds, flange, etc. These features cause the incident signal to be mode

converted into other wave modes, some of which will be reflected back along the pipe to the transducer position, where they can be recorded and stored for further analysis.

Since the waves travel at well-defined velocities, the arrival time of reflected signals can be used to determine the distance of the features from the transducer(s). The amplitudes of the reflections are found to be proportional to the size of the features, in terms of their CSA. Testing in this manner has been found to be most useful in the rapid screening of pipes to ensure their freedom from defects, particularly gross corrosion.

Table 2-1 summarises the state-of-the-art of current commercial implementations of UGW technology, within which the same physical principle is employed. The pulse-echo inspection method is utilised in these systems for monitoring long lengths of pipelines (up to 100m) to identify damage, corrosion, etc. from a single access location. Teletest®Focus+[6], Olympus®, and Wavemaker®G4 systems employ an array of piezoelectric transducers as transduction for their inspection, which covers the circumference of a specimen [16][98], [99], whereas Temate® and MsSR® systems utilise magnetostrictive coils for transduction on the pipe surface [95].

The longitudinal L(0,2) and the torsional T(0,1) wave modes are the only wave modes that are employed for inspection. However, T(0,1) is more popular as it is non-dispersive for the whole frequency range of interest and therefore it is utilised throughout this work, while L(0,2) is slightly dispersive and there is a requirement to suppress the generation of L(0,1) [95]. Note that although T(0,1) wave mode is non-dispersive its family of flexural wave modes are dispersive that needs to be reduced/removed.

2.6.5 Phase and Group Velocity

Wave propagation can be captured by two types of velocities: phase velocity and group velocity. Phase velocity, V_{ph} is the sound energy that is propagated by the movement of the changing phase in a continuous wave that propagates in space. It is more practical to employ discrete waves that transmit a short pulse containing several cycles of a particular frequency. A window function such as a Hann window is usually employed to modulate a tone burst (pulse) in order to reduce the pulse bandwidth. Group velocity, V_{gr} is the velocity of the envelope of the pulse that the pulse propagates, with its own velocity. The

[6] Teletest Focus® is a commercial UGW system that is distributed by Plant Integrity Ltd. This system is employed throughout the thesis to collect data on various pipelines for post processing.

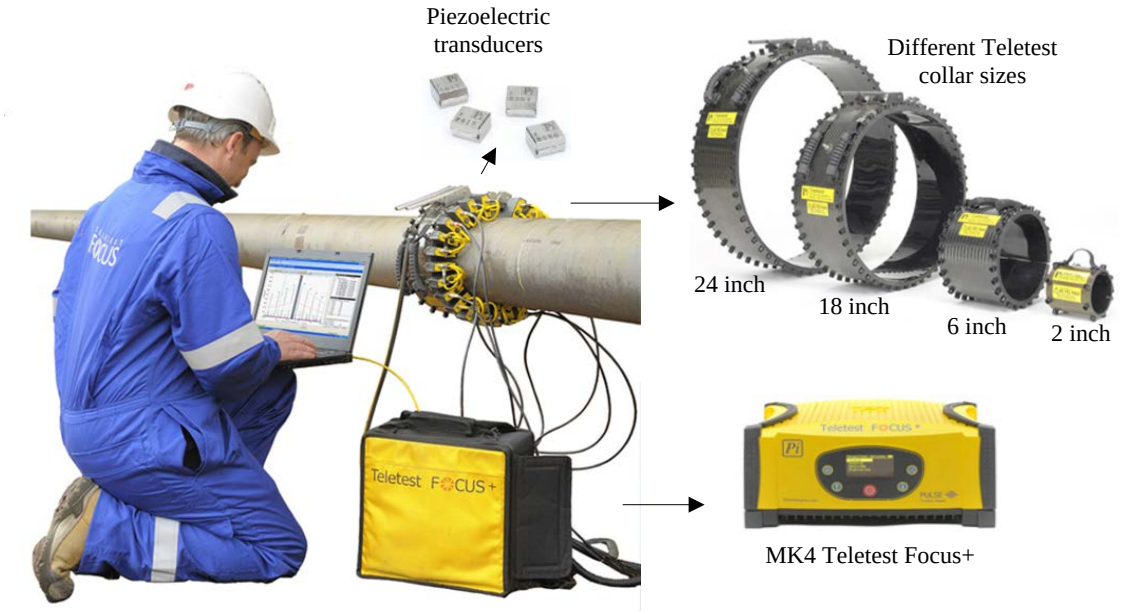

Figure 2-6: Illustration of commercial UGW pipe inspection equipment, Teletest®Focus+ system including the transducer array, the ultrasonic pulser/receiver, and an operator with a laptop [14], [16].

Table 2-1: Summary of commercial UGW systems

System	Supplier	Transduction	Frequency
Teletest® Focus+	Plant Integrity Ltd	Rings of PZT	20-100kHz
Wavemaker® G4	Guided Ultrasonic Ltd	Rings of PZT	15-80kHz
UltraWave®	Olympus Corporation	Rings of PZT	15-85kHz
PowerFocus™	Structural Integrity Associates Inc.	Rings of PZT	20-85kHz
Temate®	Inner spec Technologies Inc	Magnetostrictive coils	0.1-1MHz
MsSR® 3030R	NDT- Consultant Ltd	Magnetostrictive coils	2-250kHz

relation between the phase velocity, V_{ph} and the group velocity, V_{gr} is illustrated in (2-27) [99].

$$V_{gr} = \frac{V_{ph}}{1 - \frac{f}{V_{ph}} . \frac{dV_{ph}}{df}} \tag{2-27}$$

where f is the nominal central frequency. This equation shows that the phase velocity is equal to group velocity only when the phase velocity does not change with frequency.

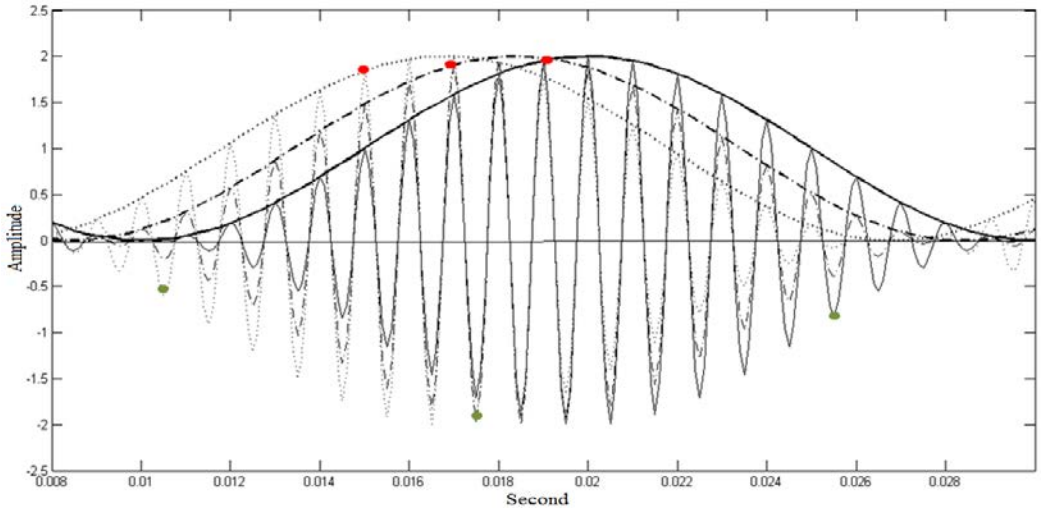

Figure 2-7: Wave propagations including phase velocity where the phase is changing but the wave propagate with zero group velocity (green dots), and group velocity where the pulse envelope propagates but the phase is not changing (red dots).

In this case, the phase propagates at the same speed as the pulse envelope. Note that in UGW testing, excepting the fundamental torsional wave mode, T(0,1) where $V_{ph} = V_{gr}$, all the other modes propagate with a frequency dependent phase velocity that causes the phase velocity to contain a different value compared to the group velocity. A phase velocity and a group velocity of a discrete pulse propagated with a changing phase or changing envelop are displayed in Figure 2-7.

2.6.6 Dispersion Curve

As shown in Equation (2-27), although the phase velocity and group velocity values are related to each other, in most cases they have a different value. Therefore, the phase can be travelling at a different speed to the envelope of the pulse (group velocity), which means a propagating pulse will have the potential to spread out over time and space. This is referred to as the *'dispersion'* behaviour of the pulse, which represents a significant impact between the UGW testing and conventional methods. In general, dispersion exists when the velocity of a wave mode is dependent on the frequency. This is defined by a 'dispersion curve' algorithm. This algorithm display two plots of the velocity variation of the phase and group velocity over a range of selected frequencies (usually kHz) for each wave mode separately. Note that if a wave mode is non-dispersive over a particular frequency range, then the value of phase and group velocity will be very close to each other.

Dispersion curves were initially investigated by Gazis [82], [83] and Viktorov [89], utilising analytical models to generate dispersion curves. Pavlakovic et al. [100] in 1997 used this knowledge and developed a software called 'Disperse', by measuring the dispersion behaviour of the UGWs and the mode propagation characteristics. This software is commercially available to generate a dispersion curve for plates and cylindrical structures, and produces dispersion curves for each particular wave mode in terms of phase and/or group velocity across the frequency range of interest. It is also able to estimate variation in attenuation over frequency for multi-layer structures, such as insulated pipes. Disperse software has been utilised throughout this thesis to generate the dispersion curves and mode shapes for all UGW testing and experiments that are investigated in this document. In general, a non-dispersive wave mode is always preferred for excitation in order to achieve a pure signal in terms of dispersion behaviour of wave modes, which makes the data interpretation easier.

The dispersion curves for a six-inch steel pipe with an 168.3mm outer diameter and 7.11mm wall thickness are illustrated in Figure 2-8. T(0,1) , L(0,1), and L(0,2) are the fundamental axisymmetric UGW modes, which have a family of flexural wave modes, F(n,2), F(n,1), and F(n,3) (where $n > 0$) that have very similar propagation characteristics, and the mode shapes of the fundamental wave modes associated with them are displayed in Figure 2-8. For example, F(n,2) of flexural modes have a similar pattern to the T(0,1) wave mode and are referred to as the 'T(0,1)' family of wave modes, which are mentioned throughout this work. As shown in this figure, the T(0,1) is the only non-dispersive wave mode with a constant velocity throughout the whole frequency range, thus its phase velocity and group velocity are equal over all frequencies. The L(0,1) mode is relatively dispersive, which is why this wave mode is not used for excitation in UGW testing; the aim of most techniques is to cancel the signal generated by this wave mode. Conversely, the L(0,2) mode is relatively non-dispersive for a wide range of frequencies employed for UGW inspection (20-100 kHz).

In addition, as shown in Figure 2-8, the number of wave modes increases at higher frequencies, and as the frequency increases, the wave modes become less dispersive. This means that the wave modes will be propagated with different velocities for higher and lower frequencies, which affects the behaviour of the wave modes in terms of spreading out in time and space. Furthermore, the properties of UGW propagation are affected by the geometry of the cylinder. These changes have been studied by Catton [95], who

demonstrates that the dispersion curves of the cylindrical structure will change depending on variations in the pipe wall thickness and its diameter.

One of the main problems in UGW testing is the dispersion behaviour of the wave modes. Therefore a wave mode must be selected carefully for a particular frequency range to minimise the effect of dispersion. Regions, where the velocity varies considerably with frequency, are known as *'dispersive regions'*. For this reason, a discrete pulse is usually employed in UGW testing to detect the reflections from the features of the specimen. To achieve this, a continuous sine wave is excited and then modulated by a window function, such as Hann windowed, to form a discrete pulse with a finite number of cycles while minimising the frequency bandwidth. Therefore, there will be a bandwidth of frequencies excited, centred over the nominal centre frequency. Thus, the lower frequency component propagates at a different frequency compared to those at a higher frequency on that particular bandwidth, especially if the frequency bandwidth is in the dispersive region.

This is the main reason that dispersive wave modes spread out in time and space. The frequency spectrum of a Hann modulated pulse with 10-cycles, and a centre frequency of 50kHz as well as the phase velocity dispersion curve of F(4,2) wave mode for the above mentioned six-inch steel pipe is illustrated in Figure 2-9. The figure is described by a `main lobe' positioned at the nominal centre frequency, with `side lobes' of diminishing amplitude either side. The frequency corresponding to the start and end of these side lobes f_k is defined as follow:

$$f_k = f_c \pm \frac{(k+2).f_c}{n} \tag{2-28}$$

Where f_k is the frequency bandwidth of side lobe k (where k = 0 refers to the main lobe), f_c is the centre frequency, and n is the number of cycles in the pulse. Thus, number of cycles plays an important role in UGW testing, as increasing the number of cycles reduces the frequency bandwidth with a longer pulse length, whereas reducing the number of cycles increases the frequency bandwidth, with a shorter pulse length. However, as most of the wave modes are dispersive, it is advisable to use a short bandwidth for processing. Figure 2-9 illustrated the dispersion behaviour of the flexural F(4,2) wave mode, where the frequency components travels at different frequencies (between ~3.5m/ms and ~4.7m/ms). Therefore, significant distortion of the pulse shape is inevitable in this case, even for short distances of a few metres. It is preferable to excite the axisymmetric wave

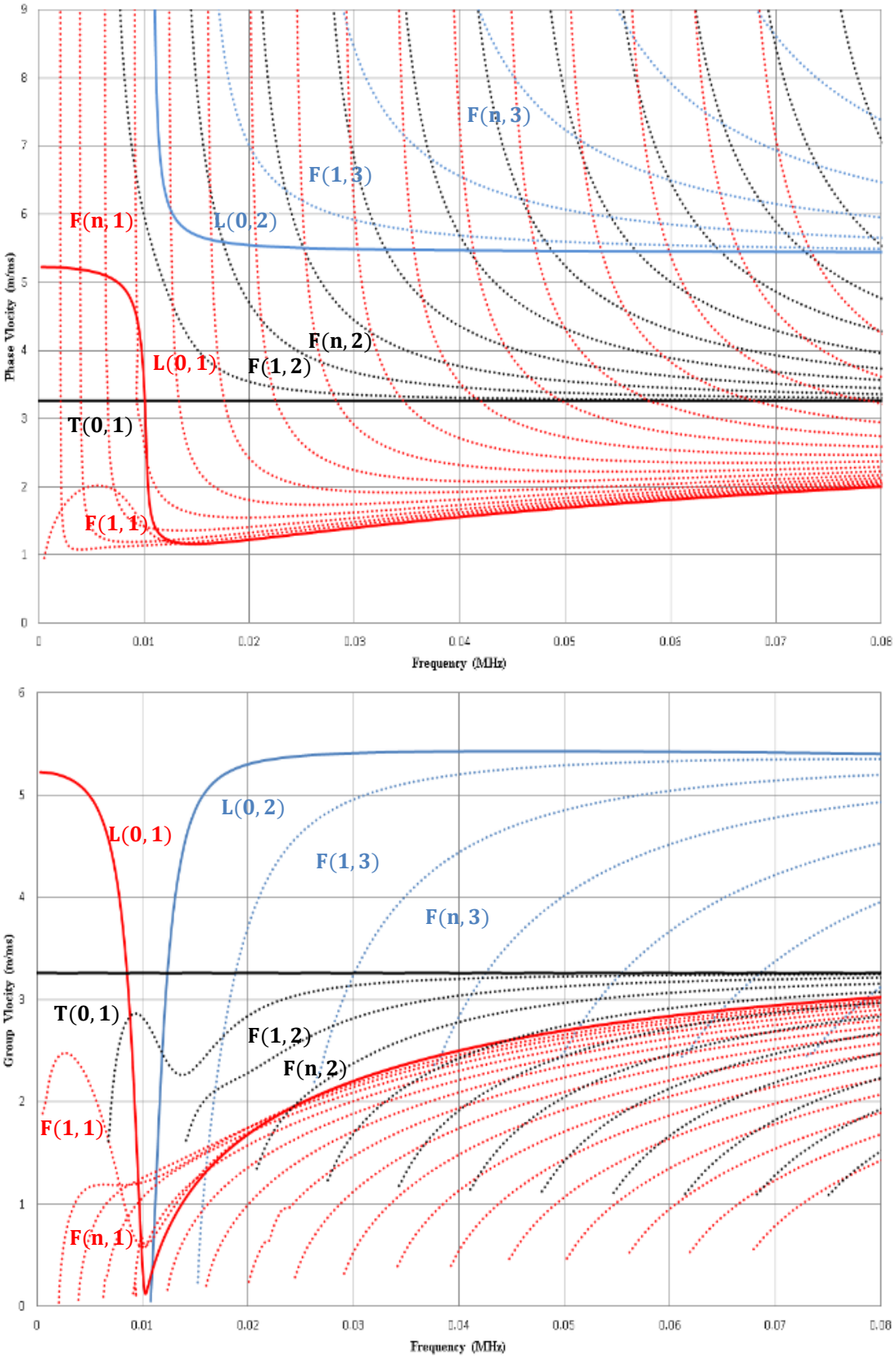

Figure 2-8 : Dispersion curves diagram for a six-inch steel pipe with 168.3mm outer diameter and 7.11mm wall thickness. a) phase velocity and b) group velocity for different axisymmetric modes and their family of flexural modes are illustrated in this figure.

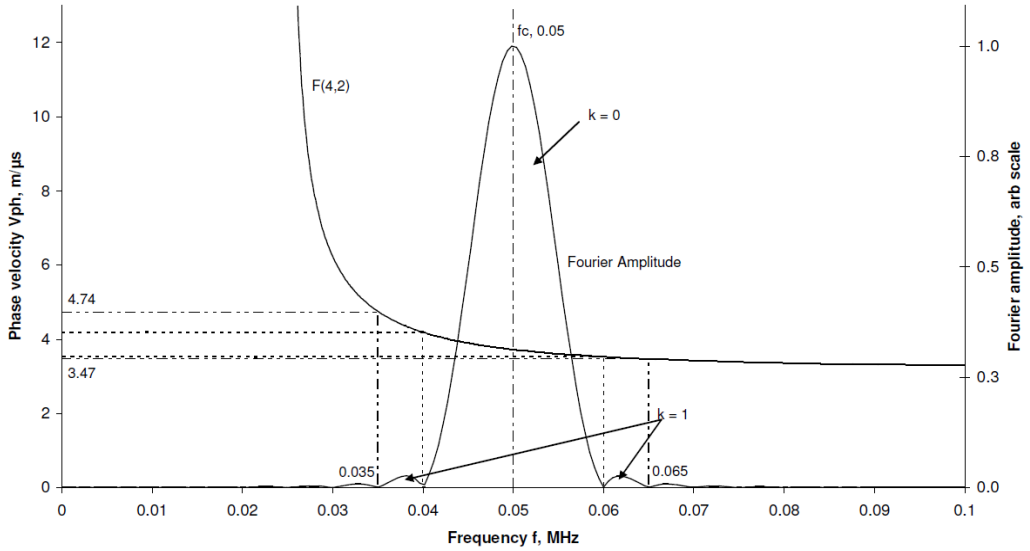

Figure 2-9: Frequency spectrum of a 50kHz, 10-cycles Hann windowed pulse overlaid with the phase velocity dispersion curve of the F(4,2) mode for a six-inch steel pipe schedule 40. The main and first side lobes are illustrated to present that the pulse has a frequency bandwidth from 35kHz to 65kHz.

mode as its dispersion behaviour is minimal, which will make data interpretation easier. However, as the excitation pulse is not always fully axisymmetric, other wave modes will produced due to mode conversion. These wave modes are the flexural family of the excited axisymmetric wave modes, which converts to coherent noise and makes the data interpretation difficult. Therefore, an advanced post-processing signal processing technique is required to analyse such signals.

2.6.7 Mode Conversion of UGWs

Mode conversion usually occurs in media when the energy of the sound propagation converts from one form into another. This could occur when an excited wave mode meets a boundary between materials of different acoustic impedances [95]. In addition, refraction usually appears at the boundary when sound waves move across the boundary between structures that have different acoustic impedances. Therefore, mode conversion in UGW testing may occur when a wave mode come across a discontinuity in the materials, hence it converts into other wave modes, with different velocity and displacement characteristics. For example, due to mode conversion, the T(0,1) mode can be converted into F(n,2) at the frequency of interest, which is its own flexural family.

2.6.8 Coherent Noise

The main challenge of guided wave inspection in pipelines is the presence of many unwanted wave modes that converts to coherent noise and makes the received signal noisy and complicated. The main reason for such a result is the excitation of multiple wave modes that travel at different velocities in different directions that in general are frequency dependent (i.e. dispersive wave mode (DWM)).

In general, the coherent noise is arising from two main sources: i) the excitation and reception of unwanted modes and mode conversion. ii) the transmission of waves in the opposite direction along the pipe and the reception of echoes from that direction.

Reducing the coherent noise is not only a challenging task for UGW inspection. It is also a problem for many other applications, such as NDE, radar, etc., where many studies and much research have been applied for over a decade to address the issue of coherent noise. In order to reduce/remove the coherent noise in UGW testing, it is vital to excite/receive a pure axisymmetric mode in one direction as well as minimising the excitation of other (i.e. dispersive) modes.

However, these unwanted modes are usually the flexural family of the excited axisymmetric wave modes that converts to coherent noise and makes the data interpretation difficult. In order to minimise the effect of unwanted modes, an advanced signal processing technique could be utilised to analyse such signals, thus improving the SNR and the spatial resolution of the UGW response.

2.6.9 Guided Wave Inspection Methods

Pulse-echo and Pitch-catch inspection methods are widely employed for UGW operations. In the pulse-echo method, a single transducer or ring of transducers is/are employed to excite the signal, before utilising same transducer(s) to receive the reflected signal; whereas in the pitch-catch method at least two sets of transducers are required for inspection to excite and receive the signal at two different locations. The pitch-catch method has the potential to provide a higher resolution compared to the pulse-echo method. Both types of inspection methods have been employed throughout the thesis.

2.7 Summary

This chapter provides the fundamental and theoretical background of acoustic applications, signal processing techniques and time-frequency analysis that are required throughout this thesis. This includes Fourier transform, windowing, etc., which are utilised in the technical Chapters 4 and 5. In addition, the fundamentals of split-spectrum processing (SSP) technique with its recombination algorithms is explored within this chapter, which is required for Chapters 5 and 6.

Furthermore, the fundamental and theoretical background of acoustic applications for sonic signals, including streaming media/protocol, describing different PLC domains, review of audio flow, etc. are provided in this Chapter, which are required in the following chapter.

Finally this chapter introduces the theoretical background of acoustic applications for UGWs, including fundamental information regarding ultrasonic applications; in particular, the development of UGW testing that has been achieved in recent years is explored, to help the reader to understand the concept of elastic wave, UGWs, which is repeatedly referred to throughout the thesis. In addition, the explanation of different wave modes and the relationship between concepts such as phase and group velocities, dispersion curve and relevant concepts, an understanding of which is required in Chapters 5 and 6, is fully covered in this chapter.

Chapter 3

3 Literature Review

3.1 Sonic Applications

3.1.1 Packet Loss Recovery Techniques

As mentioned in Chapter 1, streaming audio utilises RTP for delivery over the Internet based on UDP and because of the UDP characteristics, audio packets can be lost or discard during connection and lead to produce an annoying disturbance at the receiver sides. Since the human hearing system is very sensitive, it could easily realise the discontinuity of the sound, which is created in the waveform even by the small lost packet. Therefore, recovery and replacement of the missing packets are very important and challenging task.

It is not an acceptable solution to splicing the ends of the gap together and assumes that nothing is missing. This solution makes a timing mismatch in the playback buffer as well as possibility to interfere with server-user synchronisation in real-time process. The best solution is replacing the missing packets with the samples that are similar to the original one. There are numerous methods that have been investigated for recovery or replacement of lost packets in audio streaming [32], [101]. These techniques are divided into two broad approaches for mitigating the degradation in quality due to audio packet loss [101]:

I. Sender-based packet recovery methods, where the sender changes the encoded bit stream, adding resilience in the form of some redundancy or additional side information that the receiver side could use this information for recovery of lost packets. Forward Error Correction (FEC) [34], [101], Multiple Description Coding (MDC) and MDC-FEC method [102] are the examples of this method.
II. Receiver-based packet loss concealment (PLC) algorithms, which only utilise the received packets to estimate and/or predict the missing packets without any assistance from the sender side.

Overall, these solutions are designed to help the decoder process at the receiver side. Sender-based algorithms can employ side-information from the encoder as well as using error correction to improve the concealment process and even sometimes repairing the missing packets entirely, while receiver-based algorithms do not have access to the

encoder and employ error concealment techniques. Therefore, in order to produce the natural sound after replacing the gaps, they could only approximate the missing packets with some quality degradation.

In general, the missing gaps could be divided into short and long gaps. Replacing signal in short gaps is easier as we can estimate the characteristics similar to the lost signal by using the surrounding packets. Audio signals are often short-term or non-stationary. Hence users usually do not even realise that there was a gap. On the other hand, for long gaps or for the gaps that are very close to each other, it is usually impossible to use the same estimation method that used for short gaps; instead, gaps are commonly replacing by using other techniques and only attempt to create smooth sounds rather than annoying sounds. The concept of this work is to find a solution for receiver-based PLC technique that could be applied to both short and long gaps. Therefore, the receiver-based PLC techniques are described in more details next.

3.1.2 Receiver-Based Techniques

Sender-based methods are usually more effective than the receiver-based techniques as they have access to the encoder part and its information. However, using receiver-based techniques are more feasible and affordable in practical situations as most of the time the receiver side does not have access to the sender part. Receiver-based methods could be divided into three major categories [101]:

Insertion-based repair schemes are the simplest method to implement as the lost packets are replaced by inserting a simple fill-in segment such as a zero-length fill-in (splicing), silence/comfort noise substitution, or a repeat of a previously matched packet as the replacement. However, since the characteristics of the signal are not used to aid reconstruction, the performances of these methods are poor and not acceptable.

In splicing method, lost frame is concealed by splicing together the audio on either side of the loss, and the timing of the stream is disrupted and gives poor result as a result of makes a step reduction in the amount of available data at the buffer [103]. In order to preserve the timing relationship between the surrounding packets, silence substitution used to fill the gaps. This method is only suitable for interleaved audio over low-pass paths as when packet losses are increased; the quality will degrade rapidly [104]. Noise substitution is improved version of the silence substitution method, where, background

noise is filling the lost packet gaps. For example, using white noise compares to the silence method gives better subjectively quality and also improves the intelligibility [105][106].

In Repetition method, a gap is replaced using the previous packets which arrived immediately before the lost one. This method implemented well and involved low computational complexity. The performance of this technique could be enhanced by utilising the fading of repeated signal to zero amplitude for long gaps like that is used by GSM system [107]. Furthermore, packet repetition with fading technique is a good compromise between the other poorly performing insertion-based concealment techniques and the more complex interpolation-based and regenerative concealment methods [101]. However, the result of this method is not promising particularly for long gaps as it produces an annoying metallic sounding artefact. Hence, these schemes in general compared with the other more sophisticated schemes give poor performance result.

Time-Domain Interpolation-based repair techniques that use some form of pattern matching and interpolation to derive a replacement packet similar to the lost one from packets that surround a loss frame [101]. The advantage of this method compared to the former method is using the changing characteristics of the signal in the interpolation polynomial. Hence, better performance is achievable, although, mathematically it is more difficult to implement, and complexity/expense will be increased.

Audio signals, in general, have a time-varying behaviour, but the quasi-periodic repetitive structure, which causes most acoustic signals reoccur throughout the whole signal with some variations. The basic interpolation technique [32] used this pattern matching for reconstruction, where a lost segment of a signal is substituted by finding the best match from previous segments. This technique is particularly useful when there is a large gap in the signal. For this type of signals, it is a good idea to construct a library of patterns in order to utilise in waveform substitution [108].

Waveform Substitution is one of the popular strategies for PLC that studied by Goodman et al. [109] for packet voice structures that utilises audio before and optionally after the loss to find a suitable signal to cover the loss. The advantages of these methods are their simplicity and low computational complexity, which has obtained its popularity mainly in telecommunication industry where the computational power and memory is restricted. This method employs the buffered data of past few packets at the receiver side to analyse

them to find an appropriate substitutions samples to replace with the lost packet. The use of one or two-sided methods is evaluated to find the suitable pitch patterns for the loss.

Pitch waveform replication is presented by Wasem et al. [110] is the improved version of waveform substitution where the pitch of the substituted waveform is modified for voiced speech part to match the known pitch at both sides of the gap. Also, the packet repetition is employed for replacement of the unvoiced speech segments. Overlap-add time-scale modification scheme [111] allows the audio to be stretched across each side of the loss. This can be done by pitch synchronous overlap-add method as commonly used in the text to speech synthesis [108]. A variant of this approach has been used by Sanneck et al. [112]. Furthermore, a pitch synchronous overlap-add interpolation scheme is suggested by Valenzuela and Animalu [113] for speech signal that is similar to the technique that proposed in [114]. Although more computation is required for this technique, overall provides better result compared to the other two previous methods.

Moreover, the International Telecommunication Union (ITU) employs waveform substitution, where the missing frames are replaced by one of the previous frames using pitch replication. ITU has standardised this algorithm for extrapolation of speech signal gaps of up to 60 ms (G.711 Appendix I) [114], including ITU-T standard PLC known as G.722 Appendix III as well as ITU-T Recommendation G.728 Annex I and G729 [115], [116], [117]

Regeneration-Based Repair methods (Model-based Interpolation techniques) use knowledge of the audio compression algorithm to derive codec parameters of the received packets to synthesise a lost packet. In these methods, a large amount of state information is used to repair the losses, however; it is a codec-dependent technique and computationally intensive. These methods are widely employed in the compressed domain instead of the waveform methods.

Many researchers [118]–[120] have been investigated in the modified version of waveform substitution based methods to utilise the advantages of simplicity, and source filter model-based techniques to achieve higher quality signals. Examples include; the interpolation of transmitted state for codecs based on linear prediction (LP) or transform coding [55], where the decoder interpolate between the received states to replace lost packets. Interpolation using compressed domain parameters for speech coders [36].

Another example of this method is ITU G.723.1 where for short lost packets, the state of the LP coefficients are interpolated by speech decoder [121].

Due to adaptive nature of codec parameters, there are no boundary effects on either side of the loss, and this is one of the advantages of codecs where it is possible to interpolate the state rather than the audio signal. In addition, the computational load stays constant. However, demands of high processing may be applied in this category for interpolation. Model-based extrapolation/recovery [122] where the packet(s) on either one or both side of the loss is fitted to a model that used to generate audio to cover the lost frames. One of the well-known model-based interpolator methods in the restoration of lost samples is autoregressive (AR) model [123]-[126] that is used for reconstructing a long portion of missing samples in audio signals. AR introduced the multi-rate interpolation scheme that applied by Janssen et al. [108] for estimation of non-recoverable errors in compact disk systems. Maximum a posteriori AR (MAPAR) and least square error AR (LSAR) [124] are other common methods for estimation that could be applied to the problem of gap restoration. However, the aim of basic AR models is to restore the spectral envelope of the signal, whereas the aim of modified version is to restore the excitation-related parameters such as pitch at the same time. A pitch-based AR interpolator suggested by Vaseghi and Rayner [125] that employed the long-term correlation structure of the speech and quasi-periodic signals. Kauppinen and Roth [127] suggested a method that replaced the missing part of the excitation with zeros that effectively used the zero-exited LP model from the past samples to estimate the missing samples. A time-reversed excitation substitution technique with a multi-rate post-processing module is proposed by Esquef et al. [126] for audio gap restoration. This technique developed to prevent any artefacts signals that may generate from discontinuities of the excitation signal at the two ends of the gap.

Chen and Loizou [48] proposed repair of interleaved m-law encoded speech that combines the autoregressive analysis results with an estimate of the excitation made for the loss period. The interleaved blocks size is small enough ($8/16\ ms$) in this method, thus, the speech characteristics have a high probability to be relevant with the last received block.

Sinusoidal models [15] that operate on the source-filter components of the speech signal are the alternative approaches to modelling the excitation signals that considered by Lindblom and Hedelin [128]. They suggested an algorithm for extrapolation of lost speech packets using a LP model of the spectral envelope of the signal, and then they presented a

similar interpolation technique with some extension [129]. A LP algorithm has been proposed by Rødbro et al. [130] that applied in both symmetric and asymmetric windows as well as the overlap-add process of successive frames to predict the sinusoidal model parameters of missing frames in time-domain signal. The robustness of the inter-frame and intra-frame is investigated by Wang and Gibson [131]. They employed line spectral frequency (LSF) coders to estimate the packet loss. Most of the mentioned methods had strived to estimate and/or predict the excitation signal and the spectral envelope throughout the gap, which are the main sets of audio/speech features.

Zavarehei [55] proposed an interpolation algorithm based on a linear prediction - harmonic-plus-noise model (LP-HNM) of speech. The spectral envelope of speech is modelled using a LSF representation of a LP model, and the excitation is modelled with a HNM, for each sub-band whose parameters were the harmonic frequencies, amplitudes and harmonicity (voicing levels). These parameters are utilised for a phase prediction algorithm and then interpolated throughout the gap using a combination of autoregressive and linear interpolation techniques to produce the synthesised speech. This method is also modelled/tracked the time-varying contours of the formants and the harmonic energies across the gap. Furthermore, a codebook-mapping method is employed to mitigate abrupt changes in the envelope of the signal as well as improving the performance of the algorithm in the restoration of long gaps (e.g. > 50 ms) [55].

Alternative methods include interpolation of the missing sample by using gapped-data amplitude and phase estimation (GAPES) algorithm to reconstruct the missing data in the discrete short-time Fourier transform (DSTFT) domain. The same algorithm is also applied on a different complex domain, formed by combining the modified discrete cosine transform (MDCT) domain (real part) and the modified discrete sine transform (MDST) domain (imaginary part) [132], [133]. Advanced repair techniques are required more computation to perform [101], and although the result showed the achievement of quality improvement was incremental by following these advanced schemes, however, packet repetition method with fading sometimes preferred as it offers a good compromise between excessive complexity and achieved quality.

The main limitation of most audio/speech enhancement methods is their destructive effect on the harmonic structure of audio signals [134], particularly at low signal-to-noise ratios. This is partly a consequence of ignoring the harmonic structure of audio spectrum. HNMs method is a well-known algorithm that results in high quality synthesised and high

intelligibility for modelling the harmonic structure of audio signal that makes it popular for many applications. Sinusoidal models, and their modified version such as harmonic noise model, widely employed in text-to-speech (TTS) systems [135], bandwidth extension [136], packet loss concealment [122], [130], speech coding [137], [138], speech enhancement [69], [139] and many other audio processing applications.

Overall, most packet loss methods that mentioned in the above literature review do not specifically address the important issue of time-variation of the speech spectral parameters; their impact on the replacement of lost packets and the solutions that may account for the time-variations. A number of methods that may lend themselves to adaptation for time-varying extrapolation/interpolation, such as model-based codecs and overlap-add synthesis; have not been fully investigated in terms of their capacity to provide such improvement in time-varying environments for reconstruction of the lost packet. Due to the challenges mentioned above, these methods are not suitable for wideband audio/music signals that contain a combination of inputs from several instruments with several fundamental frequencies and spectral envelopes. Thus, a novel solution is presented in this work in Chapter 4 to address these challenges.

3.2 Ultrasonics Guided Wave

In order to increase the SNR, spatial resolution and specifically defect sensitivity, it is essential to minimise the presence of the dispersive wave modes (DWM) in UGW signals. Dispersion is one of the main sources of the coherent noise that occupies the same bandwidth as the signal of interest. Conventional methods such as band pass filters and averaging are unable to reduce the effect of DWM. Sicard et al. [140] initially studied the effect of dispersion in UGWs to compensate the dispersive behaviour of the signal. Wilcox [141] developed a technique for reversing the effect of dispersion on DWM. The technique used knowledge of the dispersion characteristics of the wave mode to map signals from the time to the distance domain. It reversed the effect of dispersion on a particular wave mode and restored it to an undispersed pulse. The dispersion pre-compensation technique is performed based on the chirp technique by Lin & Zeng [142] on the narrowband excitation signals that managed to compress the time duration of received wave packet during the extracting process. In addition, information of multiple distinct frequency ranges and responses has been extracted for a few narrowband excitations by employing the benefits of broadband chirp excitation. Moreover, this technique optimised the design

of excitation waveform. This method utilised a previous knowledge of the dispersion curve and the propagation distance. The dispersion compensation (DC) in multimodal cases is presented by Xu et al. [143] to estimate the plate thickness and propagation distance followed by a self-compensated technique for wave modes that were studied by employing a wideband dispersion reversal (WDR) algorithm [144]. This technique created a single wave mode packet that made the signal interpretation easier, but it was required to have the knowledge of the propagation distance in advance [145]. This was problematic when inspecting over a range of distances.

Toiyama and Hayashi [146] combined the DC algorithm with Pulse compression (PuC) methods by employing chirp waveforms. They investigated a scenario of single wave mode without introducing the quantitative SNR enhancement. Marchi et al. [147] employed a combination of warped frequency transform (WFT)-based DC algorithm with PuC to improve the localisation of a steel cylindrical mass in an aluminium plate. This technique was tested for a simulated defect only, and it was not practical, as the wavelength had to be filtered to reduce the effect of multimodal propagation. They also considered irregular waveguides using a triangular pulse excitation; however, no experimental validation was reported [148]. Yucel et al. [149], [150] and Fateri [151] utilised by combining of DC with PuC employ broadband maximal length sequence (MLS) excitation to improve the SNR of the UGW response for an aluminium rod. The result indicated that the propagation distance is successfully obtained for the highly dispersive flexural wave mode but not that effective for the non-dispersive longitudinal wave mode. It has been claimed that the cross-correlation compared to DC achieves a better result when the wave modes have little dispersion. Mallet [13] considered cross-correlation and wavelet de-noising for reduction of the effect of DWM on synthesised and experimental UGW response. It was shown that both techniques were not suitable for the reduction of coherent noise. This was because both methods have removed the smaller amplitudes regardless of whether or not they were signal or noise.

3.2.1 Literature review of SSP

SSP was originally developed for radar systems as a frequency diversity/agility technique [152]. Bilgutay et al. [153] in 1981 considered the frequency agility method to improve SNR in ultrasonic NDT for large grain materials. Of particular concern was microstructure scattering of the ultrasonic signal. The grain echoes, unlike flaw echoes, are highly

sensitive to shifts in the transmitted frequency, and as a result, de-correlation in grain echoes could be obtained by shifting the transmitted frequency, which improves the flaw visibility. Therefore, the grains only reflect signals that have similar size of wavelength to the grain size. This basic principle has led to the idea of SSP technique for ultrasonic flaw detection to improve the flaw to grain echo ratio of signal response. This technique reduced grain noise in a simulated UT by utilising minimisation and conventional averaging algorithms. Then, Bilgutay et al. developed a method that produced frequency diverse de-correlated signals from the received wideband signal by digital filtering instead of by transmitting many different narrowband signals. This was achieved by splitting a wideband-received spectrum of signal responses to obtain a set of sub-band signals. This was equivalent to using a frequency agility technique, where a number of pulses were transmitted with different frequencies.

Newhouse et al. [154] in 1982 considered SSP for NDE to enhance the ultrasonic signal that belongs to a flaw, above those of grains using frequency diversity. Due to destructive interference, Newhouse et al. expected that the received spectrum of a random distribution of point scatters would exhibit minima. This was an assumption from a simpler situation, where, minima of zero amplitude occur for a regularly spaced grid of scatters in the received spectrum at predictable frequency intervals. SSP was used in connection with this phenomenon to divide a received time-trace bandwidth into multiple sub-band time-traces, where each one belonged to a different frequency window. Newhouse et al. assumed that a defect's response should be presented in the sub-band signals as it manifests frequency coherence, whereas the grain noise will be incoherent. In addition, since the recombination algorithms utilised were non-linear, the amplitudes of a defect will be increased while the amplitude of noise will be reduced. However, the improvement of SNR was limited because when the original signal was divided into sub-band signals its SNR was also divided, and adding them linearly would restore the original SNR.

A theoretical analysis of SSP investigated by Amir et al. [155], who modelled a target and a set of random scatters. They obtained an improvement in SNR by utilising both linear and non-linear averaging and minimisation. They claimed that the minimisation algorithm gave the greatest SNR enhancement when the input had an SNR greater than unity.

Karpur et al. [156] proposed a theoretical basis for the selection of SSP filter bank parameters using a minimisation algorithm. They studied the dependence of the performance of SSP on various processing parameters and showed that the SNR

enhancement was mostly dependent on selecting the optimum filter bank parameters. In order to verify their theoretical basis, they carried out experiments for the selection of parameters, which were defined to predict SNR enhancement by compounding a number of frequency diverse signals. However, some of these parameters obtained a larger value than expected. This can be the result of utilising Gaussian function for filtering, whereas their calculation was based on a Sinc function.

Rose et al. [157] studied the use of SSP in a number of ultrasonic NDT applications for SNR enhancement. They considered the characterisation of the grain structure in different materials employing a polarity thresholding (PT) algorithm. They claimed that selecting an appropriate value for filter-bank parameters is one of the main factors for SNR enhancement. They have suggested that the filter bandwidth needs to be around three to four times the separation and advised that if the filter overlap was too narrow or there was no overlap at all, no improvement in SNR will be achieved. Rose et al. also claim that, if "one edge of the plane of the defect is displaced from the other edge by more than three to four times the wavelength with respect to the direction of wave propagation", SSP will not lead to SNR enhancement.

Karpur et al. [158] in 1988 proposed a technique for calculating an optimum bandwidth required for the SSP technique. It was claimed that the transmitted bandwidth and the received bandwidth in UT are not the same because scattering has a low-pass filtering effect, and based on that, the attenuation was calculated as a function of frequency for a given grain size and propagation distance. Thus, the low-pass filtering characteristics for the specified material were achieved. In order to find the bandwidth for SSP, this information along with the frequency response of the transducers were employed and compared with the results obtained experimentally. The results showed that increasing the number of filters increased the overall bandwidth. Hence, Karpur et al. claimed that as the number of filters increased, the SNR enhancement reduced to zero, as the target information did not exist at higher frequencies. Hence, the maximum SNR enhancement was obtained by selecting the optimum number of filters (optimum bandwidth).

Shankar et al. [159] proposed the PT algorithm of SSP for the reduction of coherent noise in a single target. They utilised the first deriving of the probability density function (PDF) of the output for evaluation and calculated the SNR theoretically and achieved superior noise suppression. Their results indicated that the SNR enhancement was a function of the number of filters as well as the input SNR. It was shown that the SNR experienced greater

improvement for smaller filter bandwidths. In addition, SNR enhancement was increased with the number of filters up to a certain point, beyond that SNR enhancement decreased. Furthermore, it was revealed that the detectability of the smaller targets could be seriously affected by multiple targets with different sizes of filters. Shankar et al. stated that the PT algorithm works well in conjunction with other SSP algorithms, such as minimisation. However, it should not be used when the input SNR is close to unity.

Aussel [160] implemented SSP employing finite impulse response (FIR) filters ratio rather than filtering in the frequency domain, utilising DFT that gave a delay, to obtain a real-time response. This method was more efficient for the processing of ultrasonic signals with wide frequency bandwidths or long time durations. The selection of filter bank parameters for UT signals was studied using the minimisation algorithm. However, the results were limited to fixed frequency-to-bandwidth ratio FIR filter response.

Saniie et al. [161] investigated the performance of order statistic (OS) filters in conjunction with SSP in the context of ultrasonic flaw detection to improve the flaw-to-clutter ratio of backscattered signals. They showed that an optimal rank could be obtained with a prior knowledge of the distribution of flaw and grain echoes. It has been claimed that the OS filter performs well where the flaw and clutter echoes have good statistical separation in a given quantile region representing a particular rank (e.g. minimum, median, maximum). However, its performance deteriorated with the contamination of unwanted statistical information. Thus, SSP is utilised to provide a set of observation features corresponding to different frequency bands. Through simulation and experimental studies, the robustness of OS filters was shown and the information utilised from different frequency bands to improve flaw detection.

Laugier et al. [162] considered the use of SSP for a moving target in biological tissue, employing a minimisation algorithm. They implemented an SSP technique and compared it to linear band-pass filtering of the signals. Their results showed that SSP with a non-linear minimisation algorithm gave a greater enhancement in SNR compared to linear band-pass filtering. In addition, the results indicated that the use of band-pass filters caused a loss of axial resolution, whereas the SSP did not have this problem.

Gustafsson and Stepinski [163] employed adaptive an SSP method using an artificial neural network (ANN) to implement PT for UT signals. In order to allow the relative importance of the different sub-bands to be taken into account, weighting factors were

added to the input signal, and the signal values were fed into the ANN. The results showed better performance obtained compared to PT but only for one particular sample. Gustafsson [164] in 1995 extended the method by employing both the filter bank and non-linear processing as an ANN for SSP. This method was time-consuming, although the results indicated that the ANN could “eliminate most of the noise”.

Tian et al. [165] introduced the group delay moving entropy technique to enhance the performance of SSP in detecting multiple targets that exhibit different spectral characteristics in UT applications. The technique was based on the fact that reflections from noise have a random group delay, whereas reflections from features have a constant group delay. It stated that the group delay was the derivative of the phase response. They utilised SSP to reduce the scatter noise and the targets excluding the largest. Then the target was eliminated in the time domain windows and the procedure repeated until all the remaining targets were detected. The removal of the dominant target improved the detection of the remaining weaker targets. Hence, the combination of group delay moving entropy method and multistep SSP technique offered the potential for detecting multiple targets in complex environments. Tian & Bilgutay [166] considered a statistical analysis of the performance of SSP for the detection of multiple targets for two scenarios: i) where the bandwidth and centre frequency of the features were known, ii) where the processing frequencies were obtained using group delay moving entropy as defined above. They stated that the second scenario was more effective in multiple target detection. However, the probability of detection was slightly higher when the target bandwidth was known compared to the technique when the group delay moving entropy was used.

Sun & Saniie [167] proposed the use of SSP combined with a neural network (NN) to develop a detection structure in NDE. The Gaussian bandpass filter was utilised to perform spectral splitting and an adaptive three-layer NN for the subsequent non-linear processing. They claimed that the SSP-NN technique was able to detect flaws when the SNR was $0\ dB$ or greater. Sun & Saniie [168] developed a combination of SSP with an adaptive-network-based fuzzy inference system (ANFIS) to classify features on UT signals. The inputs of ANFIS were the results of sub-bands signal that were filtered by a bank of bandpass filters. The ANFIS was trained to classify the signal from the sub-bands at a point in time as either reflection or noise. It was shown that the SNR improved only when the input signals had a SNR of 0dB or greater.

Grevillot et al. [169] proposed a moving bandwidth minimisation (MBM) method and mathematical morphology (MM) algorithms in SSP to detect multiple specular targets with different spectral characteristics in biological structures. They claimed that SSP using a minimisation algorithm could only detect a simple target or multiple targets having similar spectral characteristics. The main drawback of this algorithm was its high sensitivity to the localisation of the analysis bandwidth in the spectrum, as if the bandwidth and its position are selected incorrectly; no echo signal will be detected. They utilised SSP followed by MBM to process multiple target signals and obviate previous problems. They suggested that the MBM method could be improved by running phase thresholding in the case of the line amplitude information is lost to enhance low-level specular echoes. However, when the input SNR was less than 1dB, the detection efficiency was reduced.

Zhenqing et al. [170] proposed the SSP based on phase standard deviation (PSD) of the sub-band signals. The output of this method was equal to the input divided by the PSD for each sub-band. Hence, regions that contained high variations in phase were reduced, as they are divided by a larger value than regions surrounded by lower variations in phase. They claimed that this method is less sensitive to the filter bank parameters and since it was not a gating method, it did not require a threshold for processing.

Stepinski et al. [171] proposed Consecutive Polarity Coincidence (CPC) for determining the bandwidth for SSP. This algorithm makes use of the pulse characteristics of the target echo more easily to implement local bandwidth estimation for SSP. It was claimed that a feature exists across the bandwidth region where the sequence has a large range of consecutive values. Thus, the bandwidth was set to the region where the target signal was constant through it. Then, they considered a modified version of non-coherent detection technique for the detection of signals with additive Gaussian noise, and claimed that this technique in terms of SNR enhancement performed comparably with proposed SSP-CPC method. However, their method produced a lower temporal resolution as it offered the optimum processing parameters for a single target only. They suggested that the temporal resolution can be improved by increasing the total bandwidth but at the expense of SNR.

Drai et al. [172] considered SSP and wavelet transform for SNR enhancement in UT. They considered the maximal amplitude of the ultrasonic echo that was collected to characterize defects in nature, size and orientation. They proposed a frequency diverse ensemble to overcome the resolution limitation of the constant bandwidth windows due to the fixed time-frequency resolution over the entire region. Hence, wideband windows were utilised

at high frequencies and narrowband windows at low frequencies. They achieved a good SNR enhancement employing minimisation and the square root of product algorithms. They considered discrete wavelet transform (DWT) to decompose the signal and then reconstructed the signal a number of times, each time using only certain decomposition levels. These reconstructed signals were averaged to give the output signal and achieved better detection of the defect of the echo but not much improvement in terms of SNR.

Rubbers and Pritchard [30] gave an overview of SSP and a range of different algorithms for reconstruction in the field of UT. The selection of filter bank parameters had been discussed and the results for each algorithm for an experimental signal were shown. They stated that each of these algorithms had improved the SNR at the cost of linearity in the processed signal. However, it has been claimed that SSP does not allow for sizing of flaws as the amplitude of the processed signal is non-linear and therefore, the use of SSP application was limited, and further improvement was required. Rubbers [173] developed a complex-plane SSP (CSSP) technique for the ultrasonic inspection of castings, which was capable of suppressing SSP in terms of SNR enhancement while maintaining linearity in both the amplitude and the energy content of a flaw's signal. He measured the frequency specific phase differences in an ultrasonic signal to improve SNR without sacrificing linearity or sizing capabilities. However, further work was required for validation. Rubbers & Pritchard [174] extended CSSP further and introduced the idea of employing a weighting factor for thresholding. Hence, if the phase spread at a particular instant in time was greater than a threshold, then the output was set to zero. The input was multiplied by a weighting factor, depending on the phase spread, so if the phase spread was above the threshold, the weighting factor was linearly decreased to zero, and if it was less than the threshold, the weighting factor was equal to one. Therefore, the signal was only attenuated slightly if the threshold was not exceeded by much. Although some SNR enhancement has been achieved, in order to validate this technique, a number of criteria had to be met according to national standards of governing bodies. Rubbers & Pritchard [175] carried out a simulation of CSSP to measure its capabilities mathematically. They tried to improve the signal quality theoretically by comparing CSSP processing. They achieved a good result in reducing near-field effects, improving depth resolving power, angular resolving power and SNR. Their results showed that CSSP maintained amplitude linearity if truncation values were selected appropriately. However to achieve that, a bandwidth in excess of 100% was required. They generated a diagram of phase-spread,

presenting the spread of the sub-band phases throughout the material. Based on that, a weighting factor was applied to the simulated wave fronts that let to reducing the scattered signals from the simulation while maintaining the signal with in-phase sub-bands[7]. Johannes & Rubbers [176] continued with CSSP to improve SNR where CSSP utilised an additional mathematical dimension (the complex plane) for calculating the probability of a signal originating from a real reflector such as a flat bottom hole. They tried to validate the steps required to use this method for industrial application, such as UT technology. The CSSP system utilised was designed and manufactured by Eskom personnel to overcome problems encountered in coarse grain materials such as austenitic castings and cast materials. The aim was to assess CSSP in terms of increasing the detectability of features in the noise level and establish the procedures for selection of the CSSP frequency bands and phase spread depending on flaw size and material properties. The results showed that the improvement was significant only where the SNR was less than 6dB. Hence, CSSP is primarily a development tool and has no clear advantage for field use yet.

Mallet [13] examined cross-correlation, wavelet de-noising and SSP, to post-process UGW signals to reduce the level of coherent noise. The results showed that the cross-correlation and wavelet de-noising were not successful for the reduction of coherent noise since they removed the smaller amplitudes regardless of whether or not they are noise or signal. On the other hand, SSP was found more promising and showed great potential for improving the SNR. To the best of author's knowledge, the use of SSP in UGW testing has to date only been studied by Mallet. Their results showed that SSP is highly sensitive to its selection of filter bank parameters. He claimed that although SSP was effective in reducing the effect of DWM in both synthesised and laboratory experiments on a pipe with a saw-cut, in some cases, the processing resulted in some small erroneous features. In addition, it was less effective for a field data that had more complex signals as obtained from real pipelines. He found out that when two features were close to each other they combined, which means only one feature was presented in the processed signal, indicating a loss of temporal resolution. However, he did not mention the minimum distance for that. He stated that SSP is not yet suitable for use in UGW as it could lead to the loss of features and a high number of false calls due to the introduction of erroneous features created by

[7] Rubbers has a patent (US patent number 7,035,776, April 2006) that is entitled "low noise to signal evaluation" which is covers CSSP for a wide range of applications for complex signals.

the processing. Hence, further investigation is required to address these challenges. Donohue [177] reviewed the SSP technique to enhance ultrasonic flaw detection in materials consisting of grain-like microstructures, and with, classical approaches, such as Wiener, and matched filtering. He showed that SSP using nonlinear processing represents a unique approach relative to classical methods as it employs a statistical characterisation of the phase. SSP was examined in an automatic flaw detection scheme for multiple flaws embedded in non-stationary grain noise. The nonlinearities of the SSP effectively changed the flaw and grain echo distribution to enhance the separation of their amplitudes beyond that of simple envelope detection. He claimed that SSP is well-suited for detecting flaws embedded in large-grained material as it does not require specific knowledge of the spectral differences between the grain and flaw scatters. However, the results showed that the performance of matched filter compared to SSP is slightly better due to the statistical phase models of SSP, which was not as restrictive as the matched filter.

Rodriguez and Vergara [178] proposed a new filter bank design for SSP, based on the use of variable bandwidth filters, where filters were equally spaced in frequency and their energy gain equalised. The pruning technique was employed to reduce the number of bands required to increase the algorithm's efficiency. They carried out some simulation and experimental testing using stationary models for the grain noise with a single defect. They claimed that the simulation model was able to reproduce quite accurately the environment of the real test by simply adjusting properly the parameters involved in the design. They claimed that the frequency multiplication (FM) algorithm gave the greatest resolution and SNR enhancement when combined with the new filter bank design. They stated that this method reduced the number of filter bands compared to other algorithms; hence, it reduced the system complexity. However, this technique was not evaluated for non-stationary models, highly dispersive material, or a model with multiple defects. Therefore, further investigation with a more challenging scenario is required. In addition, the combination of a new filter bank design with another algorithm worsened the result. Rodriguez et al. [179] considered simulated ultrasonic signals using both stationary and non-stationary models for the grain noise, and real scans obtained in the laboratory from the low dispersive model (aluminium) and high dispersive model (cement) materials. The FM algorithm was revealed as the best choice among six popular recombination

algorithms[8] when combined with the new extensions. The structure was the same as for the classical filter bank, i.e. once the width of the analysis band and the number of bands were fixed, the filters were equally distributed across the inspection bandwidth, but for the new design, the bandwidth of each filter was selected proportional to its central frequency. The bands were then energy gain equalised, which did not affect the frequency distribution of the energy at the input signal, as uniformity of that distribution is essential to distinguish the presence of a possible flaw. They stated that as the bandwidth of the filters was wider than in the classical design, the time resolution improved, thus leading to a better location performance and achieved the highest SNR. Thus, making the detection process easier. Rodriguez et al. [180] considered the performance of SSP combined with spread spectrum (SS) excitation and the use of frequency selective loss compensation (FSLC) techniques for ultrasonic imaging of new composites. Since the attenuation for these materials is highly frequency dependent, SS and FSLC techniques were used to increase the energy and equalise the received signal with the aim of minimising the probability of the false alarm (PFA) while maximising the probability of detection (PD). They stated that the classic criterions were not feasible for selecting the optimum parameters, mainly due to the complex structure of the materials and their highly dispersive behaviour. The advantage of SS and FSLC combination were: obtaining higher processing gains achieved with fewer filters and increasing the range of usable frequencies leading to an improvement in resolution. It was determined that the use of FSLC techniques allows equalising the attenuation as a function of distance and frequency, thus considerably improving the SNR and flaw detection while reducing the complexity of processing. Rodriguez et al. [181] studied the problem of automatic detection of ultrasonic echo pulses in a grain noise background considering split-spectrum (SS) algorithms as sub-optimum solutions. They calculated analytically the statistics of the detectors, i.e. the PFA and PD, summarised in the receiver operating characteristics (ROC) curves, which allowed them to assess the performance of the different recombination methods[9] in terms of the number of bands and the input SNR or the defect amplitude. They tested the detectors using simulated and real scans, confirming the expectations generated from the results of the

[8] The other five-recombination algorithms included: polarity thresholding (PT) and scaled polarity thresholding (SPT) – based on the phase observation – and three classical methods, based on order statistics (OS) such as minimisation (MIN), normalised minimisation (NORM) and geometric mean (GM).

[9] PT and SPT, minimisation, normalised minimisation and FM.

theoretical analysis. They concluded that in spite of some limitations, the detector based on the FM algorithm provides the best performance and reliability, which could be applied in the automatic detection of defects in highly dispersive materials. However, the technique was tested only for simple scenarios, hence; further investigation is required for non-stationary models with highly dispersive materials having more defects.

Muthumari et al. [182] compared the Matlab simulation results of SSP using a PT algorithm over the classical approach of filtering for non-linear non-stationary time of flight diffraction (TOFD) welding defect signals. A-scan signals were used to enhance SNR while suppressing the grain noise. The results showed that the classical approach of filtering cannot remove the noise component completely due to scattering of microstructure material. Muthumari et al. stated that the high-frequency components did not have that much energy or useful information about flaws; therefore, they were filtered. In addition, the results showed that SSP was a powerful method for the easy identification of the defect location and back wall echo of the signal. However, only a simulated signal was considered that was mixed with white Gaussian noise, hence this method needs to be validated with the experimental data.

Saniie et al. [183] suggested a neural network (NN) coupled to an SSP technique for target echo detection when the input SNR was around 0dB. They claimed that an SSP-NN target detection system was capable of improving the target-to-clutter ratio (TCR) by an average of 40dB. They designed a FPGA-based hardware platform for system-on-chip realization of a real-time ultrasonic imaging system. Furthermore, order statistics (OS) and NN were utilised to improve target echo visibility in the presence of clutter that was significantly intense compared with the target echo. They claimed that the SSP-NN technique when compared with conventional methods obtained more robust detection performance by calculating the TCR. The technique was sensitive to the frequency coverage of filters. Thus, a robust target detection technique was required to minimise the sensitivity.

Syam and Sadanandan [184] employed a combination of SSP and order statistic filters to reduce the influence of reverberation for flaw detection in conventional UT. The reflections from the microstructure contribute to reverberation, which interferes with the signal being considered. They stated that by processing the multiple echoes corresponding to a set of transmitted signals, the effect of microstructure reflections could be suppressed with respect to the flaw echo. Reverberation has a complex interference structure that varies with the transmitted frequency. Therefore, a wideband signal was transmitted to

effectively reduce the influence of reverberation. It was assumed that the reflections from the flaw were insensitive to frequency and produce a steady output, which can be utilised for flaw detection. However, they did not mention which SSP parameters were selected and how they calculated the SNR. Furthermore, this technique only tested for a simulated signal, and no experimental result was given.

To summarise, SSP challenges can be divided into two main categories as follows:

i) Selection of optimum filter bank parameters, the combined effect of which were investigated and addressed for conventional UT to some extent by [156], [158], [185].

ii) Recombination algorithms for the use of SSP, such as minimisation [154], [156], Polarity thresholding [8], geometric mean [161] or other algorithms that are the combination of these three categories. Examples are PT with minimisation; frequency multiplication, etc., which are explained in more detail in Chapter 2.

The literature clearly illustrates that the outcome of SSP application is sensitive to the selection of the filter bank parameters, and successful implementation depends on this. All literature cited investigating the use of SSP in conventional UT, NDT application, and radar. Most of the work discussed claimed that their selection of filter bank parameters improved the SNR of the signal. Thus, although the important issue of filter bank parameters has been addressed for the conventional UT signal, these values are not suitable for UGW signals that contain a combination of axisymmetric and non-axisymmetric wave modes with different phase velocities operating in the kHz range. Therefore, the selection of optimum filter bank parameters requires a fuller investigation in terms of its capacity to provide such improvement in UGW signals. Thus, the core concept explored in this work in Chapters 5 and 6 is to find appropriate filter bank parameters for SSP to improve the SNR and enhance the spatial resolution of UGW signals and, as a result, a novel solution is presented in Chapter 5 to address these challenges. In addition, a variety of SSP recombination algorithms is examined to find an appropriate solution.

Chapter 4

4 Time-Varying Signal Models Using Spectral Motion Detection

4.1 Chapter overview

The focus of this chapter is the estimation/reconstruction of gaps (missing packets) in audio signals. To progress the study, two fundamental issues were identified; i) the appropriate domain for packet loss restoration, and ii) the methodologies for the gap reconstruction. In order to achieve this, a novel signal processing technique based on extrapolation and interpolation of lost audio segments is proposed to restore lost segments in audio recordings, which could be utilised for voice over IP (VoIP), streaming, voice communication over the Internet, mobile phone, audio broadcast, etc. The issue of modelling of a non-stationary frequency-spectrum is addressed in the context of packet loss concealment (PLC), and a novel solution is suggested in this part of the work by tracking and utilising the motion of spectral flow across time frames. The proposed technique employs a *time-frequency motion (TFM) matrix* representation of the signal, where each frequency is labelled with a motion vector estimate.

The technique is applied to synthesise and real audio (e.g. speech and music) signal for the restoration of signals suffering from different packet loss rates or different patterns in order to reconstruct a loss packet. It is demonstrated throughout this chapter that the proposed technique, when compared to the popular conventional techniques reported in the literature, substantially improves the audio signal quality in terms of the performance evaluation of speech quality (PESQ) and mean opinion scores (MOS).

The research conducted in this chapter has been presented in *Signal Processing and Information Technology (ISSPIT), 2013 IEEE International Symposium*, Athens, Greece on Dec. 2013 [7] and in *Acoustics, Speech and Signal Processing (ICASSP), 2014 IEEE International Conference*, Florence, Italy on 4-9 May 2014 [8]. The background theory of this technique is described in Chapter 2.

In addition, the reader is provided with details of the systematic procedure for the employment of the signal processing techniques utilised in this section, along with the necessary mathematical implementation for each step.

4.2 Introduction

One of the core communication methods in the world is that of verbal communication, on which the telecommunication industry, one of the largest industries in the world as a result of its extreme growth and development over the last few decades, is based. VoIP technology has experienced rapid growth, leading to telecommunication clients utilising any network operation in any place over any distance. Reasonable prices and a good quality of service are the most important issues to clients regarding the use of such services, while the process of the techniques employed is not of importance to them.

There are many studies, and much research that has been carried out in the past few decades to improve the quality of audio signals that are degraded by audio packet loss. In particular, various signal processing approaches have been applied in an effort to enhance the quality of audio signals by removing the effect of background noise or estimating lost segments. The enhancement of an audio signal is valuable in a variety of applications, such as VoIP, teleconferencing systems, etc. In this chapter, several aspects of the quality enhancement of audio signals that have reduced in performance and quality due to randomly lost segments at the receiver side in the telecommunication system are explored.

PLC methods employ signal models that capture the correlations of audio parameters either on one or both sides of the gap. These models can be categorised into two different classes: i) Predictive or extrapolative methods, where only the past samples are available, ii) Estimative or interpolative methods, where some future samples are also available [108]. These methods mainly endeavour to estimate and/or predict two main parts of the audio features throughout the gap: the spectral envelope and the excitation

As explained in background review in Chapter 2, packet-switching techniques are widely employed to deliver the audio signal in VoIP networks to maximise network efficiency. However, due to several reasons such as congestion at the routers, an overloaded server’s buffer, link failure, etc. audio packets may never reach their destination, which leads to degrading/deteriorate the performance and quality of signal, which may create an unpleasant sound at the receiver side. Therefore, the main aim of this chapter is to

determine a method to reconstruct the missing packets at the receiver side in order to be able to play the audio signal continuously without disruption so that the end user does not realise the loss.

Several solutions [114][123]-[126] were suggested by the extant research in order to reconstruct audio packet losses. These solutions approach the signal with different terms of performances and different computational complexity requirements that are fully covered in the literature review in Chapter 3. The algorithm proposed in this chapter is a receiver-based PLC operation, based on a time-frequency model that is investigated, developed, evaluated and discussed. The algorithm employed extrapolation and/or interpolation techniques to estimate/reconstruct the lost audio packet. A novel contribution of this work is the introduction of the TFM matrix and its application to motion-compensated extrapolation and interpolation for audio signals [8]. Furthermore, the improvement of the quality of narrowband and wideband audio signals is considered in this chapter, and an advanced model-based PLC solution is proposed.

The research is inspired by the method employed in motion-compensated image processing; however, in this work, the motion of frequencies across time frames are estimated and factored into the estimation process. In addition, the problem of the successful prediction of the signal's phase, which has a substantial effect on the quality of the reconstructed audio signal, is investigated and a solution proposed to address this issue.

4.3 Reconstruction of Lost Audio Samples

This section gives a brief concept of extrapolation and interpolation process of a band-limited signal, synthesised and real audio signals those effects by a number of missing samples that tried to reconstruct using extrapolation and/or interpolation algorithms.

Extrapolation/Interpolation are the techniques that could be utilised to estimate or predict the unknown or the lost samples of the audio signal employing a weighted average of a number of known samples at the neighbourhood point of the missing part of the signal. These techniques are widely utilised in most communication and decision making structures including conversion of a discrete-time signal to a continuous-time signal, packet loss, dropouts, low-bit-rate speech coding, sampling rate conversion in multirate communication systems, and restoration of a sequence of samples irrevocably distorted by transmission errors, etc. [101], [108].

4.3.1 Extrapolation/Interpolation Techniques

Various forms of extrapolator/interpolator techniques are employed in the field of signal processing applications in particular, for audio/video PLC. Estimation of a sequence of missing samples and pattern recognition are the obvious examples of these techniques. The aim of this chapter is to reconstruct a sequence of lost audio samples using one of these reconstruction techniques.

There is always a challenge to reconstruct a sequence of M unknown/missing sample of a signal using a number of samples on one side or both side of the gap. The perfect reconstruction technique (with zero error) is only achievable if the missing samples are redundant. This means that they do not carry any information than that already carried by the known neighbouring samples. The example of this kind of signals that could be easily predicted is sine wave signals, or in the case of a band-limited random signal if the sampling rate is greater than M times the Nyquist rate [31]. However, in reality and practical situations, the signals are typically have a random process and their sampling rate is typically slightly above the Nyquist rate. Therefore, predict the lost samples are not that easy and some interpolation error is inevitable. As a result, the aim is to find a solution to minimise the reconstruction error through utilisation of the signal models and the information confined in the neighbouring samples.

The main concept of interpolation (which are also applied for extrapolation process) is to achieve an optimum fidelity reconstruction of unknown or missing samples of a signal and below is the list of factors that affected the accuracy of the interpolation process [108].

- The sampling rate: rising sampling rate improves the interpolation performance and made the near samples of the lost samples more correlated and increased the redundant information.
- The predictability and/or correlation of the signal: the predictability of missing samples from their adjacent samples will be increased, (interpolation improves) by increasing the correlation structure of successive samples, or equivalently by decreasing the bandwidth of a signal.
- Non-stationary characteristics of the signal: audio signals could change the characteristics of their behaviour completely during the time/distance because of

their time-varying behaviour. This needs to be considered for interpolation process especially for a large sequence of samples.

- Finally, the length of the missing samples and the way of using the interpolator affected the quality of interpolation. The performance of interpolation will be reduced by increasing the length of the missing samples.

There are varieties of interpolation techniques that could be utilised for audio PLC. The main aim of interpolation is to construct a polynomial interpolator function that passes through the known samples around the missing packets to estimate the missing segments. There are some different ways to construct a polynomial interpolator such as Newton, Lagrange interpolation, power series and Hermite [108].

Cubic Spline Interpolation is another method of interpolation where the signal is divided into a number of smaller intervals. Then, in order to fit a large number of samples with a smooth curve, a low order interpolating polynomial is utilised for each interval to provide a better estimation. Hence, the cubic polynomial is fitted to each interval between two samples. However, these methods are not equipped well to make optimal use of the statistical structures of the signal. Thus they are not suitable for reconstructing a relatively large number of missing samples of the signal.

Alternatively, there is a statistical signal processing techniques referred to model-based interpolation techniques that could be utilised for interpolation of a sequence of missing samples based on predictive and/or a probabilistic model of the signal. These techniques are typically good for interpolation of small/medium sized gaps of missing samples. The examples include a frequency-time interpolation technique, an autoregressive model-based interpolation, and interpolation looking throughout a signal record to find the best matches. Furthermore, the two advanced interpolation techniques; interpolation through waveform substitution and frequency-time interpolation have the potential to replace relatively large gaps of missing samples.

The optimal interpolation model should be able to employ predictive models of signal trajectory, as well as statistical models of the distribution of the signal process that could be referred to model-based interpolation techniques, comprise least square error interpolation and maximum a posteriori interpolation based on an autoregressive model. Lastly, interpolation through searching an adaptive signal codebook and time-frequency interpolation is developed to find the best-matching signal [108].

4.3.2 Bandwidth Extension

The extrapolation/interpolation techniques of missing segments in audio signals have applications in the telecommunication industry for the restoration of band-limited signals where the audio coders filter the signal using a low-pass filter before coding or transmission to maximise the number of subscribers. Therefore, the information above 4kHz is generally not transmitted. However, the bandwidth of telephony speech is usually around 3.4kHz. Several techniques have been developed in last few decades to increase the bandwidth of telephony speech signals to a higher bandwidth (wideband) of broadcast quality to reconstruct the upper band contents of speech signals by employing the available surrounded spectrum of the speech at lower bands. The aim was to gain the sensation of higher bandwidth and higher quality of speech. Most of the approaches utilised the codebook mapping techniques to reproduce the expanded spectral envelop where the missing spectral envelope in the higher bands was achieved from codebooks trained on joint feature vectors of bandlimited and full band speech [139],[187], [188]. In addition, a similar approach is already applied and commercially available in high-quality audio compression techniques where the upper band signal is reconstructed from the lower-band as well as side information.

The spectral envelope representation was mostly based on the line spectral frequencies parameters that derived from a linear prediction model of speech [188]. The spectral envelope that calculated above is combined with the estimation of the excitation signal to obtain a wideband speech signal. In order to estimate the excitation signal, variety of algorithms such as Gaussian modulation, spectral folding, etc. could be utilised [187], [189]. However, there is a challenge to recover those parts of the signal using the mentioned algorithms when the valuable information exists in the upper band rather than the lower band such as fricatives. Therefore, to address this issue, a new approach based on time-frequency method is studied, developed and proposed that be able to estimate the excitation of the missing parts of the signal's spectrum.

4.3.3 Phase Prediction

The short-time phase spectrum is a key aspect to consider in the perceived naturalness and quality of the audio signal [190]. In order to attain an appropriate quality of the reconstructed signal, the phase estimation technique needs to be based on a model that could be able to exploit the continuity of the harmonics and preserves the randomness of

the non-harmonic sub-bands. A method employed in this work is similar to the one that used in [55] to estimate the phase in the time-domain reconstruction of the signal. This method estimates the phase spectrum entirely rather than estimating the phase of individual harmonics separately. The reason for that is because the signal is synthesised in the frequency domain; hence each frame is transformed to a waveform via the inverse Fourier transform at the final stage. The harmonics of voiced audio signal could be assumed of as a sequence of pitch parts that consistently combine at the time of occurrence of each pitch pulse [55]. The phase needs to be estimated appropriately to preserve inter-frame and intra-frame continuousness of the reconstructed audio signal.

As a result the following conditions need to be considered; i) Audio harmonics have phase continuity through successive frames, ii) Neighbouring frequency bins around each harmonic are in phase halfway across the frame, and iii) Level of randomness added to the phase of each channel rises with frequency as well as the distance from the nearest harmonic [55]. The first condition guarantees the inter-frame continuity of the harmonics. The optimistic support of the energy of signal elements around each harmonic will be provided by the second one, and the last condition is suitable for the unvoiced sub-bands reconstruction process which helps to avoid the generation of any artefacts. In addition, there are some other examples of phase reconstruction that the signal is synthesised in the time domain such as speech coding [191], text-to-speech synthesis [192] and speech morphing [190].

4.4 Spectral Flow and Motion in Time-Frequency Domain

As mentioned in the literature in Chapter 3, there are many approaches to mitigating the degradation in quality due to audio packet loss. However, most of those methods do not specifically address the important issue of time-variation of the audio spectral parameters. A number of methods that may lend themselves to adaptation for time-varying of signals have not been fully investigated in terms of their capacity to provide an improvement in the reconstruction of a lost packet. Due to the challenges mentioned above, these methods are not suitable for wideband audio signals that contain a combination of inputs from several instruments with several fundamental frequencies and spectral envelopes. Hence, the aim of this part of the research is to develop an algorithm to reconstruct the packet loss in audio streaming to address these challenges.

AR model-based and time-domain interpolation techniques may utilise for interpolation of a short length of lost samples (exp. 100 samples at a 20kHz sampling rate), but they are not suitable for estimating of a large sequence of samples as they suffer severe performance degradations due to the numerical problems associated with the inversion of a large matrix. This is usually involved in the time-domain reconstruction of a large number of samples. Hence in this work, a time-frequency matrix is employed for audio PLC in the DFT domain. This reconstruction is based on modelling the time-varying correlation of temporal trajectories of the ST- DFT components of the audio signals using motion compensated.

4.4.1 Fourier Transform and Spectrogram

Discrete Fourier Transform (DFT) as described in Chapter 2, is employed to analyse the frequency content of a finite duration discrete time signal s(t) with N samples. By adding the DFT to the spectral time representation, the problem of extrapolation and/or interpolation of a gap of N samples in the time-domain could be transformed into the problem of the reconstruction of a gap of one sample, alongside the time, in each of N discrete frequency bins. The Short-time Fourier transform (STFT) technique is employed for this purpose, which is a practical and relatively simple technique for spectral-time representation of a signal in order to create a two-dimensional STFT from a one-dimensional function of time s(t).

As shown in the flowchart of Figure 4-1, the audio input stream s(t) is segmented into overlapping windowed segments. The segments are windowed separately to reduce the spectral leakage due to the effects of discontinuities at the edges of each one. In order to perform Fourier transform of those segments, discrete-time STFT is utilised. Successive segments are transformed to frequency by a Discrete STFT and stacked along to form a time-frequency matrix given by:

$$X(l,k) = \sum_{m=0}^{N-1} s(l \times \gamma + m) w(m) e^{-j2\pi mk/N} \tag{4.1}$$

where N is the segment length , m is the discrete-time index, $k = 0, \dots, N-1$ is the discrete-frequency index, l is the frame index, γ is the segment overlap, and w is the Hann window function. The spectrum vector X_l could be defined as follows:

$$X_l = \begin{pmatrix} X(l,0) \\ X(l,1) \\ \vdots \\ X(l,N-1) \end{pmatrix} \tag{4.2}$$

Alternatively, the DCT or the MDCT can be utilised for forming TFMs [133], [193]. Theoretically, for time-varying signals, using a standard Kalman state-space formulation [56], [194], the spectral values can be formed as:

$$X_l = A_{l-1}X_{l-1} + v_l \tag{4.3}$$

where X_l is the time spectrum vector, A_{l-1} is the state transition matrix coefficient and v_l is the random driving variable. This spectral value can be also formed as an augmented matrix $X(l,k)$ that includes dynamic information on the spectral flow rates across time and frequency matrix where, $k = 0, \ldots, N-1$ is the discrete-frequency index and l is the frame index. The standard Kalman filtering does not take into account the cross-flow among frequencies, i.e. the fact that frequencies and not just their magnitudes move up/down across the spectrogram. Taking this into account, we have a modified form of state-space model that includes a *spectral motion vector* that indicates the motion of frequency component within the state vectors across time frames as described in Section 4.5. In practice, it is a challenging problem to solve (4.3) which is a modified form of state-space. The simplified solution proposed here is in the form of a TFM matrix of audio signals as shown in Figure 4-1. The audio input stream s(t) is segmented into overlapping windowed segments of length N samples and each segment is transformed into an augmented matrix of the spectrogram $X(l,k)$ as is shown in this algorithm. The spectrogram matrix is appended with the estimates of the spectral motion vectors.

Figure 4-2 shows a time domain audio signal with gaps together with the TFM representation of the signal. The received and lost audio packets can be transformed into a TFM, and then each frequency component of the lost packet is extrapolated from the previous available packets or interpolated from the previous and future frames. Note that, as shown in the illustration, a gap of N missing time-domain samples is transformed into one or several frequency column vectors in the TFM matrix.

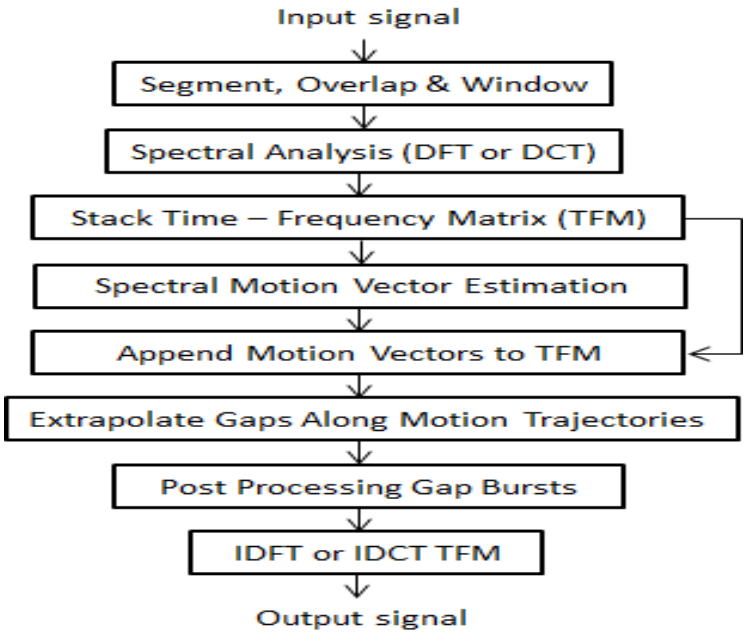

Figure 4-1: Time-frequency motion algorithms of audio signal

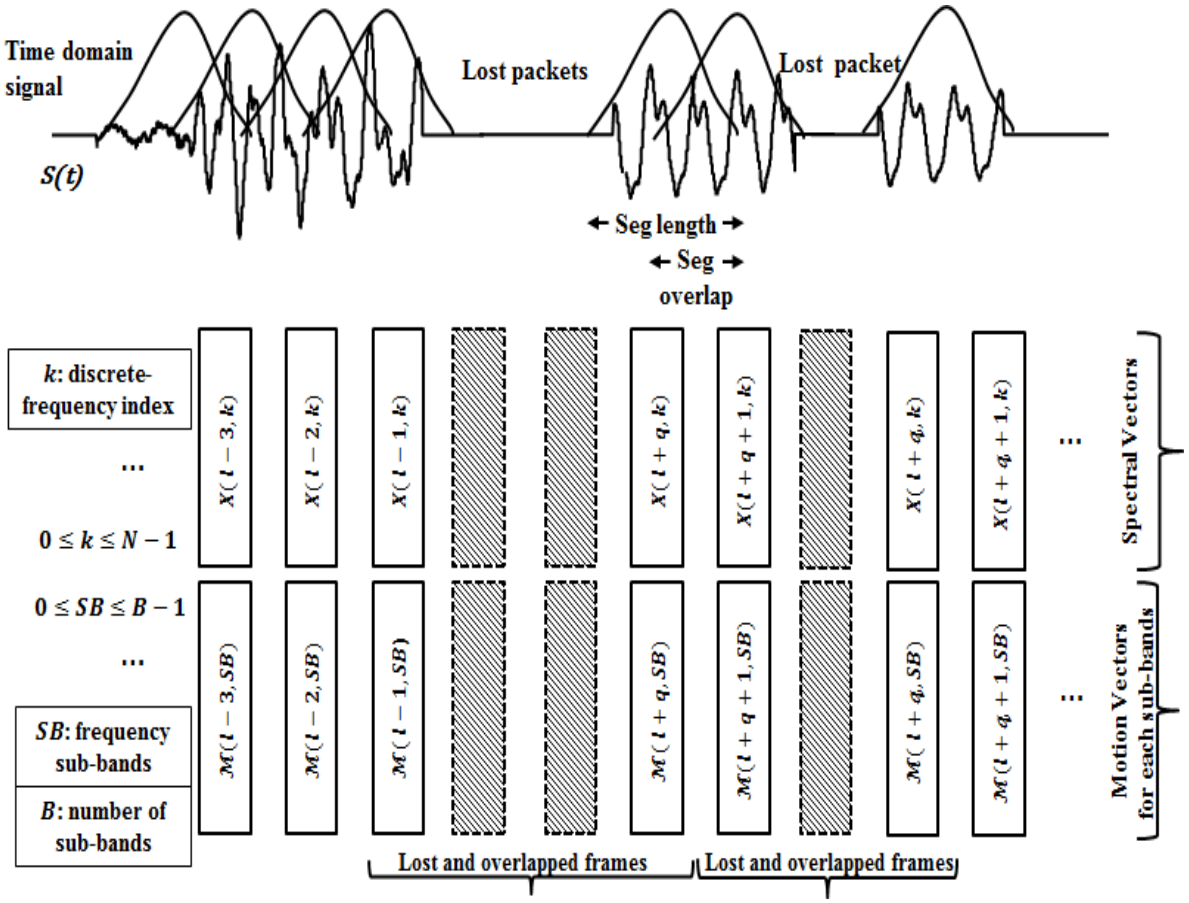

Figure 4-2: Transformation of a time-domain signal with gaps into TFMs with spectral motion vectors for each sub-bands appended.

4.5 Time-Varying Spectral Motion Vector (SMV) Model

In this section, the probability and temporal of the trajectory of the STFT elements are studied, examined, and as a result, a novel method is proposed for deriving a set of motion vectors that when combined with the spectral vector $X(l,k)$ indicates the direction along where the k^{th} frequency of the l^{th} frame has moved relative to the previous frame $l-1$. As mentioned earlier, the STFT is employed in this work, hence it is presumed that the structure of the signal frequency is time-invariant throughout of each frame, but it could be vary through the frames. The k^{th} spectral component of a signal has a time-varying character, i,e. it could be changed for some time, vanish, and then appears with a different intensity or different characteristic [108]. Therefore, it is nessasary to identify the more appropriate frames with the most similar frequency characteristics to the previous frames.

It is assumed that the STFT trajectories of the audio signal are stationary for short periods of time. Thus the autocorrelation vector or matrix of STFT trajectories is required to be regularly updated. However, since the original frame is missing and is unavailable to estimate the autocorrelation vector in the STFT trajectory, thus a technique is proposed that obtains the result from the past received frames of the signal. In addition, it is assumed that there is not a massive change for one sample delay to estimate the autocorrelation function using previous frames.

In general, the temporal correlation between DFT samples is related to the following conditions; i) the overlap between successive frames and ii) the relatively slow variation of formants of the excitation signal. In addition, the level of correlation between successive frames (temporal) of DFT/STFT varies for different frequencies and times. It is presented by Cohen [54] that the level of correlation between successive frames of speech (STSA) growths with the size of the overlap between successive windows.

4.5.1 Spectral Motion Vector Estimation

The proposed method divides the signal spectrum $X(l,k)$ into B sub-bands $X_{SB}\left(l,\hat{k}_{SB}\right)$ to estimate the spectral motion vector, $\mathcal{M}(l,SB)$ for each sub-bands individually where $k=0,\dots,N-1$ is the discrete-frequency index, $SB=0,\dots,B-1$ are the number of subbands, and frequency bandwidth $\hat{k}_{SB}$ for each sub-band could be defined as:

$$\hat{k}_{SB}=\{\frac{SB.N}{B},\frac{SB.N}{B}+1,\dots,\frac{(SB+1)N}{B}-1\} \tag{4.4}$$

Using (4.4) the sub-bands could be rewritten as $X_{SB}(l,i)$ where $i \in \hat{k}_{SB}$, are the samples in each sub-bands as shows in Figure 4-3 . This figure presents the spectral-time of an audio signal with a missing gap. The y-axis presents the frequency components which are divided into B subbands with equal number of samples i in each frequency bins. The three previous and two future frames that surronded the missing frequency-time frames has been shown that are utilised for reconstracting (extrapolation/interpolation) the missing gap.

Cross-correlation (CC) method is used to estimate the motion of the major frequency component in each sub-bands between two-time frames. To calculate a spectral motion vector, two successive spectral frames $X_{SB}(l,i), X_{SB}(l-1,i)$ has been compared that quantifies the spectral flow motion over time.The motion movements of the spectral energy are calculated for each frequency sub-bands $\mathcal{M}(l,SB)$, separately from the position of the CC lag corresponding to the peak of the CC function. This is the motion value of the B^{th} sub-bands of the l^{th} frame relative to the $(l-1)^{th}$ frame where there is a highest similarity in terms of frequency bins as:

$$\mathcal{M}(l,SB) = \underset{\ddot{k}}{argmax}\left(\sum_{i=SB(N)/B}^{((SB+1)N/B)-1} |X_{SB}(l,i)|\left|X_{SB}\left(l-1,i+\ddot{k}\right)\right|\right) \tag{4.5}$$

where $SB = 0,\dots,B-1$, are the number of subbands, $\hat{k}_{SB}$ are the frequency bandwidths for each subbands in which the frequency resides, i are the samples in each frequency bins and $\ddot{k} \in \{\hat{k}_{SB-4},\dots,\hat{k}_{SB+4}\}$ is the lag position that compares sub-bands between two successive time frames in order to find the best frame with highest similarity.

The motion movement is obtained using Matlab‘s function “*xcorr”* by calculating the absolute values where the samples are aligned in the time axis and varies in the frequency axis. In addition, since the frequency partial and the frequency motion of the missing frame l are clearly unavailable, in a case that if there is more than one lag position available with the same value, then the optimum lag position is the one that is closest to the frequency sub-bands of the missing frame l using a first order approximation.

As an alternative method, the spectral motion vector can be estimated by minimising the mean squared error (MMSE) distance between the spectral vectors similar to the algorithm that used for audio flow in [57]. However, the CC function compares with MMSE and audio flow methods provides a more robust measure. The estimates of a motion vector

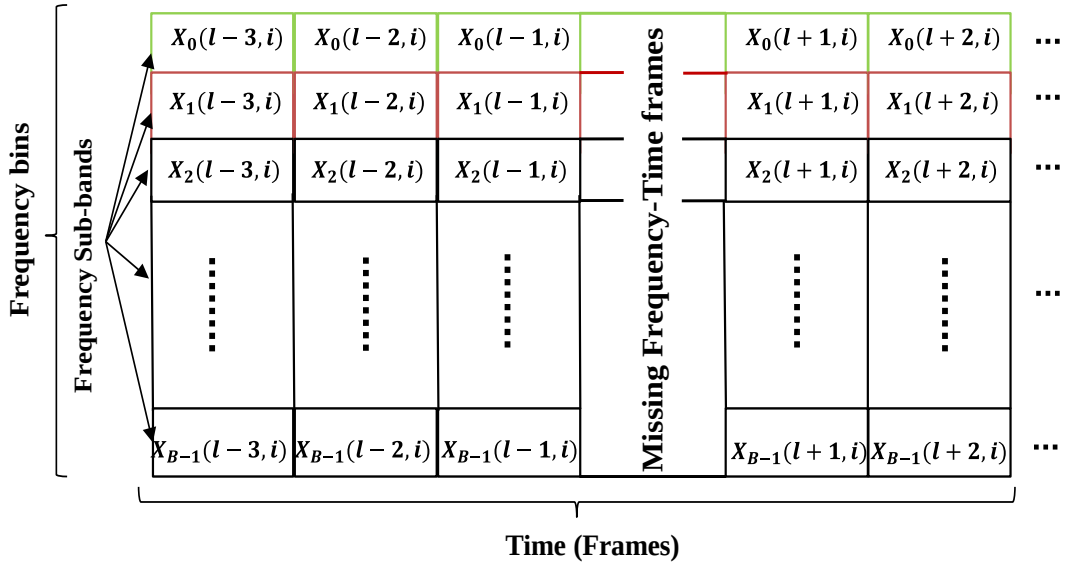

Figure 4-3: Illustration of spectral time-frequency matrix of a signal with a missing gap.

may be smoothed over time using a first order recursive equation as:

$$\widehat{\mathcal{M}}(l,SB) = a\widehat{\mathcal{M}}(l-1,SB) + (1-a)\mathcal{M}(l,SB) \tag{4.6}$$

where $\widehat{\mathcal{M}}(l,SB)$ denotes the smoothed motion vector and the variable a may be set to a value in the range of 0.95-0.99. Since the spectral motion over time would be quantised to the frequency resolution $\Delta f = F_s/N$, where $F_s = 1/T_s$ is the sampling frequency and N is the number of samples, the technique of zero-padded discrete Fourier transform is used to yeild a higher resolution interpolated spectrum and hence obtain a finer quantisation of the spectral motion variable.

4.6 Reconstruction in TFM Matrix

The main obstacle to reconstructing (extrapolate/interpolate) the signal is the time-varying nature of the spectral envelope and the fundamental frequencies of the audio signals. It would be incorrect to extrapolate a missing frequency partial $X(l,\hat{k}_{SB})$ from the same frequency bin, $\hat{k}_{SB}$, of the previous frames, $l-j, X(l-j,\hat{k}_{SB})\ j = 1,2\ \cdots$, if, as shown in Figure 4-4, over the time frames, the spectral power is moving across the frequency bins. A more appropriate process would be to estimate the trajectory of motion of the frequency partials across time frames and to extrapolate the k^{th} frequency partial from $X\left(l-1, SB-\widehat{\mathcal{M}}(l-1,SB)\right), X\left(l-2, SB-\widehat{\mathcal{M}}(l-2,SB,)\right), \ldots$ where the variable $\widehat{\mathcal{M}}(l-1,SB)$ indicates the relative motion of the k^{th} frequency partial between the frames $l-1$ and l.

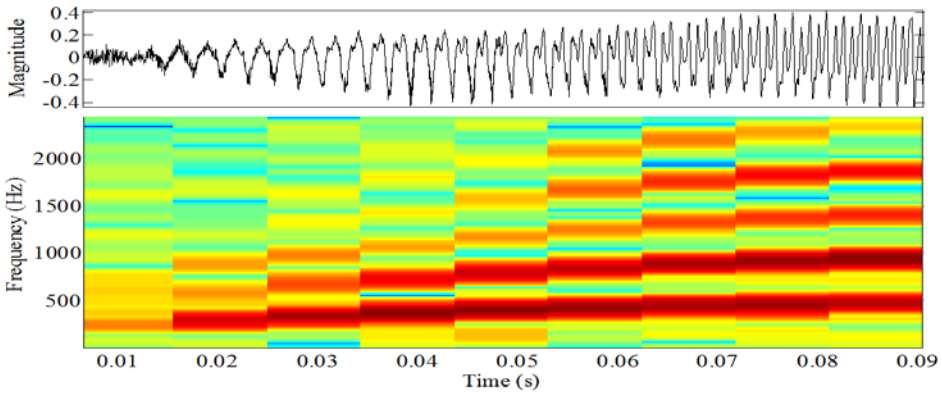

Figure 4-4: Illustration of a speech segment where the spectral power is moving across the frequency over the time frames.

In general, the aim is to fill in the missing frame especially at the beginning and at the end of the gap to maintain the continuity of both the magnitude and the phase of each frequency component of the signal. There are several choices for the formulation of the interpolator polynomials such as linear, quadratic, cubic spline polynomials, or a low-order linear prediction model [195]. A moving average motion-compensated (MAMC) extrapolation/interpolation method was developed in this work. This method produced satisfactory results when a few adjacent blocks (three previous frames for extrapolation and adding two future frames for interpolation) employed on either side of the gap.

4.6.1 Extrapolation in TFM Matrix

Assume that the l^{th} packet is lost, and needs to be extrapolated using the previous Q packets, the spectral motion-compensated extrapolation formula is expressed as;

$$X_{SB}\left(l,\hat{k}_{SB}\right)=\sum_{j=1}^{Q}c_jX\left(l-j,\hat{k}_{SB}-\widehat{\mathcal{M}}(l-j,SB)\right) \tag{4.7}$$

where c_j are the coefficients of an extrapolation polynomial of order Q. The polynomial coefficients can be calculated and updated from a least square error fit of an n^{th} order polynomial such as a linear, second order or spline function to the frequency tracks immediately preceding the missing gaps [55].

4.6.2 Interpolation in TFM Matrix

Equation (4.7) can be modified to a spectral motion- compensated interpolation method, using Q past and P future spectral vectors as;

$$X_{SB}\left(l,\hat{k}_{SB}\right)=\sum_{j=1}^{Q}c_jX\left(l-j,\hat{k}_{SB}-\widehat{\mathcal{M}}(l-j,SB)\right)+\sum_{j=1}^{P}c_{Q+j}X\left(l+j,\hat{k}_{SB}-\widehat{\mathcal{M}}(l+j,SB)\right) \tag{4.8}$$

where the coefficient vector $[c_1,\dots\ c_Q,c_{Q+1},\dots\ c_{Q+P}]$ operates on the available past and future frames $[l-1,\dots\ l-Q,l+1,\dots,l+P]$. This is useful in cases where a delay of one or two frames is not critical and when the future frames have not been lost. A linear extrapolator is used for this work that passing through the past $Q=3$ frames for extrapolation of each frequency frame. For interpolation in TFM matrix, $P=2$ future frames are also included. These rules can be extended for burst losses and reconstructed in the same manner.

4.7 Performance Evaluation

4.7.1 Packet Loss Model

There are two widely used packet loss models that introduce frame loss in speech signals: (i) Bernoulli distributed frame loss model for independent and identically distributed (i.i.d.) losses where the probability of a frame loss is p and is independent from the state of other frames [55], and (ii) Gilbert-Elliott, 2-state hidden Markov model (HMM) [196], [197], for burst data loss as shown in Figure 4-5. In the Gilbert model, the duration and rate of burst loss are controlled by state transition probabilities, p and q.

Since the results of these methods are comparable, the Bernoulli model is operated for objective evaluation, and Gilbert model is employed for the subjective test. Note that, the Bernoulli model is a special case of the 2-state HMM when the $q=1-p$. The loss rate, α_L , and the average gap length, β_L , of a 2-state model can be calculated as follow:

$$\alpha_L=\frac{p}{p+q}\ \text{ and }\ \beta_L=\frac{1}{q} \tag{4.9}$$

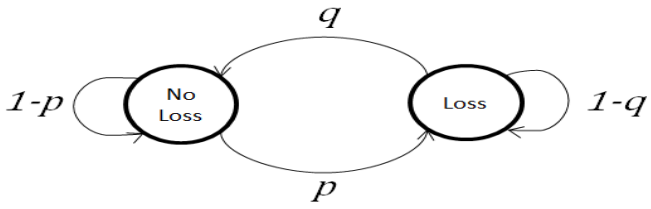

Figure 4-5: Gilbert-Elliott 2-state HMM model for packet loss.

Furthermore, the performance of the algorithm for the restoration of different gap lengths is also evaluated.

4.7.2 Experiment Setup

The proposed PLC method is evaluated for both objective and subjective tests on audio (speech and music) signal with bandwidths of 10kHz to 20kHz and the corresponding sampling rates of 44kHz to 48kHz which were resampled to 8kHz or 16kHz to do the objective evaluation test. The segment length was set to 25ms and segment shift to a quarter the segment length. Each sample is represented by 16 bits.

Note that, as shown in Figure 4-2, for the purpose of forming TFM, successive speech segments are overlapped. When a packet loss occurs, only one previous TFM frame that overlaps with the lost one is unavailable for extrapolation if half overlap is chosen, whereas three previous TFM frames that overlap with the lost one are unavailable for extrapolation if 75% speech segments overlap is selected. This rule is applied to the interpolation method as well.

As declared before, the DFT format is developed for forming the TFMs and then compared with the DCT format. Furthermore, it is common practice to apply a window to signal segments to mitigate end-discontinuity effects. The Hann window is also engaged to perform a Fourier transform of signal segments. The signal before and after the gap is windowed using a 25ms long Hann window (segment length) with a 6.25ms overlap (a quarter of the segment length). The gap length is a multiple of 6.25ms. The parameters are then extracted from the overlapping frames and extrapolated-interpolated through the gaps that result in a smooth transition period of 6.25ms on each side of the gap. In addition, the packet loss model used for the objective test is the Bernoulli model with packet loss rates varying between 5% and 20%. To mitigate unnatural sound that was produced during the extrapolation of a long sequence of missing packets, attenuation technique is applied when more than one packet frames are lost. This method is common and similar to the one that is engaged in ITU standards such as G.711, G.729, and G7.28 [114], [116], [117].

The results are compared to some alternative methods including i) a LP-HNM model of speech where the spectral envelope is modelled using an LSF representation of a linear prediction (LP) model [55], ii) method proposed by Lindblom and Hedelin [128] which is based on interpolation of harmonics in a sinusoidal model (SM) for excitation, iii) The multirate technique [126] based on time-domain AR modelling of the signals, and iv) The

ITU standard packet loss concealment algorithm G.711 [114]. The results presented in this chapter relate to DFT and comparison with DCT.

4.7.3 Experiments on Synthesised Time-Varying Signals

The proposed method is tested and applied to a selection of synthesised time-varying signals to compare the proposed DFT-TFM technique with DFT method without motion as shown in Figure 4-6 and Figure 4-7. These figures provide a comparison of two synthesised time-varying signals. Both figures show part of the spectrogram of a synthesised signal with lost packets, the proposed DFT-TFM signal, and DFT method without motion. It is clear that the proposed technique improves performance especially when the loss occurred in different frequency bins.

In addition, the DFT interpolation (DFTI) model without motion is also presented in Figure 4-7. The DFTI model utilises the future frames as well as previous frames for estimating a missing gap and achieves better result compared to the DFT method. However, since the frequency partial changes rapidly between time frames, the proposed DFT-TFM method performs better than both the DFTI and DFT methods. This is because the proposed method employs motion trajectory for reconstruction, although it only uses the previous frames. These figures clearly illustrated that the frequency bins of the spectral power could change across time frames and extrapolation/interpolation from the previous frequency frames or from previous and future frames for estimating the lost packets are not always give the correct result especially when the motion trajectory follows some movements. This is highlighted (circled) in all three reconstruction methods in Figure 4-7.

In these experiments, the overlap between successive signal windows is set to three-quarter overlap. Hence due to overlap, three previous and future frames are affected and cannot be used to estimate the lost frames. In terms of packet loss model, the Bernoulli frame loss model employed for objective tests and Gilbert model loss utilised for subjective tests.

In addition, the DFT-TFM and DCT-TFM techniques were compared, and as we expected, both methods perform well and give a similar result. However, when two or more packet losses happen close to each other, the DFT-TFM method performs slightly better. Thus in this work, the result related to DFT-TFM model is presented.

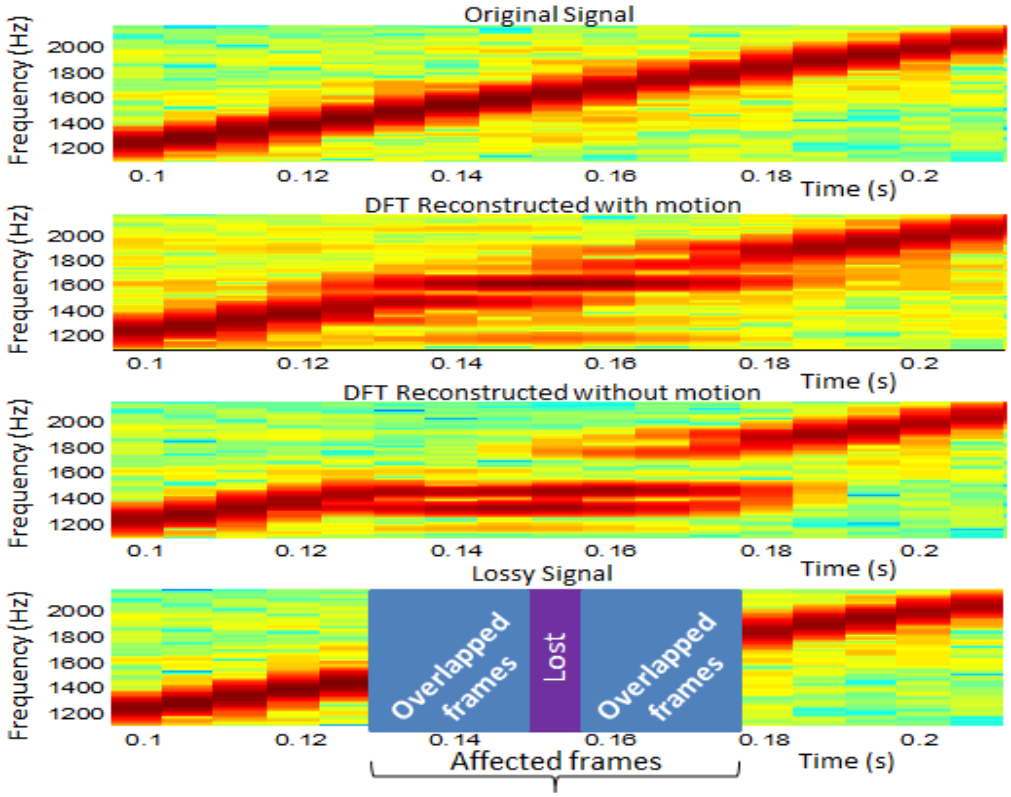

Figure 4-6: Spectrogram of synthesised signal, from top: original signal, DFT-TFM, DFT, and signal with 20% Bernoulli frame loss

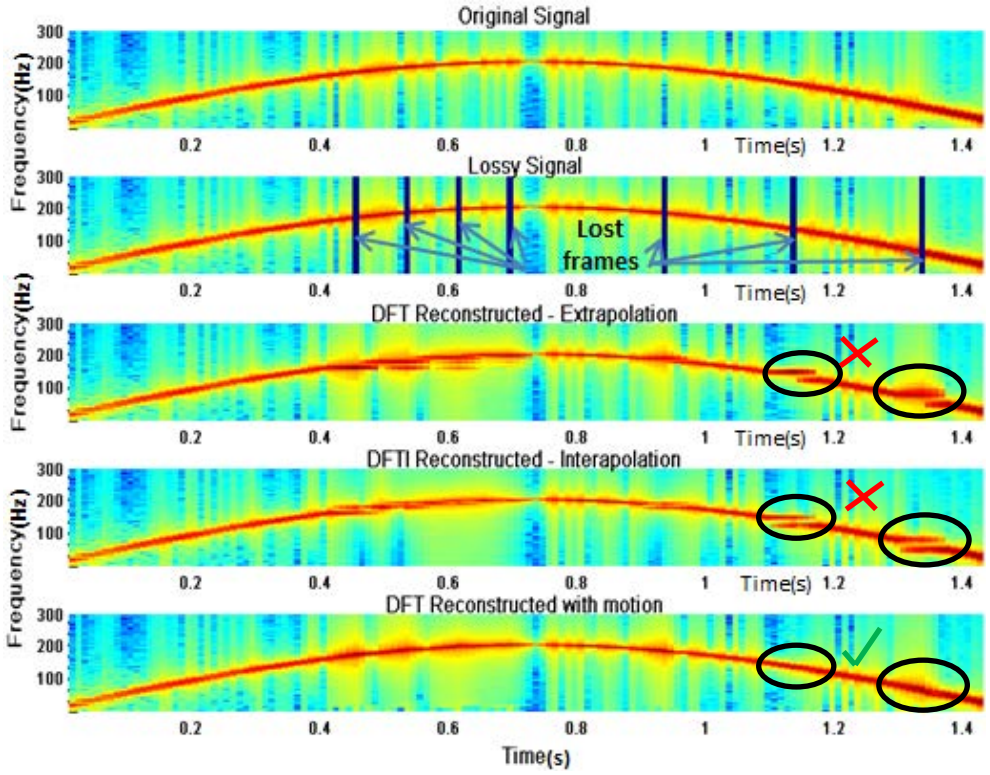

Figure 4-7: Spectrogram of the synthesised time-varying signal, from top: original signal, lossy signal, DFT- Extrapolation, DFTI- Interpolation and DFT-TFM signal.

4.7.4 Experiments on Audio/Speech signals

In this section, the proposed technique is applied to the database containing speech and music samples. Figure 4-8 shows part of the spectrogram of a Civil-Right's speech signal, a signal with lost, DFT and DFT-TFM reconstructed signals. The result illustrates that the proposed technique performs well compared to DFT method, especially for reconstructing the first and last lost frames, where the spectral power moved across the frequency bins.

Furthermore, Figure 4-9 displayed the time-domain signal of the Civil-Rights speech, a signal with three random lost packets, DFT without motion and proposed DFT-TFM reconstructed the signal. The result indicates that the DFT method is not effective as the proposed DFT-TFM method. This is because, in DFT method, the motion trajectory cannot be tracked as effectively as the proposed method.

4.7.5 Objective Evaluation

For this experiment, the signals that contain gaps employing the Bernoulli distributed random lost frames [55], [197], are reconstructed by using the proposed DFT-TFM method and the conventional methods mentioned earlier. Perceptual Evaluation of Speech Quality, (PESQ, ITU-T P.862) [198], is utilised for comparison. The results are calculated and averaged for one hundred sentences randomly selected from TIMIT database are summarised in Table 4-1.

The results in Table 4-1 indicate that the proposed method performs well and achieves higher score compare to other algorithms in terms of PESQ measurement and improve performance by an average of 2.85% compared to the best conventional method [55]. The improvement calculated as:

$$improvement = \frac{ps - cs}{cs} \times 100 \tag{4.10}$$

where ps is the score of proposed method and cs is the score of best conventional technique. As an example for 10% loss rate according to Table 4-1 we have:

$$Improvement = \frac{3.28 - 3.20}{3.20} \times 100 = 2.5\% \tag{4.11}$$

where values 3.28 and 3.20 belong to the DFT-TFM and the LP-HNM "*pesq*" scores respectively. Moreover, Table 4-1 shows that the performance of G.711 and LP-HNM

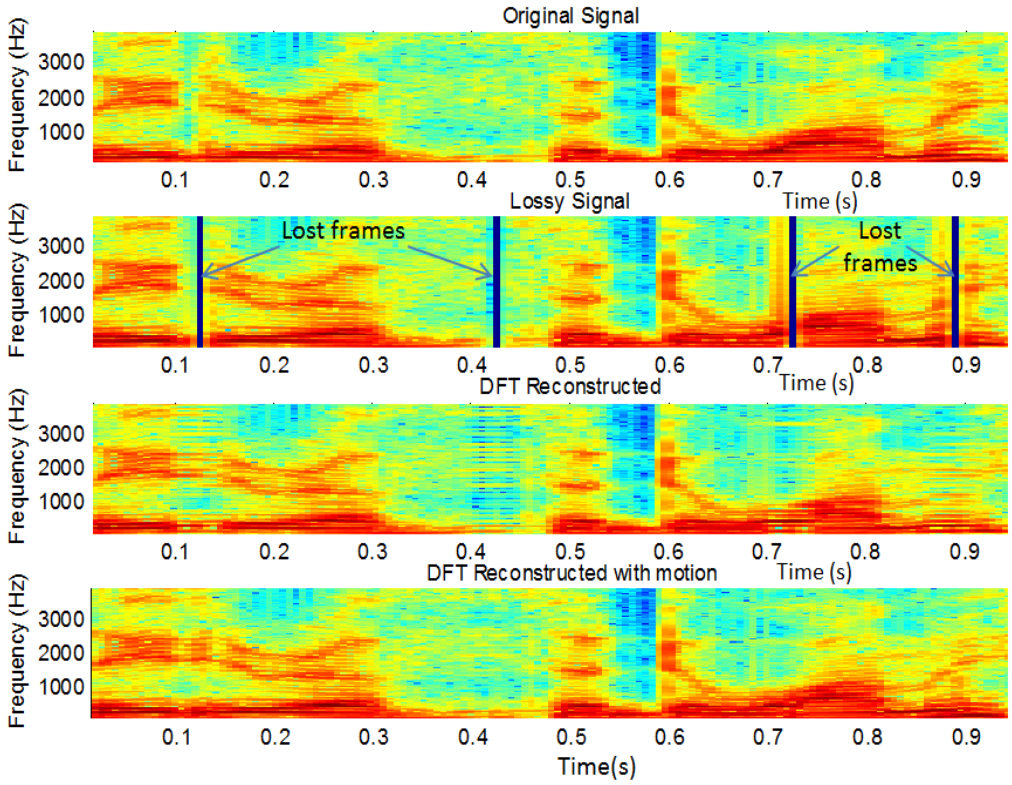

Figure 4-8: Spectrogram of the Civil Rights speech from the - United States, from top: original signal, lossy signal, DFT-without motion and DFT-TFM signal.

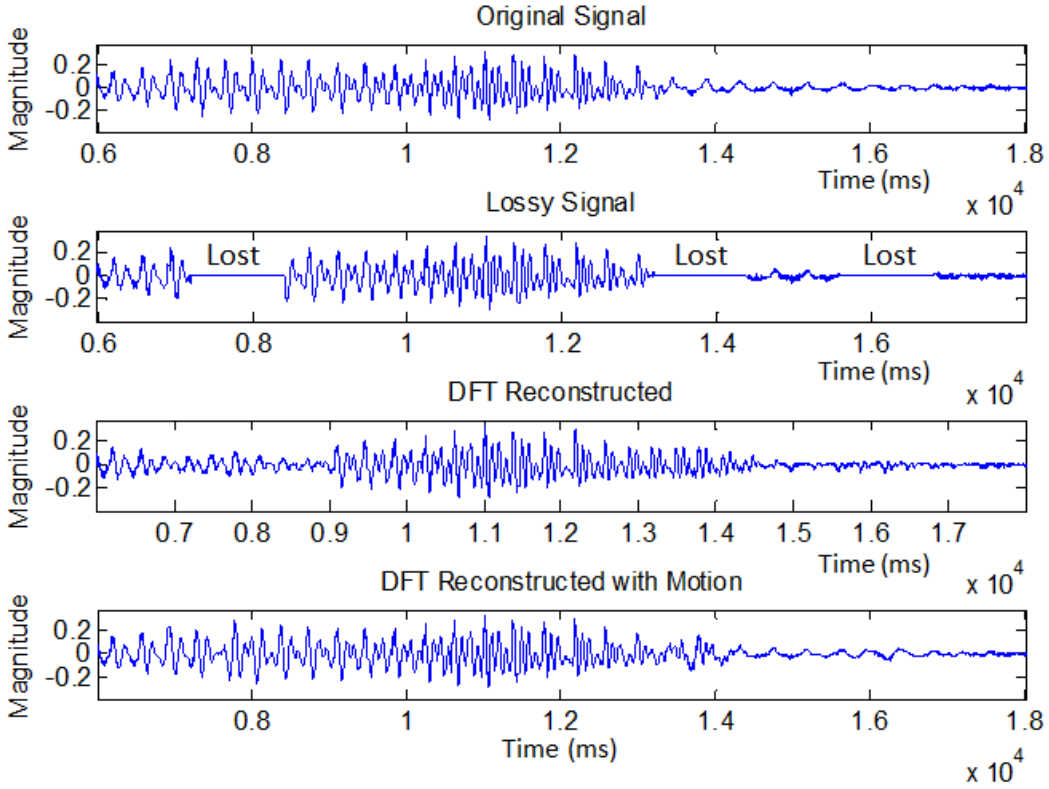

Figure 4-9: Time-domain signal of Civil Rights speech, from top: original signal, lossy signal, DFT-without motion and DFT-TFM (with motion) signal

models are good at lower loss rates, but deterioration is increased for higher loss rates. The LP-HNM and SM algorithms interpolated the envelopes throughout the gap and performed better than the multirate method and G.711 at higher loss rates or longer gaps.

Furthermore, the proposed technique illustrates better performance to longer frame loss compared to other methods. It should be considered that the G.711 method is designed to cope with 60ms of loss and deteriorates quickly for loss periods more than that.

4.7.6 Subjective Listening Test

A set of five random wideband speech and music samples that are used for this experiment are listed in Table 4-2. Signals are about 14-18 seconds long, with a fixed packet loss rate of 20% and different average gap lengths of 2, 5 and 7 frames employing the Gilbert model introduced in the previous section. The reason that 20% gap has been chosen because this range of packet loss rate is more difficult and challenging to reconstruct by the conventional methods and it is one of the worst-case scenarios. In particular, when the average gap length is 7 frames, that equivalent to 70ms, which may represent a burst of packet loss in telecommunication system.

To evaluate the result after applying the gaps, each sample was reconstructed using the proposed DFT-TFM and DCT-TFM techniques, LP-HNM method [55] and G.711 [114] algorithm. Subjective tests were carried by 12 subjected listeners aged between 22 to 31 years in a quiet room using headphones. The listeners were asked to compare the quality of the speech that degraded by packet losses with the enhanced speech where the lost packets were replaced using DFT-TFM, DCT-TFM, LP-HNM and G.711 algorithms in random order. Listeners' preferences were recorded by using the mean opinion score (MOS) point-based assessment where the scores vary from 1 (bad) to 5 (imperceptible degradation). Table 4-3 displays the score results of this analysis where the average of corresponding confidence intervals for 95% was ± 0.25. The result verifies that the proposed technique performs better than other methods and achieves higher subjective quality. Note that, the extent of validity of these outcomes is limited by the number of listeners and audio samples employed. The average improvement of 5.9% has been achieved in terms of MOS using (11) where ps was the score of proposed algorithm and cs was the score of LP-HNM method from Table 4-3. Furthermore, Table 4-3 indicates that the proposed DFT-TFM method achieves slightly better result than the DCT-TFM technique.

Table 4-1. Performance of different algorithms for restoration of Bernoulli generated gaps (PESQ Result)

Loss Rate %	5%	10%	15%	20%
Av.Gap Length	1.05	1.11	1.18	1.25
Distorted Signal	3.43	2.71	2.49	2.28
LP-HNM [13]	3.82	3.20	3.02	2.81
G.711 [7]	3.80	3.19	2.97	2.73
SM [15]	3.60	2.98	2.71	2.56
Multirate [16]	3.58	2.75	2.54	2.35
DFT-TFM	3.91	3.28	3.10	2.92

Table 4-2. Audio, speech and music samples

No.	File Name	Sampling Rate	Type of Audio
1	Barack Obama - Berlin	22050	Speech
2	Speech on Women's Right		
3	Civil Rights – United States	44100	
4	Abraham Lincoln		
5	Adele – Take It All	48000	Music

Table 4-3. Comparative subjective results of proposed methods with a loss rate of 20% against LP-HNM and G.711

(q,p)	(0.5,0.3)	(0.2,0.13)	(0.14,0.95)
Loss Rate%	6.67	16.67	23.33
Av.Gap Length	2	5	7
DFT-TFM	4.17	3.42	3.00
DCT-TFM	4.08	3.33	2.92
LP-HNM [13]	3.92	3.25	2.83
G.711 [7]	4	3.25	2.75

4.8 Conclusions

In this chapter, a technique is proposed for the enhancement of audio signals that have been degraded in quality and performance by missing segments. The proposed algorithm is shown to improve the audio signal's quality particularly in Figure 4-7 and Figure 4-8.

Time-frequency matrix algorithms developed and discussed in this chapter and industry were explored. The time-frequency algorithm of spectral motion was the main focus of this chapter. This algorithm utilised short time DFT components and tried to reconstruct the lost segments in the received audio signal.

The problem of the restoration of gaps in an audio signal was addressed and a novel solution of packet loss concealment is presented in connection with audio signals based on a *time-frequency motion (TFM) matrix*. It is observed that the proposed technique gives better performance compared to the conventional methods in terms of objective and subjective quality evaluations for audio enhancement.

The novel aspect of this methodology is the introduction of TFM and its application to spectral motion-compensated extrapolation and/or interpolation for audio signals. The spectral motion vectors were estimated by dividing the signal bandwidth into several sub-bands. The cross-correlation of the frequency bands across time frames has been used for motion estimation. The objective and subjective evaluation experiments reveal that the proposed method compares well with conventional methods, with the results superior in output quality in terms of PESQ and MOS measurement scores.

The PESQ scores were utilised as the objective quality measurement of the audio enhancement technique as according to Zavarehei [199] (appendix. A) it is highly correlated with MOS scores.

Moreover, there are some complex statistical algorithms that may estimate the lost packets more accurately, but the majority of these algorithms are very computationally demanding, to the extent that they are not feasible in practical applications.

Chapter 5

5 Optimisation of SSP input parameters for Synthesised UGW Signals

5.1 Chapter overview

The motivation of this chapter is to find a solution to address the problem of coherent noise[10] in UGW signals that can obscure reflections from features in the pipe under inspection. Therefore, the main concern of this part was to find a post-processing solution to reduce the level of coherent noise in the received signal. The literature review in Chapter 3 confirmed that conventional signal processing approaches are not fully successful in reducing/removing the coherent noise of UGW signals and therefore an advanced method is required. As a result, in this chapter, a novel signal processing technique, based on time-frequency analysis, called split-spectrum processing (SSP) is proposed for the reduction of coherent noise due to the presence of dispersive wave modes (DWM) and enhanced the spatial resolution for such signals. To progress the study of SSP, two fundamental issues have been identified; i) the selection of optimum filter bank parameter values, and ii) its appropriate recombination algorithms for the use of SSP in UGW testing.

The SSP technique that we have developed is applied to the synthesised experimental UGW signal for the restoration of signals suffering from coherent noise, to increase the sensitivity and inspection range of UGW testing. The fundamental knowledge and literature review of SSP is fully explained in Chapter 2 and Chapter 3 respectively. In this chapter its implementation, including an explanation of selecting optimum filter bank parameters, and processing of filter sub-bands is fully covered. In addition, the initial signal processing of generating synthesised signals is described in this chapter, which is required to analyse and find the limitations of SSP application.

It is demonstrated throughout this chapter that the proposed technique, when compared to the conventional techniques reported in the literature, substantially improves the

[10] [10] The explanation of coherent noise in the UGWs testing is given in Chapter 2.

sensitivity and spatial resolution of signals in terms of signal-to-noise ratio (SNR), detecting smaller defects hidden below the noise level, as well as increasing the inspection range. The research conducted in this chapter has been presented at the *International Congress of Ultrasonics (ICU)*, Metz, France, 2015 and the *1st National Structural Integrity Research Centre (NSIRC) Annual Conference*, TWI Cambridge, United Kingdom, 23 June 2015. Moreover, the result of this chapter is published on Special Issue of Ultrasonics Journal paper on ‘‘*Ultrasonic advances applied to materials science*”, Feb 2017. The background theory of this technique is described in Chapter 2. In addition, the reader is provided with a step-by-step procedure for the employment of the SSP application utilised in this section, followed by the necessary mathematical implementation for each step.

5.2 Split-Spectrum Processing (SSP)

Reducing coherent noise is not only a challenging task for UGW inspection. It is also a problem for many other applications, such as NDE, medical ultrasound, radar, etc., where many studies and much research have been applied for over a decade to address the issue of coherent noise. SSP is one of the most advanced post-processing techniques to gain recent attention, particularly for grain noise suppression in NDE applications.

The background and the literature review of SSP application are described in Chapter 2 and Chapter 3 respectively. This chapter covers the development of SSP applications. Then, the structure of the fundamental parameters that are the key elements in the use of SSP is described, followed by an explanation of the selection of the filter-bank parameter values. Furthermore, the calculation methods are discussed and the optimised filter-bank parameters are proposed to improve the SNR and the spatial resolution of the UGW signal. The selection of filter-bank parameter values was first inspired by the values introduced for the use of SSP application in conventional ultrasonic testing (UT). The performance of the SSP technique is highly sensitive to the selection of filter-bank parameter values. The literature review of SSP clearly shows that the selection of filter-bank parameter values for the use of SSP in conventional UT are not suitable for use in GWT. Therefore, the core concept of this chapter is to investigate and propose suitable filter-bank parameter values in order to optimise the results of SSP by quantifying the enhancement of SNR and spatial resolution of signals. To obtain this, an empirical approach is utilised, whereby the parameter values are varied, and the test performed more than 100 times for synthesised

UGW signals to investigate the optimum values, and then in order to validate the results experimental tests are carried out in the lab, as will be explained in Chapter 6. In addition, the proposed technique with the optimum filter-bank parameter values is applied to the synthesised signals in order to find a distance limitation of SSP application when a feature (i.e. defect) with small amplitude is close to a dominant feature (i.e. welds, flange) with high amplitude.

In GWT, the velocity of DWM is a function of frequency, so dispersive components of the received signal will vary across the SSP sub-bands, whereas the non-dispersive components stay constant. Therefore, SSP technique may be used to suppress regions of the signal that vary across the bandwidth, reducing the effects of DWM. Since the coherent noise mostly appears to be due to the presence of DWM, thus, the SSP technique has the potential to improve the SNR and enhance the spatial resolution of the received UGW signals. The use of SSP in UGW testing is relatively new and to the best of the author's knowledge, this technique has not been fully investigated previously in the field of UGW.

5.3 Implementation of SSP

In this section, the implementation of SSP application is explained in more detail. The input signal is the unprocessed UGW signal in the time domain, converted to the frequency domain for post-processing. This signal is filtered in the frequency domain to generate a set of sub-band signals, as described in Section 5.2. The result is then multiplied by a Gaussian window function in each sub-band signal individually to produce the sub-band outputs. Subsequently, in order to create the output signal, a number of different SSP recombination algorithms are introduced to the outputs of the sub-band signals. Furthermore, to achieve a good SNR enhancement, the selection of the SSP filtering scheme is studied.

5.3.1 Filter Bank Parameters

The SSP filter-bank parameter values were first investigated by trial-and-error for NDT applications as they were processed. However, this was not very practical for field inspection as there are typically large amounts of data to analyse; therefore, several researchers sought to find the optimum value of the filter-bank parameters in the use of NDT, and particularly for conventional UT. Hence, the optimum values of filter bank parameters have been proposed, developed and examined for the conventional UT

techniques, as described in the literature review in Chapter 3. However, these values are not suitable for UGW signals due to the long duration and narrow bandwidth of the UGW signal that operates in the kHz range, whereas the traditional UT operates in the MHz range [200]. Therefore, further investigation was required to find an optimum value, suitable for UGW testing. As a result, the rules and key factors of parameter selection for conventional UT have been reviewed, followed by a discussion of the selection of the optimum filter-bank parameter values for UGW testing.

The general SSP filtering scheme is displayed in Figure 5-1. The parameters that require to be specified for spectral splitting are: i) the number of filters (N), ii) the total bandwidth for processing (B), iii) the filter bandwidth (B_{filt}), iv) the filter crossover point (δ), and v) the filter separation (F). These parameters are listed in Table 5-1 with its recommended values that are briefly explained here. These parameters are dependent on each other, which mean that their values have a direct effect on other parameter values. Therefore, it is necessary to search for the optimum parameters and select them appropriately. As an example, increasing the number of filters (N), would require to increase the total bandwidth for processing (B) or reduce the filter separation (F), or a combination of both. Therefore, according to Figure 5-1 the number of filters (N), could be calculated as follows:

$$N = B/F \ + 1 \tag{5-1}$$

5.3.1.1 Total Bandwidth for Processing

The total operating bandwidth for processing (B) should be such that the signal's reflection from features in the specimen are constant across this range and the reflection from coherent noise varies. If the bandwidth is too wide then at least one of the filter outputs will not include the feature signal, and this may cause the feature to be lost and reduce the

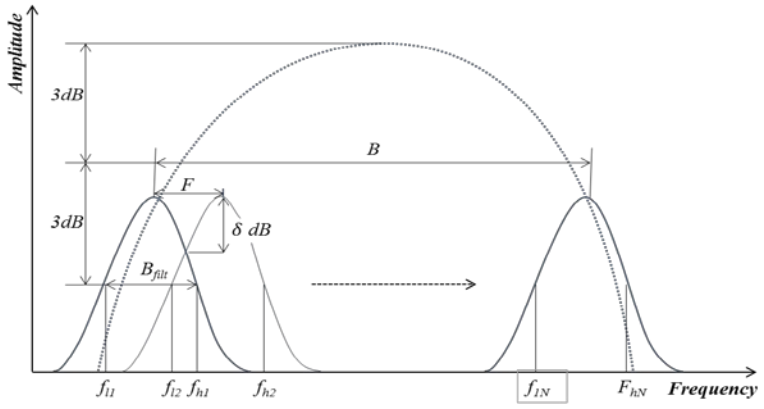

Figure 5-1: SSP filter bank parameters

Table 5-1: The recommended values for SSP parameters

SSP parameters	Symbols	Recommended values
The total bandwidth	B	99% of total energy
Sub-band filter bandwidth	B_{filt}	$B/11$
Filter crossover point	δ	$B_{filt}/3.5$
Filter separation	F	$1\ dB$
Number of filters	N	$B\ /\ F + 1$

spatial resolution in the processing. In conventional UT, the transmitted signal is usually an impulse function and, therefore, the bandwidth is limited by the frequency response of the transducers. As a result, the processing bandwidth in conventional UT is often the frequency response of the ultrasonic transducers.

Many researchers have investigated the effect of the material on the bandwidth of the transmitted pulse in conventional UT signals, such as Karpur et al. [158] who proposed the optimum processing bandwidth for this purpose.

In order to reduce the effect of unwanted wave modes and to suppress the dispersion effect in UGW testing, narrowband waveforms (such as Hann windowed sine waves of 5 to 10-cycles in length) were used as the excitation signals. Therefore, the bandwidth of the transmitted signal can be used for SSP total bandwidth of processing while considering the frequency response of the transducers. Alternatively, Stepinski et al. [171] proposed consecutive polarity coincidence, which involved identifying the region in time where the signal was constant across the largest frequency range and setting the total bandwidth for processing equal to this frequency range. This was an adaptive method to define the optimum processing bandwidth from the input signal.

5.3.1.2 Sub-band Filter Bandwidth

Sub-band filter bandwidth (B_{filt}) is the width to be used for each filter in the filter bank. It was recommended by many researchers, such as Shankar et al. [159], Aussel [160], and Rose et al. [157] that the value of the filter bandwidth (B_{filt}), needs to be set at three to four times the filter separation (F). It should be noted that a bandpass filter could reduce the temporal resolution of the signal. This is because reducing the bandwidth of a time-limited signal will increase its duration. This means that applying the SSP filter banks could lead to a reduction in temporal resolution if not chosen appropriately, as the pulses that correspond to reflections from features spread out in time and mask one another.

Mallet [13] investigated the effect of band-pass filtering on the temporal resolution of a signal and looked at the changes in duration of a simulated reflection after filtering. The result of filtering showed that the pulse became lengthened in time and its amplitude was reduced. The Gaussian filters in SSP are spread across the total processing bandwidth, which leads to poorer temporal resolution. This result is unchanged regardless of whether the deviation is negative or positive. Therefore it was suggested that the centre frequency that can use for the filters needs to be equal to the upper 3dB cut-off frequency of the input signal. This is the maximum deviation that can be used for a bandpass filter in SSP from the signal centre frequency.

Additionally, the filter overlap could affect the correlation between adjacent sub-bands, such that as the overlap increases, the correlation increases [156]. However, little or no overlap can lead to loss of information. In SSP, the noise signal in adjacent filters should be uncorrelated, and the features should be correlated. Therefore, the overlap chosen should minimise the correlation between coherent noise regions in adjacent sub-bands without losing information. Furthermore, the cosine filters have been investigated by Karpur and Canelones [185], who found that compared to Gaussian window function, cosine filters achieved a better result in terms of correlation without losing any information.

5.3.1.3 Filter Separation

Filter Separation (F) is the distance between sub-band filters, as is shown in Figure 5-1. Karpur et al. [21] in 1987 developed a theoretical scheme of parameter selection in SSP for conventional UT. It was reported that optimum spectral splitting could be achieved using the frequency-sampling theorem. The frequency-sampling theorem says that the spectrum of a time-limited signal can be reconstructed from its sample points in the frequency domain separated by $2\pi/T$ rad/s or $1/T$ Hz, where T is the total duration of the signal; based on this, the SSP filter separation for UT is calculated as:

$$F = {}^{1}/_{T} \tag{5-2}$$

However, this is based on the use of Sinc functions, whereas in practice the Gaussian filter is employed for the filter bank because of its simplicity, and, as a result, some parameters obtain a larger value than expected.

5.3.2 Implementation of the Filter Bank

A Matlab program is developed throughout the research that takes an unprocessed signal in time domain and converts it to the frequency domain. Then it filters the signal in the frequency domain to generate a set of sub-bands signal and applies a number of different SSP recombination algorithms, as explained in Chapter 2, into these sub-bands. The filter bank covers the total bandwidth, (B) as illustrated in Figure 5-1. The received unprocessed signal is filtered using a Gaussian bandpass filter in the frequency domain by multiplying its Fourier transform by a Gaussian window. The input to this function is the signal to be filtered, its sampling frequency and the upper and lower 3dB cut-off frequencies. In order to implement the filter bank, a set of 3dB cut-off frequencies for the Gaussian filters are applied. The lower cut-off frequen*cy* f_l *a*nd the higher cut-off frequency f_h for each sub-band filters are calculated as follows:

$$f_{l_n} = \begin{cases} f_{min} - \dfrac{B_{filt}}{4} & n = 1 \\ f_{l_{n-1}} + F & n = 2,3, \dots N \end{cases} \tag{5-3}$$

$$f_{h_n} = f_{l_n} + B_{filt} \qquad n = 1,2, \dots N \tag{5-4}$$

where N is the number of filters, F is the filter separation, B_{filt} is the sub-band filters and f_{min} is the lower cut off frequency of B. The lower cut off frequency for the first sub-band f_{l_1} needs to cover the start point of the signal, thus it is selected as shown in (5-3). The selections of these values are inspired by the values that have been employed in conventional UT. In order to find the optimum values for UGW testing, a brute force search is applied. The selection of filter bank parameters is explained in this Section. However, as stated before, these parameters are interrelated, hence, it is required to specified some parameters and check the others and vice versa to find the optimum values.

The filter bandwidth (B_{filt}) in a case where the 3dB cut off frequencies send to the Gaussian filter function is calculated as follows:

$$B_{filt} = \frac{B}{N} \tag{5-5}$$

This equation (5-5) is only applicable to the crossover point values of δ=3dB while for other crossover point values it is necessary to find a new filter bandwidth ($B_{new-filt}$) as:

$$B_{new-filt} = \left(\frac{p_{3dB} - x_c}{p_\delta - x_c}\right) \times B_{filt} \tag{5-6}$$

where p_δ is a new crossover point, and p_{3dB} is the crossover point when δ=3dB for a Gaussian filter function, as presented in Figure 5-2.

5.3.3 Selection of SSP Filter Bank Parameters for UGW testing

The SSP parameter selection rules utilised for conventional UT signals were soon found to be unsuitable for UGW applications. This is due to the long duration and narrow bandwidth of the UGW signal, which operates in the kHz range whereas the traditional UT operates in MHz range [200]. Karpur et al. [156] described a way to calculate the filter separation using (5-2). This led to a large number of sub-band filters, requiring either a large overlap or a narrow bandwidth. The large overlaps between the sub-band filters mean that the filters are highly correlated, which can compromise the performance of SSP at removing coherent noise. On the other hand, using narrowband filters can lead to the loss of signal responses when applied to the sub-band filters and subsequently in the output of SSP application.

Therefore, the optimum SSP parameters are determined synthetically using a brute force search through the essential SSP parameters, i.e. the total operating bandwidth (B), the sub-band filter bandwidth (B_{filt}), the filter crossover point (δ), and the filter separation (F). Moreover, the number of filters (N) is calculated using (5-1). As mentioned before, the filter bank parameters are interdependent, hence it is necessary to search for the optimum parameters in parallel and select them appropriately. The ranges of values selected for the brute force search algorithm are inspired by the values employed for conventional UT. This offers the benefit of having an appropriate bandwidth that can be applied to different frequencies or different pulse lengths signals. Note that, the operation bandwidths of processing will be increased by selecting the shorter pulse lengths or higher

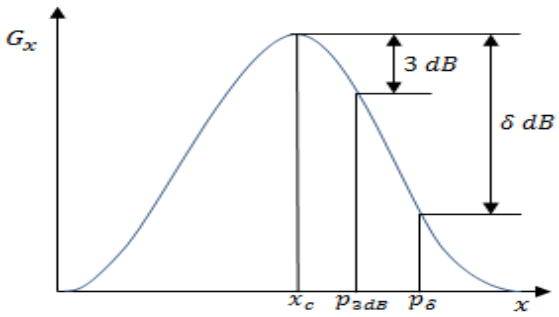

Figure 5-2: A Gaussian filter function

frequency signal. However, this condition is not valid when the operation bandwidth is defined in Hertz. It would be an advantage to select the sub-band filter bandwidth (B_{filt}) as a portion of the total operation bandwidth, thus the optimum values could be fixed for any UGW signal.

Therefore, to start searching for the optimum filter bank parameter values, a portion of the frequency spectrum of the signal selected as the total operating bandwidth (B) and fed into the brute-force search algorithm as follows:

- Step 1: The range of the total operating bandwidth of processing (B) is altered from the signal bandwidth containing 84% to 100% of the frequency spectrum in steps of 3%.
- Step 2: The sub-band filter bandwidth (B_{filt}) is varied from the total operating bandwidth value (B) divided by 3 to the total operating bandwidth value divided by 15 in steps of 2. The selection of the sub-band filter bandwidth range is a tradeoff between loss of temporal resolution and the number of filters.
- Step 3: The filter separation (F) is varied from the value of sub-band filter bandwidth (B_{filt}) divided by 1 to 7 in steps of 1.
- Step 4: The filter crossover point (δ) is varied from 1 dB down from the filter peak to 9 dB down.

The performance of SSP is quantified by measuring the SNR and spatial resolution of the output UGW signals.

5.4 Signal Synthesis

The initial development and implementation of synthesised UGW data employed for analysis of SSP application are explained in this section.

5.4.1 Synthesised UGW Data

The signal synthesis presented by Wilcox [141] is employed in order to synthesise the propagation of the DWM in time/space [73], [96]. The technique is based on applying a frequency-dependent phase shift to the wave packet of interest. This phase shift depends on the phase velocity of the wave mode, which is a function of frequency. This can be extracted from the dispersion curves generated via DISPERSE software, which is

developed by Imperial College [100]. It is assumed that the dispersive wave packet g(t), has been propagated at a distance of x= 0. This signal has been converted to the frequency domain by taking the fast Fourier transform as follows:

$$G(\omega) = \int_{-\infty}^{\infty} g(t)e^{-j\omega t}dt \tag{5-7}$$

where ω=2πf, is the angular frequency and f is the frequency. A transfer function, H(ω), is then required to find g(t) at a given distance, x = d, related to g(t) at x= 0 which for the dispersion of a single wave mode can be calculated as [100]:

$$H(\omega) = \frac{[G(\omega)]_{x=d}}{[G(\omega)]_{x=0}} \tag{5-8}$$

the transfer function for a single DWM is:

$$H(\omega) = e^{j\omega\frac{x}{v_{phase}(\omega)}} \tag{5-9}$$

where $v_{phase}(\omega)$ is the phase velocity of the wave mode, which is a function of frequency, thus:

$$[G(\omega)]_{x=d} = [G(\omega)]_{x=0} \times e^{-j\omega\frac{x}{v_{phase}(\omega)}} \tag{5-10}$$

$k(\omega)$ is the circular wave number as given in (5-11):

$$k(\omega) = \frac{\omega}{v_{phase}(\omega)} \tag{5-11}$$

Then (5-10) can be written as:

$$[G(\omega)]_{x=d} = [G(\omega)]_{x=0} \times e^{-jk(\omega)x} \tag{5-12}$$

So, the inverse Fourier transform could be defined as:

$$f(t) = \frac{1}{2\pi}\int_{-\infty}^{\infty} F(\omega)e^{j\omega t}d\omega \tag{5-13}$$

Therefore, the dispersive wave packet at a distance of $x = d$, $[g(t)]_{x=d}$, could be calculated as by employing the inverse FFT as below:

$$[g(t)]_{x=d} = \frac{1}{2\pi}\int_{-\infty}^{\infty} G(\omega)e^{j(\omega t - k(\omega)x)}d\omega \qquad (5\text{-}14)$$

Figure 5-3 shows the phase velocity dispersion curve for the axisymmetric signal, T(0,1) wave mode, with its family of flexural wave modes: F(1,2), F(2,2), F(3,2), F(4,2), F(5,2), and F(6,2) using DISPERSE software. This is a six-inch diameter steel pipe with an outside diameter of 168.28 mm and a wall thickness of 7.11mm. The combination of these wave modes is used in a single complicated waveform. Figure 5-3 presents the behaviour of phase velocity of these wave modes in terms of frequency; for instance, it is shown that the phase velocity of the T(0,1) wave mode is constant across the frequency bandwidth of interest, whereas all the flexural wave modes' velocities are frequency dependent. The excitation centre frequency of 50kHz is employed for this test and a dashed line illustrates the behaviour of all wave modes around this particular centre frequency. Higher order flexural wave modes also exist, but as they are more dispersive in this region; the first six orders modes employed here, which are more difficult to remove.

Figure 5-4 illustrates the propagation of a dispersive wave mode F(5,2), using the aforementioned synthesised modelling technique for a nominal six-inch steel pipe. The distance incrementally varies from x=1 to x=5 metres. It is clearly shown that as the propagation time increases, the signal's energy spreads out over space.

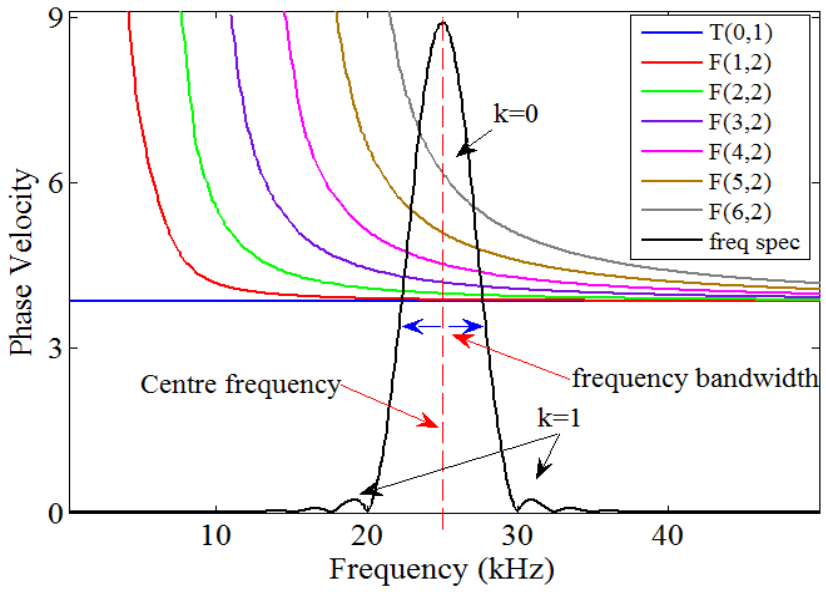

Figure 5-3: Phase velocity dispersion curves for a six-inch pipe overlaid with the frequency spectrum of a 50kHz 10-cycle Hann windowed pulse. The main and first side lobes are displayed to clarify that the pulse will have a frequency bandwidth corresponding to a phase velocity bandwidth of each wave modes.

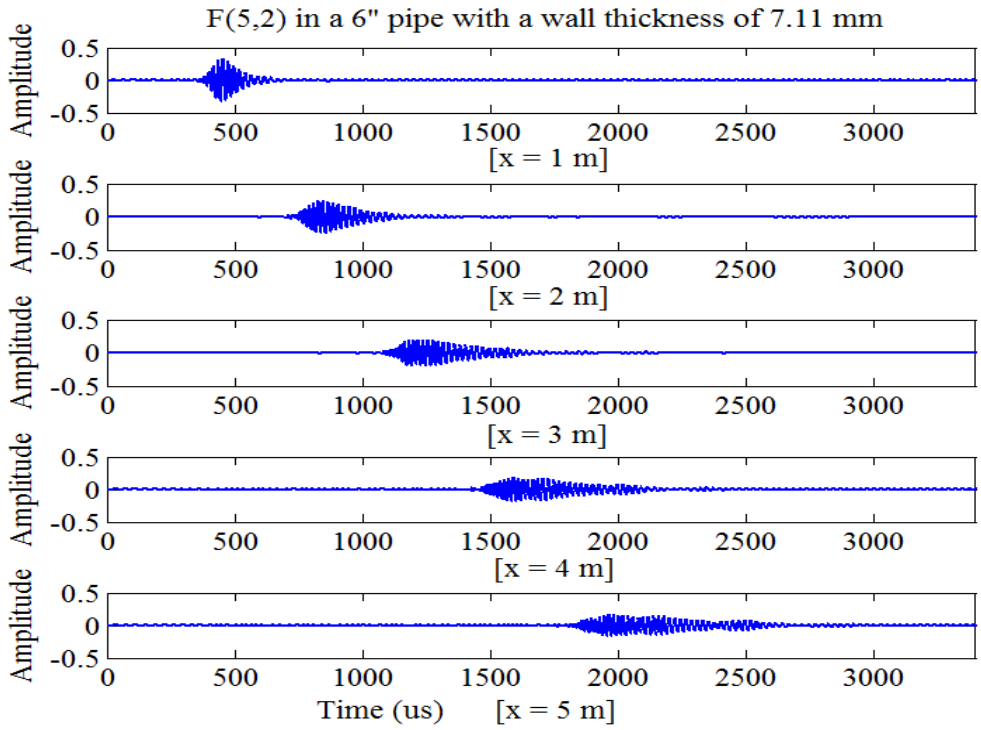

Figure 5-4: Synthesised dispersive propagation of, F(5,2) wave mode. Frequency = 50kHz

5.4.2 Implementation of Synthesised UGW Signals

The technique described above is used to generate a synthesised UGW signal [11], [141]. Figure 5-5 illustrates a 10-cycles pulse with a centre frequency of 50kHz including T(0,1) and its flexural wave modes family up to F(6,2). These wave modes are propagated three meters along a six-inch steel pipe with an outside diameter of 168.28mm and a wall thickness of 14.3mm.

A synthesised ideal reflection signal from T(0,1) is shown in Figure 5-6-(a). The input pulse is a 50kHz, 10-cycles, Hann windowed sine signal. The received signal illustrated in Figure 5-6-(c) is the sum of the abovementioned wave modes as shown in Figure 5-5 containing T(0,1) and its flexural wave modes family up to F(6,2). Since the flexural wave modes are dispersive and frequency dependent, the received signal is spread out in time and converts to background (coherent) noise. The spectra of the ideal reflection signal and the received signal are presented in Figure 5-6-(b) and Figure 5-6-(d) respectively. It is notable that the received signal occupies the same bandwidth as the ideal reflection signal, which makes the interpretation difficult.

For techniques based on a single axisymmetric mode, other wave modes present in the signal (generally dispersive ones) can be considered as noise. These dispersive modes

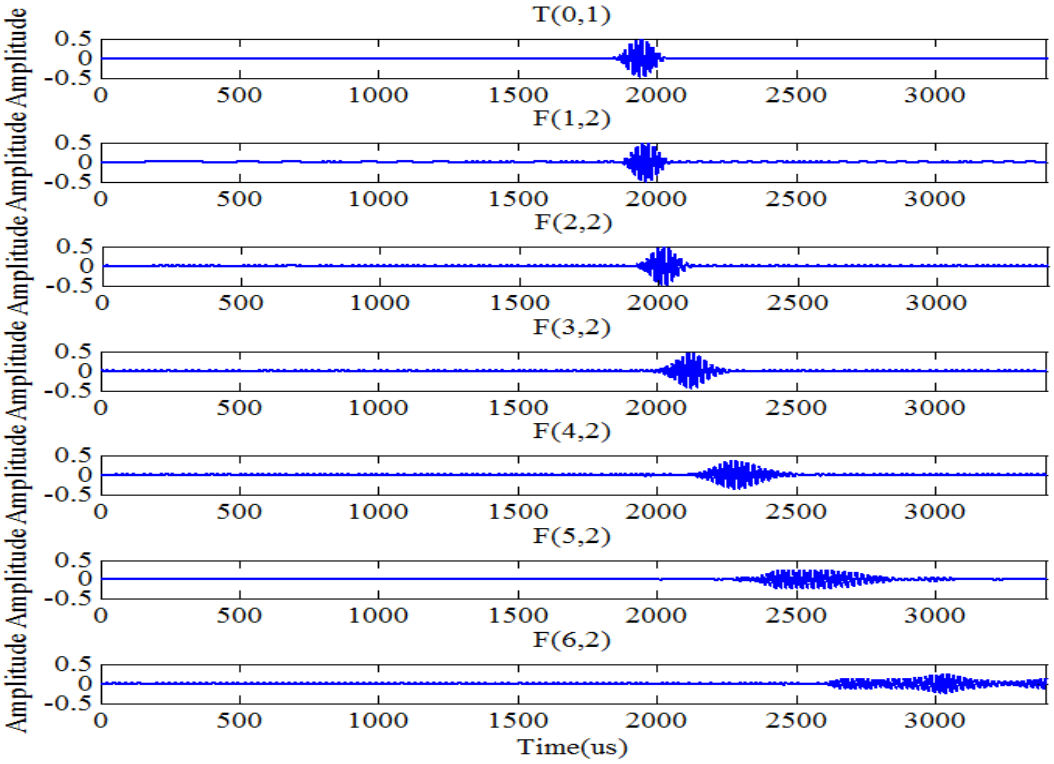

Figure 5-5: Synthesised UGW signals: Torsional T(0,1) and its family of flexural wave modes: F(1,2), F(2,2), F(3,2), F(4,2), F(5,2) ,F(6,2).

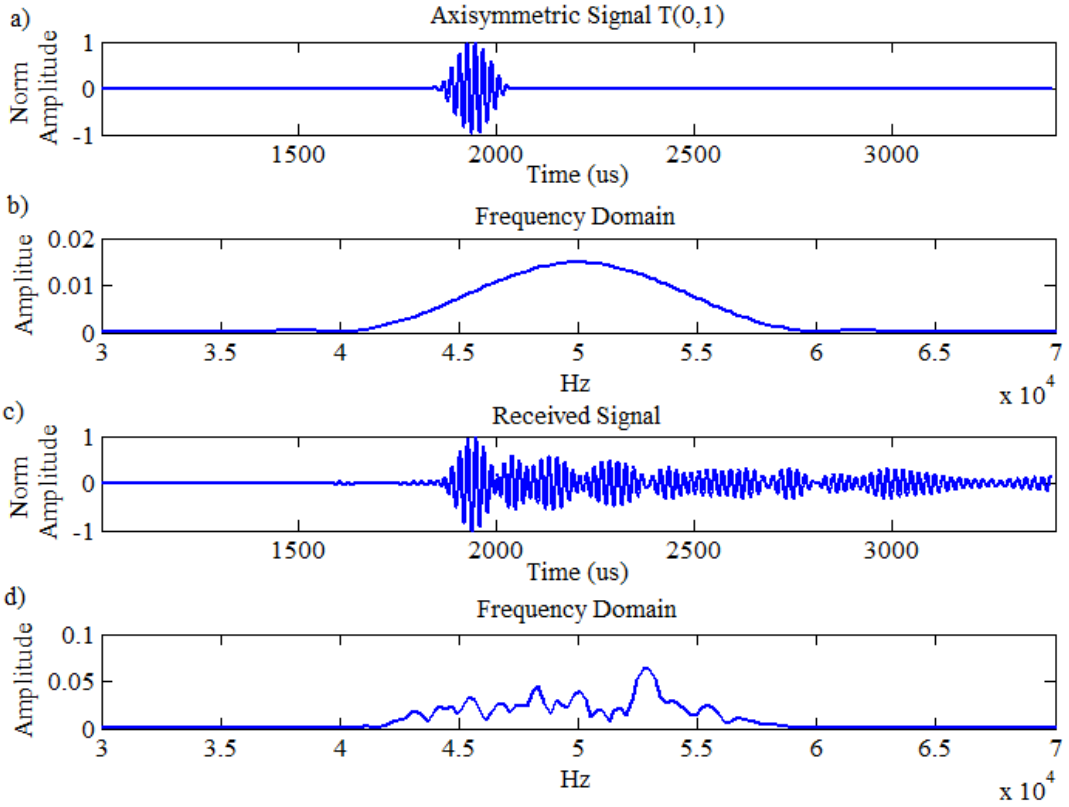

Figure 5-6: Synthesised UGW signal: a) ideal reflection signal T(0,1), b) spectrum of ideal reflection signal c) received signal including T(0,1) and its family of flexural wave modes: F(1,2),…, F(2,6), and d) spectrum of received signal

degrade the spatial resolution and SNR of the axisymmetric wave mode of interest, i.e. T(0,1). The synthesised UGW signal illustrated in Figure 5-6-(c) is employed to investigate the SSP application with different recombination algorithms.

The advantage of using a synthesised signal is to generate the particular wave modes that must be considered in the signal, whereas in the experimental data there are always other wave modes that are not clearly identified in the signal. In addition, the synthesised signal does not contain any unwanted wave modes, so it is an ideal signal. In reality, and especially in field data, there are always some dispersive and non-dispersive wave modes that travel at different velocities. Therefore, the synthesised signals are very useful to begin the analysis of a signal processing technique as all the wave modes that exist are known and are no undefined peaks or unwanted wave modes in the signal. Furthermore, the typical attenuation effect of the UGW signal is not included in the synthesised signal. However, the attenuation only affects the amplitude of the signal and, as the signal processing technique is investigated in this work, this it is not an issue.

5.5 SSP of Synthesised UGW Signal

5.5.1 First Synthesised Signal Analysis

The synthesised UGW signal generated in the previous section is employed to test the SSP application using the Matlab program. In order to find the optimum SSP filter-bank parameter values,[11] their values must be varied during the test to find an optimum value for each parameter. Therefore, the brute force search is applied, as explained in Section 5.3.3 for this purpose. In addition, five different SSP recombination algorithms, described in Chapter 2, are utilised that non-linearly sum the outputs of the sub-band filters. These algorithms include: polarity thresholding (PT), PT with minimisation (PTM), mean, minimisation, and frequency multiplication (FM), which are applied to each set of SSP parameters on the signal displayed in Figure 5-7-(a) to find: i) the best recombination algorithms for UGW inspection, and ii) identify the most suitable parameter values of SSP. The spectrum of the synthesised signal, which is split into several sub-band signals using Gaussian band-pass filters, is shown in Figure 5-7-(b). The performance of SSP, as

[11] The filter-bank parameters that vary are: the total bandwidth (B), the filter bandwidth (B_{filt}) and the start points of total bandwidth (f_{min}). The number of filters (N) and their peak separation (F) are inferred from these values.

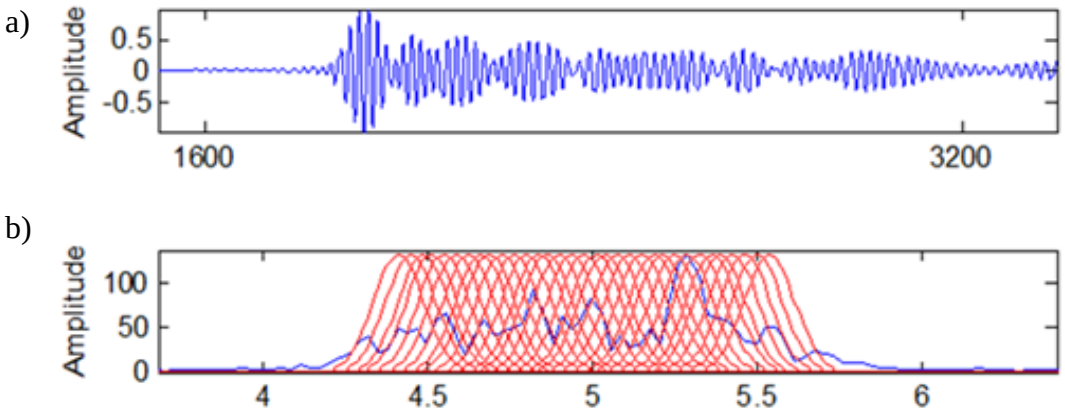

Figure 5-7: Received synthesised UGW signal: a) Time domain, b) frequency domain with Gaussian band-pass filters

mentioned earlier, is quantified by measuring the SNR and spatial resolution of the output UGW signals. The highest SNR is obtained when the parameters have been set as follow:

- 99% of the total operation frequency,
- A sub-band filter bandwidth that is equal to the total operating bandwidth divided by 11,
- A filter separation that is equal to sub-band filter bandwidth divided by 3.5,
- A filter crossover of 1dB.

These values are therefore selected as the optimum SSP parameters for UGW testing. In addition, the aforementioned parameters are subsequently used in the processing of the synthesised data, as described in the following section.

Moreover, using the optimum SSP filter bank parameter values, different SSP recombination algorithms are employed to combine the output signals from each sub-band signal to obtain an output signal. The results are displayed in Figure 5-8. In order to quantify the performance of the synthesised signal and find the optimum SSP parameters, the SNR of the original (unprocessed) signal and the received signal after applying different SSP recombination algorithms has been calculated as follows:

$$SNR = 20 \times \log_{10}\left(\frac{S}{N}\right) \tag{5-15}$$

where S is the maximum amplitude of the signal and N is the noise level, which is taken as the root mean square (RMS) of the whole signal. The SNR value of the unprocessed synthesised signal before applying SSP is 15.6dB.

Figure 5-8 illustrates the unprocessed signal and the results of applying different SSP recombination algorithms on the signal. The outputs from all of the SSP recombination algorithms illustrate a dominant wave, which arrives at a particular time for all of the algorithms i.e. T(0,1), however; the level of coherent noise caused by the flexural wave modes is different.

It can be seen that all of the algorithms have improved the SNR significantly, except for the mean algorithm. Figure 5-8 demonstrates that the PTM gives the highest SNR enhancement with the proposed parameters, followed by the PT. It also represents that although the FM and minimisation algorithms have improved the SNR, the spatial resolution of the result compared to PT and PTM algorithm is poorer. This is due to the presence of DWM. In addition, it should be noted that the SNR enhancement depends on the level of input noise as well as the level of dispersion, therefore, when the signal is less noisy or less dispersive then the performance of the other algorithms will be improved.

The improvement is regarded as the increase in SNR due to SSP using the optimum parameters that were proposed in Section 5.3.3. Table 5-2 gives the SNR enhancement achieved by each SSP recombination algorithm, as given in (5-16):

$$SNR_{improvment} = SNR_{output} - SNR_{input} \tag{5-16}$$

where $\mathrm{SNR}_{\mathrm{output}}$ and $\mathrm{SNR}_{\mathrm{input}}$ are the SNR after and before applying SSP, respectively. Table 5-2 shows that taking the mean of the sub-bands has negative results in the improvement of the SNR, whereas the remaining algorithms have all improved the SNR of the received UGW signal, with PTM giving the greatest SNR enhancement, followed by the PT and the FM.

Although the FM and minimisation algorithms give reasonably good SNR enhancement, they are not able to remove the presence of DWM entirely and therefore they have a distorting effect on the signal as shown in Figure 5-8. On the other hand, PTM and PT, which are the best algorithms in terms of SNR, do not have such a distorting effect. Therefore, PTM and PT were selected as the most appropriate SSP recombination algorithms for the remainder of this thesis.

Table 5-2: SNR enhancement of synthesised UGW signal

SSP Recombination Techniques	SNR Enhancement (dB)
Mean	-0.26
Minimisation	9.61
Frequency Multiplication	16.82
Polarity Thresholding (PT)	29.30
PT with Minimisation (PTM)	30.61

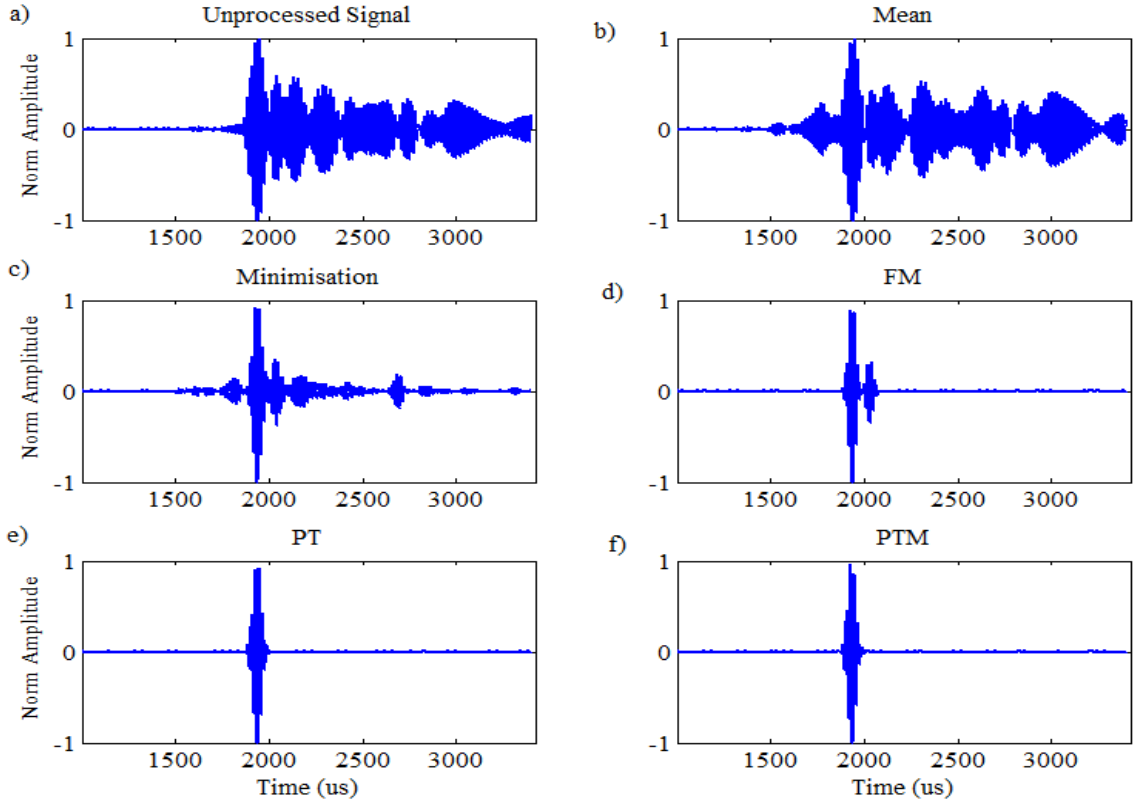

Figure 5-8: Results of synthesised UGW signal before and after applying SSP: a) Unprocessed input signal, b) Mean, c) Minimisation, d) Frequency Multiplication, e) Polarity Thresholding, f) Polarity Thresholding with Minimisation

5.5.2 Second Synthesised Signal Analysis

The core concept of this section is to identify the limitation of SSP in terms of finding the smallest defect size that can be detected by the proposed technique; and in addition, to find the distance limitation when the location of the defect is close to a dominant feature with high amplitude such as weld, flange, etc. In order to achieve this, 10-cycles pulse with a centre frequency of 44kHz with the axisymmetric torsional T(0,1) wave mode is excited using the synthesised model, as explained in Section 5.4, and it is assumed that there are only two reflections, from i) the defect, and ii) the pipe's end respectively. Since the proposed method has already demonstrated the capability to remove the DWM

(Section 5.5), in this part it is assumed that only the axisymmetric T(0,1) signal is reflected from the features on the pipe.

According to Böttger et al. [91], there is a linear relationship between the amplitude of the reflected signal of T(0,1) wave mode and the CSA of its defect. Hence, the attenuation of T(0,1) is linear, which means if 10% of the excited signal reflects from the defect, then the rest of the energy (90%) will reflect from the pipe end.

The set-up of this synthesised experiment is shown in Figure 5-9. The distances of the defect and end of the pipe are X=3m and X=4.5m from the excitation signal, respectively. It is assumed that the defect reflects 10 % of the total energy and the rest of the energy (90%) is reflected by pipe end, as displayed in Figure 5-10 (a). The reflection from defects are reduced gradually in order to find the smallest size of defect that can be recognised by the proposed method. These are illustrated in Figure 5-10, where the defect sizes are gradually reduced from 10% CSA to 1% CSA by steps of 2%. The results shown in Figure 5-10 demonstrate that the proposed method has the potential to detect defects down to 1% CSA when the distance between two features is 1.5m.

Furthermore, in order to find the distance limitation, it is assumed that the defect (10% CSA) is 1m from the end of the pipe and it is moving towards the pipe's end by steps of $0.1\ m$ as illustrated in Figure 5-11. It is clearly illustrated that the defect is recognisable until its distance from the pipe's end is around 0.7m, as illustrated in Figure 5-11-(d). Then, the resolution is gradually reduced until the distance is $0.5\ m$, as shown in Figure 5-11-(f). Afterward, the defect reflection starts to superpose with the pipe's end reflection and as a result reduces the temporal resolution. Therefore, according to this result, SSP technique can detect small amplitudes close to the dominant amplitude only when the distance between them is greater than 0.5m. However, this is the result for 10-cycles excitation signal modulated by Hann window with a defect size of 10% CSA and centre frequency of 50kHz.

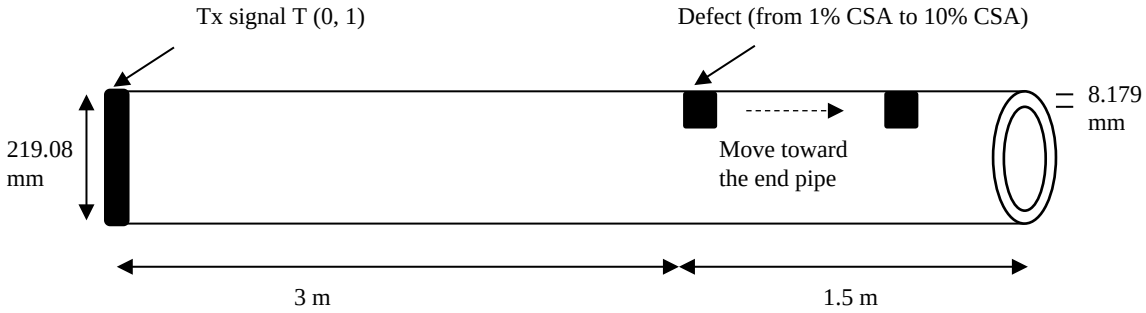

Figure 5-9: Synthesised setup for eight-inch pipe with WT =8.179 mm and OD=219.08 mm.

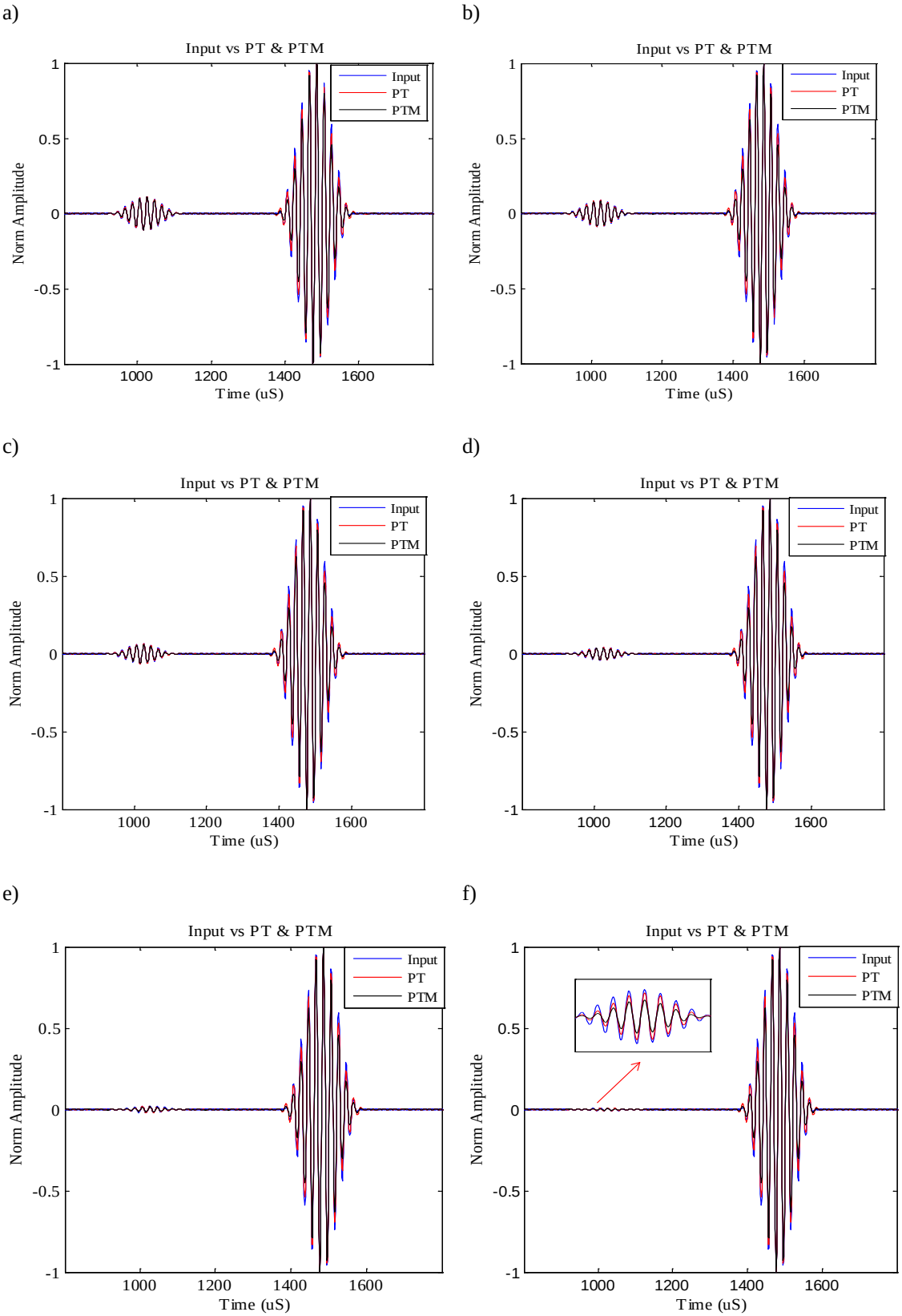

Figure 5-10: Results for synthesised UGW signal before and after applying SSP (PT & PTM algorithms). The defect and the pipe end are located at X=3 m and X=4.5 m from the excitation signal. The defect sizes are a)10% CSA, b)8% CSA, c)6% CSA, d)4% CSA, e)2% CSA and f)1% CSA

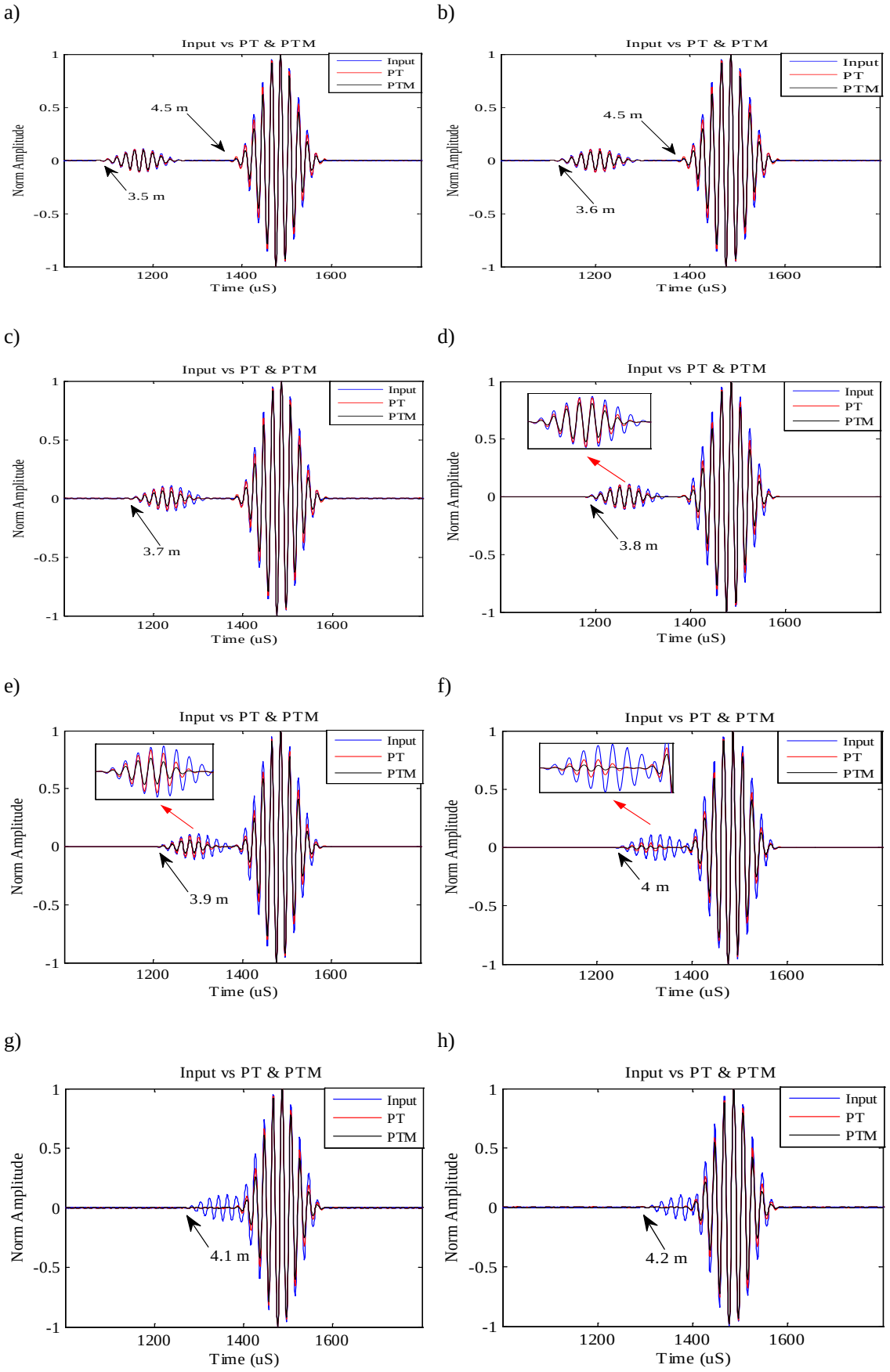

Figure 5-11: Results for synthesised UGW signal before and after applying SSP (PT & PTM). The defect location (X=3.5m) is moved towards the pipe end (X=4.5 m) with steps of 0.1m.

In addition, the results of the PT and PTM recombination algorithms as shown in Figure 5-11, are almost identical, while the distance between two peaks is greater than 0.8m but the PT algorithm, when compared to the PTM algorithm, gives a better spatial resolution result when the distance is around or less than 0.5m (Figure 5-11-(f)). In these regions, the PT algorithms identify defects with poor resolution, whereas the PTM loses the information. In order to validate the outcome of these synthesised results, the experimental test was carried out in the lab followed by the field data analysis, which are described in the next chapter.

5.6 Discussion of Initial SSP Studies

The result of the synthesised signal analysis showed that SSP application has the potential to reduce the level of coherent noise significantly due to the presence of dispersive wave modes in UGW signals. Therefore it can considerably improve the SNR and spatial resolution of the received such signals. The optimum filter bank parameter values were applied by trial and error, using the brute force search algorithms to find the optimum parameter values by checking the SNR and spatial resolution of the received signal. The initial values tested for SSP application were inspired by the values introduced for conventional UT and then modified. The results obtained from this chapter showed that, among the other recombination algorithms, the PT and PTM algorithms give the best SNR enhancement, and both algorithms significantly reduced the effects of dispersive wave modes without distorting the signal.

In addition, in order to address the distance limitation of SSP when two features are close together, a threshold has been defined, below which threshold the temporal resolution will be reduced. To sum up, SSP application as it is implemented here could be applied for UGW inspection. However, further work is required to test the SSP application for different scenarios. Furthermore, in order to validate the results obtained in this chapter, SSP has been applied to experimental data in the lab and field data. These validations are fully covered in Chapter 6.

5.7 Conclusions

A novel solution based on advanced signal processing technique is proposed in this chapter to address the problem of coherent noise in UGW signals using SSP as a post-processing technique. The fundamental knowledge and the literature review of SSP is explained in details in Chapter 2 and Chapter 3 respectively. In addition, the fundamental development of SSP is fully covered within this chapter, which mostly related to conventional UT for SNR enhancement. Two main challenges of SSP were investigated for synthesised UGW signals, which were: i) finding the optimum filter bank parameter values, and ii) selecting the appropriate recombination algorithms for the use of SSP in GWT. Furthermore, the initial signal processing of generating synthesised UGW signals is described in the chapter, with regard to the analysis and determination of the limitation of SSP application.

In order to address above issues, SSP application is applied to two different synthesised experimental signals for the restoration of signals suffering from coherent noise and the reduction of the effect of dispersive wave modes to increase the sensitivity, SNR and inspection range of UGW testing. Theses synthesised signals were utilised to find the optimum filter bank parameter values which were varied during the tests. The brute force search algorithms is employed to find the optimum parameter values by checking the SNR and spatial resolution of the received signal. The five most common SSP recombination algorithms are employed for each set of parameters to find the appropriate one. Result showed that the *polarity thresholding (PT)* and *PT with minimisation (PTM)* among the other recombination algorithms achieved the highest SNR enhancements in both scenarios without distorting the signal.

It is demonstrated throughout this chapter that the proposed method has the potential to improve the sensitivity and spatial resolution of UGW signals in terms of SNR (enhancing the SNR approximately by 30dB), detecting smaller defects (down to 2% CSA), finding the distance limitation when the location of the defect is close to a dominant feature with high amplitude as well as increasing the inspection range.

Therefore, this chapter shows that SSP application as it is implemented here could be applied for UGW inspection. However, further work is required to validate the SSP application for experimental and field data which are covered in the next chapter.

Chapter 6

6 Application of SSP to experimental GWT data and field trials for validation

6.1 Chapter overview

The focus of this chapter is to validate the proposed SSP application with the optimum parameters that were proposed in Chapter 5 for the reduction of coherent noise in the UGW signal. The synthesised analysis in Chapter 5 confirmed that the proposed method has the potential to enhance the SNR and spatial resolution of the UGW signal. This chapter presents the details of two experiments have were undertaken in the lab on six-inch and eight-inch diameter steel pipes, followed by a presentation of field data to validate the proposed method experimentally. The technique applied uses pitch-catch and pulse-echo methods. In addition, a different type of SNR calculation is defined here in order to address the challenges identified in the literature about SSP with regard to reducing the temporal resolution and creating erroneous features in the processed signal.

It is verified throughout this chapter that the proposed technique, when compared to the conventional techniques reported in the literature, substantially improves the sensitivity and spatial resolution of UGW signals in terms of SNR, detecting smaller defects that might be hidden below noise level as well as increasing the inspection range. Fundamental to SSP, the development of GWT is explained in Chapter 2; while, the step by step procedures for the implement of SSP is covered in Chapter 5.

6.2 Application of SSP to Experimental Signal

To validate the proposed technique for the reduction of the presence of dispersive wave modes (coherent noise) in UGW signals and enhance the spatial resolution, it is necessary to perform experimental testing. This section discusses, two laboratory experiments implemented in the lab to gather experimental data, following which SSP was applied to these data to validate the proposed technique. These experiments have been carried out using the following methods for gathering data;

i) Vibrometry measurement using the pitch-catch method and
ii) Guided wave inspection system employing the pulse-echo method

6.2.1 Experiment #1: using Pitch-Catch Technique

In this experiment, the pipe under investigation was a nominal six-inch, six-meter long steel pipe, with an outside diameter of 168.28mm and 14.3mm wall thickness. The pipe included an axisymmetric defect of 12.5% depth, which represented a loss in cross-section area (CSA) of 13.5%. Figure 6-1 displays the experimental set-up using the pitch-catch method to maintain directionality during the experiment in order to achieve an accurate experimental result.

The Teletest Focus+ system pulser/receiver [14] was employed to transmit a signal (Tx) and a Polytec 3D Laser Doppler Vibrometer (3D-LDV) [15] was utilised to receive the signal (Rx). The laser vibrometry was engaged to measure the vibration of the surface of a spatial position of the wave packets of interest (i.e. flexural wave modes family of T(0,1) that spread out in time/space). This was a specific project set-up plan, used in this research as a first experimental result to validate the proposed technique regarding reducing the effects of DWM (coherent noise) in the received UGW signal.

The optical receiver has the capability to remove the uncertainty of the coupling and to receive the transfer function of the piezoelectric ceramic. Also, the vibrometry could be used to perform a circumferential variation analysis to determine what modes are present. Thus, the presence of wave modes that are generated purely by transmission could be validated. The 3D-LDV is equipped with three laser heads, as illustrated in Figure 6-1, to detect the motions of the surface that are produced by the circumferential excitation of the UGW signal at 60kHz. This pulse is 10-cycles Han-windowed sine wave pulse, transmitted into the pipe specimen, as illustrated in Figure 6-2, to generate a pure T(0,1) wave mode.

The Teletest system has an external trigger that initiates synchronisation with the 3D-LDV during data collection. To remove/reduce any random noise, the collection was averaged on the vibrometer and set to 512. The vibrometer was focused at a distance of two-metres and in line with the transducers that deliver the input signal. In addition, the sampling frequency of the received signal was set to 1MHz. As shown in Figure 6-1, the transducers (Tx) are located at the very end of the pipe to avoid receiving any backwards propagation complicating the received signals.

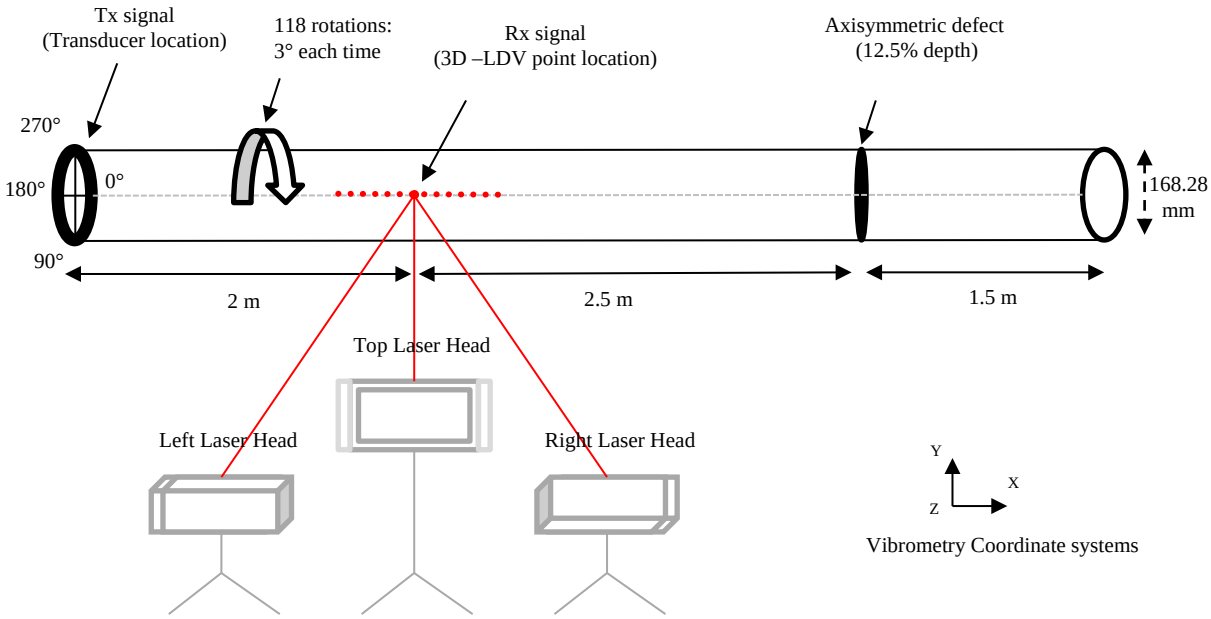

Figure 6-1: Illustration of 3D-LDVexperimental set-up

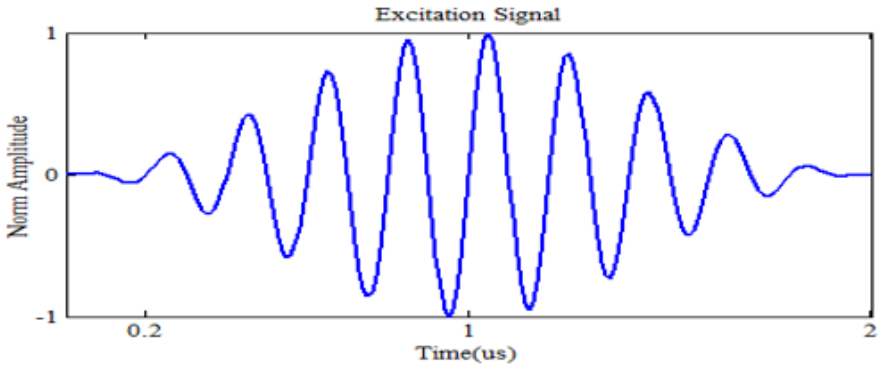

Figure 6-2: Excitation Time-domain signal

An array comprised of 64 laterally polarised piezoelectric transducer elements equally distributed around the circumference was used. The elements create circumferential displacement and can be used in-phase to generate torsional wave modes. The elements are glued to the pipe specimen using Araldite epoxy. The vibrometer receives at one circumferential point, and the test is repeated to gather received points around the circumference. The pipe is rotated 3° each time to gather 118 vibrometry points during the scan to capture the UGW signal. The results of this scan are illustrated in Figure 6-3-(a), summing all results of 118 points to generate the pure T(0,1), and Figure 6-3-(b), a single point scan.

The aim of the proposed method is to obtain a fairly pure T(0,1) signal by utilising only one point of scan and removing/reducing the coherent noise. Since the transducers are

a)

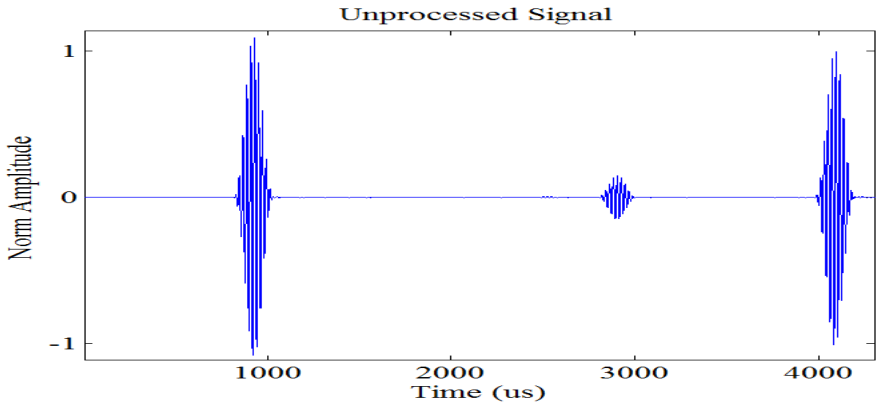

b)

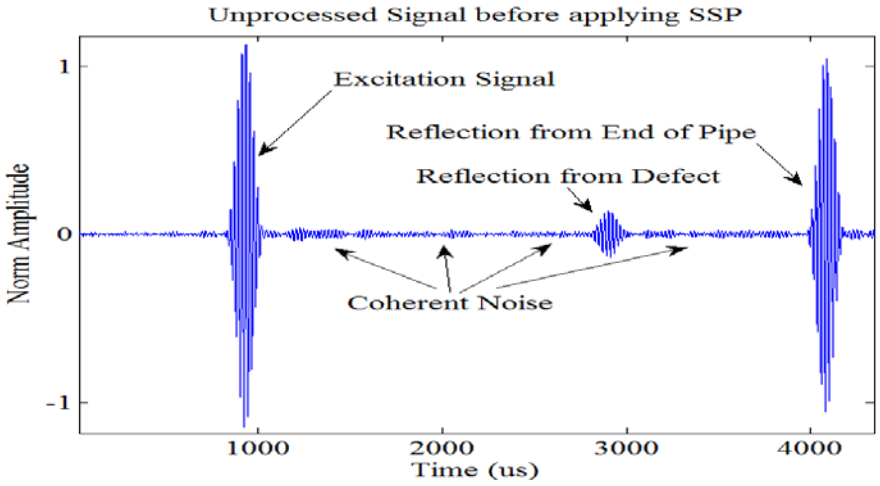

Figure 6-3: Experimental signal using 3D-LDV: a) sum of 118 points b) one point scan

placed at the end of the pipe, the wave peaks represent the incident T(0,1), the defect response, and the reflection from the pipe-end respectively. As shown in Figure 6-3-(b) the level of coherent noise between these wave packets is clearly noticeable that mainly caused by the presence of dispersive wave modes and needs to be reduced. In order to quantify the improvement given by the different SSP recombination algorithms, the SNR of the UGW response is calculated as follows:

$$SNR = 20 \times \log_{10}\left(\frac{S}{N}\right) \tag{6-1}$$

where S is the peak value of the defect's reflection and N is the RMS value of the coherent noise region, as illustrated in Figure 6-3-(b). The SNR of the unprocessed signal is 21.9dB. The selection of SSP recombination algorithms with the proposed filter bank parameters are applied to the experimental data and the results are displayed in Figure 6-4. Since the

reflections of the excitation signal and the pipe-end have high amplitude, it is required to re-scale the results to see the coherent noise and reflection from the defects more clearly. Therefore, Figure 6-4 is re-scaled (zoomed-in) to highlight the presence of the coherent noise and the defect's reflection for a better representation in different SSP recombination algorithms, as illustrated in Figure 6-5. This figure clearly illustrates that the PTM has resulted in the greatest spatial resolution without distortion, followed by PT and minimisation. These three SSP algorithms enhanced the spatial resolution of the signal by reducing/removing the noise level significantly. In addition, taking the mean of sub-bands and FM have a distorting effect on the unprocessed signal where the FM algorithms have removed the defect's reflection completely and reduced the amplitudes of the pipe end's reflection considerably.

Table 6-1 displays the SNR enhancement of each recombination algorithm using equation (6-1). The improvement is regarded as the increase in SNR due to SSP. The results illustrate that the PTM algorithms have the greatest increase in SNR, 32dB, without distortion the signal. The second best performing method was the PT algorithm, which gave a 23dB enhancement. On the other hand, FM algorithms removed the defect's reflection signal and reduced the pipe-end amplitude. This distortion is caused by multiplying the frequency of each sub-band without considering the sign of their signals. As a result, PTM and PT are chosen as the most appropriate SSP recombination algorithms for UGW data.

Additionally, another comparison similar to that used in [201] is employed for performance evaluation, which calculates the strength of the defect's reflection to the largest surrounding coherent noise signal. This is referred to as defect-to-coherent noise ratio (DCR) and is measured in dB as:

$$DCR = 20 \times \log_{10}\left(\frac{F}{C}\right) \tag{6-2}$$

where F and C are the maximum output echo amplitude of the defect and the largest amplitude of the coherent noise respectively. The improvement is calculated as the rise in the DCR due to SSP. The DCR enhancement is calculated as follows:

$$DCR_{improvment} = DCR_{output} - DCR_{input} \tag{6-3}$$

where $\mathrm{DCR_{input}}$ and $\mathrm{DCR_{output}}$ calculates the DCR enhancement before and after applying the SSP technique respectively.

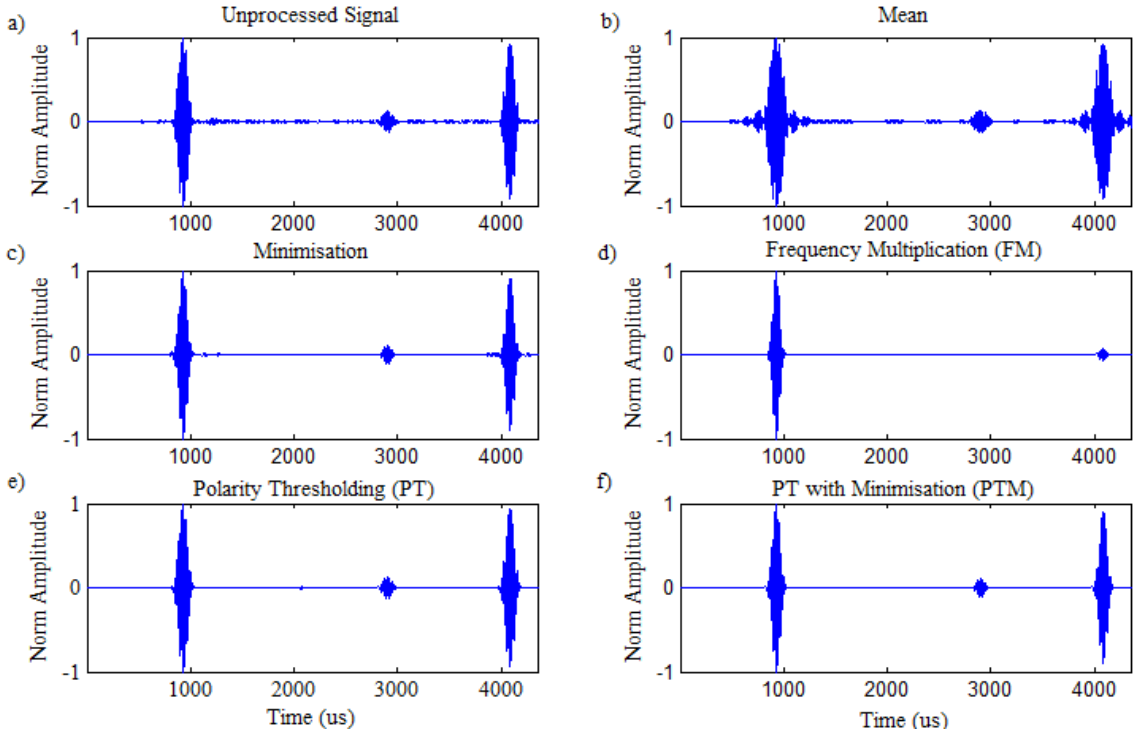

Figure 6-4: Results from applying various SSP techniques: a) unprocessed signal, b) result of mean, c) result of minimisation, d) result of frequency multiplication, e) result of polarity thresholding f) result of polarity thresholding with minimisation

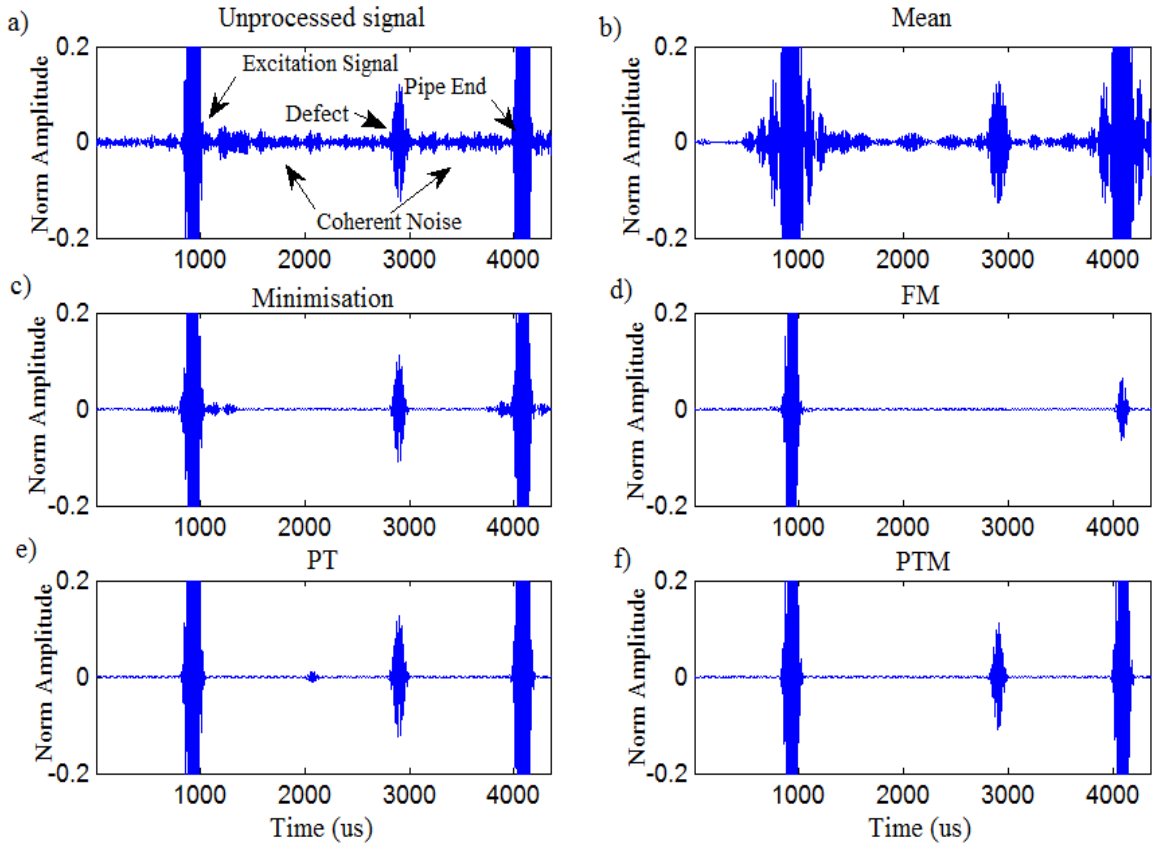

Figure 6-5: Re-scaled results from applying various SSP techniques: a) unprocessed signal, b) result of mean, c) result of minimisation, d) result of FM, e) result of PT f) result of PTM

Table 6-1: SNR and DCR enhancement of experimental UGW signal

SSP Recombination algorithms	SNR Enhancement (dB)	DCR Enhancement (dB)
Mean	-1.92	-
Minimisation	7.78	-
Frequency Multiplication	- 39.97	-
Polarity Thresholding (PT)	22.87	14.29
PT with Minimisation (PTM)	32.14	22.34

Since the PTM and the PT algorithm have produced the most promising results among others in terms of SNR with the same filter bank parameters, thus, the DCR is calculated only for these algorithms and the results are presented in Table 6-1. As expected, the PTM and PT have improved the DCR by 22.3dB and 14.3dB respectively.

6.2.2 Experiment #2: using Pulse-Echo Technique

The second experiments were conducted in the lab using a nominal eight-inch pipe, six meters long with a wall thickness of 8.28mm and outer diameter of 219.08mm. The setup for the experiment is illustrated in Figure 6-6. The signal is excited using a '5 Ring Torsional' Teletest system [14] to transmit a 10-cycles, Hann window modulated tone burst of T(0,1) wave mode. The ring spacing between transducers was 30mm.

The frequencies that give the best result for this particular pipe size according to the dispersion curve are 27kHz, 36kHz, 44kHz, 64kHz and 72kHz. Therefore, the data has been collected on these frequencies for analysis. The Teletest Collar placed at 1.5m away from the near pipe-end and a saw cut defect is created 1.5m away from the far pipe-end. The size of the defect has incrementally increased from 0.5% CSA to 8% CSA. In total, 9 defects have been created, the flaw size plan is displayed in Table 6-2. Although the pipe length is six metres, in order to see the attenuation, the test runs for 25m to collect more data.

In order to reduce incoherent noise, the collection is repeated 512 times, and the received signals averaged. The sampling frequency of the received signal is set to 1MHz. A pulse-echo method is employed for this experiment and the Teletest system is utilised to excite/receive (Tx/Rx) the signal. Since PT and PTM algorithms gave the best results regarding SNR and spatial resolution for the synthesised and the vibrometry experiments, both are utilised in this experiment.

a)

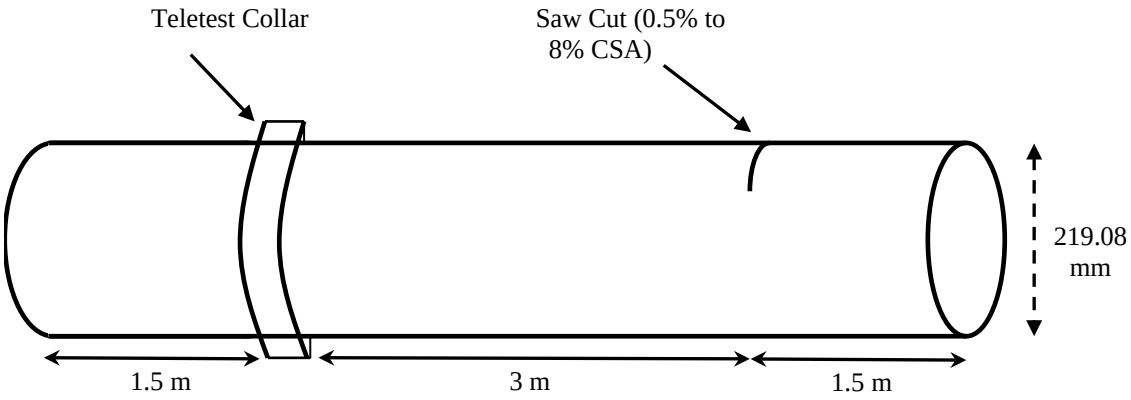

b)

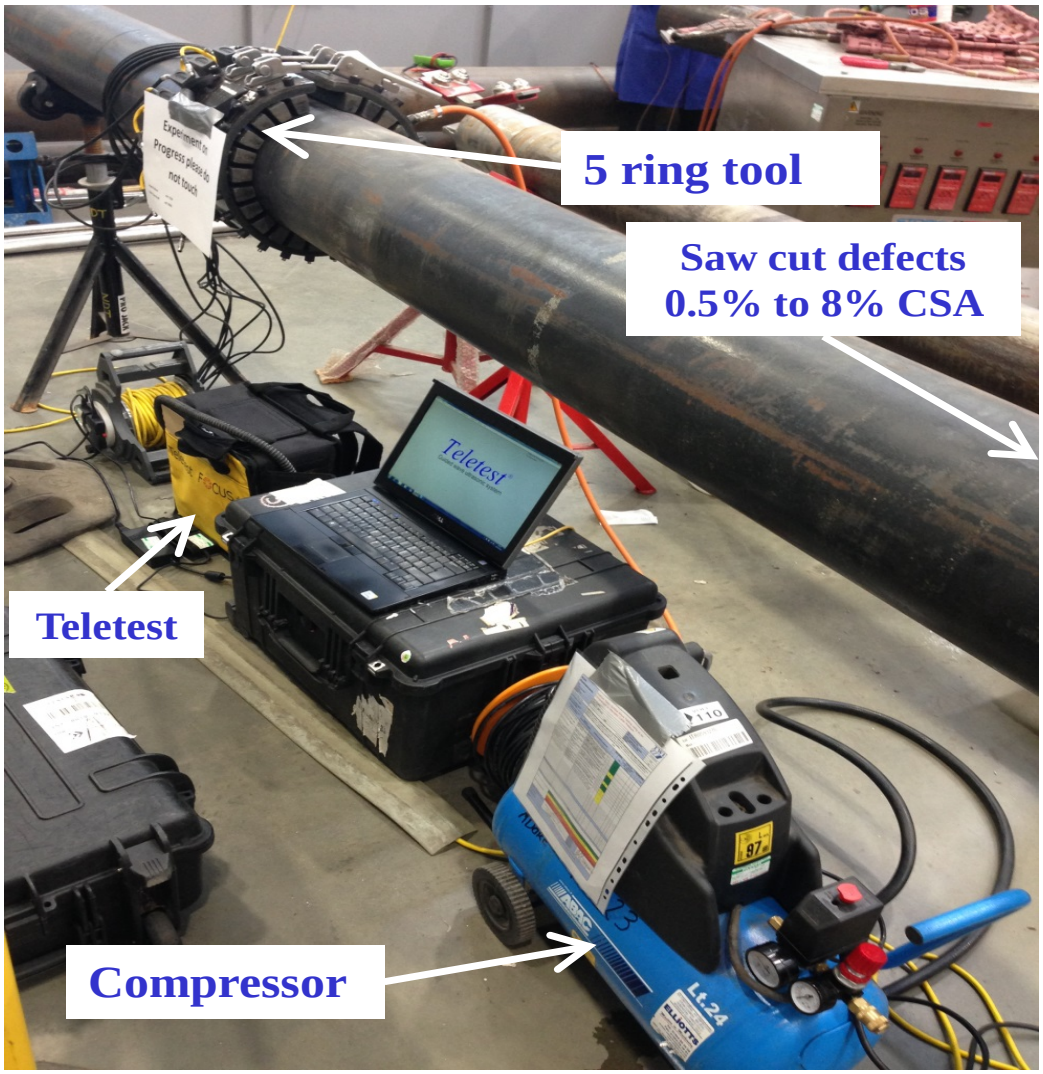

Figure 6-6: Experimental setup up for eight-inch steel pipe with a wall thickness of 8.179 mm and OD of 219.08 m

Table 6-2: Flaw size plan for eight-inch steel pipe

Outside diameter	219.08
Inside diameter	202.722
Wall thickness	8.179

Index	Flaw depth (mm)	Cord length (mm)	Arc length (mm)	% C.S.A.
Defect 1	1.2	32.33920222	32.45781306	0.5%
Defect 2	2	41.67301285	41.92850407	1.0%
Defect 3	3.1	51.75086473	52.2446449	2.0%
Defect 4	4.1	59.37736943	60.12945843	3.0%
Defect 5	5	65.43393615	66.44806334	4.0%
Defect 6	5.8	70.34270396	71.61112785	5.0%
Defect 7	6.5	74.34433401	75.8506566	6.0%
Defect 8	7.2	78.11622111	79.87403667	7.0%
Defect 9	7.9	81.69019525	83.71248272	8.0%
Through Wall Flaw (8")	8.55	84.8535562	87.13258361	9.0%

In addition, the same SSP filter bank parameters as defined, recommended in Table 5-1 in Chapter 5 are employed here.

As mentioned earlier, the experiment has been run for different frequencies, and the result of each frequency compared with the same frequency of the conventional model that is currently employed in the Teletest system. However, the comparison for 44kHz is presented in greater detail in this section. The results indicate that defects smaller than 2% CSA are almost impossible to identify before and/or after applying the proposed technique. Therefore, the investigation and comparison takes place only when the defect size is greater than 2% CSA. It is notable that the current sensitivity for reliable detection of Teletest system is 9% CSA which is equivalent to 5% amplitude reflection.

Figure 6-7 illustrated a) the actual scale result, and b) the zoomed-in result of the unprocessed signal and the proposed SSP technique with PT and PTM algorithms respectively when the saw cut defect size is 3% CSA. The results show that the unprocessed signal has less chance and certainly to identify defects of a similar level to the surrounding coherent noise produced by the presence of DWM.

By contrast, the proposed SSP method, both PT and PTM, removes the noise entirely and only the defect's reflection remains, without distortion of the signal or creating artefacts. Therefore, as a result, the proposed technique has the potential to detect a defect with confidence down to 3% CSA. These data are gathered using the Teletest unit, collected by

a)

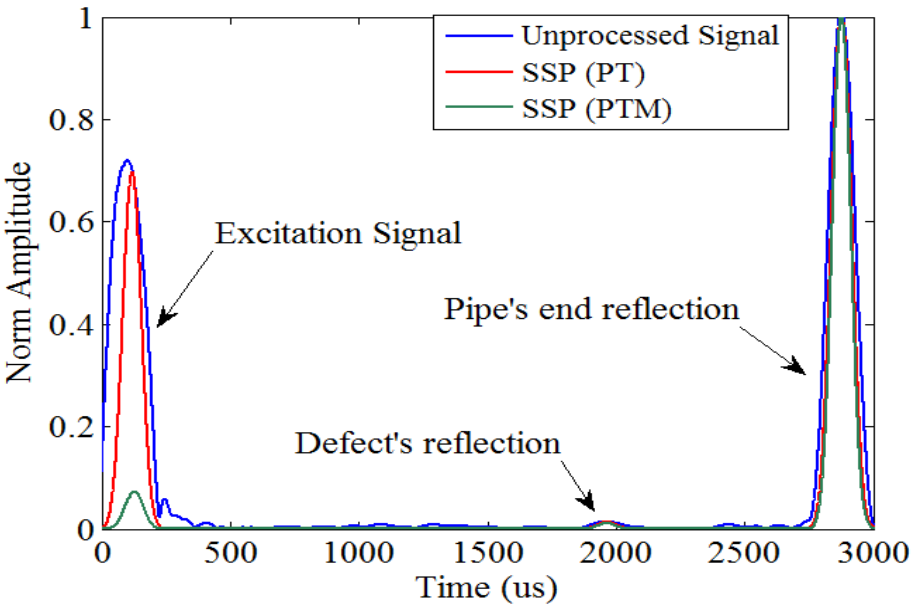

b)

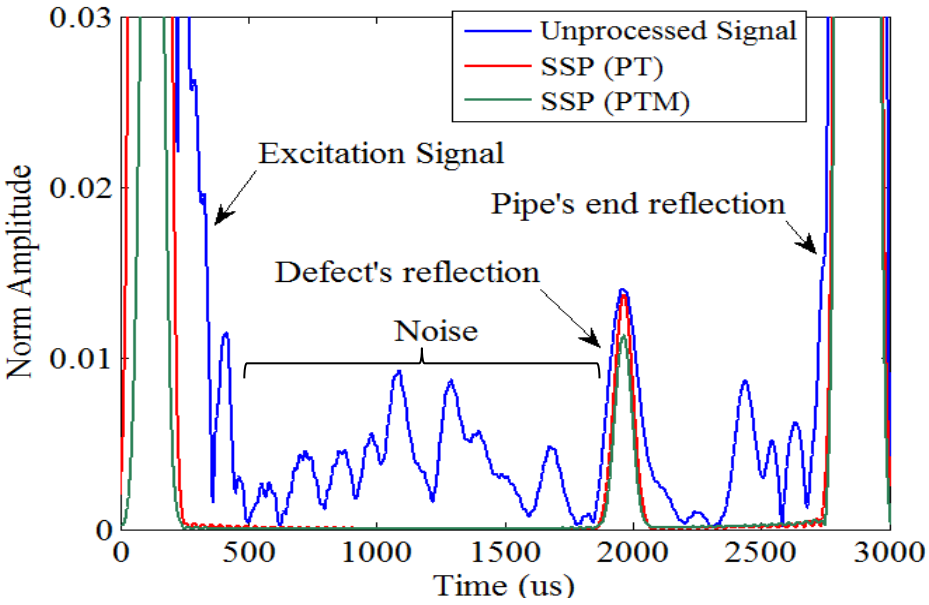

Figure 6-7: Result of unprocessed signal vs. SSP- 3% CSA defect - 44kHz: a) result b) zoom-in

PC and then analysed using Matlab program to generate the output signal for both unprocessed and SSP signal. In addition, to quantify the improvements shown by the proposed technique, the SNR enhancement is calculated by using (6-1) where S is the maximum amplitude of the defect's reflection and N is the RMS value of the noise region as defined in Figure 6-7-(b). The SNR of the unprocessed signal is 13.25dB. The results presented in Table 6-3 show that both algorithms enhanced the SNR by 38.9dB and 36.9dB respectively.

Table 6-3: SNR enhancement of experimental UGW signal with 3% CSA

SSP recombination techniques	SNR enhancement (dB)
Polarity thresholding (PT)	36.9
PT with minimisation (PTM)	38.9

Furthermore, a comparison of the amplitude of the pipe-end reflection and the defect reflection was undertaken in order to evaluate how well the SSP maintains the amplitude of the signal features of interest. The results are given in Table 6-4 and indicate that no significant amplitude proportionality changes occurred for either method. However, since the PTM used the sum of minimum amplitudes of the PT for each individual sub-band, the amplitude of the defect's reflection reduced slightly. This is the main reason that the PTM gives a slightly higher value than PT for peak-to-peak comparison of pipe-end to defect.

The same scenario is then applied to check the proposed method when the saw cut defect size is 2% CSA. Figure 6-8 presents a) the actual scale result and b) the zoomed-in result of the unprocessed signal and the proposed SSP technique, with the PT and PTM algorithms respectively. It is clear that the defect is almost hidden by the noise level and it is impossible to identify it with the conventional technique used in the Teletest system. The result of proposed technique clearly indicates that the SSP technique with PT algorithm is able to identify defects down to 2% CSA. It is shown that the amplitude of the defect's reflection is at the level of coherent noise amplitude for the unprocessed data, whereas the PT algorithms has removed all the surrounding noises and only the defect's reflection remains. In addition, while the PTM algorithm removed the coherent noise significantly, the defect amplitude is also reduced.

The SNR of the unprocessed signal is 7.8dB and the result of SNR enhancement is shown in Table 6-5. The PT algorithm, as illustrated in Figure 6-8, gives the highest SNR enhancement (33.9dB), and although the PTM gives 25dB SNR enhancement it reduced the defect's reflection considerably.

Table 6-4: Peak to peak measurement of pipe-end to defect with 3% CSA

Received signal	Pipe-end to defect (dB)
Unprocessed signal	37.15
Polarity thresholding (PT)	37.35
PT with minimisation (PTM)	38.95

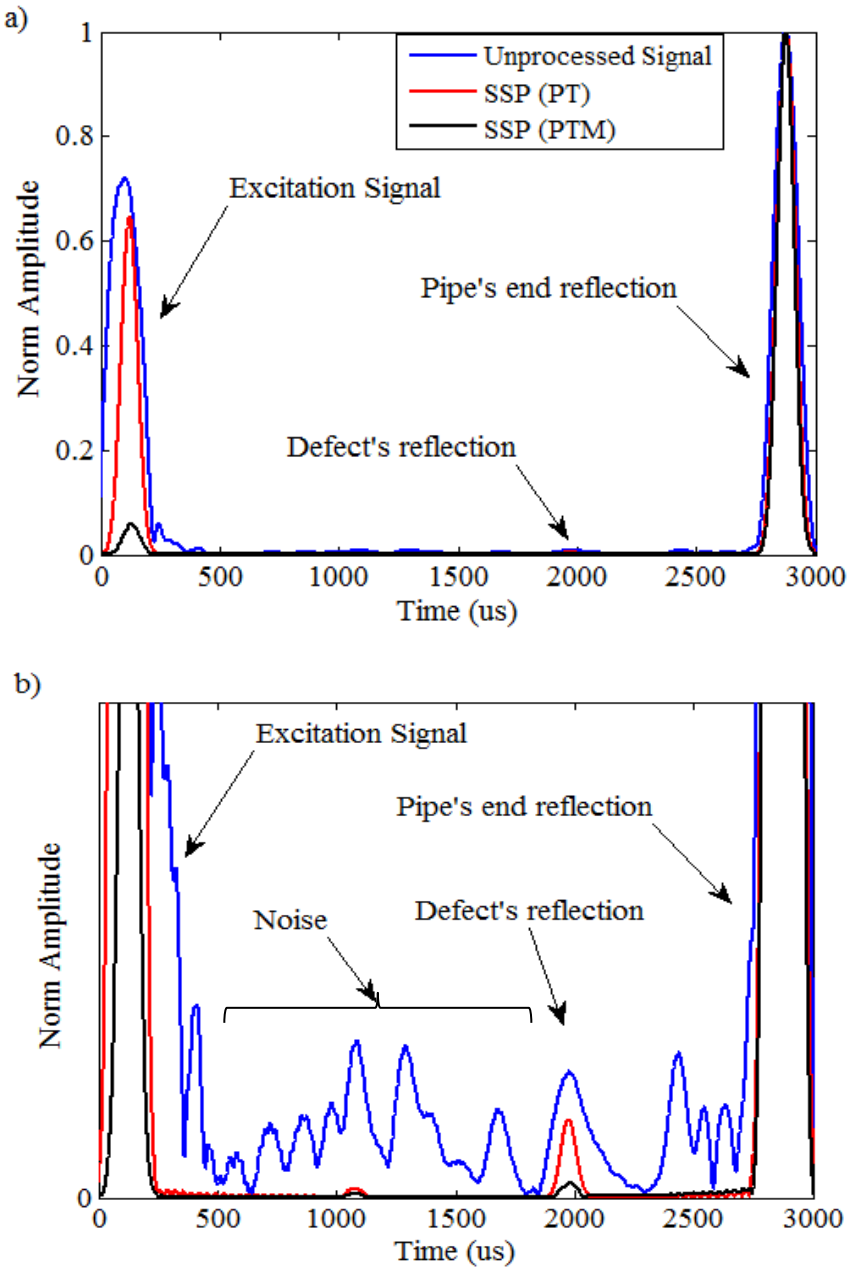

Figure 6-8: Result of unprocessed signal vs. SSP- 2% CSA defect- 44kHz: a) result b) zoom-in

Figure 6-9 illustrates the Hilbert transform zoom-in of the defect's reflection from baseline up to 8% CSA, obtained by a) Teletest system before applying SSP and b) the proposed SSP technique using PT algorithms.

These results indicate that defects up to 2% CSA can be identified with both Teletest and SSP techniques. However, as explained earlier and illustrated in Figure 6-7 and Figure 6-8, the conventional technique utilised in Teletest system was unable to identify defects below 4% CSA, as they are hidden in the noise level, whereas the SSP identified defects down to 2% CSA as it reduced/removed the effect of DWM. Therefore, SSP reduced the coherent noise level around the signal of interest.

Since SSP divides the frequency bandwidth to a set of overlapping sub-bands signal and then non-linearity sums up entire sub-bands together to obtain the output signal, as illustrated in Figure 6-9-(b), it is slightly narrower/stretched compared to the conventional results, as displayed in Figure 6-9-(a).

In addition, Figure 6-10 shows the zoom-in plot around the defects area from 0.5% CSA to 8% CSA using Matlab software for both unprocessed data (blue) and the SSP technique with PT algorithm (red). The figure confirms that the SSP technique using optimum parameters with PT algorithm enhances defect sensitivity down to 2% CSA, which was hidden below the noise level. Even for 3% CSA, as shown in Figure 6-10, is still difficult to identify it using conventional techniques, whereas after using SSP it is easily noticeable and can with confidence be identified as a defect. This size flaw is typical of that which can be challenging to reliably detect with UGW inspection systems.

Furthermore, in order to show how the proposed SSP technique removes/reduces the coherent noise on the received UGW signal, and as a result has the potential to increase the inspection range, the unprocessed signal (blue) and SSP signal using PT (red) with 8% CSA at 44kHz is displayed in Figure 6-11. It can be seen in the unprocessed signal that there some coherent noise exists between peaks and the level of the noise increases as the distance increases.

This proves that it is more difficult to find a small defect in a longer distance. By contrast, the result of SSP clearly shows that this technique has removed the entire coherent noise and only the signal of interest remains, without distorting the signal, therefore it increases the sensitivity as well as increasing the inspection range.

Table 6-5: SNR enhancement of experimental UGW signal with 2% CSA

SSP recombination techniques	SNR enhancement (dB)
Polarity thresholding (PT)	33.9
PT with minimisation (PTM)	25

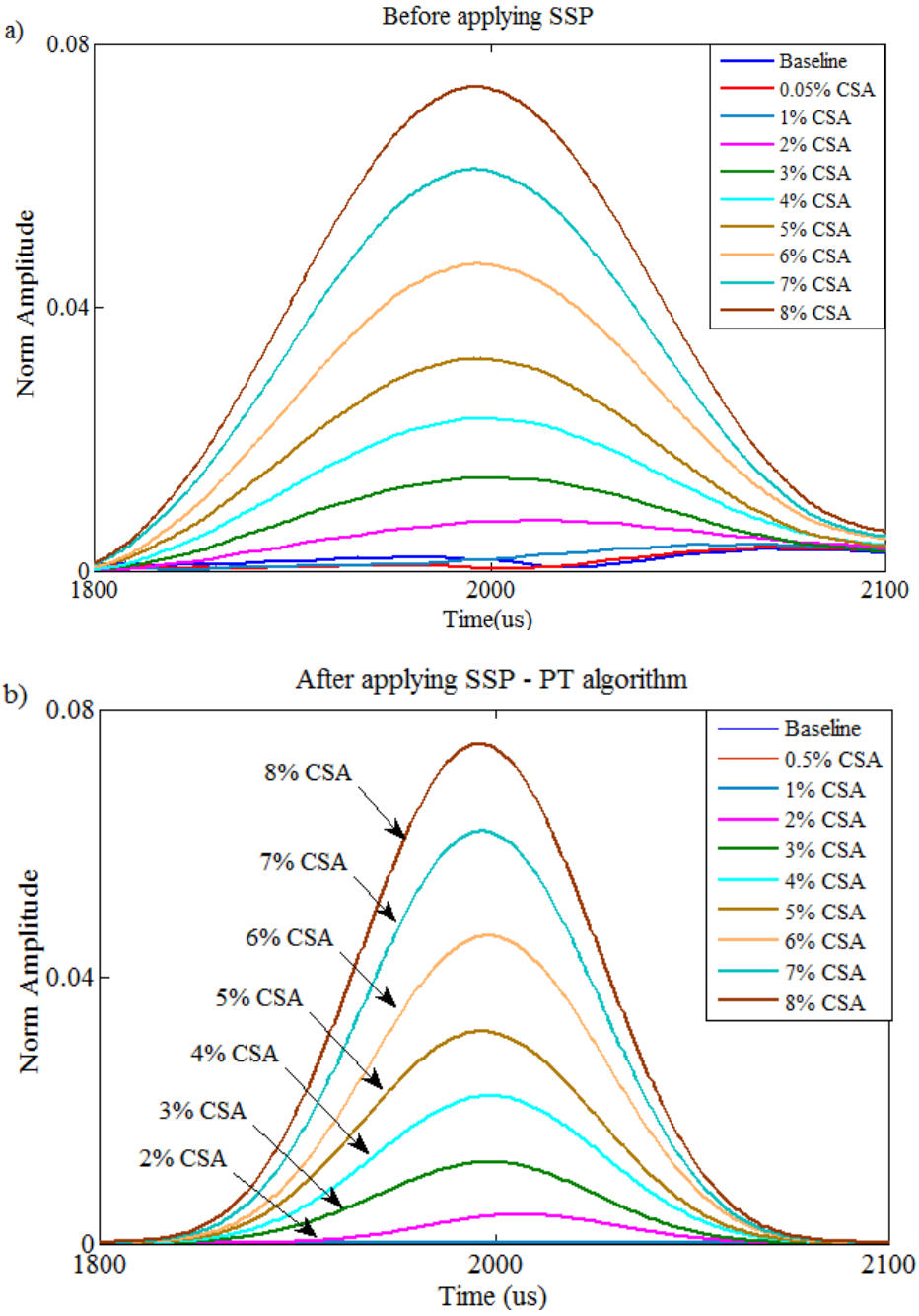

Figure 6-9: Illustrates the zoom-in result of experimental data for the defect's reflection from baseline up to 8% CSA, obtained by a) Teletest unit and b) the proposed SSP technique using PT algorithms.

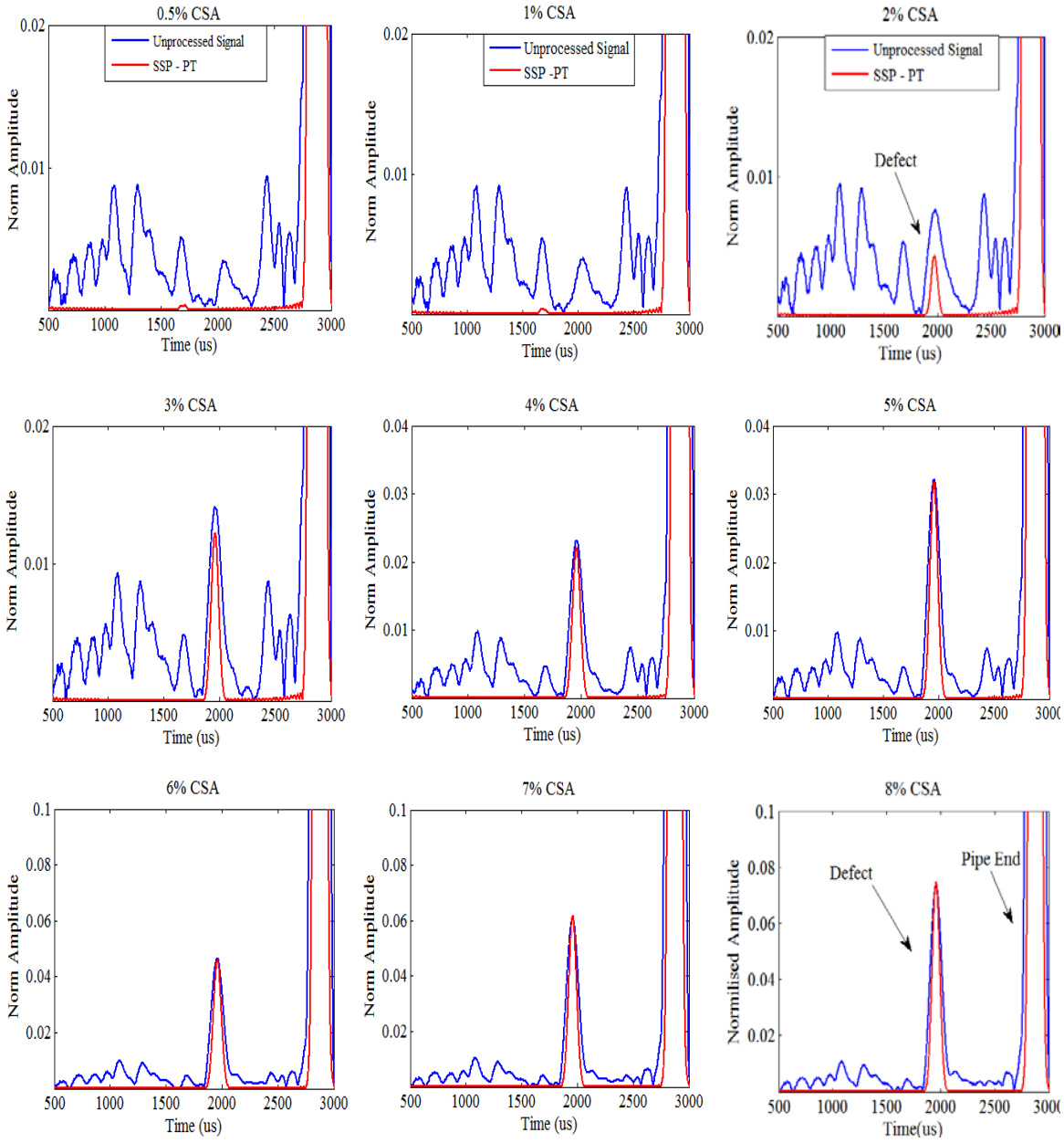

Figure 6-10: Zoom in around defect area from 0.5% CSA up to 8% CSA

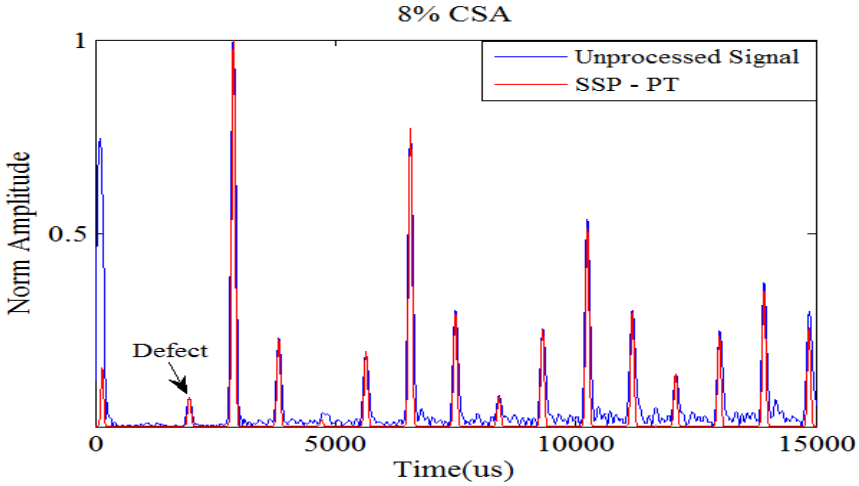

Figure 6-11: Result with 8% CSA; Unprocessed Signal (blue) and SSP Signal (red)

6.2.3 SNR Calculations

In order to determine how the proposed technique improves the performance and enhances the spatial resolution of the UGW response, the SNR has been calculated for different frequencies to see which improves the SNR most. Three types of SNR are calculated for this purpose, using equation (6-1) as follows:

i) The peak amplitude of the defect (S) to the RMS value of the noise region (N)
ii) The peak amplitude of the pipe-end (S) to the RMS value of the noise region (N)
iii) The peak amplitude of the pipe-end (S) to the peak amplitude of the defect (N)

Figure 6-12 illustrates those parts of the signal which are utilised to calculate the SNR for the above cases. This figure presents the response of the experimental data for the eight-inch pipe with 8% CSA defect, as described in the previous section.

In the first SNR calculation, the peak amplitude of the defect is selected as (S) and the RMS value of the noise region is selected as (N) and the SNR is calculated for all frequencies, which as mentioned earlier are 28kHz, 36kHz, 44kHz, 64kHz and 72kHz. Note that, since the PT algorithm gave the best SNR enhancement as well as spatial resolution, only the result of the PT is presented for this analysis. Figure 6-13 illustrates the result of the unprocessed signal (blue) and SSP–PT algorithm (red) for the above experiment when there is no defect (baseline) up to a defect size of 8% CSA.

The results clearly illustrate that the performance of the proposed technique massively improves the SNR of the UGW response compared to the unprocessed data for each frequency tested, achieving a 30dB improvement for 44kHz. However, as mentioned

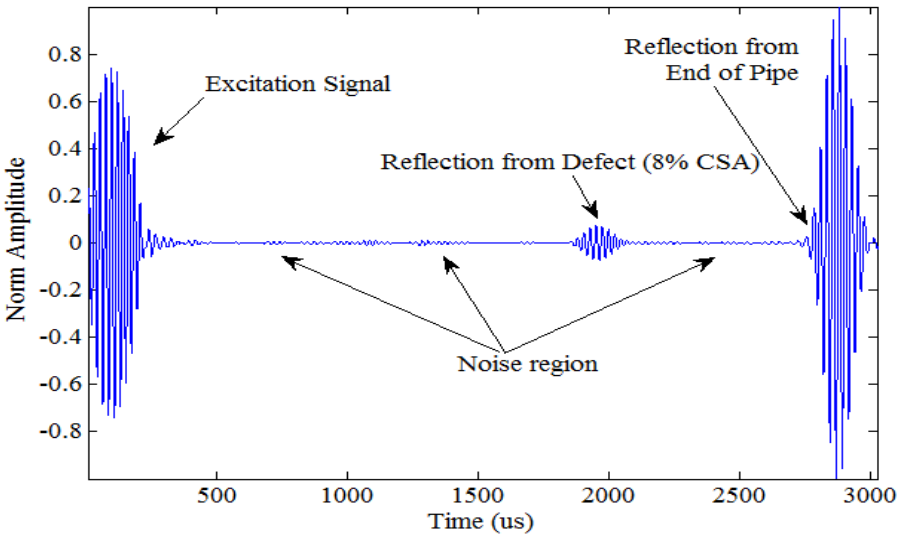

Figure 6-12: Regions to calculate SNR

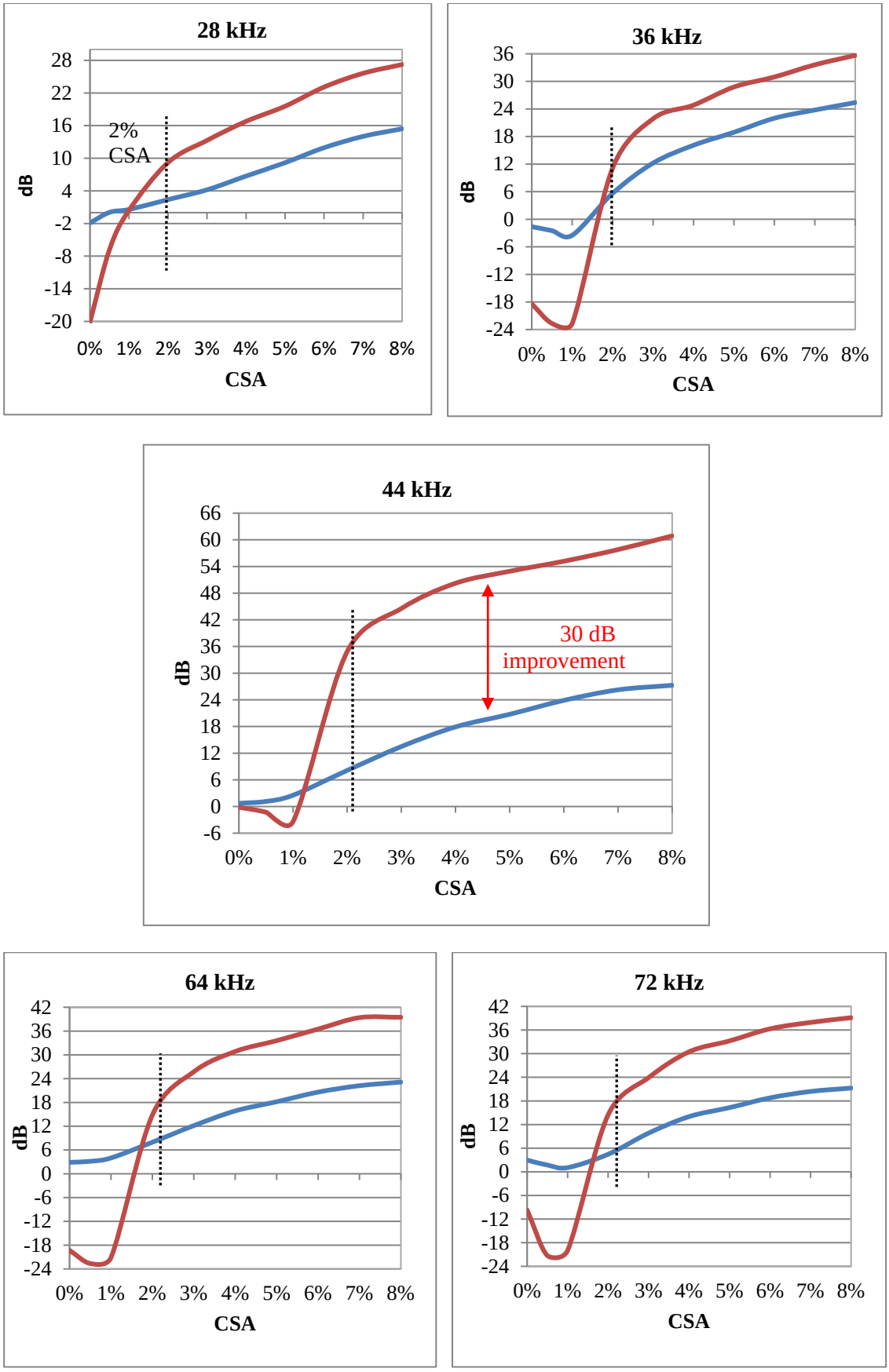

Figure 6-13: SNR calculation - peak amplitude of the defect (S) to the RMS value of the noise region (N) for 28 kHz, 36 kHz, 44 kHz, 64 kHz and 72 kHz.

earlier, the comparison commences when the defect size is at least 2% CSA. Hence, in order to clarify, we show a dotted line at 2% for each frequency response.

In addition, Figure 6-14 illustrates the SNR results for both unprocessed UGW data and SSP–PT technique for the selected frequencies and indicates that overall the result of 44kHz gives the best enhancements, although the SSP-PT improves the SNR for each frequency from 2% CSA upwards. The reason that 44kHz gives the highest SNR even before applying the SSP technique is that this frequency is in the peak of dispersion curve for this particular pipe size and geometry as explained in Section 2.6.6.

Figure 6-15 illustrates the results of two other SNR calculations. Figure 6-15-(a) calculates the SNR by selecting the peak amplitude of the pipe end to RMS value of the noise region, and clearly demonstrates that in all cases the proposed technique improves the SNR significantly, in particular at 44kHz, which improves the frequency approximately by 30dB. Figure 6-15-(b) presents the SNR of the peak amplitude of the pipe end reflection to the peak amplitude of the defect reflection, and as shown, the SNR for the UGW response before and after applying SSP follows the same trend. This means that no information is lost in terms of reducing the noise.

It is very important in UGW testing that the post-processing technique does not remove any small features. The results above evidently present that the SSP with the proposed optimum parameters has the potential to remove coherent noise while preserving small

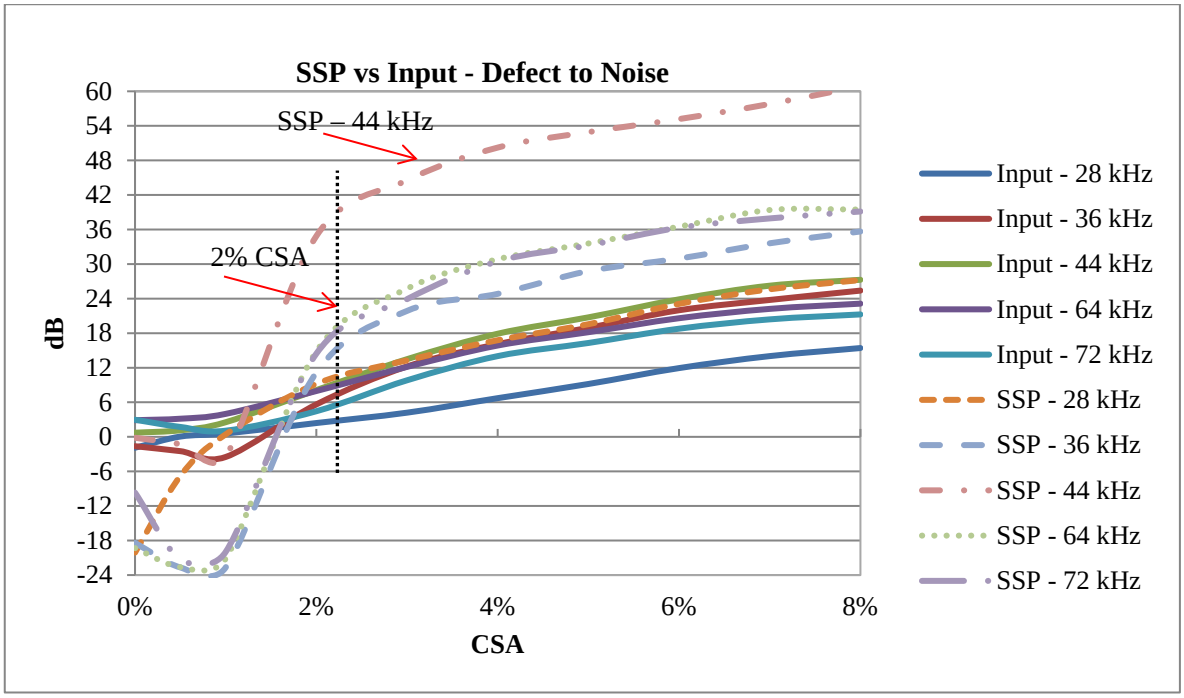

Figure 6-14: Result of SNR for original respond and SSP respond for different frequencies

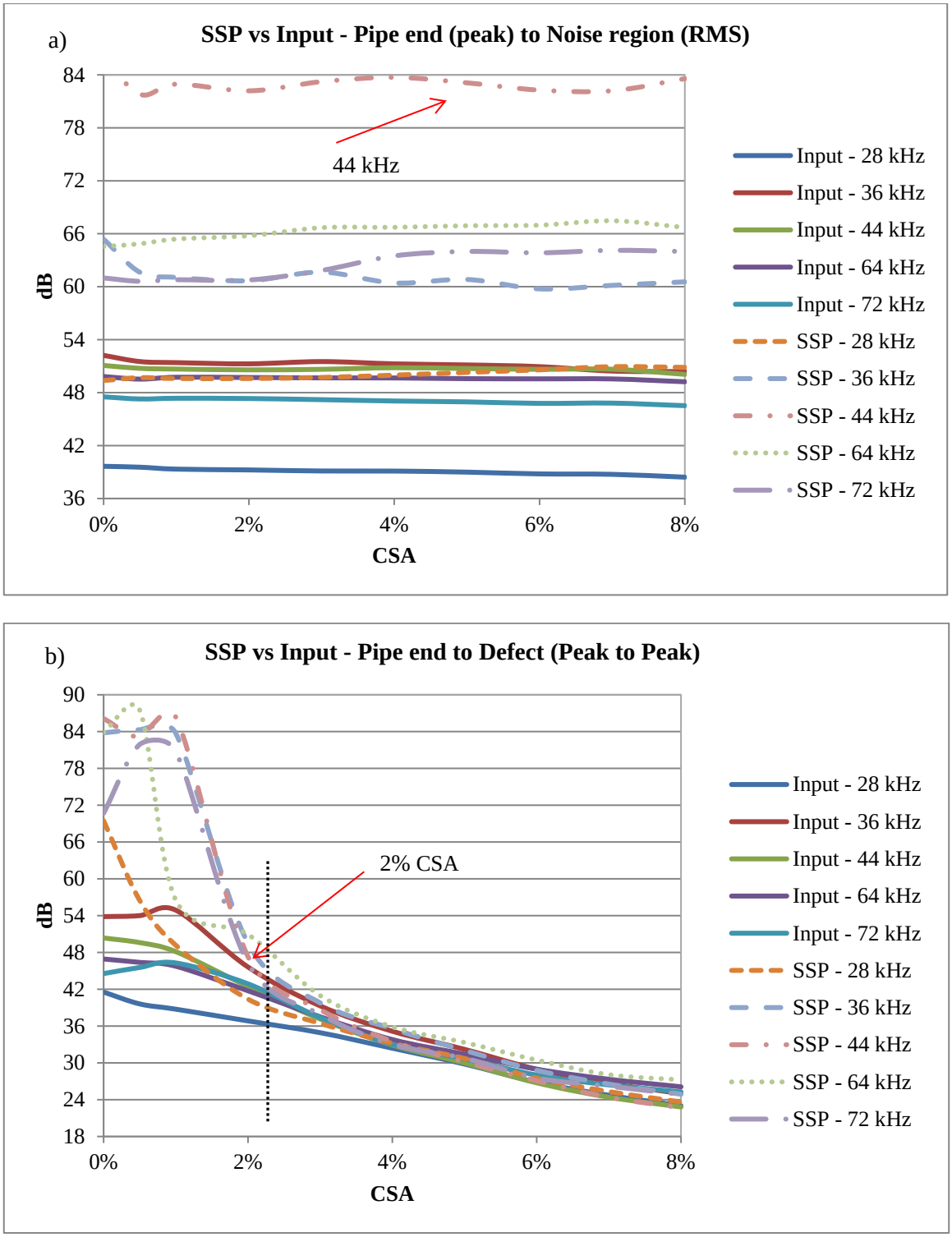

Figure 6-15: Result of SNR calculation a) peak of pipe end to RMS of noise region, b) peak of pipe end to peak of defect

features down to 2% CSA. Therefore, as a result of this experiment, SSP shows great potential to enhance the SNR, increase the sensitivity and spatial resolution of UGW response and identify potential defects down to 2% CSA.

6.3 Experiment with Two Saw Cut Defects

6.3.1 Objectives

The aim of the work within this section is to investigate the spatial resolution (distance limitation) of SSP where a small feature (i.e. defect) is close to a dominant features (such as a weld, pipe end and flange). The initial investigation starts with the proposed optimum SSP parameters utilised for a single saw cut defect, as explained in Section 6.2.2, to evaluate the outcome of the SSP distance limitation, obtained for the synthesised signal defined in Chapter 5.

6.3.2 Overview

To find the SSP distance limitation, experiments were carried out in the lab on the same eight-inch steel pipe that was utilised for the previous experiments, presented in Section 6.2.2. It has been claimed by Mallet [13] that when two features are close to each other, the SSP technique will remove the one that has a smaller amplitude. However, he did not mention the exact parameters that produce this result, or the exact distance limitation, etc.

In the synthesised test described in Chapter 5, it was revealed that when the distance between two features is less than 50cm, then the reflection of those signals will be superposed and the output of SSP technique is the combination of those signals as a single peak. However, other techniques, such as pulse compression, dispersion compensation, etc. offer the separation of superposed signals, as already mentioned in the literature.

6.3.3 Experiment Setup Up

The experiments setup up was the same as for the previous experiment, using the same eight-inch pipe, six meters long with a wall thickness of 8.28mm and outer diameter of 219.08mm. In this experiment, another saw cut defect is added to the pipe at a location 48cm from end of the pipe, as shown in Figure 6-16. The size of the defect is incrementally increased from 1% CSA to 8% CSA. Note that another 8% CSA saw cut defect already exists 1.5m from the pipe end. The signal is excited using a ‘5 Ring Torsional’ Teletest system [14] to transmit a 10-cycles, Hann window modulated tone burst of T(0,1) wave mode. The ring spacing between transducers was 30mm. The Teletest Collar was placed 1.5m from the near end of the pipe, using the pulse/echo method to excite/receive (Tx/Rx) the signal. The same frequencies as for the previous experiment were used to collect the

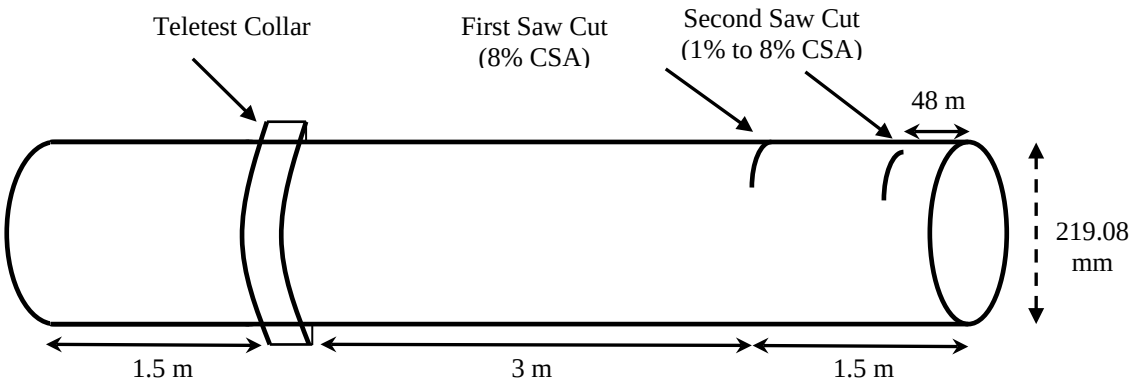

Figure 6-16: Experimental setup for the same eight-inch pipe with two saw cut defects.

data, but only the results relating to 44kHz are presented here because, according to the previous experiment, this frequency gives the best SNR enhancement.

6.3.4 Implementation of SSP

In this section, the proposed SSP technique was applied to the UGW response of the experimental data gathered with two defects. The SSP parameters were the same as those utilised for the previous experiment for this pipe with one defect. The initial result obtained with these parameters was not as successful and was only able to identify defects down to 4% CSA.

Therefore, the brute force search was applied to find the optimum parameter values for this scenario, again in order to improve the performance/resolution of the defects and capability to find smaller defect size. As a result, the optimum values were discovered that give the chance to detect defects down to 2% CSA for a second defect while the pipe already had another 8% CSA. The unprocessed signal and signal after applying SSP with the new optimum parameters are presented in Figure 6-17. This figure clearly demonstrates that the data after applying SSP are tidier in general and, in terms of defect detection, down to 2% CSA is noticeable. However, it can be seen that the coherent noise is hardly removed/reduced by the new parameters and SNR is slightly improved. The SNR enhancement is presented in Table 6-6 for 2% CSA and 3% CSA. Therefore, it is confirmed that there is a trade-off between detecting small features next to a dominant signal and improving the SNR.

The result shows that the same as synthesised analysis the distance limitation of SSP to identify any features is around 50cm when using 10-cycles Hann windowed at 44kHz.

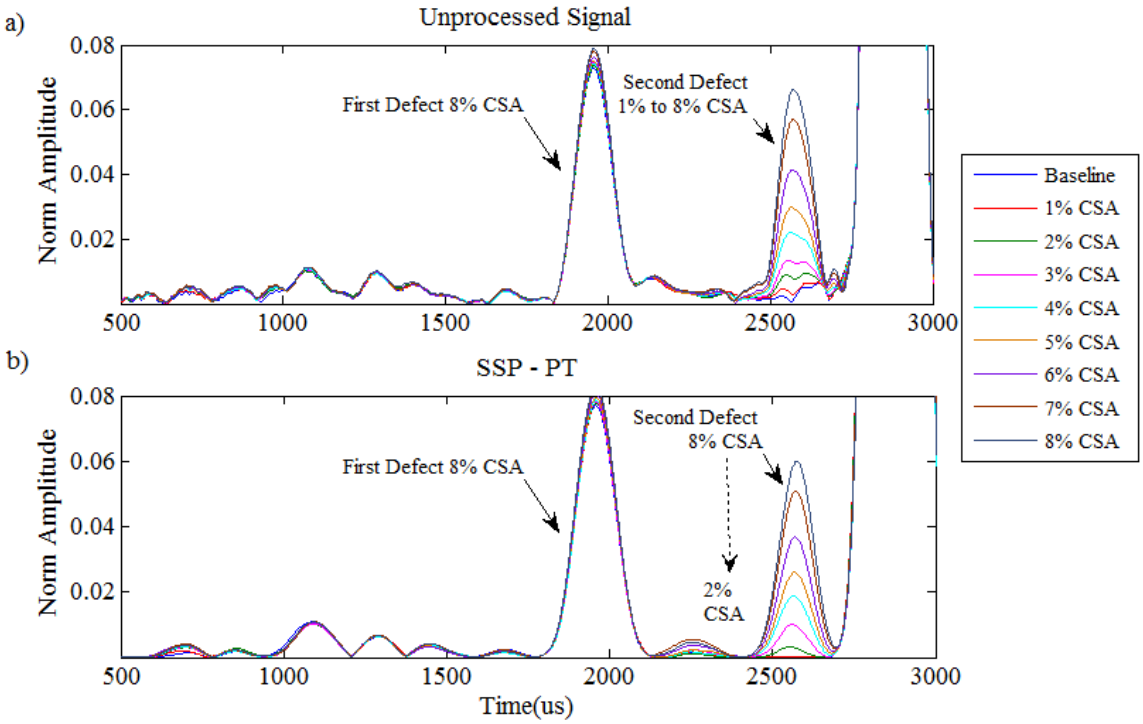

Figure 6-17: Zoom in result with two defects a) Unprocessed Signal b) SSP -PT

Table 6-6: SNR enhancement of experimental UGW signal with two defects

SSP recombination techniques	2% CSA	3% CSA
Polarity thresholding (PT)	1.5	2.2
PT with minimisation (PTM)	2.1	3.1

6.4 Application of SSP to field data

The set of experiments in the previous section had the purpose of applying the proposed SSP technique to the GWT data gathered in the lab. In this section, the technique is tested for actual GWT field inspection data. These data were gathered in different areas and at different frequencies. A key point of this section is to show how the proposed technique can improve the SNR and enhance the spatial resolution of the field GWT signal compared to the conventional results obtained from the Teletest system.

This section presents field inspection data collected using the Teletest system with the standard narrowband excitation routine. The narrowband data responses were examined by a trained GWT inspection to identify damage such as corrosion during the field inspection before the data were processed using the proposed SSP technique with PT and PTM, which were found to be the best SSP algorithms regarding SNR enhancement.

It is notable that these data only cover a torsional tool configured in three/five rings, 10-cycles Hann windowed.

6.4.1 Objectives

The main motivation of the work within this section is to study the SSP technique that proposed throughout this thesis to actual GWT field inspection data. Thus, the specific objectives are as follow:

- Define an optimum SSP filter bank parameters that could be applied in the Teletest system for all the data that obtained in the field inspection.
- Implement the SSP with PT and PTM algorithms that proposed in Chapters 6, to the data gathered in the field.
- Extract quantitative information from the inspection plots to assess the performance of SSP technique within an actual GWT field inspection data.

6.4.2 Field data collection

The data used in this section were collected during inspections using a commercial Teletest system and covering a variety of sizes of pipes at several locations, mainly in Alaska. There were many data available for processing. However only eight scenarios have been presented, and a summary of these inspections is presented in Table 6-7:

Table 6-7: Schedule of field tests

Test ID	Pipe size (inch)	Ring Spacing (mm)	Frequency (kHz)	Plot Number	Test Direction
TK104	8	30	36	Figure 6-18	Backward
Tank 13	16	30	36	Figure 6-19	Forward
Tank 13	16	30	36	Figure 6-20	Backward
C9 Sewage	12	30	44	Figure 6-21	Forward
C9 Sewage	12	30	44	Figure 6-22	Backward
GW SES	12	30	64	Figure 6-23	Forward
153	14	30	36	Figure 6-24	Backward
516	12	45	54	Figure 6-25	Forward

6.4.3 Pre-Processing

To assess the data, a function written in Matlab received the field data and processed it to generate the output signal. Note that a GWT inspection contains a few wave modes that are overlaid on the same plot, but in our processing we have only used the result of T(0,1) wave mode, and the SSP technique is applied to these data. In addition, the Hilbert transform is used to present the absolute value of a sinusoidal signal and to display its envelope.

6.4.4 Data Analysis and Results

The results presented in this section belongs to the eigth sets of data that are summarised in Table 6-7 among the many data available to the author for post-processing which contains different level of coherent noise. The results of Test 1 are shown in Figure 6-18. This test utilised an eight-inch pipe with a wall thickness (WT) of 8.18mm and an outside diameter (OD) of 8.625 inches. This figure presents the logarithmic A-Scan in the distance domain that the operator employs to analyse the data and decide whether there are any features within the pipeline or not. The logarithmic A-scan is preferred over a linear A-

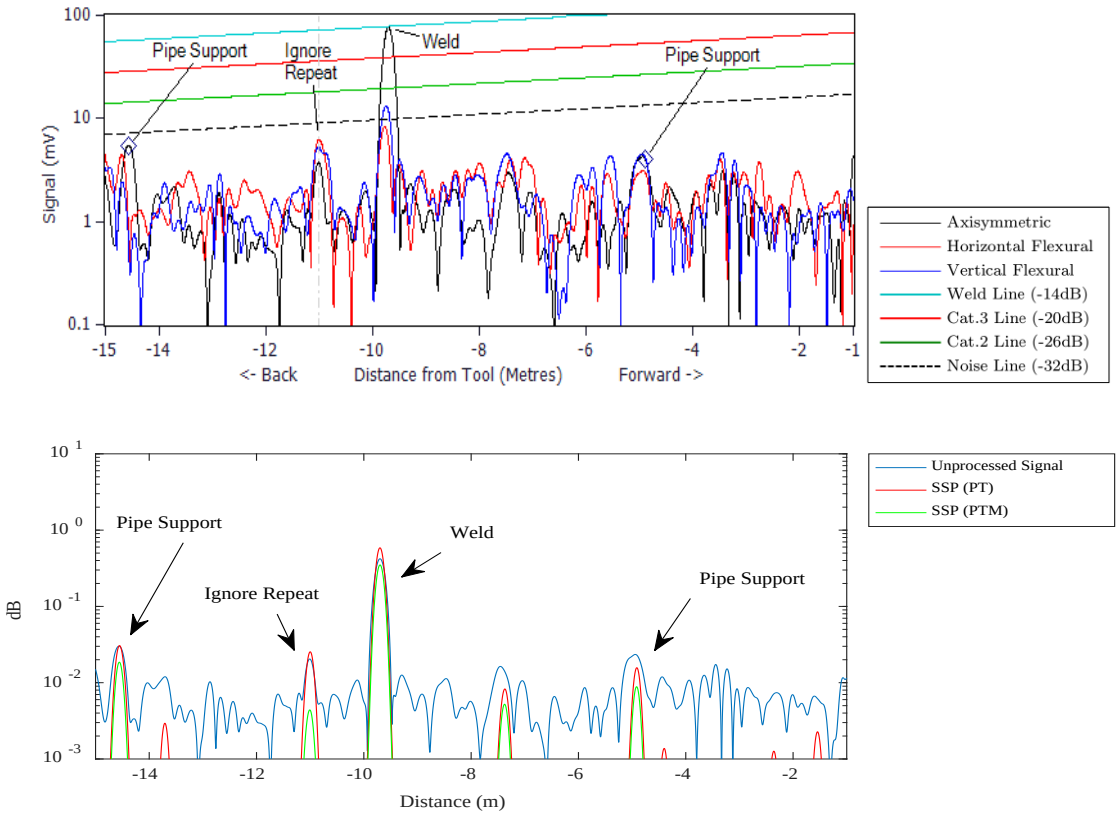

Figure 6-18: Comparison between unprocessed signal and proposed SSP with PT and PTM algorithms. Test ID: TK104, 8-inch pipe with OD: 8.625 and WT: 8.18mm at 36 kHz.

Scan, as the linear results usually do not show up the data effectively due to material attenuation, which has a negative exponential effect on amplitude with propagated distance from mechanical waves in this type of material. The black trace is the axisymmetric, T(0,1) wave mode, response in both plots. The blue and red traces are flexural responses of F(1,2) in Figure 6-18 (top plot), where the blue trace presents the vertical cross-section displacement of F(1,2) and the red trace displays the horizontal trace of F(1,2) in terms of cross-section displacement. Distance amplitude correction (DAC) is used in the Teletest system to set the reference signals for measuring the sensitivity of the scan, which is explained by many researchers (such as [81], [95]). In addition, responses from flaws are categorised as follow:

- Category 3: where the line is set at -20dB and used for a severe anomaly that is -6dB below the weld line.
- Category 2: where the line is set at -26dB and used for a moderate anomaly that is -12dB below the weld line.
- Category 1: Any response that exceeds the general noise level by 6dB and below category 2 are categorised as Cat.1.

Test file 1, as illustrated in Figure 6-18, contains four features identified by the inspector, and no anomalies were identified throughout inspected length. The results show that the proposed method enhanced the SNR and spatial resolution of this test by approximately 5dB. The SNR enhancement of all test files is presented in Table 6-8.

Table 6-8: SNR of all test files

Test file number	**Unprocessed signal SNR**	**PT SNR**	**PTM SNR**
1 – TK104	21.8	25.6	26.8
2 – Tank 13	22.3	26	26
3 – Tank 13	22.8	26.1	27
4 - C9 Sewage	18.7	26.4	27.2
5 – C9 Sewage	20.9	25.7	28.8
6 – GW SES	28.1	31.6	31.8
7 – 153	24.4	26	26.8
8 – 516	18.5	24.5	24.7

Test file 2, shown in Figure 6-19, states that the signal identified as welds on the A-scan cannot be confirmed, so a degree of assumption has been made. This was a noisy signal within the tested range. Hence, the inspection length is down to 5.5 meters from the tool location. Note that the grey colour indicated the end of the inspection range by the site engineer. The proposed method identified the weld, reduced the coherent noise, and only a few peaks remained that required further investigated. In addition, the SNR was improved by 4dB for both PT and PTM algorithms.

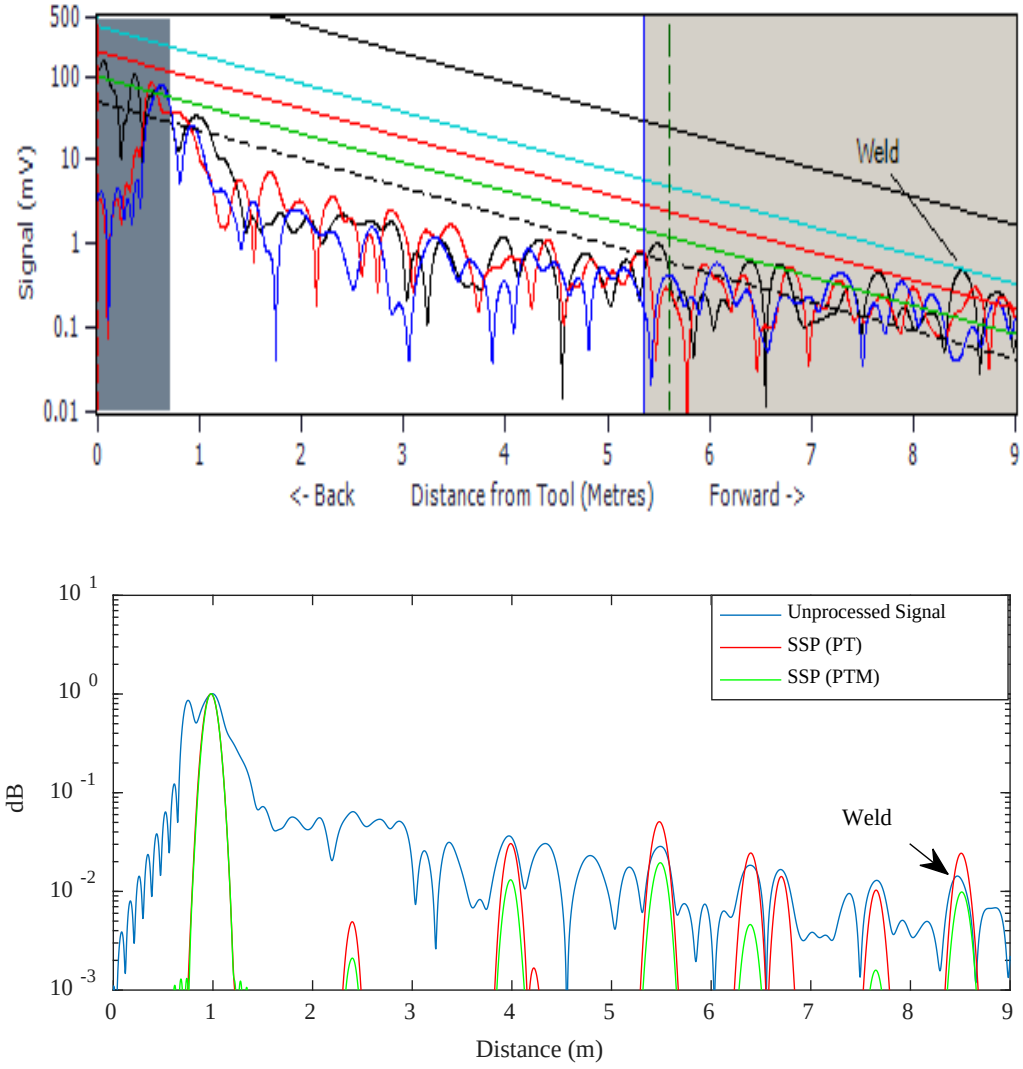

Figure 6-19: Comparison between unprocessed signal and proposed SSP with PT and PTM algorithms. Test ID: Tank 13, 16-inch pipe with at 36kHz, forward direction.

Two category 2 anomalies were reported in the inspection length of Test file 3, as shown in Figure 6-20. This was a 16-inch tank, which was inspected at 36kHz. In general, 36kHz is an optimum frequency for the tool configuration. Both PT and PTM algorithms identified these flaws as well as the weld and enhanced the SNR approximately by 4dB.

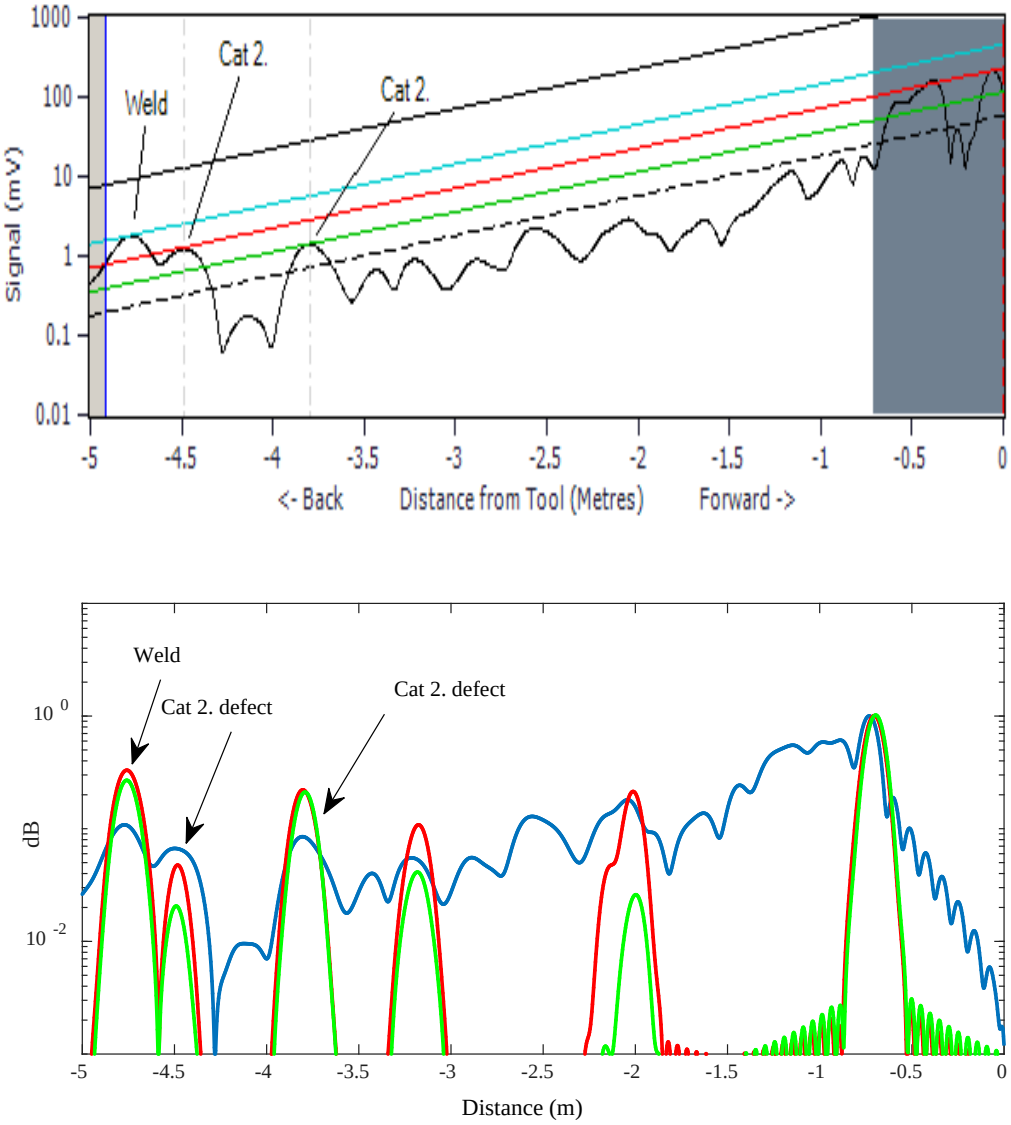

Figure 6-20: Comparison between unprocessed signal and proposed SSP with PT and PTM algorithms. Test ID: Tank 13, 16-inch pipe with at 36 kHz, backward direction.

The report of Test 4, as shown in Figure 6-21, stated that this pipe had high levels of noise. However, the inspection engineer identified one Cat.2 flaw, a weld, and the pipe end was on the diagnostic length for the 12-inch pipe at 44kHz. The results of the proposed method illustrated that the reported features are recognised by the proposed SSP method and the SNR was improved by approximately 9dB.

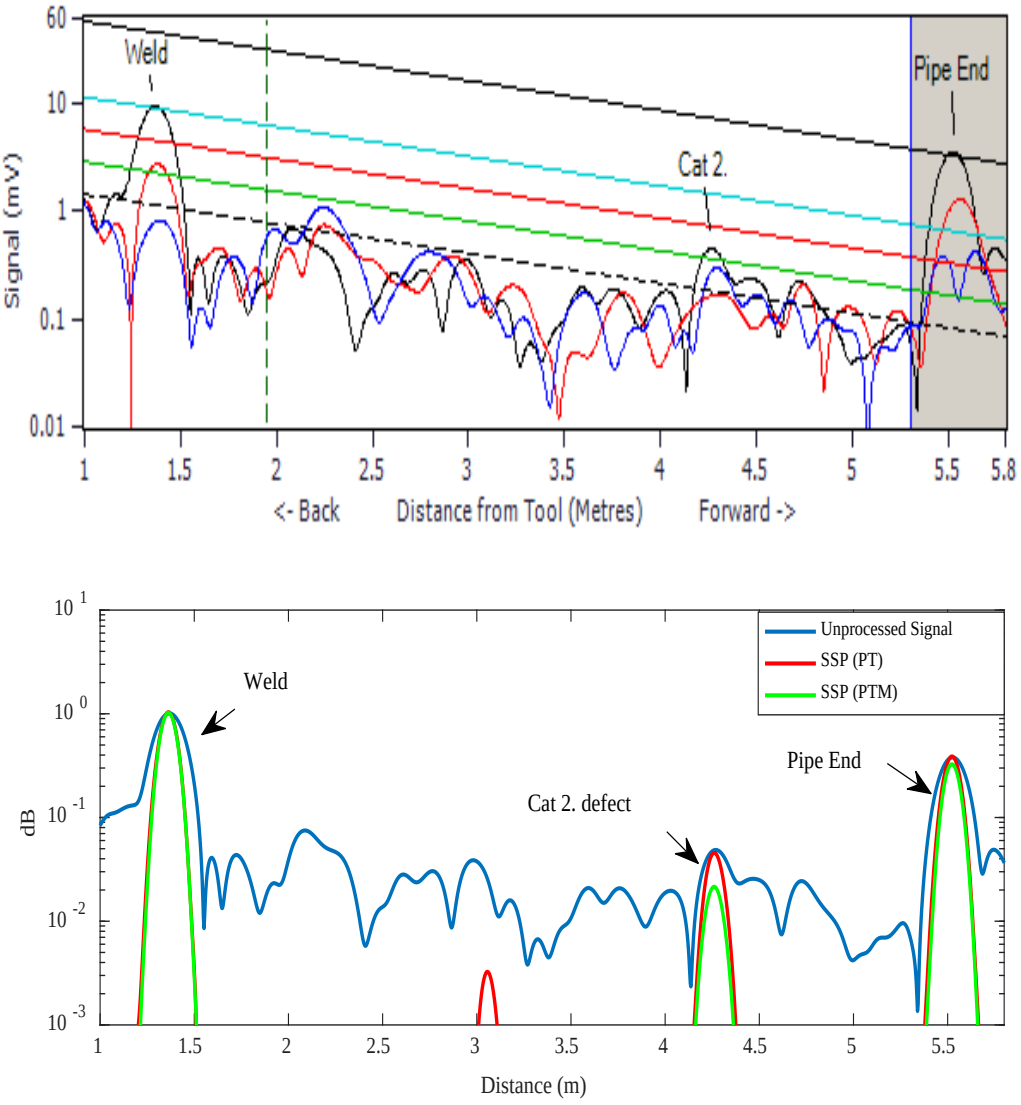

Figure 6-21: Comparison between unprocessed signal and proposed SSP with PT and PTM algorithms. Test ID: C9 Sewage, 12-inch pipe with OD: 12.75 and WT: 19.05mm at 44kHz, forward direction.

A-scan in Figure 6-22, illustrates for Test file 5 at 44kHz that the level of noise was high; hence, the length of inspection was reduced. One Cat.1 flaw was identified by the inspector, which was also detected by SSP. The results showed that SSP reduced the coherent noise while preserving all features, and increased the SNR by 8dB for PTM algorithm.

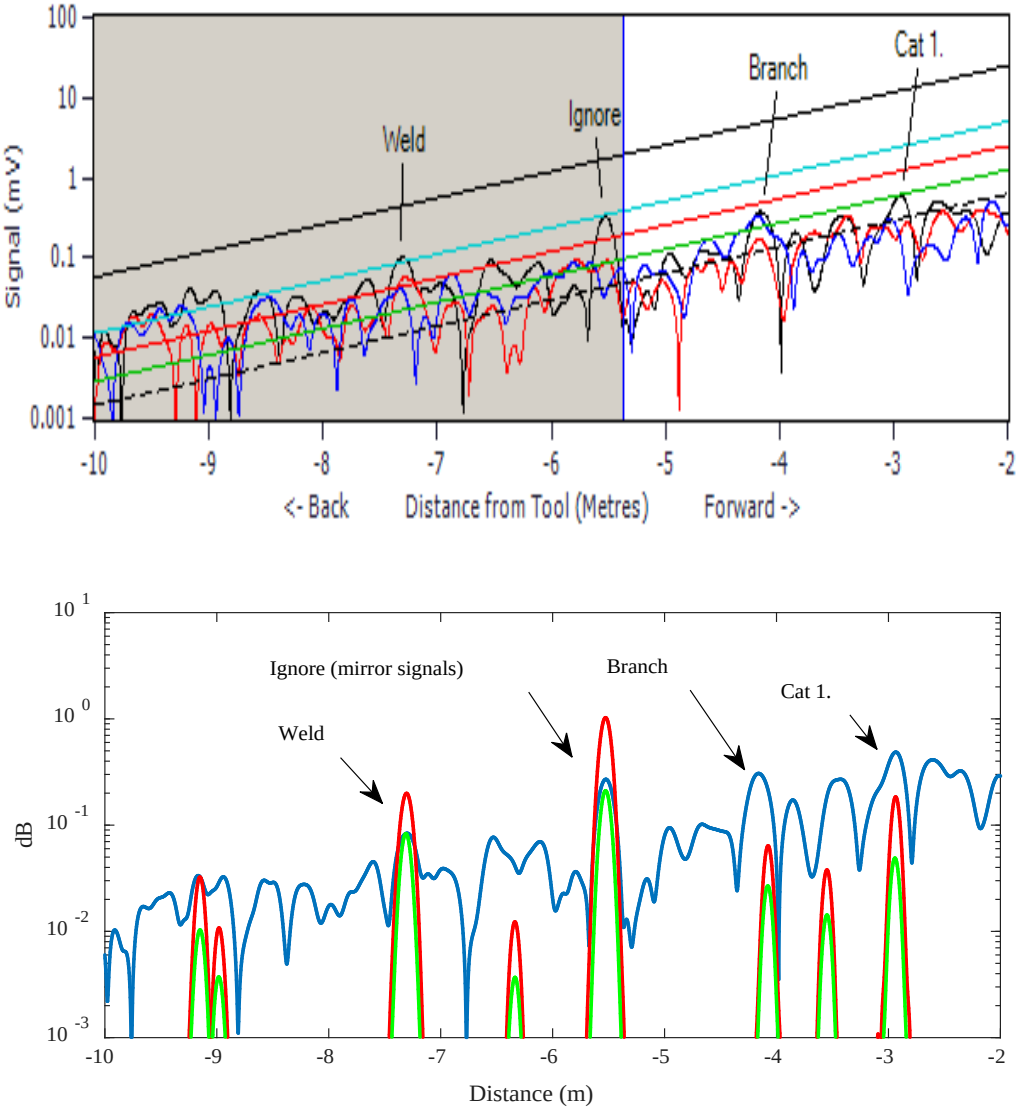

Figure 6-22: Comparison between unprocessed signal and proposed SSP with PT and PTM algorithms. Test ID: C9 Sewage, 12-inch pipe with OD: 12.75 and WT: 19.05mm at 44kHz, backward direction.

The data collected for Test 6 contain three responses, which were classified as two welds and one Cat.1 anomaly, as shown in Figure 6-23. The inspection engineer identified these features, which were also detected by SSP. The SNR was improved by about 3.5dB for both PT and PTM algorithms.

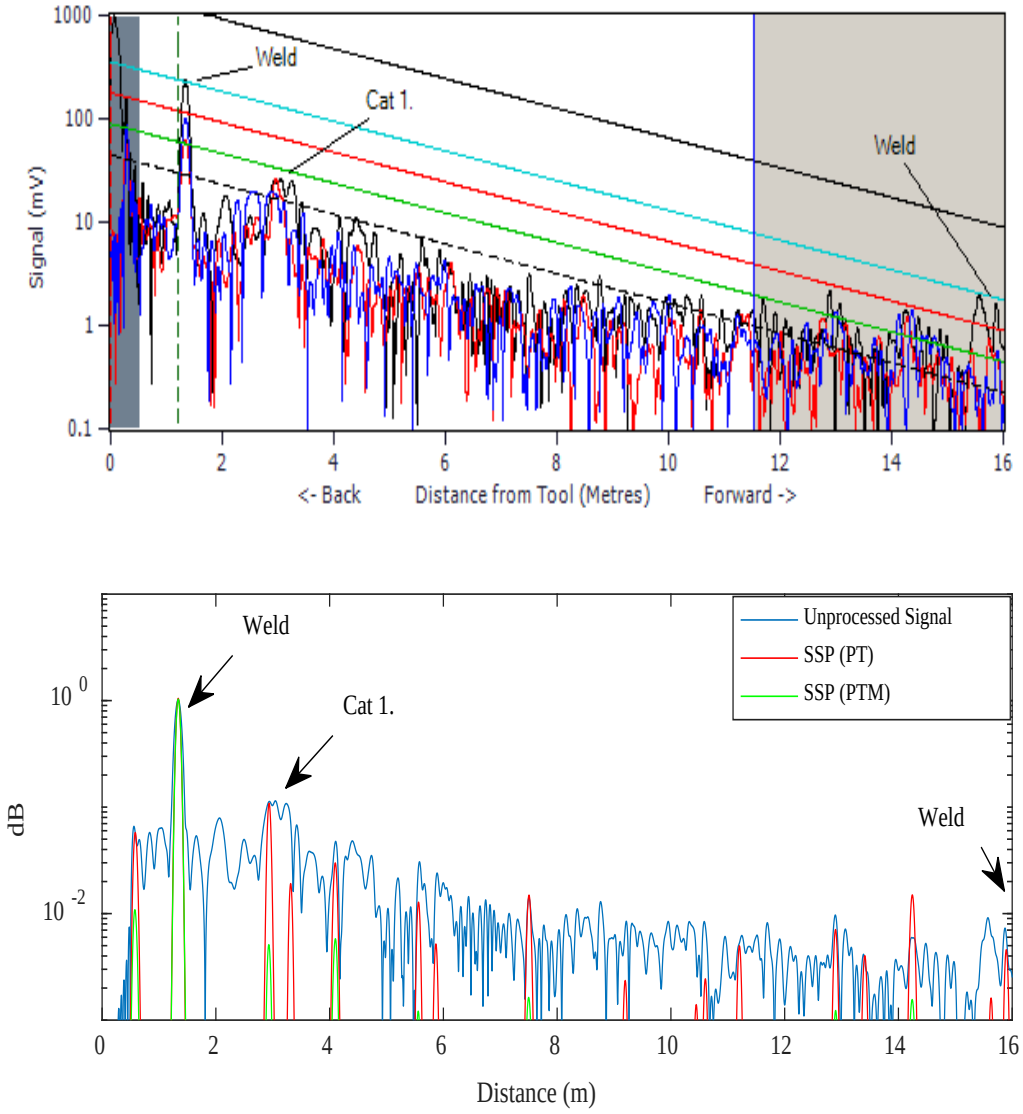

Figure 6-23: Comparison between unprocessed signal and proposed SSP with PT and PTM algorithms. Test ID: GW SES, 12-inch pipe with OD: 12.75 and WT: 5.16mm at 64kHz, forward direction.

A-Scan of Test file 7 is presented in Figure 6-24. The figure shows that no usable data were obtained. It is suggested by the inspector that the pipe may have Denso wrap applied. The proposed method identified the clamp, weld, reduced the coherent noise level, and enhanced the SNR by 2dB.

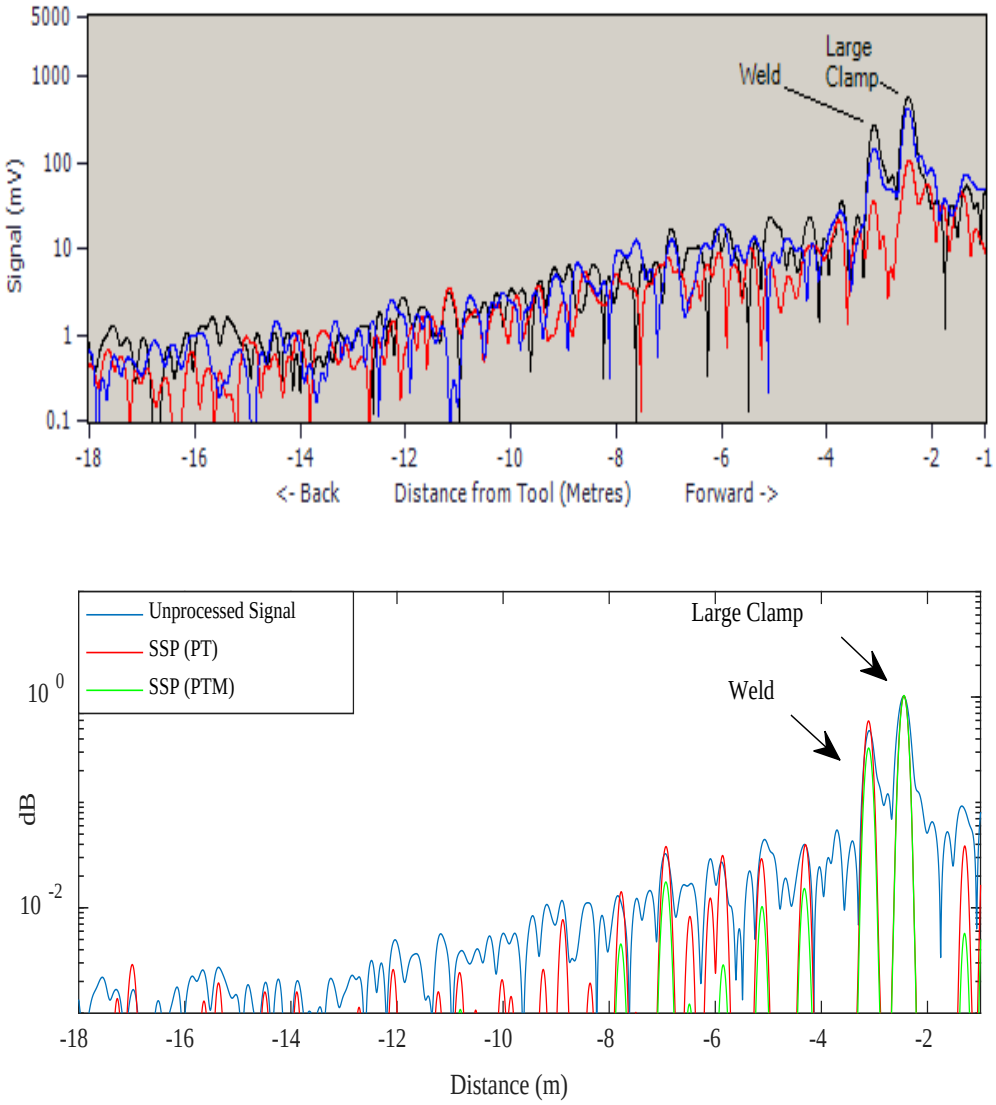

Figure 6-24: Comparison between unprocessed signal and proposed SSP with PT and PTM algorithms. Test ID: 153, 14-inch pipe with OD: 14 and WT: 7.92mm at 36kHz, forward direction.

Finally, Test file 8 presents the A-Scan of a 12-inch pipe at 54kHz containing two Cat. 2 defects and a few other peaks, as illustrated in Figure 6-25, where the signal contains a high level of noise. The proposed SSP increased the SNR by approximately 6dB due to removing the coherent noise. Also, it detected most of the features identified by the inspection engineer, but was unable to identify the second defect. This could be the result of a distance limitation of SSP, as defined in the previous section.

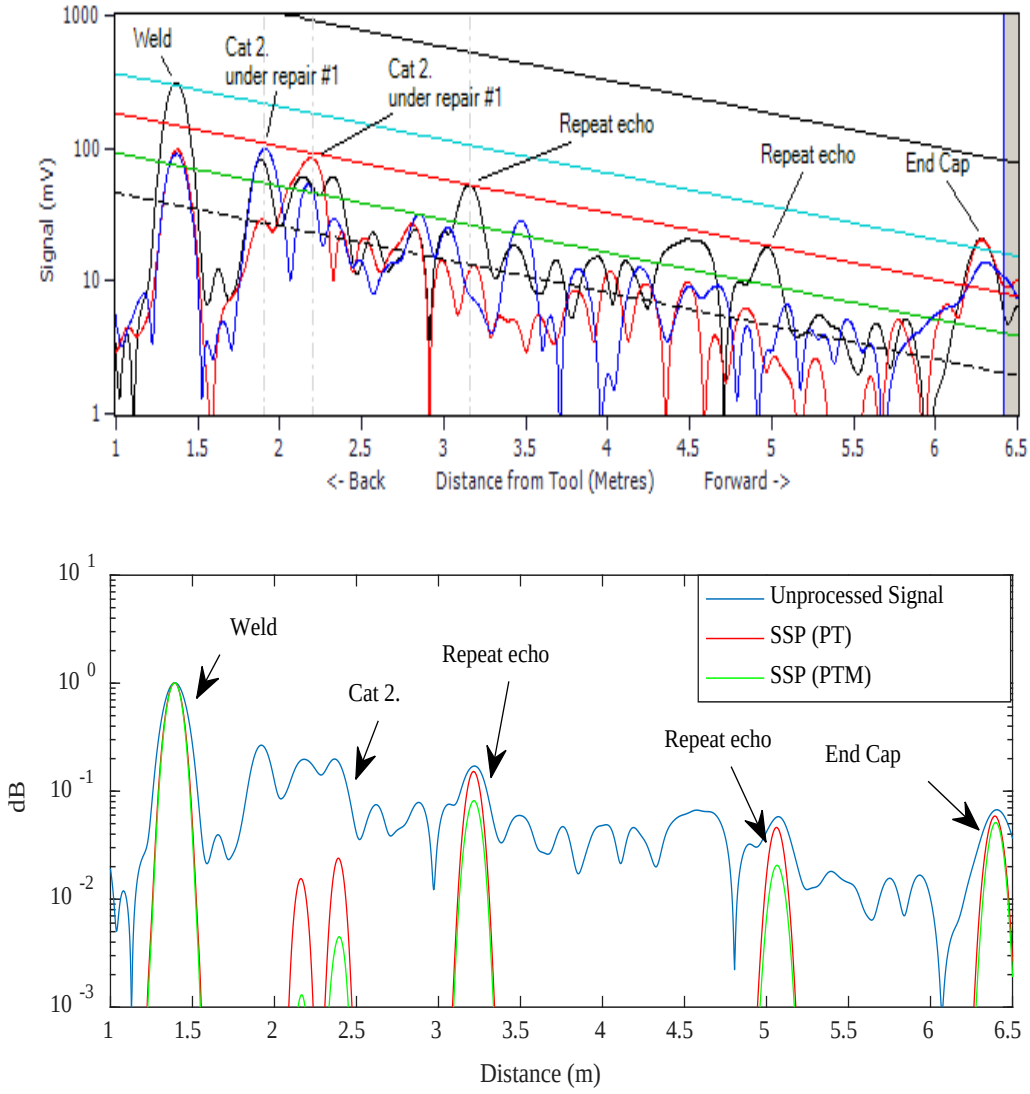

Figure 6-25: Comparison between unprocessed signal and proposed SSP with PT and PTM algorithms. Test ID: 516, 12-inch pipe with OD: 12.75 and WT: 10.31mm at 54kHz, forward direction.

6.5 Discussion

The use of SSP in GWT and identification of its optimum set of parameters carried out in this chapter follows a relatively new approach [13]. The signal synthesis presented in the previous chapter showed that SSP with the proposed parameters has generated promising results to enhance the SNR and spatial resolution of GWT signals by minimising the coherent noise. Hence to validate the synthesised outcome, laboratory experiments were carried out to assess the suitability of those proposed parameters.

6.5.1 Experiment #1: Pitch-catch using Teletest Focus+ and 3D-LDV scan (axisymmetric defect)

The first experiment used the pitch-catch method on a six-inch, six-meter long steel pipe with an outside diameter of 168.28mm and 14.3mm wall thickness. The pipe included an axisymmetric defect of 12.5% depth, which represented a loss in CSA of 13.5%. The Teletest Focus+ system pulser/receiver was employed to transmit a signal (Tx) and a Polytec 3D Laser Doppler Vibrometer (3D-LDV) was utilised to receive the signal (Rx). The excitation signal was a 10-cycles Han-windowed sine wave pulse at 60kHz that transmitted into the pipe specimen to generate a pure T(0,1) wave mode. The aim of this experiment was to analyse a scan point captured by 3D-LDV and minimise the coherent noise using SSP.

The level of coherent noise in this experiment was noticeable, mainly caused by the presence of dispersive wave modes. To quantify the improvement given by different SSP recombination algorithms, the SNR of the UGW response was calculated.

The results illustrated that the PTM algorithms have the greatest increase in SNR, 32dB, without distortion of the main signal arising from T(0,1) wave mode. The second best performing method was the PT algorithm, which exhibited 23dB enhancements. On the other hand, the FM algorithm removed the defect's reflection signal and reduced the pipe-end amplitude. This distortion is caused by multiplying the frequency of each sub-band without considering the sign of the signal. As a result, PTM and PT are chosen as the most appropriate SSP recombination algorithms for GWT data.

6.5.2 Experiment #2: Pulse-echo using Teletest Focus+ system (single saw cut defect)

The second experiment was carried out on an eight-inch steel pipe, six meters long with a wall thickness of 8.28mm and outer diameter of 219.08mm using a pulse-echo technique. The '5 Ring Torsional' Teletest system was utilised to transmit a 10-cycles, Hann window modulated tone burst of T(0,1) with a centre frequency of 44kHz. The Teletest Collar was placed 1.5m from the near pipe-end, and a saw cut defect was created 1.5m from the far pipe-end. Nine-saw cut defects were created, the sizes of which gradually increased from 0.5% CSA to 8% CSA. Since the PT and PTM algorithms gave the best results in terms of SNR and spatial resolution for the synthesised and the pitch-catch method, these algorithms were employed here.

The results of this experiment demonstrate that the SNR was improved by approximately 30dB compared to the unprocessed signal. The results indicated that defects smaller than 2% CSA cannot be identified both before and after SSP. This is due to the sensitivity of the system[12]. Therefore, the investigation and comparison were conducted only when the defect size was greater than 2% CSA. It was shown that the 2% CSA defect's reflection was almost masked by the coherent noise level and identification of responses using conventional signal interpretations is not feasible. However, SSP removed all the surrounding coherent noise but the defect's reflection. Therefore, this provides a good evidence that SSP has the potential to identify defects down to 2% CSA and enhance the spatial resolution.

6.5.3 Experiment #3: Pulse-echo using Teletest Focus+ system, (two saw cut defects)

The third experiment was carried out on the same eight-inch pipe mentioned in the previous experiment. In this test, a new saw cut defect was created which varied in size 1% CSA to 8 % CSA in each test, in addition to the already existing 8% CSA defect. The aim was to find and validate the distance limitation of SSP, as proposed in the synthesised UGW exercise with two adjacent features. Therefore, the defects were created 48cm from

[12] Sensitivity of Teletest monitoring system vary in different applications. However, typically a -32dB signal to coherent noise (100% reflector to coherent noise level) is considered in the field of guided waves [203]. This is the reason where a defect response remains unnoticed where its relative amplitude falls below -32dB.

the far pipe-end. The results illustrated that defects up to 4% CSA are detectable with the same filter bank parameters as used for the previous scenarios. However, in terms of identifying smaller defects, the parameters were required to be modified and was undertaken using brute force search algorithm described in Chapter 6. As a result, new filter bank parameters were introduced to identify defects down to 2% CSA. However, this was achieved at the cost of reducing the SNR enhancement.

6.5.4 Field data analysis using SSP

Furthermore, the proposed technique was applied to a series of field data using pipelines of different dimensions, collected in Alaska. These pipelines had a few known features, which were employed to assess the proposed parameters, where signal responses were more complex than those previously examined. The excitation signal in all test files was a 10-cycles Han-windowed sine wave pulse at different frequencies that were transmitted into the pipe specimen to generate a pure T(0,1) wave mode. The results showed that the proposed method significantly reduced the coherent noise in all test files and increased the SNR and spatial resolutions of the UGW response.

In addition, some peaks were identified that corresponded to unidentified peaks in the unprocessed signals. It is unclear if these are actual features or erroneous features introduced by the SSP technique. However, in some cases the proposed method reduced the amplitude of the features, in particular the response of defects. Therefore, this requires further investigation as the relative amplitude of the defect is required for flaw sizing. Moreover, although the SNR of the PTM algorithm was slightly higher than the SNR of the PT algorithm in most cases, in terms of identifying features and preserving the amplitudes, PT achieved the greatest response. Therefore, SSP using PT algorithm as implemented in this work, is suitable for GWT; however, the pre-defined parameters that can be applied for any inspection are not yet defined. As a result, further investigation is required to address this issue. In addition, more field data sets are required to assess the proposed method by utilising all known features in the A-Scan to ensure that SSP technique does not produce any erroneous features.

6.6 Conclusions

This chapter presents the GWT experimental and field data containing features and a high coherent noise level. The SSP technique is applied to these data to assess the outcome of synthesised signal analysis, as presented in Chapter 5. The main concern was to reduce the coherent noise by minimising the effect of DWM, hence, improving the SNR and the spatial resolution of UGW response.

A selection of commercial GWT tools, such as Teletest system and a 3D-LDV were utilised to demonstrate the advantage of the proposed method compared to the current inspection process. To meet the objective, three sets of experiments were conducted in the lab on six and eight-inch diameter steel pipes, followed by field tests, to validate the proposed SSP filter bank parameters, using the best recombination algorithms. The proposed parameters were tested for T(0,1) wave mode and its flexural wave modes family using different frequencies.

The experimental results confirmed that the proposed technique considerably reduces the level of DWM in UGW response, and significantly enhances the SNR up to 38.9dB for pulse-echo measurement in Section 6.2.2. These levels of SNR improvement can potentially make signal interpretations easier and lead the users to do more reliable UGW inspections. Enhancements in UGW sensitivity and spatial resolution can pave the way to detecting smaller defects and increasing the inspection range. It is shown that the proposed technique identified defects down to 2% CSA that were hidden below the noise level. Thus, it is suggested that these parameters are suitable for UGW signal using T(0,1) wave mode for this specific application. To the best of the author's knowledge, this technique has not previously been used successfully in the field of GWT.

Furthermore, in order to validate the distance limitation of SSP, as illustrated for the synthesised signal in Chapter 5, another experiment was conducted in the lab, where a saw cut defect was created 48cm from the pipe-end, the size of defect gradually increased from 1% to 8% CSA. To start the investigation, the same SSP filter bank parameters as utilised for the first experiments were tested. The results indicated that the proposed method, with those parameters defined earlier, was able to identify defects only when the size of the defect was larger than 4% CSA. Therefore, in order to check the ability of SSP to find smaller defects in this case, a brute force search was applied. As a result, new optimum values were discovered enabled the detection of defects down to 2% CSA when the defect was close to the pipe end. However, this achievement is at the cost of losing resolution

and SNR enhancement, as this set of parameters were unable to remove the coherent noise entirely.

Moreover, some field data were processed in this chapter, where the signal was much more complex. The results showed that the SNR and spatial resolution were improved for the majority of the features. However, in some cases, particularly when the features were close to one another, SSP combined the features, and hence reduced the temporal resolution.

To sum up, it is shown throughout the synthesised, experimental and field data results that the performance of SSP technique is sensitive to the selection of filter-bank parameters. The optimum parameters are proposed that significantly reduced the effect of DWM, as a result; removing/minimising the coherent noise, enhancing the SNR, and spatial resolution. However, it was shown in some cases that the SSP parameters need to be modified, and further investigation is required to find the best parameters for every scenario. Also, the limitation of SSP regarding a distance limitation should be studied and a solution proposed to address it. Although SSP shows great promise for use in the industry, the pre-defined parameters need further investigation, which could result in a more reliable application to cover every scenario.

.

Chapter 7

7 Conclusions and Recommendations for Future Work

7.1 Main Finding of this Thesis

The focus of the work presented in this thesis was to develop advanced signal processing techniques for acoustic (sonic and ultrasonic) applications. In these applications, signal responses are usually incomplete, distorted and noisy. Therefore, reconstructing the signal, noise reduction and the removal of any distortion/interference were the main goals of signal processing techniques presented. The primary aim was to study and develop an advanced time-frequency signal processing technique for acoustic applications to enhance the quality of the signals. The phenomenon was studied in detail with useful recommendations for future works.

7.1.1 Signal processing technique applied to Audio Signal

A time-varying signal model based on time-frequency analysis was introduced using motion detection to reconstruct the audio packet loss signal. The literature related to the audio signal was provided and the limitation of conventional techniques was highlighted. The proposed algorithm was a receiver-based that is designed for wide-band and narrow-band audio signals to address the problem of the restoration of gaps in the signal.

The problem of modelling the time-varying frequency spectrum in the context of packet loss concealment (PLC) was addressed, and a novel solution therefore is proposed for tracking and using the temporal motion of spectral flow to reconstruct the signal based on a *time-frequency motion (TFM) matrix*. The novel aspect of this methodology was the introduction of TFM and its application to motion-compensated extrapolation or interpolation algorithms using a discrete Fourier transform (DFT) or discrete cosine transform (DCT).

The spectral motion vectors are estimated by dividing the signal bandwidth into several sub-bands. The cross-correlation of the frequency bands across time frames is used for motion estimation. The proposed algorithm is applied to synthesised and real audio signals

that contain random frame loss or gaps, in order to reconstruct/estimate the missing frames and enhance the quality of audio signals that have been degraded by packet loss.

To compare the proposed method with conventional approaches both objective and subjective evaluations tests, in packet loss range of 5% to 20% were carried out, the details of which were fully discussed in Section 4.7. The evaluation results demonstrated that the proposed algorithm improved performance by an average of 2.85% and 5.9%, regarding PESQ and MOS scores respectively. Furthermore, the proposed algorithms are being considered for commercial applications by Brunel Innovation Centre.

7.1.2 Signal processing method applied to Ultrasonic Guided Wave Signal

A slightly different signal processing technique has been extended and applied to address another challenging problem in the Guided Wave Testing (GWT) industry, where shortcomings in pipeline inspections could result in catastrophe. Therefore, the focus was on a signal processing technique that could be utilised as the post-processing technique for Ultrasonic Guided Waves (UGW) response. This has been achieved by employing the modified version of time-frequency algorithms that were proposed and developed for audio signals.

The proposed signal processing technique, called split-spectrum processing (SSP), was investigated for the reduction of coherent noise in GWT due to multi-modality and the presence of unwanted dispersive wave modes (DWM). The SSP method with respect to its application in UGW inspection has been reviewed quantitatively to measure the enhancement regarding SNR and spatial resolution.

The research into this application of SSP demonstrated that the performance of the technique was sensitive to the parameter values employed in its implementation. This research therefore investigated a parametric study of the filter bank parameter values to determine their influence on SSP performance for pipe inspection using GWT. Parameters such as processing bandwidth, filter bandwidth, and filter separation with resultant estimated optimum values were investigated for pipeline inspection.

Initial signal processing of generating synthesised UGW signals was developed, to address challenges of excessive coherent noise arising from ultrasonic signals gathered during inspection, which was required to analyse the SSP application. Once the synthesised signal was generated, a brute force search algorithm was used to find the optimum values of the SSP parameters to give the highest SNR.

In addition, a range of SSP recombination algorithms was studied in this research, before being selected for synthesised experimental data. Polarity Thresholding (PT) and PT with Minimisation (PTM) algorithms among other recombination algorithm were found to be the best SSP methods recombining the signal. An SNR improvement of up to 30dB of received synthesised UGW signal was observed with the proposed optimal filter bank parameters employing PTM. To the best of the author's knowledge, these optimum parameters have not previously been recognized or identified in the field of GWT. It also represents that although the Frequency Multiplication (FM) and Minimisation algorithms have improved the SNR, the spatial resolution of the result compared to PT and PTM algorithm was poorer as they were unable to remove the presence of DWM entirely and therefore they have a distorting effect on the signal. The limitations of each SSP algorithms are investigated in this research. The research identifies that if the distance of two features (e.g. defect and weld) was less than 0.4cm; the SSP algorithm may combine the reflection of two features as a single feature and presents a single peak. The amplitude of this single peak was the value of the larger of the two original peaks this effect reduces the temporal resolution. A minimum distance of 0.5cm was found to be effective with the proposed technique.

It should be mentioned that this examination utilised an excitation frequency of 44kHz with 10-cycles modulated with Hann window. However, this result may vary slightly for different excitation frequencies and pulse width. The frequency optimisation study indicated that the distance limitation could be reduced up to 0.35cm by increasing the excitation frequency up to 70kHz.

A range of experimental data was introduced to validate the proposed filter bank. The usefulness of SSP to minimise the coherent noise was tested in different scenarios, with two different types of defects (axisymmetric and saw cut defects), using the commercial GWT tools, "Teletest", designed/manufactured by Plant Integrity Ltd. The optimum parameters obtained were validated using these experiments. The experimental set up used three-rings of torsional transducers to generate T(0,1) wave mode (the only non-dispersive wave mode). The results for a selection of frequencies showed that SSP using the optimum parameters successfully minimised the coherent noise and helped identifying defects down to 2% Cross-Sectional Area (CSA), where it was hidden below noise level for the unprocessed signal. An SNR improvement of up to 38dB of received UGW signal was observed in pulse-echo experiment in Section 6.2.2 However, it was revealed that when

the defect was close to the pipe-end (48cm), the defect identification for that particular defect, close to the anomaly signal, reduced to 4% CSA.

Therefore, another brute force search algorithm was applied to find the optimum parameters to identify smaller defects. The results showed that the new parameters have the potential to identify defects down to 2% CSA, even when the defect was close to the pipe-end. However, in terms of SNR enhancement and temporal resolution, the new parameters when compared to the previous optimum parameters were less effective as shown in Figure 6-17., which the SNR is improved by an average of 2dB for 2% and 3% CSA defect. In addition, the results of SSP algorithms revealed that the SSP in terms of defect sensitivity has the potential to identify defects down to 2% CSA. Hence, SSP showed good potential to increase the inspection range from a single test location as it significantly reduced the level of coherent noise, enhanced the SNR, and improved the spatial resolution of UGW response. Furthermore, the development of the SSP technique was considered in respect of its application to sets of field data, which were more complex and difficult to analysis. It was revealed that SSP with optimum parameters has the potential to remove/reduce the coherent noise and significantly enhance the SNR and spatial resolution of field data, leading to the identification of smaller defects that may be hidden below the noise level.

The field data were extracted from raw data collected at different locations, and of different areas, pipe sizes, etc. the post-processing methods were applied to make comparison of the Teletest result and the result of proposed technique that explained earlier. The results showed that the proposed method significantly reduced the coherent noise in all test files and the SNR and spatial resolutions were improved for the majority of the features. However, in some cases, particularly when the features were close to one another, SSP combined the features, and hence reduced the temporal resolution.

The conclusions reached in this thesis will contribute to the progression of the GWT technique through more reliable signal interoperation and defect detection. Moreover, since this thesis has highlighted the performance of SSP in minimising the coherent noise and enhancing the SNR, this technique is being considered as a potential candidate to be used in the next release of Teletest software, produced by Plant Integrity (TWI Ltd). However, before software integration, the distance limitation needs to be addressed after future validations.

7.2 Recommendation for Future Works

7.2.1 Time-Frequency Motion Matrix using Modified Discrete Cosine Transform or Wavelet Transform

The proposed TFM matrix was designed to reconstruct audio packet loss with application to VOIP. The parameters defined in this work can be varied for better resolution, such as changing the frame length and reducing the overlap between adjacent frames.

There is strong potential to examine the proposed TFM method using either MDCT domain or wavelet transforms. In addition, the comparison between the proposed DFT method with MDCT and wavelet transform may result in a better solution for enhancing the signal quality regarding packet loss. This approach may result in significant reduction in computational complexity of the system.

Since the proposed technique is computationally demanding in terms of recent technology development, certain adjustments are required in order to implement the proposed algorithm on real-time embedded applications. This will involve tailoring and adjustment include numerical shortcuts, in particular with regards to matrix and vector calculations.

In order to reduce the complexity, it may worth to pre-define the optimal frequency bins. This can be done by investigating the optimum frequency bandwidth and using either cross-correlation or autocorrelation for estimating the motion movement. In addition, the choice of interpolation algorithms is further area that could be the subject of future research.

Furthermore, adding side information to the coded signal at a sender-side such as information about the signs of the DFT, DCT and MDCT coefficients, or a polynomial approximation of the coefficients (along frequency or time) needs to be investigated as it may improve the reconstruction process.

7.2.2 Automation of SSP Algorithm

A set of synthesised, experimental data, as well as field data, were investigated in this work. Since the result showed promise regarding SNR enhancement and spatial resolution of GWT data, there is clear potential to automate the SSP technique based on pre-defined parameters. For this reason, further investigation is required in respect of different asset frequencies for each pipe's size and geometry. Furthermore, the possibility of creating a procedure that can be utilised for working out the optimum parameters without using a brute force search. In addition, the use of a chirp signal (larger bandwidth excitation) may improve the results of SSP in terms of temporal resolution; however increasing the bandwidth increases the number of possible wave modes in the test, which can worsen the result.

7.2.3 Application of the SSP Method on Flexural Wave Modes

The proposed SSP method is designed to reduce the effect of coherent noise and increase the SNR and spatial resolution of GWT data. Dispersive wave modes (DWM) are one of the main sources of coherent noise, which occupies the same bandwidth as the signal of interest. Flexural wave modes are all dispersive, whereas higher order flexural wave modes are more dispersive as their energy is spread further over space/time during propagation. However, fundamental flexural wave modes are less dispersive (i.e. F(1,2)), as is presented in the Teletest software plot for field data in Chapter 6. Therefore, as most of the time defects were identified by looking at the trace of these wave modes, future work can concentrate on applying the SSP method on these wave modes.

7.2.4 Apply the SSP Method on Hybrid Active Focusing Technique

Initial test of SSP application on Hybrid Active Focusing technique [202] shows promise result to improve the SNR and spatial resolution of focused GWT up to 6dB when applying with the PT algorithms as shown in Figure 7-1. Therefore, further investigation is required in this area to enhance the sensitivity of inspections.

a)

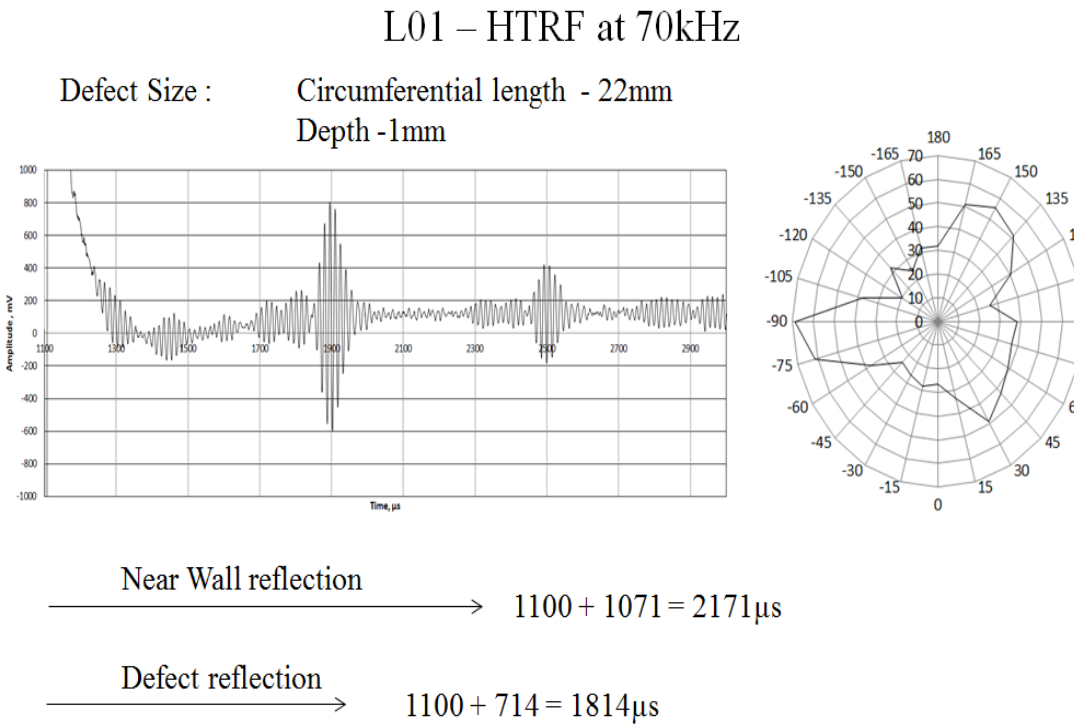

b)

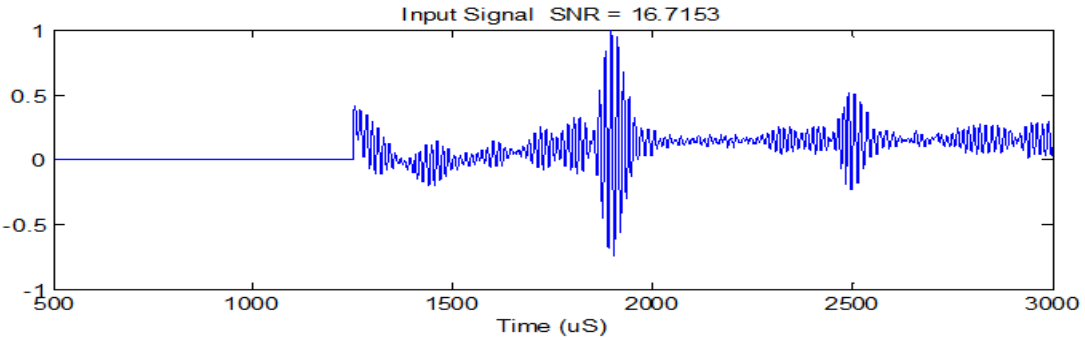

c)

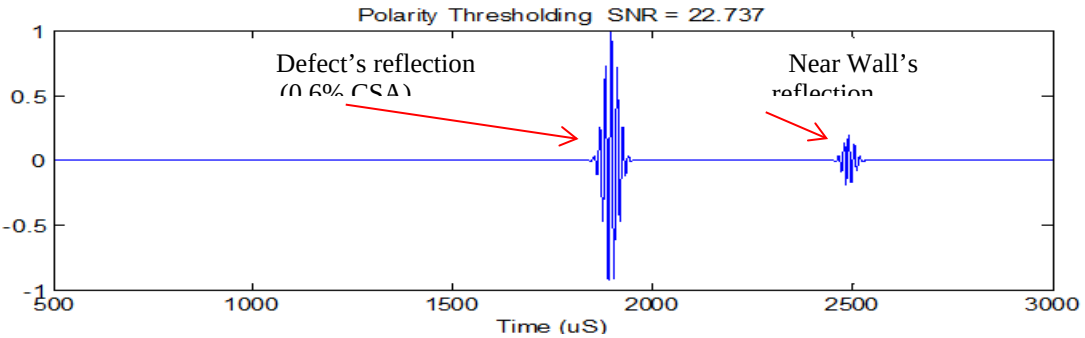

Figure 7-1: Focusing technique a) HTRF set up b) HTRF signal c) result of SSP-PT

References

[1] The United States Department of Justice, “United States V. BP Products North America (D. ALASKA),.” [Online]. Available: http:%0A//www.justice.gov/enrd/3509.htm. [Accessed 29 01 2015]. [Accessed: 10-Mar-2015].

[2] R. Bonner, “Trans-Alaska Pipeline, United States,” *Building the World*, 1997. [Online]. Available: http://blogs.umb.edu/buildingtheworld/tunnels/trans-alaska-pipeline-united-states/. [Accessed: 10-Aug-2015].

[3] M. Kaste, “Republican Sweep Highlights Climate Change Politics In Alaska,” *ncpr*, 2014. [Online]. Available: http://www.northcountrypublicradio.org/news/npr/361896179/republican-sweep-highlights-climate-change-politics-in-alaska. [Accessed: 10-Aug-2015].

[4] B. Xu, L. Yu, and V. Giurgiutiu, “Lamb wave dispersion compensation in piezoelectric wafer active sensor phased-array applications BT - Health Monitoring of Structural and Biological Systems 2009, March 9, 2009 - March 12, 2009,” vol. 7295, 2009.

[5] N. Testing, U. Testing, L. Range, and U. Testing, “The Basics – An Introduction to Guided wave testing Phil Catton 2 Ultrasonic Testing (UT) 3 Long Range Ultrasonic Testing,” pp. 1–26, 2011.

[6] K. R. Leonard and M. K. Hinders, “Guided wave helical ultrasonic tomography of pipes.,” *J. Acoust. Soc. Am.*, vol. 114, no. August 2002, pp. 767–774, 2003.

[7] S. K. Pedram, S. Vaseghi, and B. Langari, “Audio Packet Loss Concealment using Motion-Compensated Spectral Extrapolation,” *Signal Process. Inf. Technol. 2013 IEEE Int. Symp.*, pp. 434–439.

[8] S. K. Pedram, S. Vaseghi, and B. Langari, “Audio packet loss concealment using spectral motion,” *ICASSP, IEEE Int. Conf. Acoust. Speech Signal Process. - Proc.*, no. 3, pp. 6707–6710, 2014.

[9] L. Garverick, “Corrosion in the petrochemical industry, USA: ASM International,” 1995.

[10] “ASME B36.10M,” 2004.

[11] S. K. Pedram, A. Haig, P. S. Lowe, K. Thornicroft, L. Gan, and P. Mudge, “Split-spectrum signal processing for reduction of the effect of dispersive wave modes in long-range ultrasonic testing,” *Phys. Procedia*, vol. 70, pp. 388–392, 2015.

[12] S. K. Pedram, K. Thornicroft, L. Gan, and P. Mudge, “Reduction of Dispersive Wave Modes in Guided Wave Testing using Split-Spectrum Processing,” pp. 1–6, 2016.

[13] R. Mallet, “SIGNAL PROCESSING FOR NON- DESTRUCTIVE TESTING A thesis submitted in part fulfilment of the requirements for the award of Doctor of Engineering (EngD) by Robin Mallett,” no. August, p. 242, 2007.

[14] “Plant Integrity Ltd., TWI, 2015. [Online]. Available: http://www.plantintegrity.com/.,” 2015.

[15] D. Oliver, “Tutorial: 3D Scanning Vibrometry for Structural Dynamics Measurements,” *SEM IMAC-XXVII Conf. Expo. Struct. Dyn.*, 2009.

[16] Plant Integrity Ltd., “Teletest Focus Long Range Ultrasonic System Specification,” *TWI, Cambridge, United Kingdom,*. 2007.

[17] D. T. Blackstock, *Fundamentals of Acoustics*. John Wiley and Sons, 2000.

[18] R. Resnick, D. Halliday, and K. and Krane, *Physics*, 4th ed. John Wiley and Sons, 1992.

[19] Liang Tao, Hon Keung Kwan, L. Tao, H. K. Kwan, and S. Member, “Novel DCT-based

real-valued discrete Gabor transform and its fast algorithms," *IEEE Trans. Signal Process.*, vol. 57, no. 6, pp. 2151–2164, 2009.

[20] A. T. Poyil and K. M. Nasimudeen, "Multi resolution signal analysis using improved Wigner Ville Distribution," *Proc. - 2012 Int. Conf. Commun. Inf. Comput. Technol. ICCICT 2012*, pp. 1–4, 2012.

[21] L. Srinivasan, Y. Rakvongthai, and S. Oraintara, "Microarray image denoising using complex gaussian scale mixtures of complex wavelets," *IEEE J. Biomed. Heal. Informatics*, vol. 18, no. 4, pp. 1423–1430, 2014.

[22] J. W. Cooley and J. W. Tukey, "An Algorithm for Machine Calculation of Complex Fourier Series," *Math. Comput.*, vol. 19, no. 90, p. 297-, 1965.

[23] L. Cohen, "Time-Frequency Distributions-A Review," *Proc. IEEE*, vol. 77, no. 7, pp. 941–981, 1989.

[24] P. Flandrin and P. Gon, "Geometry of Affine Time – Frequency Distributions," pp. 10–39, 1996.

[25] A. H. Nuttall, "Some Windows with Very Good Sidelobe Behavior," *IEEE Trans. Acoust.*, vol. 29, no. 1, pp. 84–91, 1981.

[26] P. Cawley and D. Alleyne, "The use of Lamb waves for the long range inspection of large structures," *Ultrasonics*, vol. 34, no. 2–5, pp. 287–290, 1996.

[27] S. R. Taghizadeh, "Digital Signal Processing Case Study: Part-3 Discrete- Time Signals & Systems," 2000.

[28] J. Watkinson, *The Art of Digital Audio*. 1988.

[29] R. E. Crochiere and L. R. Rabiner, "Interpolation and decimation of digital signals - A tutorial review," *Proc. IEEE*, vol. 69, no. 3, pp. 300–331, 1981.

[30] P. Rubbers and C. J. Pritchard, "An overview of Split Spectrum Processing," *NDT.net*, vol. 8, no. 8, pp. 1–11, 2007.

[31] S. V Vaseghi, *Multimedia signal processing: theory and applications in speech, music and ...*. 2007.

[32] H. Ofir, "Packet Loss Concealment for Audio Streaming," 2006.

[33] S. Kumar and S. Rai, "Survey on Transport Layer Protocols : TCP & UDP," *Int. J. Comput. Appl.*, vol. 46, no. 7, pp. 20–25, 2012.

[34] J.-C. Bolot, H. Crépin, and A. V. Garcia, "Analysis of audio packet loss in the internet," *Netw. Oper. Syst. Support Digit. Audio Video*, pp. 154–165, 1995.

[35] J. C. Bolot, "Characterizing end-to-end packet delay and loss in the internet," *J. High Speed Networks*, vol. 2, no. 3, pp. 305–323, 1993.

[36] T. Moriya, R. Sugiura, Y. Kamamoto, H. Kameoka, and N. Harada, "Progress in LPC-based frequency-domain audio coding," *APSIPA Trans. Signal Inf. Process.*, vol. 5, p. e11, 2016.

[37] S. Quackenbush and P. F. Driessen, "Error Mitigation in MPEG-4 Audio Packet Communication Systems," *Audio engineering society*. pp. 5981–5991, 2003.

[38] J. M. TRIBOLET and R. E. Crochiere, "Frequency Domain Coding of Speech," *IEEE Trans. Audio, Speech Lang. Process.*, no. 5, pp. 512–530, 1979.

[39] D. L. Wang and J. S. Lim, "The Unimportance of Phase in Speech Enhancement," *IEEE Trans. Acoust.*, vol. 30, no. 4, pp. 679–681, 1982.

[40] K. Paliwal and L. Alsteris, "Usefulness of phase spectrum in human speech perception.,"

Interspeech, pp. 2117–2120, 2003.

[41] J. S. Lim and A. V. Oppenheim, “Enhancement and Bandwidth Compression of Noisy Speech,” *Proc. IEEE*, vol. 67, no. 12, pp. 1586–1604, 1979.

[42] S. Boll, “Suppression of acoustic noise in speech using spectral subtraction,” *IEEE Trans. Acoust. Speech Signal Process.*, vol. 27, no. 2, pp. 113–120, 1979.

[43] M. K. Hasan, S. Salahuddin, and M. R. Khan, “A modified \emph{a priori} {SNR} for speech enhancement using spectral subtraction rules,” vol. 11, no. 4, pp. 450–453, 2004.

[44] H. Nawab, A. V. Oppenheim, and J. S. Lim, “IMPROVED SPECTRAL SUBTRACTION FOR SIGNAL RESTORATION,” *Proc. IEEE ICASSP*, pp. 1105–1108, 1981.

[45] I. Y. Soon and S. N. Koh, “Low distortion speech enhancement,” *IEE Proc. - Vision, Image, Signal Process.*, vol. 147, no. 3, p. 247, 2000.

[46] R. Martin, “Speech Enhancement Using Mmse Short Time Spectral Estimation with gamma distributed speech priors,” *IEEE Int. Conf. Acoust. Speech, Signal Process. (ICASSP)*, pp. 253–256, 2002.

[47] R. Martin and C. Breithaupt, “Speech Enhancement in the DFT Domain using Laplacian Speech Priors,” *Iwaenc 2003*, pp. 87–90, 2003.

[48] B. Chen and P. C. Loizou, “Speech enhancement using a mmse short time spectral amplitude estimator with laplacian speech modeling,” *ICASSP, IEEE Int. Conf. Acoust. Speech Signal Process. - Proc.*, vol. I, no. 2, pp. 1097–1100, 2005.

[49] B. Chen and P. C. Loizou, “A Laplacian-based MMSE estimator for speech enhancement,” *Speech Commun.*, vol. 49, no. 2, pp. 134–143, 2007.

[50] Y. Ephraim and D. Malah, “Speech Enhancement Using a- Minimum Mean- Square Error Short-Time Spectral Amplitude Estimator,” *IEEE Trans. Acoust. Speech Signal Process.*, no. 6, pp. 1109–1122, 1984.

[51] I. Cohen, “On the decision-directed estimation approach of Ephraim and Malah,” *Acoust. Speech, Signal Process. 2004. Proceedings. (ICASSP ’04). IEEE Int. Conf.*, vol. 1, pp. 17–21, 2004.

[52] I. Cohen, “Speech enhancement using a noncausal a priori SNR estimator,” *IEEE Signal Process. Lett.*, vol. 11, no. 9, pp. 725–728, 2004.

[53] Y. Ephraim and D. Malah, “Speech enhancement using a minimum mean-square error log-spectral amplitude estimator,” *IEEE Trans. Acoust.*, vol. 33, no. 2, pp. 443–445, 1985.

[54] I. Cohen, “Relaxed statistical model for speech enhancement and a priori SNR estimation,” *IEEE Trans. Speech Audio Process.*, vol. 13, no. 5, pp. 870–881, 2005.

[55] E. Zavarehei and S. Vaseghi, “Interpolation of lost speech segments using LP-HNM model with codebook post-processing,” *IEEE Trans. Multimed.*, vol. 10, no. 3, pp. 493–502, 2008.

[56] Q. Yan *et al.*, “Kalman tracking of linear predictor and harmonic noise models for noisy speech enhancement,” *Comput. Speech Lang.*, vol. 22, no. 1, pp. 69–83, 2008.

[57] T. Ezzat, E. Meyers, J. R. Glass, and T. Poggio, “Morphing spectral envelopes using audio flow,” *Interspeech*, pp. 2545–2548, 2005.

[58] B. K. P. Horn and B. G. Schunck, “Determining optical flow,” *Artif. Intell.*, vol. 17, no. 1–3, pp. 185–203, 1981.

[59] M. Slaney, M. Covell, B. Lassiter, P. M. Road, and C. Building, “Automatic Audio Morphing,” pp. 1001–1004, 1801.

[60] K. K. Paliwal, “Interpolation properties of linear prediction parametric representations,” *Proc. Eurospeech*, vol. 2, pp. 1029–1032, 1995.

[61] D. T. Chappell and J. H. L. Hansen, “A comparison of spectral smoothing methods for segment concatenation based speech synthesis,” *Speech Commun.*, vol. 36, no. 3–4, pp. 343–374, 2002.

[62] H. R. Pfitzinger, “DFW-based spectral smoothing for concatenative speech synthesis.,” *Interspeech*, pp. 2–5, 2004.

[63] R. . McAULAY and T. . Quatieri, “Speech Analysis/Synthesis Based on a Sinusoidal Representation,” *IEEE Trans. Acoust.*, vol. 15, no. 4, pp. 113–123, 1986.

[64] V. Goncharoff and M. Kaine-Krolak, “Interpolation of LPC spectra via pole shifting,” *Ieee Int. Conf. Acoust. Speech Signal Process.*, vol. 1, pp. 780–780, 1995.

[65] D. Schwarz and X. Rodet, “Spectral Envelope Estimation and Representation for Sound Analysis – Synthesis,” *Proc. ICMC*, pp. 351–354, 1999.

[66] R. E. Kalman, “A New Approach to Linear Filtering and Prediction Problems,” *J. Basic Eng.*, vol. 82, no. 1, p. 35, 1960.

[67] R. E. Kalman and R. S. Bucy, “New results in linear filtering and prediction theory,” *J. Basic Eng.*, vol. 83, no. 1, pp. 95–108, 1961.

[68] L. Joon Woong, K. Mun Sang, and K. In-So, “A Kalman filter based visual tracking algorithm for an object moving in 3D,” *Proc. 1995 IEEE/RSJ Int. Conf. Intell. Robot. Syst.*, vol. 1, pp. 342–347, 1995.

[69] S. Gannot, D. Burshtein, and E. Weinstein, “Iterative and sequential kaiman filter-based speech enhancement algorithms,” *IEEE Trans. Speech Audio Process.*, vol. 6, no. 4, pp. 373–385, 1998.

[70] M. Gabrea, “Robust adaptive Kalman filtering-based speech enhancement algorithm,” *Acoust. Speech, Signal Process. 2004. …*, vol. 1.1, pp. 301–304, 2004.

[71] K. Y. Lee, S. McLaughlin, and K. Shirai, “Speech Enhancement Based on Extended {Kalman} Filter and Neural Predictive Hidden {Markov} Model,” *Proc. Intl. Work. Neural Networks Signal Process.*, pp. 302–310, 1996.

[72] J. L. Rose, Z. Sun, P. J. Mudge, and M. J. Avioli, “Guided wave flexural mode tuning and focusing for pipe testing,” *Materials evaluation*, vol. 61, no. 2. pp. 162–167, 2003.

[73] P. Wilcox, M. Lowe, and P. Cawley, “The effect of dispersion on long-range inspection using ultrasonic guided waves,” *NDT E Int.*, vol. 34, no. 1, pp. 1–9, 2001.

[74] P. Cawley and M. J. S. Lowe, “Practical long range guided wave inspection-applications to pipes and rail,” *Mater. Eval.*, pp. 66–74, 2003.

[75] K. F. Graff, *Wave Motion in Elastic Solids*. 1975.

[76] J. L. Rose, “An Introduction to Ultrasonic Guided Waves,” 2007.

[77] J. W. Strutt, *The Theory of Sound*. 1896.

[78] Noé Jiménez, “Wave simulations,” 2015. [Online]. Available: http://www.nojigon.webs.upv.es/simulations_waves.php. [Accessed: 01-Feb-2016].

[79] H. Lamb, “On Waves in an Elastic Plate,” *Proc. R. Soc. London Ser. A*, pp. 114–128, 1971.

[80] D. C. Worlton, “Experimental Confirmation of Lamb Waves at Megacycle Frequencies,” *J. Appl. Phys.*, vol. 32, pp. 697–971, 1961.

[81] K. Thornicroft, “Ultrasonic Guided Wave Testing of Pipelines using a Broadband Excitation,” no. May, 2015.

[82] D. C. Gazis, “Three-Dimensional Investigation of the Propagation of Waves in Hollow Circular Cylinders . I . Analytical Foundation Three-Dimensional Investigation of the

Propagation of Waves in Hollow HE propagation of free harmonic waves in an," *J. Acoust. Soc. Am.*, vol. 568, no. 31, pp. 568–573, 1959.

[83] D. C. Gazis, "Three-dimensional investigation of the propagation of waves in hollow circular cylinders. II. numerical results.," *J. Acoust. Soc. Am.*, vol. 573, no. 31, pp. 573–578, 1959.

[84] A. H. Meitzler, "Mode Coupling Occurring in the Propagation of Elastic Pulses in Wires," *J. Acoust. Soc. Am.*, vol. 435, no. 33, pp. 435–445, 1961.

[85] Joseph Zemanek Jr., "An Experimental and Theoretical Investigation of Elastic Wave Propagation in a Cylinder," *J. Acoust. Soc. Am.*, vol. 265, no. 51, pp. 265–283, 1972.

[86] H. Helmholtz, *On the Sensations of Tone*. New York: Dover Publications, 1954.

[87] L. Rayleigh, "On Waves Propagated along the Plane Surface of an Elastic Solid," *Proc. London Math. Soc.*, vol. 17, pp. 4–11, 1887.

[88] H. Lamb, *The Dynamical Theory of Sound*. New York: Dover Publications, 1960.

[89] I. A. Viktorov, *Rayleigh and Lamb Waves Physical Theory and Applications*. New York: NY: Plenum Press, 1967.

[90] M. G. Silk and K. F. Bainton, "The propagation in metal tubing of ultrasonic wave modes equivalent to Lamb waves," *Ultrasonics*, vol. 17, no. 1, pp. 11–19, 1979.

[91] W. Bottger, H. Schneider, and W. Weingarten, "Prototype EMAT system for tube inspection with guided ultrasonic waves," *Elsevier, Nucl. Eng. Des.*, vol. 102, no. 3, pp. 369–376, 1987.

[92] P. Mudge, A. M. Lank, and D. N. Alleyne, "Long Range Method of Detection of Corrosion under Insulation in Process Pipework," in *5th European Union Hydrocarbons Symposium*, 1996.

[93] J. L. Rose, "A Baseline and Vision of Ultrasonic Guided Wave Inspection Potential," *J. Press. Vessel Technol.*, vol. 124, no. 3, p. 273, 2002.

[94] H. J. Shin and J. L. Rose, "Guided Wave Tuning Principles for Defect Detection in Tubing," *J. Nondestruct. Test. Eval.*, vol. 17, no. 1, pp. 27–36, 1998.

[95] P. Catton, "Long Range Ultrasonic Guided Waves for the Quantitative Inspection of Pipelines," Brunel University, 2009.

[96] D. N. Alleyne, M. J. S. Lowe, and P. Cawley, "The Reflection of Guided Waves From Circumferential Notches in Pipes," *J. Appl. Mech.*, vol. 65, no. 3, pp. 635–641, 1998.

[97] P. J. Mudge, *PRACTICAL ENHANCEMENTS ACHIEVABLE IN LONG RANGE ULTRASONIC TESTING BY EXPLOITING THE PROPERTIES OF GUIDED WAVES PJ Mudge Plant Integrity Limited, Cambridge, United Kingdom*, no. 1. 2004, pp. 1–7.

[98] G. Gautschi, *Piezoelectric Sensorics: Force, Strain, Pressure, Acceleration and Acoustic Emission Sensors, Materials and Ampli ers*. Springer, 1st edn, 2002.

[99] J. Krautkramer, H. Krautkramer, and H. Krautkramer, J. Krautkramer, *Ultrasonic testing of materials*, 4th ed. Newyork: Springer Verlag, 1990.

[100] B. Pavlakovic, M. Lowe, D. Alleyne, and P. Cawley, "Disperse: A General Purpose Program for Creating Dispersion Curves," *Rev. Prog. Quant. Nondestruct. Eval.*, pp. 185–192, 1997.

[101] C. Perkins, O. Hodson, and V. Hardman, "A Survey of Packet-Loss Recovery Techniques for Streaming Audio 1 Introduction 2 Multicast Channel Characteristics," *Media*, no. October, pp. 1–15, 1998.

[102] X. Zheng and C. Ritz, "Hybrid FEC and MDC models for low-delay packet-loss recovery,"

5th Int. Conf. Signal Process. Commun. Syst. ICSPCS'2011 - Proc., 2011.

[103] J. G. Gruber and L. STRAWCZYNSKI, "Subjective Effects of Variable Delay and Speech Clipping in Dynamically Managed Voice Systems," *IEEE Trans. Commun.*, vol. COM-33, no. 8, pp. 801–808.

[104] N. s. JAYANT and S. W. CHRISTENSEN, "Effects of Packet Losses in Waveform Coded Speech and Improvements Due to an Odd-Even Sample-Interpolation Procedure," *IEEE Trans. Commun.*, vol. COM-29, no. 2, pp. 101–109.

[105] G. A. Miller and J. C. R. Licklider, "The Intelligibility of Interrupted Speech," *J. Acoust. Soc. Am.*, vol. 22, no. 2, pp. 167–173, 1950.

[106] H. Schulzrinne, "RTP profile for audio and video conferences with minimal control," *IETF Audio/Video Transp. WG, Work Prog.*

[107] E. R. G. 6.11, "Substitution and muting of lost frames for full rate speech channels." 1992.

[108] S. V Vaseghi, *Advanced Digital Signal Processing and Noise Reducion*, Fourth. 2008.

[109] D. J. Goodman, G. B. Lockhart, O. J. Wasem, and W. Wong, "Waveform Substitution Techniques for Recovering Missing Speech Segments in Packet Voice Communications," *IEEE Trans. Acoust.*, vol. ASSP-34, no. 6, pp. 1440–1448.

[110] O. J. Wasem, D. J. Goodman, C. A. Dvorak, and H. G. Page, "The Effect of Waveform Substitution on the Quality of PCM Packet Communications," *IEEE Trans. Acoust. Speech Signal Process.*, vol. 36, no. 3, pp. 1–7.

[111] F. Merazka, "Packet Loss Concealment Using Time Scale Modification for CELP Based Coders in Packet Network," *Syst. Theory (SSST), 40th Southeast. Symp. Syst. Theory*, pp. 84–87.

[112] H. Sanneck, A. Stenger, K. Ben Younes, and B. Girod, "A New Technique for Audio Packet Loss Concealment," *IEEE Glob. Internet*, pp. 48–52.

[113] R. A. Valenzuew and C. N. Anlmalu, "A new voice-packet reconstruction technique," *Proc. IEEE Int. Conf. Acoust. Speech, Signal Process.*, pp. 1334–1336, 1989.

[114] Appendix I, "A High Quality Low-Complexity Algorithm for Packet Loss Concealment With G.711, ITU-T Recommend. G.711," 1999.

[115] J. Thyssen, R. Zopf, J. H. Chen, and N. Shetty, "A candidate for the ITU-T G.722 packet loss concealment standard," *ICASSP, IEEE Int. Conf. Acoust. Speech Signal Process. - Proc.*, vol. 4, pp. 549–552, 2007.

[116] ITU-T Recommendation G.728 Annex I:, *Frame or packet loss concealment for LD-CELP decoder*. 1999.

[117] ITU-T Recommendation G.729:, *Coding of speech at 8 kbit/s using Conjugate Structure Algebraic-Code-Exited Linear-Prediction (CS-ACELP)*. 1996.

[118] E. Gündüzhan and K. Momtahan, "A Linear Prediction Based Packet Loss Concealment Algorithm for PCM Coded Speech," *IEEE Trans. Speech Audio Process.*, vol. 9, no. 8, pp. 778–785, 2001.

[119] M. Elsabroulj, M. Borrchard, and T. Aboulnasr, "A NEW HYBRID LONG-TERM AND SHORT-TERM PREDICTION ALGORITHM FOR PACKET LOSS ERASURE OVER IP-NETWORKS," *Proc. 7th Int. Symp. Signal Process. Its Appl.*, vol. 1, pp. 361–364, 2003.

[120] J. Wang and J. D. Gibson, "PARAMETER INTERPOLATION TO ENHANCE THE FRAME ERASURE ROBUSTNESS," *Proc.IEEE Int. Conf. Acoust. Speech, Signal Process.*, vol. 2, pp. 745–748, 2001.

[121] ITU Rec. G.723.1, “Dual rate speech coder for multimedia communications transmitting at 5.3 and 6.3 kbit/s,” 1996.

[122] C. A. Rødbro, M. N. Murthi, S. V. Andersen, and S. H. Jensen, “Hidden Markov model-based packet loss concealment for voice over IP,” *IEEE Trans. Audio, Speech Lang. Process.*, vol. 14, no. 5, pp. 1609–1623, 2006.

[123] N. J. Veldhuis, “Adaptive Interpolation of Discrete-Time Signals That Can Be Modeled as Autoregressive Processes,” *IEEE Trans. Acoust. Speech Signal Process.*, vol. ASSP-34, no. 2, pp. 317–330, 1986.

[124] S. J. Godsill and P. J. W. Rayner, *Digital Audio Restoration - a statistical model based approach*. 1998.

[125] S. V Vaseghi and P. J. W. Rayner, “Detection and suppression of impulsive noise in speech communication systems,” *IEE Proceedings, Part 1*, vol. 137(1), no. February, pp. 38–46, 1990.

[126] P. A. A. Esquef and L. W. P. Biscainho, “An efficient model-based multirate method for reconstruction of audio signals across long gaps,” *IEEE Trans. Audio, Speech Lang. Process.*, vol. 14, no. 4, pp. 1391–1400, 2006.

[127] I. Kauppinen and K. Roth, “Audio signal restoration- theory and applications,” in *in Proc. 5th Int. Conf. on Digital Audio Effects*, 2002, pp. 105–110.

[128] J. Lindblom and P. Hedelin, “Packet Loss Concealment based on Sinusoidal Extrapolation,” *IEEE*, pp. 173–176, 2002.

[129] J. Lindblom and P. Hedelin, “Packet loss concealment based on sinusoidal modeling,” *Proc. IEEE Work. Speech Coding*, pp. 65–67, 2002.

[130] C. A. Rødbro, M. G. Christensen, S. V. Andersen, and S. H. Jensen, “COMPRESSED DOMAIN PACKET LOSS CONCEALMENT OF SINUSOIDALLY CODED,” in *in Proc. IEEE Int. Conf. Acoustics, Speech, Signal Processing*, 2003, no. 1, pp. 104–107.

[131] J. Wang and J. D. Gibson, “Performance comparison of intraframe and interframe LSF quantization in packet networks,” in *2000 IEEE Workshop on Speech Coding. Proceedings. Meeting the Challenges of the New Millennium*, 2000, pp. 126–128.

[132] H. Ofir and D. Malah, “Packet loss concealment for audio streaming based on the GAPES and MAPES algorithms,” *IEEE Conv. Electr. Electron. Eng. Isr. Proc.*, pp. 280–284, 2006.

[133] H. Ofir, D. Malah, and I. Cohen, “Audio packet loss concealment in a combined MDCT-MDST domain,” *IEEE Signal Process. Lett.*, vol. 14, no. 12, pp. 1032–1035, 2007.

[134] C. Plapous *et al.*, “SPEECH ENHANCEMENT USING HARMONIC REGENERATION,” in *ICASSP, IEEE International Conference on Acoustics, Speech and Signal Processing - Proceedings*, 2005, no. 5, pp. 157–160.

[135] Y. Stylianou, “Applying the Harmonic Plus Noise Model in Concatenative Speech Synthesis,” *IEEE Trans. Speech Audio Process.*, vol. 9, no. 1, pp. 21–29, 2001.

[136] S. Vaseghi, E. Zavarehei, and Q. Yan, “SPEECH BANDWIDTH EXTENSION : EXTRAPOLATIONS OF SPECTRAL ENVELOP AND HARMONICITY QUALITY OF EXCITATION,” in *ICASSP, IEEE International Conference on Acoustics, Speech and Signal Processing - Proceedings*, 2006, no. 1, pp. 844–847.

[137] D. W. Griffin and J. A. E. S. Lim, “Multiband Excitation Vocoder,” *IEEE Trans. Acoust.*, vol. 36, no. 8, pp. 1223–1235, 1988.

[138] A. M. Kondoz, *Digital Speech: Coding for Low Bit Rate Communication Systems*. John Wiley & Sons, Ltd., 1999.

[139] D. G. Raza and C. Chan, “Enhancing quality of CELP coded speech via wideband

extension by using voicing GMM interpolation and HNM re-synthesis," *IEEE Acoust. Speech, Signal Process.*, vol. 1, pp. 1–4, 2002.

[140] R. Sicard, J. Goyette, and D. Zellouf, "A numerical dispersion compensation technique for time recompression of Lamb wave signals," *Ultrasonics*, vol. 40, no. 1–8, pp. 727–732, 2002.

[141] P. D. Wilcox, "A rapid signal processing technique to remove the effect of dispersion from guided wave signals," *IEEE Trans. Ultrason. Ferroelectr. Freq. Control*, vol. 50, no. 4, pp. 419–427, 2003.

[142] L. Zeng and J. Lin, "Chirp-based dispersion pre-compensation for high resolution Lamb wave inspection," *NDT E Int.*, vol. 61, pp. 35–44, 2014.

[143] K. Xu, D. Ta, P. Moilanen, and W. Wang, "Mode separation of Lamb waves based on dispersion compensation method," *J. Acoust. Soc. Am.*, vol. 131, no. 4, pp. 2714–2722, 2012.

[144] K. Xu, D. Ta, B. Hu, P. Laugier, and W. Wang, "Wideband dispersion reversal of lamb waves," *IEEE Trans. Ultrason. Ferroelectr. Freq. Control*, vol. 61, no. 6, pp. 997–1005, 2014.

[145] K. Xu, C. Liu, and D. Ta, "Ultrasonic Guided Waves Dispersion Reversal for Long Bone Thickness Evaluation : a Simulation Study *," vol. 0, no. 3, pp. 1930–1933, 2013.

[146] K. Toiyama and T. Hayashi, "Pulse compression technique considering velocity dispersion of guided wave," *Rev. Quant. Nondestruct. Eval.*, vol. 27, pp. 587–593, 2008.

[147] L. De Marchi, A. Perelli, and A. Marzani, "A signal processing approach to exploit chirp excitation in Lamb wave defect detection and localization procedures," *Mech. Syst. Signal Process.*, vol. 39, no. 1–2, pp. 20–31, 2013.

[148] L. De Marchi, A. Marzani, and M. Miniaci, "compression," no. 2013, p. 2013.

[149] M. K. Yücel *et al.*, "Pulse-compression based iterative time-of-flight extraction of dispersed Ultrasonic Guided Waves," *Proceeding - 2015 IEEE Int. Conf. Ind. Informatics, INDIN 2015*, pp. 809–815, 2015.

[150] M. K. Yucel, "Signal Processing Methods for Defect Detection in Multi-Wire Helical Waveguides using Ultrasonic Guided Waves by," no. March, 2015.

[151] S. Fateri, "Advanced Signal Processing Techniques for Multimodal Ultrasonic Guided Wave Response," 2015.

[152] H. R. Beasley, Eric W and Ward, "A Quantitative Analysis of Sea Clutter Decorrelation with Frequency Agility," *IEEE Trans. Aerosp. Electron. Syst.*, vol. 4, no. May, pp. 468–473, 1968.

[153] N. . M. Bilgutay, V. L. Newhouse, E. S. and Furgason, and E. S. Furgason, "FLAW VISIBILITY ENHANCEMENT BY SPLIT-SPECTRUM PROCESSING TECHNIQUES," *Ultrason. Symp.*, pp. 878–883, 1981.

[154] V. L. Newhouse, N. M. Bilgutay, J. Saniie, and E. S. Furgason, "Flaw-to-grain echo enhancement by split-spectrum processing," *Ultrasonics*, vol. 20, no. 2, pp. 59–68, 1982.

[155] I. Amir, N. M. Bilgutay, and V. L. Newhouse, "Analysis and comparison of some frequency compounding algorithms for the reduction of ultrasonic clutter.," *IEEE Trans. Ultrason. Ferroelectr. Freq. Control*, vol. 33, no. 4, pp. 402–11, 1986.

[156] P. Karpur, P. M. Shankar, J. L. Rose, and V. L. and Newhouse, "Split Spectrum Processing - Optimizing the Processing Parameters Using Minimization.pdf," *Ultrasonics*, vol. 25, pp. 204–208, 1987.

[157] J. L. Rose, P. Karpur, and V. L. and Newhouse, "Utility of Split-Spectrum Processing in

Ultrasonic Nondestructive Evaluation," *Mater. Eval.*, vol. 46, pp. 114–122, 1988.

[158] P. Karpur, P. M. Shankar, J. L. Rose, and V. L. and Newhouse, "Split spectrum processing:determination of the available bandwidth for spectral splitting," *Ultrasonics*, vol. 26, pp. 204–209, 1988.

[159] P. M. Shankar, V. L. Newhouse, P. Karpur, and J. L. Rose, "Split-Spectrum Processing: Analysis of Polarity Thresholding Algorithm for Improvement of Signal-to-Noise Ratio and Detectability in Ultrasonic Signals," *IEEE Trans. Ultrason. Ferroelectr. Freq. Control*, vol. 36, no. 1, pp. 101–108, 1989.

[160] J. . Aussel, "Split-Spectrum Processing with Finite Impulse Response Filters of Constant Frequency-to-Bandwidth Ratio," *Ultrasonics*, vol. 28, pp. 229–240, 1990.

[161] J. Saniie, D. T. Nagle, and K. D. Donohue, "Analysis of Order Statistic Filters Applied to Ultrasonic Flaw Detection Using Split-Spectrum Processing," *IEEE Trans. Ultrason. Ferroelectr. Freq. Control*, vol. 38, no. 2, pp. 133–140, 1991.

[162] P. Laugier, E. Cherin, and G. Berger, "ULTRASONIC ECHO OF A MOVING TARGET IN BIOLOGICAL TISSUES," pp. 999–1004, 1993.

[163] M. G. Gustafsson and T. Stepinski, "Adaptive split spectrum processing using a neural network," *Res. Nondestruct. Eval.*, vol. 5, no. 1, pp. 51–70, 1993.

[164] M. G. Gustafsson, "Towards Adaptive Split Spectrum Processing," *Ultrason. Symp. 1995. Proceedings., 1995 IEEE*, pp. 729–732, 2000.

[165] Q. Tian, X. Li, N. M. Bilgutay, and S. Member, "Multiple Target Detection Using Split Spectrum Processing and Group Delay Moving Entropy," *IEEE Trans. Ultrason. Ferroelectr. Freq. Control*, vol. 42, no. 6, pp. 1076–1086, 1995.

[166] Q. Tian and N. M. Bilgutay, "Statistical analysis of split spectrum processing for multiple target detection," *IEEE Trans. Ultrason. Ferroelectr. Freq. Control*, vol. 45, no. 1, pp. 251–256, 1998.

[167] H. C. Sun and J. Saniie, "Nonlinear Signal Processing for Ultrasonic Target Detection," pp. 855–858, 1998.

[168] H. C. Sun and J. and Saniie, "Ultrasonic Flaw Detection Using Split-Spectrum Processing Combined with Adaptive-Network-Based Fuzzy Inference System," *IEEE 1999 Ultrason. Symp.*, pp. 801–804, 1999.

[169] M. Grevillot, C. Cudel, J. J. Meyer, and S. Jacquey, "Two approaches to multiple specular echo detection using split," vol. 37, pp. 1–6, 1999.

[170] L. Zhenqing, T. Dean, and L. Xiao, "A Phase Deviation Based Split-spectrum Processing Algorithm for Ultrasonic Testing in Coarse Grained Materials," *NDT.net*, pp. 1–5, 2000.

[171] T. Stepinski and L. Ericsson, "Signal Processing for Ultrasonic Testing of Material with Coarse Structure Signal Processing for Ultrasonic Testing of Material with Coarse Structure," *NDT.net*, pp. 1–9, 2000.

[172] R. Drai, M. Khelil, and A. Benchaala, "Time frequency and wavelet transform applied to selected problems in ultrasonics NDE," *NDT E Int.*, vol. 35, no. 8, pp. 567–572, 2002.

[173] P. Rubbers, "Forging ahead with the Ultrasonic Inspections of castings," *NDT.net*, vol. 5, no. 10, pp. 2–6, 2000.

[174] P. Rubbers, G. S. Africa, and C. J. Pritchard, "Complex plane Split Spectrum Processing: an introduction," *NDT.net*, vol. 8, no. 11, pp. 1–8, 2003.

[175] P. Rubbers and C. J. Pritchard, "Complex plane Split Spectrum Processing: simulations of zero degree long waves," *J. Br. Inst. NDT*, vol. 27, no. 1, pp. 20–24, 2005.

[176] M. S. JOHANNES and P. Rubbers, “An Investigation into the Performance of Complex Plane Spilt Spectrum Processing Ultrasonics on Composite Materials,” *NDT.net*, pp. 1–7, 2008.

[177] K. D. Donohue, “Split Spectrum Processing and Automatic Flaw Detection,” 2007, pp. 517–546.

[178] A. Rodríguez, “A new filter bank design for split-spectrum algorithm,” *Ndt*, pp. 1–7, 2009.

[179] A. Rodríguez, R. Miralles, I. Bosch, and L. Vergara, “New analysis and extensions of split-spectrum processing algorithms,” *NDT E Int.*, vol. 45, no. 1, pp. 141–147, 2012.

[180] A. Rodriguez *et al.*, “Split Spectrum processing applications for new composite materials imaging,” *IEEE Int. Ultrason. Symp. IUS*, vol. 23403, pp. 1473–1476, 2012.

[181] A. Rodríguez, A. Salazar, and L. Vergara, “Analysis of split-spectrum algorithms in an automatic detection framework,” *Signal Processing*, vol. 92, no. 9, pp. 2293–2307, 2012.

[182] S. Muthumari, K. Vijayarekha, and A. Chatterjee, “Comparative Investigation of Split Spectrum Processing over Classical Approach of Filtering for Non-Linear and Non-Stationary Signals,” *Int. J. Comput. Appl.*, vol. 10, no. 3, pp. 35–38, 2010.

[183] J. Saniie, E. Oruklu, and S. Yoon, “System-on-chip design for ultrasonic target detection using split-spectrum processing and neural networks,” *IEEE Trans. Ultrason. Ferroelectr. Freq. Control*, vol. 59, no. 7, pp. 1354–1368, 2012.

[184] G. Syam and G. K. Sadanandan, “Flaw Detection using Split Spectrum,” *Int. J. Adv. Res. Electr. Electron. Instrum. Eng.*, vol. 3, no. 3, pp. 8118–8127, 2014.

[185] P. Karpur and O. J. Canelones, “Split spectrum processing: a new filtering approach for improved signal-to-noise ratio enhancement of ultrasonic signals,” *Ultrasonics*, vol. 30, no. 6, pp. 351–357, 1992.

[186] T. Q. Nguyen and S. Jayasimha, “Polarity-coincidence filter banks and nondestructive evaluation,” *Circuits Syst. 1994. ISCAS ’94., 1994 IEEE Int. Symp.*, vol. 2, pp. 497–500 vol.2, 1994.

[187] Y. Qian and P. Kabal, “Dual-Mode Wideband Speech Recovery from Narrowband Speech,” in *Eurospeech 2003 - Geneva*, 2003, pp. 1433–1436.

[188] R. Hu, V. Krishnan, and D. V Anderson, “Speech Bandwidth Extension by Improved Codebook Mapping Towards Increased Phonetic Classification,” in *Interspeech*, 2005, pp. 1501–1504.

[189] I. Ist and R. A. Redol, “Pitch-Synchronous Time-Scaling for High-Frequency Excitation Regeneration,” in *Interspeech*, 2005, pp. 1513–1516.

[190] H. Ye, “Voice Morphing Using a Sinusoidal Model and Linear Transformation,” Cambridge University.

[191] D. S. Processing, “LPC Methods Digital Speech Processing — Linear Predictive Coding (LPC) - Introduction LPC Methods LPC Methods Basic Principles of LP LP Estimation Issues Solution for { α k } Solution for { α k } Solution for { α k } Solution for { α k },” pp. 1–14.

[192] Y. Stylianou, “Removing linear phase mismatches in concatenative speech synthesis,” *IEEE Trans. Speech Audio Process.*, vol. 9, no. 3, pp. 232–239, 2001.

[193] M. Y. Zhu, M. Zhang, X. Q. Yu, and W. G. Wan, “Streaming audio packet loss concealment based on sinusoidal frequency estimation in mdct domain,” *IEEE Trans. Consum. Electron.*, vol. 56, no. 2, pp. 811–819, 2010.

[194] G. Welch and G. Bishop, “An Introduction to the Kalman Filter,” *In Pract.*, vol. 7, no. 1, pp. 1–16, 2006.

[195] T. Moriya, R. Sugiura, Y. Kamamoto, H. Kameoka, and N. Harada, “Progress in LPC-based frequency-domain audio coding,” *APSIPA Trans. Signal Inf. Process.*, vol. 5, no. 2016, p. e11, 2016.

[196] G. Hasslinger and O. Hohlfeld, “The Gilbert-Elliott Model for Packet Loss in Real Time Services on the Internet,” *Meas. Model. Eval. Comput. Commun. Syst. (MMB), 2008 14th GI/ITG Conf.* -, pp. 1–15, 2008.

[197] E. N. Gilbert, “Capacity of a Burst-Noise Channel,” *Bell Syst. Tech. J.*, pp. 1253–1265, 1960.

[198] a. W. Rix, J. G. Beerends, M. P. Hollier, and A. P. Hekstra, “Perceptual evaluation of speech quality (PESQ)-a new method for speech quality assessment of telephone networks and codecs,” *IEEE Int. Conf. Acoust. Speech, Signal Process. Proc. (Cat. No.01CH37221)*, vol. 2, pp. 2–5, 2001.

[199] E. Zavarehei, “SPEECH ENHANCEMENT USING HARMONIC-PULSE-NOISE MODELS,” 2007.

[200] K. T. and C. M. and P. Mudge, “Time-Frequency Analysis of Long Range Ultrasonic Signals,” *J. Phys. Conf. Ser.*, vol. 382, no. 1, p. 12060, 2012.

[201] J. Weber, S. S. Member, E. Oruklu, S. S. Member, and J. Saniie, “FPGA-Based Configurable Frequency-Diverse Ultrasonic Target-Detection System,” vol. 58, no. 3, pp. 871–879, 2011.

[202] W. A. A. P. S. Lowe, “Advances in Resolution and Sensitivity of Ultrasonic Guided Waves for Quantitative Inspection of Pipelines by Declaration of Authorship,” no. June, 2016.

[203] S. Fateri, “Advanced Signal Processing Techniques for Multimodal Ultrasonic Guided Wave Response by,” 2015.